DE GRUYTER

ZEITSCHRIFT FÜR KRISTALLOGRAPHIE SUPPLEMENT

26TH ANNUAL CONFERENCE
OF THE GERMAN CRYSTALLOGRAPHIC SOCIETY

MARCH 5-8, 2018
ESSEN, GERMANY

ABSTRACTS

2018 · NUMBER 38

26th Annual Conference of the German Crystallographic Society

Zeitschrift für Kristallographie Supplement

2018 Number 38

26th Annual Conference of the German Crystallographic Society

March 5–8, 2018
Essen, Germany

Abstracts

DE GRUYTER

ISBN 978-3-11-059535-2
e-ISBN (PDF) 978-3-11-059599-4
e-ISBN (EPUB) 978-3-11-059294-8
ISSN 0930-486X

Library of Congress Cataloging-in-Publication Data
A CIP catalog record for this book has been applied for at the Library of Congress.

Bibliographic information published by the Deutsche Nationalbibliothek
Die Deutsche Nationalbibliothek verzeichnet diese Publikation in der Deutschen Nationalbibliografie; detaillierte bibliografische Daten sind im Internet über http://dnb.dnb.de abrufbar.

Druck und Bindung: Frantz X. Stückle Druck und Verlag e.K., Ettenheim
♾ Printed on acid-free paper
Printed in Germany

www.degruyter.com

Table of content

Plenary talks

P01
Temperature dependent structures studied by synchrotron radiation

S. Lidin[1], L. Folkers[1]
[1]Lund University, CAS ,Lund, Sweden

The power of synchrotron radiation allows us to study weak ordering phenomena that develop with changing temperature *in situ*. This has been used to study the temperature dependence of the 3+3 dimensionally modulated strudture of Sn3Sb2 and two ordered variants of the TlI type structure. AuIn and BiPd.

Sn3Sb2 is stable only in a narrow temperaturer ange and decomposes to tin-rich stistaite Sn4Sb3 and pure tin on cooling. Sn3Sb2 was synthesized *in-situ* by heating a single crystal of stistaite together with a piece of tin. The stistaite single crystal takes up tin at temperatures above the melting point of the element and forms Sn3Sb2 in a topochemical reaction. The elemental contrast was enhanced by using radiation with a wave-length close to the absorption edge of tin.

At room temperature, AuIn adopts an incommensurately modulated super structure of TlI. If the temperature in the measurement is increased the satellites of this modulation change in number as the ordering deteriorates, they give way to diffuse scattering and finally, the super structure disappears altogether and the high temperature modufication is simple TlI.

BiPd behaves analogously to AuIn, but here the room temperature modufication appears to be a commensurate super structure. This is replaced first by an incommensurately modulated structure at moderate heating and then by a disordered superstructure as indicated by diffuse scattering.

Figure caption: Temperature dependent single crystal X-ray diffraction data from BiPd. Note the discommensuration at 200oC and the diffuse scattering from 235oC

Figure 1

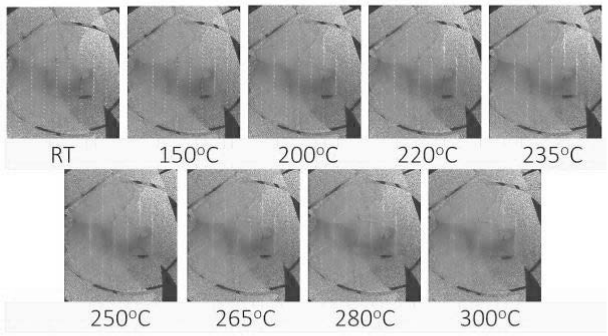

P02
Carbon Oxide Activation at Biological Ni,Fe Centers

H. Dobbek[1]
[1]Humboldt-Universität zu Berlin, Structural Biology and Biochemistry, Berlin, Germany

Anoxic niches provide habitats for a diversity of microorganisms adapted to seemingly hostile environments. Carbon monoxide and carbon dioxide are used by several anaerobic microorganisms as carbon and energy source. Different pathways of growth with CO/CO2 have been described among which the reductive acetyl-CoA pathway is likely of primordial origin and developed a rich bioorganometallic chemistry. Productive utilization of carbon dioxide is relying on oxygen sensitive the metalloenzymes exploiting the chemistry nickel/iron-sulfides and cobalt to synthesize acetyl-CoA from two molecules of CO2. The central catalysts to reversibly reduce carbon dioxide to carbon monoxide are the Ni,Fe-containing carbon monoxide dehydrogenase (CODH) – the central topic of the talk. Recently, we could show that CODH activates carbon dioxide for reduction by binding it between Ni and Fe (Fig.). In this trapped state, carbon dioxide is already reduced by two-electrons and is stabilized by strong p-backbonding interactions with the Ni ion. Furthermore, recent insights indicate that CODH-isoforms vary surprisingly in their kinetic efficiency and tolerance towards dioxygen. The talk will give an overview on the current status of our work and how protein crystallography helps resolving the reaction and inactivation mechanisms of CODHs.

Figure 1

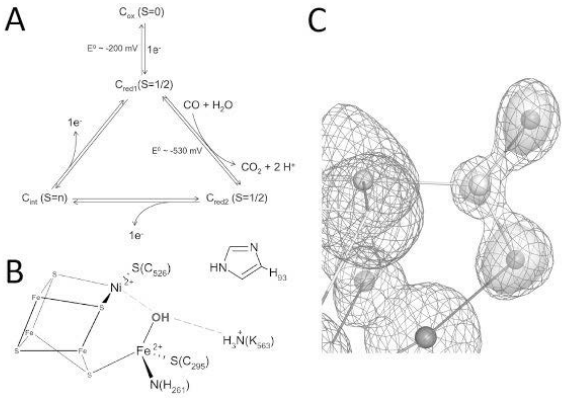

P03
Crystallography taken to the extreme

L. Dubrovinsky[1], N. Dubrovinskaia[1]
[1]University of Bayreuth, Bayerisches Geoinstitut ,Bayreuth, Germany

The impact of high-pressure studies on fundamental physics and chemistry, and especially on the Earth and planetary sciences, has been enormous. Modern science and technology rely on the fundamental knowledge of matter that is provided by crystallographic studies. The most reliable information about crystal structures and their response to changes in pressure and temperature is obtained from single-crystal diffraction experiments. Advances in diamond anvil cell (DAC) techniques and double-stage DACs, as well as in modern X-ray facilities have increased the accessible pressure range for structural research up to multimegabar range. We have developed a methodology to perform single-crystal X-ray diffraction experiments in double-side laser-heated DACs. Our results demonstrated that the solution of crystal structures, their refinement, and accurate determination of thermal equations of state of elemental materials, oxides, carbides, borides, carbonates, and silicates from single-crystal diffraction data are possible above 200 GPa at temperatures of thousands of degrees. These resulted in findings of novel compounds with unusual compositions, crystal chemistry, and physical properties. We illustrate application of new methodology for simultaneous high-pressure and high-temperature single crystal diffraction studies using examples of investigations of chemical and phase relations in the Fe-O system, nitrides, transition metals carbonates, and silicates.

P04

New Experimental Techniques for Exploring Crystallization Pathways and Structural Properties of Solids

K. Harris[1]
[1]Cardiff University, School of Chemistry ,Cardiff, United Kingdom

The lecture will highlight two experimental strategies that we have developed recently for exploring crystallization pathways and structural properties of solids: (i) *in-situ* solid-state NMR techniques to probe the time-evolution of crystallization processes, and (ii) the study of X-ray birefringence and X-ray dichroism to determine molecular orientations in materials.

Our *in-situ* solid-state NMR technique [1] for studying crystallization pathways exploits the ability of NMR to *selectively* detect the solid phase in heterogeneous solid/liquid systems of the type that exist during crystallization from solution. This technique has been shown to be able to establish the sequence of solid phases formed during crystallization, and to enable the discovery of new transient polymorphs. The most recent development [2] is an *in-situ* NMR strategy (called "CLASSIC NMR") that yields simultaneous information on the time-evolution of *both* the solid phase *and* the liquid phase during crystallization, significantly extending the scope and capability of *in-situ* NMR for gaining fundamental insights on the evolution of crystallization processes.

Following our earlier studies of the phenomenon of X-ray birefringence, we recently reported [3] a new experimental set-up that allows X-ray birefringence of materials to be measured in a spatially resolved manner. This technique (called *X-ray Birefringence Imaging*) represents, in many respects, the X-ray analogue of the polarizing optical microscope. By presenting a range of recent results, the lecture will demonstrate the utility and potential of *X-ray Birefringence Imaging* for establishing the local orientational properties of anisotropic materials, including the characterization of changes in molecular orientational ordering associated with solid-state phase transitions, and determination of the size, spatial distribution and temperature dependence of domain structures in materials. Recent results will be presented of the use of the related phenomenon of X-ray dichroism [4] to explore molecular orientations in solids.

References

[1] K.D.M. Harris, C.E. Hughes, P.A. Williams, G.R. Edwards-Gau, *Acta Crystallogr.* **2017**, *C73*, 137.
[2] C.E. Hughes, P.A. Williams, K.D.M. Harris, *Angew. Chemie Int. Ed.* **2014**, *53*, 8939.
[3] B.A. Palmer, G.R. Edwards-Gau, B.M. Kariuki, K.D.M. Harris, I.P. Dolbnya, S.P. Collins, *Science* **2014**, *344*, 1013.
[4] B.A. Palmer, S.P. Collins, J. Hulliger, C.E. Hughes, K.D.M. Harris, *J. Am. Chem. Soc.* **2016**, *138*, 16188.

P05

An unexpected crystallographic insight into renin secretionYahui

Yan[1], Aiwu Zhou[2], Randy J Read[1]
[1]Cambridge Institute for Medical Research, Wellcome Trust/MRC Building, Hills Road, Cambridge CB2 0XY, UK.
[2]Key Laboratory of Cell Differentiation and Apoptosis of Ministry of Education of China, Shanghai Jiaotong University School of Medicine, Shanghai 200025, China.

The action of renin on angiotensinogen to produce the prohormone peptide angiotensin-1 is the first and rate-limiting step in production of the hormone angiotensin-2, which plays a key role in the control of blood pressure and fluid balance. Most renin in the body is secreted in a proenzyme form as prorenin, which is activated later by proteolytic cleavage. When studying the structure of prorenin from human, mouse and rat, we made the surprising observation that the protein from all three species crystallises in the same crystal form, with an unusual packing. This led us to literature describing an alternative renin synthesis pathway that occurs only in the juxtaglomerular cells of the kidney. In this pathway, prorenin is trafficked to immature secretory granules where it forms microcrystals referred to as “rhomboid protogranules”. Renin activation occurs in the course of granule maturation before secretion.

I will discuss evidence that our crystals are the same as the “rhomboid protogranules”, as well as the implications for the events that take place during renin secretion.

P06

Intermolecular interactions from electron density and electrostatic potential perspective

P. M. Dominiak[1]
[1]University of Warsaw, Biological and Chemical Research Centre, Department of Chemistry ,Warszawa, Poland

Understanding and quantitative characterization of interactions among molecules place key role in structure – property studies. To achieve even deeper understanding, access not only to geometry, but also to electron density, is crucial. Electrostatic potential, which combines electron charge density with nuclei charges, is vital as well. Electrostatic interactions are always important contributors to interaction energies and often driving force for molecular recognition.

Nowadays crystallographers are accustom to usage of various electron density models (IAM, Stewart-Hansen-Coppens multipole model, pseudoatom databanks, etc.) to interpret diffraction data. The models may also be used to characterize intermolecular interactions and to estimate interaction energies and electrostatic contributions to them.

I will give brief overview of electron density models developed in my group (UBDB, aug-PROmol model) to be used in crystallography and structural chemistry or biology. Then, after short report from our studies on interactions in macromolecules (RNA, protein kinases, etc.), I will focus on nucleobase interactions in their hydrochloride crystals studied with high-resolution X-ray diffraction and theoretical calculations.

We confirmed that interaction energies in studied ionic crystals are dominated by contributions from electrostatics. Electrostatic interactions energies (Ees) usually constitute 95% of total interaction energies. Ees were several times larger in absolute value when compared to neutral bases. However, they were not as big as some of the theoretical calculations predicted. This was because molecules appeared not to be fully ionized. Apart from chlorine to protonated base charge transfer, small but visible, charge redistribution within cations was observed. Some pairs of protonated bases exhibited attractive interactions or unusually low repulsion despite same molecular charges. This was because strong hydrogen bonding overcompensated overall cation-cation repulsion, the latter being weakened due to charge transfer and molecular charge density polarization. We also discovered strong correlation between interaction energies estimated from QTAIM analysis, and the charge penetration component of Ees. The relation holds regardless of interaction types or whether interacting molecules bear the same or opposite charges.

With all the above I aim to show how modern crystallographic tools help to understand the importance of electrostatics.

Bio-Crystallography I: Hot new structures

S01-01

A symmetry break in a symmetric homodimer results in crystals with alternating layers of order and disorder

W. Bleymüller[1], M. Ebbes[1], C. Geerds[1], H. Niemann[1]
[1]Universität Bielefeld, Fakultät für Chemie ,Bielefeld, Germany

The vast majority of protein homodimers follows C_2 point group symmetry. Extensive structural and functional studies of the bacterial invasion protein InlB led us to the conclusion that InlB is a notable exception to this rule. InlB has three functional regions, the N-terminal internalin domain, the central B-repeat and three C-terminal GW domains. Here, we suggest that the N-terminal domain forms a C_2-symmetric functional homodimer, while the central domain forms a rare asymmetric homodimer.

Full length InlB crystallizes with one molecule in the asymmetric unit forming a functional homodimer mediated by a crystallographic 2-fold axis [1,2]. In the structure of full-length InlB the N-terminal and the C-terminal regions are well resolved. However, the central B-repeat domain could never be modeled into existing difference density between the N- and C-terminal regions.

Our high-resolution structure of the central B-repeat with four molecules in the asymmetric unit revealed two virtually identical asymmetric homodimers [3]. Using mutagenesis in combination with receptor activation assays we could show that the contact area mediating this asymmetric homodimerization is important for InlB function [4]. The arrangement of protomers in this potential asymmetric B-repeat homodimer is akin to a skrew axis with a 176.5° rotation coupled to a 3 Å translation. Placing the asymmetric B-repeat homodimer into the hitherto uninterpretable region of the full-length InlB structure produces an acceptable fit of the electron density.

This leads to a structural model, in which the N- and C-terminal region of InlB obey crystallographic symmetry, while the B-repeat is modeled as a domain present in two conformations with 50% occupancy each. As a result, the crystals would be made up of an ordered layer containing the N- and C-terminal region and a partly disordered layer containing the B-repeat in a double conformation.

References

[1] Marino M, Banerjee M, Jonquières R, Cossart P, Ghosh P (2002) EMBO J., 21, 5623-5634.

[2] Ferraris DM, Gherardi E, Di Y, Heinz DW, Niemann HH (2010) J. Mol. Biol. 395, 522-532

[3] Ebbes M, Bleymüller WM, Cernescu M, Nölker R, Brutschy B, Niemann HH (2011) J. Biol. Chem. 286, 15496-15506

[4] Bleymüller WM, Lämmermann, N, Ebbes M, Maynard D, Geerds C, Niemann HH (2016) J. Biol. Chem. 291, 25567-25577

S01-02

IL-1 Family Cytokines Use Distinct Molecular Mechanisms to Signal through Their Shared Co-receptor

S. Günther[1,2], D. Deredge[3], A. L. Bowers[2], A. Luchini[4], D. A. Bonsor[2], R. Beadenkopf[2], L. Liotta[4], P. L. Wintrode[3], E. J. Sundberg[2]
[1]Deutsches Elektronen-Synchrotron DESY, Hamburg, Germany
[2]University of Maryland School of Medicine, Institute of Human Virology, Baltimore, Germany
[3]University of Maryland School of Pharmacy, Baltimore, United States
[4]George Mason University, Center for Applied Proteomics and Molecular Medicine ,Manassas, United States

Cytokines of the IL-1 family are potent stimulators of the immune system. As seen in other cytokine families, cytokine redundancy due to receptor sharing is characteristic for the IL-1 family. Today five primary receptors have been described that each bind a subset of the 11 known cytokines within this family. Once an agonistic cytokine-receptor pair has formed, it can engage one of the two co-receptors and initiate signaling through MyD88. While IL-18Rβ is the unique co-receptor for the IL-18/IL-18Rα pair, IL-1RAcP is shared between the other four primary receptors, IL-1RI, IL-1RII, ST2 and IL-36R. Crystal structures of IL-1β bound to IL-1RI or IL-1RII in complex with IL-1RAcP previously revealed the general architecture of signaling complexes in the IL-1 family. IL-33 is the latest cytokine to be discovered in the IL-1 family. Since its first description in 2005 it has been recognized as a central driver of type 2 immunity. Here we present the crystal structure of IL-33 in complex with its receptors ST2 and IL-1RAcP. The structure reveals a remarkable conservation of the ternary architecture of signaling complexes in the IL-1 family. We observe common principles of co-receptor binding, also seen in the other two ternary structures containing IL-1RAcP. However, hydrogen/deuterium mass exchange spectroscopy and extensive alanine-scanning analysis combined with direct binding analysis of the IL-1β and IL-33 signaling complexes demonstrate that the binding energy is distributed quite differently within the two. Co-receptor binding of ST2/IL-33 is much less dependent on the cytokine than on the receptor, while for IL-1β/IL-1RI the cytokine plays a much more important role.

S01-03

Insight into a synthetic TetR-derived protein – RNA aptamer switch.

F. Grau[1], F. Groher[2], B. Suess[2], Y. Muller[1]
[1]Friedrich-Alexander-Universität Erlangen-Nürnberg, Department Biologie; Lehrstuhl für Biotechnik, Erlangen, Germany
[2]Technische Universität Darmstadt, Institute for Biology ,Darmstadt, Germany

Introduction

During the past decade, the ever-expanding toolkit of synthetic biology has seen the introduction of several new and promising additions. RNA-based systems are becoming increasingly popular for gene expression control due to the inherent versatility of RNA in interacting with both molecular ligands (see riboswitches) and proteins (ribosome), as well as the relative ease by which RNA can be modified. The SELEX-derived TetR-binding aptamer and the TetR protein provide an ideal basis for the design of a robust framework upon which regulation systems for various applications can be built [1]. On the most basic level, the TetR-binding RNA aptamer was shown to induce TetR controlled gene expression in *E. coli* with an efficiency comparable to that of tetracycline (tc) by competitively displacing the *tetO* operator DNA. RNA aptamer interaction with TetR can be disrupted *via* the addition of tc, thus providing an additional level of regulatory control which has enabled the implementation of the system into more complex gene regulatory networks in both pro- and eukaryotes [2, 3].

Objectives

The aim of this work was the structure determination of the complex between TetR and the TetR-binding RNA aptamer *via* X-ray crystallography in order to provide insight into the mechanism of RNA-binding toTetR.

Results

We present the first structure of TetR in complex with a SELEX-derived TetR-binding RNA aptamer. The complex consists of one homodimer of TetR and a single aptamer. The flexibility of the aptamer allows it to adopt a conformation that is compatible with the canonical nucleotide-binding conformation of TetR, allowing for an interaction that somewhat resembles the interaction between TetR and the naturally occurring *tetO* operator DNA in terms of affinity and specificity.

Conclusion

Our results provide insight into the mechanism by which the synthetic TetR-derived protein – RNA aptamer switch functions. In addition, the data could serve as a structural blueprint for the design of future generations of RNA aptamers that will be able to specifically control single repressor proteins from the very large family of TetR-like bacterial repressors.

References

[1] Steber, M., et al.. ChemBioChem, 2011. **12**(17): p. 2608-2614.
[2] Ausländer, D., et al.. Nucleic Acids Research, 2011. **39**(22): p. e155-e155.
[3] Atanasov, J., et al.. Nucleic Acids Research, 2017. **45**(22): p. e181-e181.

S01-04

Structural basis of modulation of host protein synthesis by a virus: The SARS-CoV macrodomain II binds human Paip1

J. Lei[1], Y. Ma-Lauer[2], A. von Brunn[2], R. Hilgenfeld[1]
[1]University of Lübeck, Institute of Biochemistry, Lübeck, Germany
[2]Ludwig-Maximilians-Universität München, Max-von-Pettenkofer Institute, München, Germany

Introduction

Coronaviruses (CoVs) possess the largest genome of all currently known RNA viruses. CoVs infect humans or other mammals, leading to respiratory or enteric diseases. In particular, two human CoVs, severe acute respiratory syndrome CoV (SARS-CoV) and Middle-East respiratory syndrome CoV (MERS-CoV), cause severe pneumonia, with high case/fatality rates (~10% during the SARS-CoV outbreak of 2003 and ~35% during the ongoing MERS-CoV epidemic (www.who.int; last accessed on December 13, 2017)). Many antiviral targets of these two CoVs (such as the main protease (or 3C-like protease) and the papain-like protease) have been used for inhibitor design. However, none of the lead compounds discovered has yet been turned into a clinically approved drug. Therefore, specific interactions between viral proteins and host components would be of high interest, but because of structures of such complexes are extremely scarce, the development of antiviral approaches targeting such interactions is seriously hampered.

Objectives

Coronavirus-host interactions play essential roles in the whole virus life cycle - virus entry, replication and transcription, assembly and release as well as interference with host innate immunity. The goal of the present project is to identify and characterize novel virus-host interactions as a valuable strategy to find new antiviral targets.

Results

Using the SARS-CoV unique domain (SUD) as a bait, we performed a high-throughput yeast-two-hybrid screen of the human proteome. We found that poly(A)-binding protein (PABP)-interacting protein 1 (Paip1), a factor of the host translation machinery, interacts with SUD. Furthermore, we discovered that the N-terminal subdomain of SUD (SUD-N, now called "macrodomain II" (Mac2)) is responsible for binding Paip1. A crystal structure of Mac2 in complex with the middle domain of Paip1 (Paip1M) was determined. We confirmed by SAXS that the complex has the same overall structure. Interestingly, SUD enhances the interaction between PABP and Paip1, thereby indicating a possible novel mechanism by which SARS-CoV may regulate the host translation machinery. The SUD-Paip1 interaction can potentially be used as a new antiviral target.

Conclusions

1) The SARS-CoV SUD domain binds human Paip1 *in vitro* and *in vivo*; 2) The crystal structure of the viral macrodomain II in complex with Paip1M was determined; 3) SUD enhances the Paip1-PABP interaction.

S01-05

A family of unconventional deubiquitinases with modular chan specificity determinants

T. Hermanns[1], C. Pichlo[2], I. Woiwode[1], K. Klopffleisch[1], K. F. Witting[3], H. Ovaa[3], U. Baumann[2], K. Hofmann[1]
[1]Universität zu Köln, Institute for Genetic, Köln, Germany
[2]Universität zu Köln, Institut für Biochemie, Köln, Germany
[3]Leiden University Medical Center, Department of Chemical Immunology, Leiden, Netherlands

Deubiquitinating enzymes (DUBs) regulate ubiquitin signaling by trimming ubiquitin chains or removing ubiquitin from modified substrates. Similar activities exist for ubiquitin-related modifiers, although the enzymes involved are usually not related. Here, we report human ZUFSP and fission yeast Mug105 as founding members of a new DUB family different from the six known DUB classes. The crystal structure of human ZUFSP in covalent complex with propargylated ubiquitin shows that the new DUB family shares a fold with UFM1- and Atg8-specific proteases, but uses a different active site more similar to canonical DUB enzymes. ZUFSP family members differ widely in linkage specificity through differential use of modular ubiquitin-binding domains (UBDs). While the minimalistic Mug105 prefers K48 chains, ZUFSP uses multiple UBDs for its K63specific endo-DUB activity. K63-specificity, localization, and protein interaction network suggest a role for ZUFSP in DNA damage response.

S01-06

Structural basis for antibacterial peptide export by bacterial ABC transporters

K. Beis[1]
[1]Imperial College London, Life Sciences, London, United Kingdom

Bacteria under nutrient starvation produce antibacterial peptides, which target closely related species for survival, and can either be lytic or non-lytic. Lytic peptides disrupt the membrane that results in nutrient loss whereas non-lytic peptides hijack membrane bound receptors for internalisation. The lasso peptide MccJ25 is an interesting class of non-lytic peptide that can be used as novel antimicrobial. MccJ25 is also toxic to the producing bacteria, which utilise the ABC transporter McjD to transport it out of the cell and provide them with resistance. Once it has been secreted it hijacks the outer membrane siderophore receptor FhuA and inner membrane transporter SbmA for internalisation inside the target cell. Inside the cell it targets the RNA polymerase. We have determined the crystal structure of the ABC transporter McjD in distinct conformations (1, 2), apo inward-occluded and nucleotide-bound outward occluded. These conformations were further chatacterised by predictive cysteine cross-linking and PELDOR in *E. coli* membranes and bicelles, respectively, that have allowed us to refine the mechanism of antibacterial peptide ABC transporters. Our functional data in proteoliposomes show that MccJ25 is specific to McjD and not to other antibacterial peptides or drugs. We are also investigating which portion of the peptide is important for recognition by NMR and non-denaturing mass spectrometry. We have also determined the structure of the siderophore receptor FhuA in complex with MccJ25 (3). These data provide new avenues for the design of novel antibacterials to fight bacterial multidrug resistance.

References

[1] Bountra K, Hagelueken G, Choudhury HG, Corradi V, ElOmari K, Wagner A, Mathavan I, Zirah S, Wahlgren WY, Tieleman DP, Schiemann O, Rebuffat S, Beis K (2017) Structural basis for antibacterial peptide self-immunity by bacterial ABC transporters. EMBO J, 36, 3062-3079
[2] Choudhury H, Zhen T, Mathavan I, Li Y, Zhirah S, Iwata S, Severine S., Rebuffat S, van Veen H, Beis K (2014) An antibacterial peptide ABC transporter in a novel outward occluded state. PNAS 111, 9145-9150

[3] Mathavan I, Zhirah S, Mehmood S, Choudhury H, Goulard C., Li Y, Robinson CV, Rebuffat S, Beis K (2014) Structural basis for hijacking siderophore receptors by antimicrobial lasso peptides. Nature Chemical Biology 10: 340-342

Figure 1. Structure of the lasso peptide MccJ25 and ABC transporter McjD.

Figure 1

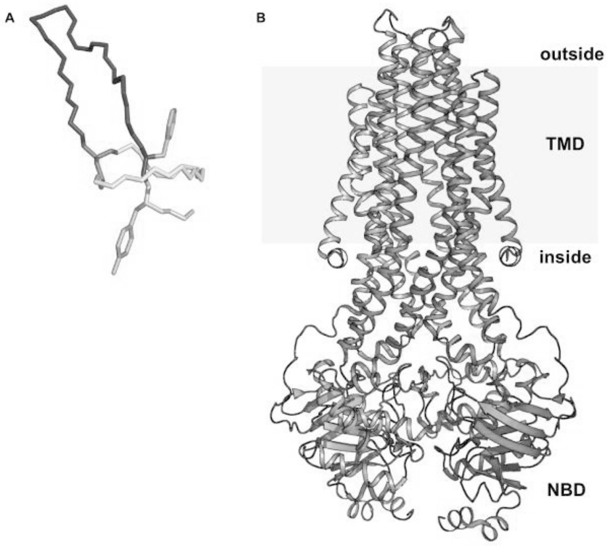

Measurements and syntheses under extreme conditions

S02-01

The crystal chemistry of calcite-type structure carbonates at extreme conditions

S. Chariton[1], E. Bykova[2], M. Bykov[1], V. Cerantola[3], G. Aprilis[4], C. McCammon[1], L. Dubrovinsky[1]
[1]University of Bayreuth, Bayerisches Geoinstitut, Bayreuth, Germany
[2]Deutsches Elektronen-Synchrotron DESY, Hamburg, Germany
[3]European Synchrotron Radiation Facility (ESRF), Grenoble, France
[4]University of Bayreuth, Bayreuth, Germany

There are compelling evidences that carbon and carbonates are present inside the Earth"s mantle and thus studies of carbonate minerals at high pressures and temperatures are important for the understanding of the carbon-related geological processes inside the Earth [1]. Recent discoveries of the high-pressure CO_4-containing carbonated phases, accompanied by novel oxide compounds, provide new insights in the most stable carbonate and carbon forms of the lower mantle, speculating its oxidation state, and further invite analogies to the SiO_4-metasilicates [2, 3]. Transition metals play a crucial role in the crystal chemistry of carbonates at such extreme conditions. Studying their structural and chemical stability can be useful when searching for systematics in their high pressure behavior with respect to the size of their cationic radius. Thus, we synthesized pure single crystals of various carbonates $(Fe,Mg,Mn,Co,Zn,Ni)CO_3$ and studied them by single-crystal X-ray diffraction and Raman spectroscopy in synchrotron (ESRF, DESY, APS) and in-house (BGI) facilities, respectively. Additionally, Fe-bearing samples were measured by Mössbauer spectroscopy (ESRF). High pressures were generated by diamond anvil cells, while high temperatures were obtained by utilizing a double-sided laser heating system. We first performed a compressibility study, and obtained the equations of state of six different compositions. We observed that carbonates, which incorporate metals with big cationic radii, such as Mn^{2+}, remain stable in the R-3c structure over a shorter pressure range, compared to carbonates with small cations, such as Zn^{2+}. After heating at various pressure points, carbonates decomposed to one or several phases. These phases were either known or novel metal oxides, such as the CoO (Fm-3m) at 56 GPa or the Mn_5O_7 (C2/m) at 66 GPa, respectively. On the other hand, we also found new or known high-pressure carbonate polymorphs with CO_3 or CO_4 units, such as the MnCO3-III ($P2_1/c$) at 66 GPa or the $(Fe, Mg)_3C_3O_9$ (C2/m) tetracarbonate at 95 GPa. We conclude that carbonates are important players in the geochemical processes and their high-pressure behavior is interesting from the point of view of fundamental crystal chemistry and solid-state physics, and thus experiments continue.

References

[1] Dasgupta & Hirschmann (2010), EPSL, 298, 1-13
[2] Cerantola et al. (2017), Nat Commun, 8, 15960
[3] Merlini et al. (2015), Am Min, 100, 2001-2004

S02-02

Pressure-induced spin transitions in garnets at 45-70 GPa

A. Friedrich[1,2], M. Koch-Müller[3], I. Efthymiopoulos[3], W. Morgenroth[2], J. Cott[4], R. Wentzcovitch[5]
[1]Julius-Maximilians-Universität Würzburg, Institut für Anorganische Chemie, Würzburg, Germany
[2]Goethe-Universität Frankfurt am Main, Institut für Geowissenschaften, Frankfurt am Main, Germany
[3]GFZ Potsdam, Potsdam, Germany
[4]University of Minnesota, Department of Chemical Engineering and Materials Science, Minneapolis, United States
[5]Columbia University, Department of Applied Physics and Applied Mathematics, New York, United States

The importance of garnets within the Earth"s mantle, the high symmetry of the garnet structure (space group *Ia*-3*d*), and the manifold cation and anion substitution mechanisms make garnets an ideal model system to study pressure-induced spin-pairing transitions of 3*d*-transition-metal cations. We have already reported on pressure-induced spin-pairing transitions in cubic andradite, $Ca_3Fe_2[SiO_4]_3$ (for Fe^{3+}) and tetragonal henritermierite, $Ca_3Mn_2[SiO_4]_2[O_4H_4]$ (for Mn^{3+}) [1,2], which occur in the pressure range of 55-70 GPa. In this study we will present our results on the high-pressure structural compression and spin transitions of OH-free manganese garnets $Ca_3Mn_2[SiO_4]_3$ and blythite, $Mn_3Mn_2[SiO_4]_3$ up to 73 GPa from experiment and theoretical calculations based on density functional theory.

$Ca_3Mn_2[SiO_4]_3$ and $Mn_3Mn_2[SiO_4]_3$ single crystals were synthesized at high pressure and temperature in a multi-anvil press and subsequently pressurized in diamond anvil cells for single-crystal X-ray diffraction data collections at the PETRA III synchrotron facility (beamline P02.2, DESY, Hamburg, Germany) and for Raman spectroscopy measurements.

While the unit-cell compression does not show a distinct discontinuity at high pressure, the compression of the MnO_6-octahedra clearly shows a pronounced compression at about 45-65 GPa in both compounds, which can be related to the occurrence of a spin-pairing transition in Mn^{3+}. The spin transition is also apparent in the discontinuous pressure shifts of Raman modes and confirmed by our theoretical calculations. Results will be discussed with respect to our recent data on andradite and henritermierite [1,2].

Financial support from the DFG, Germany (Fr2491/2-1), the BMBF, Germany (05K13RF1), Goethe University Frankfurt, and University of Würzburg is gratefully acknowledged. Portions of this research were carried out at PETRA III (DESY), a member of the Helmholtz Association. We thank H.-P. Liermann for support.

References

[1] A. Friedrich, B. Winkler, W. Morgenroth, J. Ruiz-Fuertes, M. Koch-Müller, D. Rhede, V. Milman. *Phys. Rev. B* 2014, **90**, 094105
[2] A. Friedrich, B. Winkler, W. Morgenroth, A. Perlov, V. Milman. *Phys. Rev. B* 2015, **92**, 014117

S02-03

In situ X-ray diffraction studies on tournalines at high pressures and temperature

K. D. Grevel[1], B. Marler[2], A. Ertl[3], C. Lathe[4]
[1]Friedrich Schiller Universität Jena, Institut für Geowissenschaften, Jena, Germany
[2]Ruhr-Universität Bochum, Institut für Geologie, Mineralogie und Geophysik, Bochum, Germany
[3]Universität Wien, Institut für Mineralogie und Kristallographie, Wien, Austria
[4]Helmholtz Centre Potsdam – GFZ German Research Centre for Geosciences, Potsdam, Germany

Tourmaline-supergroup minerals are ubiquitous accessory minerals in rocks of the Earth"s crust with the general formula: $X\ Y_3\ Z_6\ [T_6\ O_{18}]\ (BO_3)_3\ V_3W$; X = o (vacancy), Na, K, Ca, Pb^{2+}; Y = Li, Mg, Fe^{2+}, Mn^{2+}, Cu^{2+}, Al, Fe^{3+}, V^{3+}, Cr^{3+}, Mn^{3+}, Ti^{4+}; Z = Mg, Fe^{2+}, Al, V^{3+}, Cr^{3+}, Fe^{3+}; T = Si, B, Al; V = O, OH; W = O, OH, F [1]. Although tourmaline is stable over a wide pressure-temperature (*P-T*) interval, data describing its volumetric behaviour at elevated *T* and *P* are almost not available.

In this study, the *P-V-T* behaviour of synthetic Al-rich (olenitic) tourmaline was investigated. Additionally, the bulk moduli of two natural samples, a blue dravite from Koksha Valley, Afghanistan and the elbaitic rim of a colour-zoned tourmaline crystal (sample HIM5) from the Himalaya Mine, California are reported.

The volumetric behaviour of all samples has been determined by in situ X-ray diffraction up to 8.5 GPa and 700°C for olenite respectively 5.5 GPa for the natural samples using a MAX 80 cubic anvil high-pressure apparatus (DESY, HASYLAB, Hamburg, Doris III, Beamline F.2.1). The powdered samples were mixed with Vaseline as pressure medium to ensure hydrostatic pressure transmitting conditions. NaCl served as a diffraction standard to define the pressure. Energy dispersive diffraction patterns were collected at a fixed 2θ angle ($\theta \approx 3.67°$).

By fitting a third-order Birch-Murnaghan EOS to the data, the bulk modulus of olenite was determined as 91.18 ± 4.84 GPa, ($K' = 4$), $V_{T,0} = (1484.93 \pm 3.79)$ Å^3 $\exp\ [\int(0.137 \pm 0.090) \times 10^{-4}\ dT]$, $(\partial K_T/\partial T)_P = 0.023 \pm 0.017$ GPa K^{-1}. The fit is improved if K' is taken as a variable, but results in a negative value for K' which suggests the olenite might be heading for a structural phase transition.

The bulk moduli of dravite and elbaite were determined as 119.5 ± 4.8 GPa, respectively 115.7 ± 2.6 GPa, ($K' = 4$).

Recently, Xu et al. (2016) [2] conducted in situ X-ray diffraction experiments on a natural tourmaline sample by using an externally heated diamond anvil cell up to 18 GPa and 450 °C. Based on electron microprobe analyses, they stated this tourmaline sample to be uvite-dominated. In contrast, they indexed their spectra following JCPDS card 71-0716, which belongs to an elbaite-dominated tourmaline with significantly smaller cell parameters. Their reported volumes are very similar to the elbaite volumes obtained in this study (Fig. 1).

References

[1] Henry DJ et al. (2011) *Am. Min.* **96**, 895
[2] Xu J et al. (2016) *Phys. Chem. Min.* 43, 315

Figure 1

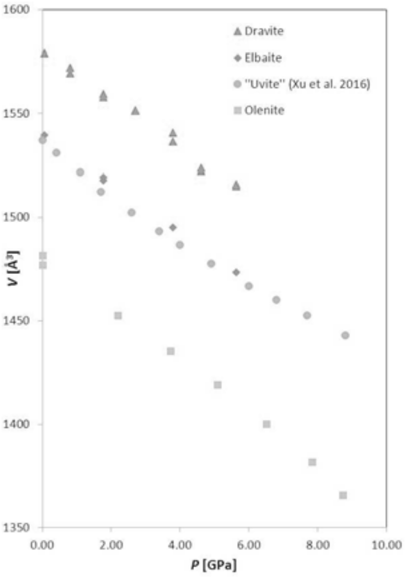

Fig. 1: *P-V* data for olenite, dravite, and elbaite [this study] and for uvite [2].

S02-04

New insights on the high pressure behaviour of the $GeSe_xTe_{1-x}$ solid solution

M. Herrmann[1], R. Stoffel[2], M. Küpers[2], M. Ait Haddouch[1], A. Eich[3], K. Glazyrin[4], A. Grzechnik[3], K. Friese[1]
[1]Forschungszentrum Jülich GmbH, JCNS-2, Jülich, Germany
[2]RWTH Aachen, Institute of Inorganic Chemistry, Aachen, Germany
[3]RWTH Aachen, Institute of Crystallography, Aachen, Germany
[4]Deutsches Elektronen-Synchrotron DESY, P02.2 ECB, Hamburg, Germany

The high pressure behaviour of GeTe was studied previously [1,2] and the results revealed contradicting results. The high pressure behaviour of the $GeSe_xTe_{1-x}$ solid solution is less known. High pressure experiments on powder of $GeSe_xTe_{1-x}$ (x=0, 0.2, 0.5, 0.75) compounds were performed on the beamline P02.2 at DESY. We aimed a) to improve the understanding of the high pressure behaviour of GeTe and b) to study the influence of Se on the stability fields of the observed phases.

At ambient conditions GeTe-I crystallizes in a rhombohedral structure (*R3m*) [1]. The high temperature and ambient pressure phase diagram of the $GeSe_xTe_{1-x}$ solid solution was determined previously [3]. While mixed crystals with $0<x<0.52$ are isostructural to GeTe-I, a hexagonal phase (*P63mc* [4]) was found for $0.58<x<0.85$ [3]. Mixed crystals with $x>0.95$ are isostructural to GeSe [3].

Figure 1 shows the results of our study. For GeTe, $GeSe_{0.2}Te_{0.8}$ and $GeSe_{0.5}Te_{0.5}$ we found a phase transition from GeTe-I into the FCC structure of GeTe-II. At higher pressure we found a mixture of the FCC and an additional phase. Indexing of our high pressure data using the published *Pbnm* and *Pbcn* structure of GeTe-III failed. In the high pressure experiment on GeTe the pattern of a single crystal was visible and we have indexed the corresponding reflections with an orthorhombic lattice. First attempts to solve the structure of GeTe-III indicate a structure similar to the one published by [2], although the obtained lattice parameter seem to have a close relation with the cell reported by [1]. By using the lattice parameter obtained from the single crystal of GeTe-III, we have refined all high pressure data collected for $GeSe_{0.2}Te_{0.8}$ and $GeSe_{0.5}Te_{0.5}$. $GeSe_{0.75}Se_{0.25}$ is stable up to at least 36 GPa.

Fig. 1.: High pressure phase diagram of the $GeSe_xTe_{1-x}$ solid solution between 0-25 GPa . The *Pbnm* phase corresponds to our GeTe-III structure.

We have studied the influence of high pressure on the rhombohedral and hexagonal phase of the $GeSe_xTe_{1-x}$ solid solution. For rhombohedral $GeSe_xTe_{1-x}$ three phases are present between 0-25 GPa. We have shown how Se influences the stability fields of these phases. We are currently working on the determination of the structure of GeTe-III.

References
[1] Onodera, et al., Phys. Rev. B, 56:7635-41, (1997)
[2] Serebryanaya, et al., Phys. Lett. A, 197:63-66, (1995)
[3] Wiedemeier, et al., High Temp. Sci., 17:395-408, (1984)
[4] Küpers, et al., Angew. Chem. 56:10204, (2017)

Figure 2

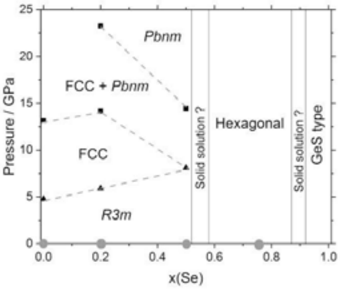

S02-05

A new high-pressure and high-temperature polymorph of $FeCO_3$

C. J. Fruhner[1], L. Bayarjargal[1], D. Zimmer[1], R. Luchitskaia[1], E. Bykova[2], W. Morgenroth[1], B. Winkler[1]
[1]Goethe-Universität Frankfurt am Main, Institut für Geowissenschaften, Frankfurt am Main, Germany
[2]Deutsches Elektronen-Synchrotron DESY, P02.2 Extreme Conditions Beamline, Hamburg, Germany

Carbonate inclusions in diamonds are an evidence for the existence of carbonates in the Earths lower mantle [1]. Siderite is one potential carbon carrier in subduction zones [2]. However, the properties, phase stabilities and crystal structures of carbonates under extreme conditions are poorly understood. In this study we investigated the behavior of Europium doped siderite at high pressure and temperature.

High-pressure experiments were carried out in laser-heated diamond anvil cells (LH-DAC). DACs were loaded with Eu-doped siderite, ruby chips for pressure determination, potassium chloride for thermal insulation and argon as pressure transmitting medium. For laser heating a double sided fiber laser was used. XRD data was recorded prior, during and after LH at the extreme conditions beamline P02.2 at PETRA III [3].

After laser heating of the samples at 18.5 GPa and 2000 K we observed appearance of new reflections on the diffraction frames. Using single-crystal X-ray diffraction data we could identify several grains of a new hexagonal phase with unit cell parameters: a = 4.5912(2), c = 7.1636(2) (based on the procedure described by Bykova in [4]). Figure 1 shows the crystal structure of the $FeCO_3$ polymorph. The difference between siderite and the new polymorph is a 60° rotation of the CO3-groups in every second layer. DFT calculations are in good agreement with our data.

Fig 1. Structural representations along c-axis. Left: new polymorph of $FeCO_3$, Right: Siderite structure

The relation between the structures of the two $FeCO_3$ polymorphs resembles that between $CaCO_3$-IV and $CaCO_3$-V [5]. The relative arrangement of the carbonate groups is the same. Our DFT model calculations support our structure model.

Financial support from the DFG grant BA4020/2-1 (within in the DFG research unit FOR 2125 "CarboPaT") is gratefully acknowledged.

References
[1] F. E. Brenker *et al., Earth and Planetary Science Letters*, **260**, 1–9 (2007).
[2] V. Cerantola et al., *Nature Comm.* **8** 15960 (2017).
[3] H. P. Liermann *et al., Journal of synchrotron radiation*, **22**, pp. 908–924 (2015).
[4] E. Bykova Dissertation, Universität Bayreuth (2015).
[5] S. A. T. Redfern et al., *Contr. Mineral. and Petrol.* **101**, 479–484 (1989).

Figure 1

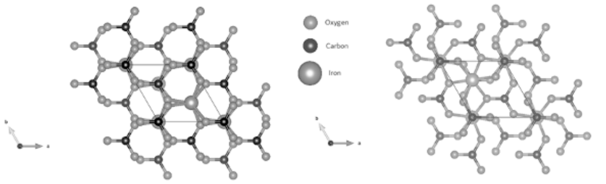

S02-06

Using Raman scattering to measure strains in crystals under non-hydrostatic stress conditions

R. Angel[1], M. Murri[1], M. Mazzucchelli[1], M. Prencipe[2], B. Mihailova[3], M. Alvaro[1]
[1]University of Pavia, Earth and Environmental Sciences, Pavia, Italy
[2]University of Torino, Dept. Earth Sciences, Torino, Italy
[3]Universität Hamburg, Dept. Earth Sciences, Hamburg, Germany

The majority of in-situ high-pressure crystallographic studies aim to understand the behavior of crystals under hydrostatic pressure by immersing the sample in a fluid pressure medium. Deviatoric stress states are avoided because they are very difficult to characterise. In single-crystal high-pressure diffraction studies the stress can be calculated by measuring the unit-cell parameters and calculating the strains relative to hydrostatic conditions, from which the stress state can be determined from the elastic tensor of the crystal at high pressure [1].

If the sample crystals are small, then precise measurements of cell parameters can be challenging. Raman spectroscopy provides an alternative method of measuring strains eij because the shifts of band positions, Δw, are determined by the Grüneisen tensor γ by $\Delta w/w = -\gamma : e$ [2]. But determination of the components of γ requires measurements under carefully-characterised deviatoric strain states! To solve this conundrum, we have performed ab-initio HF/DFT (Hartree-Fock/Density Functional Theory) calculations to determine the crystal structure, lattice parameters and Raman shifts of quartz, as a test case, under various strain states (e11= e22 ≠ e33) that preserve the trigonal symmetry. For most modes the lines of constant Raman shift are neither parallel to isochors nor to lines of constant mean normal stress, showing the Raman shift of single mode cannot be used to determine the mean stress state of a quartz crystal under non-hydrostatic stress. For small strains (up to 2% linear) the Raman shifts of most modes are linear in the strains, and can be used to determine the two symmetry-independent components γ11 (= γ22) and γ33 of the Grüneisen tensor of quartz. These reproduce the experimentally-observed shifts in Raman modes of quartz under hydrostatic stress and the limited data with deviatoric stress. In-situ diffraction and Raman measurements of quartz crystals trapped inside cubic garnets as inclusions are under way to provide further validation of the DFT results. Once validated, the measurement of several Raman lines of quartz will allow the determination of the strain state of crystals under any conditions of strain.

This work has been supported by ERC-StG TRUE DEPTHS (grant number 714936) and MIUR-SIR Mile Deep (grant number RBSI140351) to M. Alvaro

References
[1] Zhao et al. (2010) Journal of Applied Crystallography 43:743-751.
[2] Key (1967) Journal of Applied Physics 38:2923-2928.

New crystal structures I

S03-01

Polymorphism and Isomerism in Coordination Compounds: The Nemesis of Crystal Design

C. Näther[1], T. Neumann[1], A. Jochim[1], C. Wellm[1], I. Jess[1], M. Rams[2], Z. Tomkowicz[2], L. S. Germann[3], R. E. Dinnebier[3]
[1]Christian-Albrechts Universität zu Kiel, Institut für Anorganische Chemie, Kiel, Germany
[2]University of Krakow, Institute of Physics, Krakow, Germany
[3]Max-Planck-Institut für Festkörperforschung, X-ray diffraction, Stuttgart, Germany

The development of strategies for a rational synthesis of coordination compounds is still a major field in coordination chemistry because if one have no control over the structure one have also no control over the properties of such compounds. Moreover, for any physical characterization pure amounts of the compounds are required, which is sometimes difficult to achieve. In most cases coordination compounds are prepared from solution where different species are in equilibria and therefore, crystallization can lead to mixtures of compounds, polymorphs or isomers. Some other compounds might be thermodynamically metastable and thus, can be easily overlooked.

This lecture will give a brief introduction into this topic, which includes some basics on the thermodynamic and kinetic aspects and on the transition behavior of polymorphs or isomers. Several examples are shown, where different metastable compounds, isomers or polymorphic modifications of "simple" luminescent or magnetic coordination compounds were obtained. It is shown how metastable coordination compounds can selectively be prepared by, e.g., thermal decomposition of suitable precursor compounds.

Unfortunately, because coordination compounds usually do not melt and decompose before they transform, the experimental possibilities for their investigations are limited. Nevertheless, some examples will be presented how to prove which of the different forms are thermodynamically stable or metastable and how these forms can be transformed into each other. However, even if all these phenomena can limit a structure prediction they are very useful for the investigation of structure property relationships, because the chemical composition is identical and all changes in the physical properties can be traced back to differences in the crystal structures. Representative examples supporting these facts were given using coordination polymers that show cooperative magnetic phenomena including single chain magnetism.

References

[1] J. Werner, M. Rams, Z. Tomkowicz, T. Runčevski, R. Dinnebier, S. Suckert, C. Näther, Inorg. Chem., **2015**, 54, 2893.

[2] S. Suckert, M. Rams, L. Germann, R. Dinnebier, C. Näther, Cryst. Growth. Des. **2017**, 17, 3997.

[3] S. Suckert, M. Rams, M. Böhme, L. Germann, R. Dinnebier, W. Plass, J. Werner, C. Näther, Dalton Trans., **2016**, 45, 18190.

[4] M Rams, Z. Tomkowicz, M. Böhme, W. Plass, S. Suckert, J.Werner, I. Jess, C. Näther, Phys. Chem. Chem. Phys., **2017**, 19, 3232.

S03-02

From Giant Supramolecules to Coordination Polymers with Supramolecules as Nodes

A. Virovets[1], E. Peresypkina[1], B. Krämer[1], M. Scheer[1]
[1]Universität Regensburg, Institut für Anorganische Chemie, Regensburg, Germany

Since 2003 [1], we have been investigating pentaphosphaferrocene $[Cp^RFe(\eta^5\text{-}P_5)]$ ($Cp^R = \eta^5\text{-}C_5R_5$, R = Me, CH_2Ph, PhC_4H_9) in supramolecular chemistry. The phosphorus atoms of the planar P_5-rings coordinate to Cu^+ and Ag^+ cations resulting in self-assembled spherical supramolecules of 2.1 – 4.6 nm in diameter [1-4]. Due to possessing fullerene or fullerene-like topologies, the central metallophosphorus core is sometimes able to encapsulate various guest molecules [2, 3].

A new direction of our research is to connect giant supramolecules to form coordination polymers by using flexible bitopic linkers $N{\equiv}C(CH_2)_nC{\equiv}N$ (L^n, n = 5-10). The coordination of Ag^+ cations to the P_5-rings results in the in situ formation of supramolecules, while the additional coordination of Ag^+ to N-donor atoms of L^n in turn leads to 1D, 2D and 3D coordination polymers in one-pot reactions. The composition and structure of the supramolecules as well as the dimensionality of the polymer can be controlled by changing the reaction stoichiometry or by adding the guest molecules as e.g. white phosphorus, P_4 (Fig. 1a).

In addition to the usual methodological problems as for instance difficulties in the crystallization or the presence of a severe crystallographic disorder, the structural studies are occasionally encumbered by the appearance of modulated or incommensurate structures. Depending on experimental conditions, e.g. $[(Cp^*FeP_5)_{12}Ag_{12}L^{10}{}_6](SbF_6)_{12}$, can crystallize in two different monoclinic unit cells with $a_2{=}a_1$, $b_2{=}b_1$, $c_2{=}3c_1$ and $\beta_2{=}\ \beta_1$ (Fig. 1b,c). The superstructural phase shows additional pseudo-$P2_1/n$ symmetry, whereas the true space group is $P2_1$.

Fig. 1. *a*) inclusion of P_4 molecule into $[Ag_9(Cp^*FeP_5)_9]^{9+}$ cage. Fe atoms, Cp* ligands and CH_2 groups are omitted; *b*) 3D coordination polymer $[(Cp^*FeP_5)_{12}Ag_{12}L^{10}{}_6](SbF_6)_{12}$, Fe atoms, Cp* ligands and counteranions are omitted; *c*) reciprocal space with superstructural reflections along *c** axis.

Financial support from the ERC grant ADG 339072 is gratefully acknowledged. The research was partly done at the light source PETRA III at DESY.

References

[1] J. Bai, A. Virovets, M. Scheer (2003), *Science*, **300**, 781

[2] E. Peresypkina, C. Heindl, A. Virovets, M. Scheer (2016) *Structure and Bonding* (2016) **174**, 321

[3] F. Dielmann, M. Fleischmann, C. Heindl et al (2015) *Chem.-A Eur. J.*, **21**, 6208

[4] C. Heindl, E.V. Peresypkina, A.V. Virovets et al (2017) *Angew. Chem. Int. Ed.* **56**, 13237

Figure 1

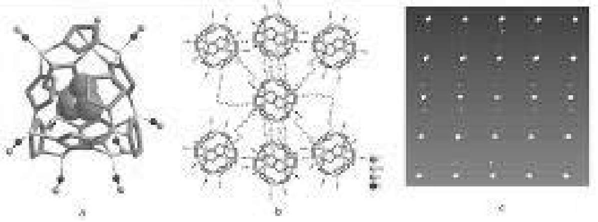

S03-03

New data on incorporation of rare-earth elements into uranyl layers: synthesis and crystal structures of novel praseodymium(III) compounds

T. Spano[1], S. Aksenov[1], M. Turner[1], P. Burns[1]
[1]University of Notre Dame, Department of Civil and Environmental Engineering & Earth Sciences, South Bend, United States

Praseodymium analogues of protasite $Ba[(UO_2)_3O_2(OH)_2]\cdot 4(H_2O)$ and carnotite $K_2[(UO_2)_2(VO_4)_2]\cdot 3H_2O$ have been synthesized by mild hydrothermal reactions at 170°C for 120 hours. Reagents were combined in approximate 1:1:1, 1:1:2, or 2:2:1 molar ratios of U:V:Pr. The initial pH of the reactions were adjusted from ~3.7 to the desired value by the drop-wise addition of 0.5 M NH_4OH.

Raman spectroscopy shows that at low pH, the 1:1:1 and 1:1:2 U:V:Pr systems are dominated by formation a carnotite-like, whereas at pH > 7, the 1:1:1 U:V:Pr system also crystallizes the protasite-like phase. Across the range of pH values in this study, the 2:2:1 U:V:Pr system, the uranyl vanadate species remains the dominant phase.

Crystals of novel phases praseodymium uranyl hydroxide hydrate (**PrUOH**) and praseodymium uranyl vanadate (**PrUV**) have been studied by single crystal X-ray analysis. Unit-cell parameters are: a = 6.7956(8) Å, b = 11.871(1) Å, c = 6.8861(8) Å, V = 555.52(11) Å^3, sp. gr. $Pnm2_1$ for **PrUOH**; a = 9.707(4) Å, b = 10.542(4) Å, c = 24.818(10) Å, β = 98.405(5)°, V = 2512(3) Å^3, sp. gr. $P2_1/n$ for **PrUV**. Crystal structures refined to final R_1 = 3.29 for **PrUOH**, and R_1 = 6.62 for **PrUV**.

Crystal chemical formulas can be written as: $Pr_{1.35}[(UO_2)_3O_2(O,OH)_3](OH,H_2O)_3$ (Z = 2) for **PrUOH** and $Pr_{0.66}[(UO_2)_2(V_2O_8)]\cdot 6H_2O$ (Z = 6) for **PrUV**. Crystal structure of studied compounds are based on uranyl layers with protasite (**PrUOH**) and francevillite (**PrUV**) anion-type topology which are intercalated by Pr^{3+}-ions which partly occupy large $PrØ_{9\text{-}10}$-polyhedra (Ø = O, H_2O) and water molecules.

Our new data are in a good agreement with previous work where Ln^{3+}-ions were incorporated into uranyl layers and frameworks. Incorporation of Ln in secondary U(VI)-minerals has important implications for the behavior of minor actinides such as Am^{3+} and Cm^{3+} upon corrosion of used nuclear fuel as Ln^{3+} are important analogues for the minor An^{3+} resulting from nearly identical ionic radii radii (Choppin, 1983; Cotton, 2013; Krauskopf, 1986; Wang et al., 2015). Furthermore, we found, that over a range of conditions, **PrUOH** and **PrUV** are crystallized simultaneously thus indicating potential paragenetic relationships between these minerals in natural systems.

References

[1] Choppin, G.R. (1983) J. Less Common Metals, 93(2), 323-330.
[2] Cotton, S. (2013) Lanthanide and actinide chemistry. John Wiley & Sons.
[3] Krauskopf, K.B. (1986) Chem. Geol. 55(3), 323-335.
[4] Wang, Y. et al. (2015) Inorg. Chem. 54(17), 8449-8455.

S03-04

High-Pressure Synthesis of the New Binary Superconductor Lutetium trigermanide $LuGe_3$

J. M. Hübner[1], M. Bobnar[1], Y. Prots[1], U. Schwarz[1]
[1]Max Planck Institute for Chemical Physics of Solids, Chemical Metals Science, Dresden, Germany

Silicon and germanium form various binary compounds with alkaline-, alkaline earth- and rare earth metals at ambient conditions. The application of high-pressure methods to such binary system enabled the synthesis of numerous new modifications and new phases. These compounds exhibit both covalent and ionic interactions and a large fraction follows the Zintl-Klemm concept [1].

Various rare earth-tetrel compounds of the structure MTt_3 (M = Y, La, Eu, Ho, Yb, Lu; Tt = Si, Ge) exist. Some of them possess interesting physical properties, such as superconductivity [2-7]. No phases with a 1:3 composition are known for the system Lu-Ge, but the analogue $LuSi_3$ has been described [6].
In this study, we focused on reactions of the system Lu-Ge with a 1:3 composition.

The new metastable binary compounds $LuGe_3$ has been synthesized under high-pressure, high-temperature conditions at pressures between 8(1) and 14(2) GPa and temperatures in the range of 1100(150) to 1500(150) K.

$LuGe_3$ crystalizes in the $DyGe_3$-type structure (space group Cmcm, a = 3.97541(3) Å, b = 20.3768(2) Å and c = 3.86957(3) Å, without standard). The lattice parameters and magnetic properties were determined. The compound $LuGe_3$ exhibits superconductivity below 4 K.

Examinations of the analogue Ba-Si system with a 1:3 composition indicate the new barium silicide $BaSi_3$ with a $CaGe_3$-type structure (space group I4/mmm).

References

[1] Demchyna, R.; Leoni, S.; Rosner, H.; Schwarz, U. *Z. Kristallogr.* **2006**, 221, 420-434
[2] Fukuoka, H.; Suekuni, K.; Onimaru, T.; Inumaru, K. *Inorg. Chem.* **2011**, 50, 3901-3906
[3] Meier, K.; Cardoso-Gil, R.; Schwarz, U. *Z. Kristallogr.* **2011**, 226, 297-298
[4] Wosylus, A.; Prots, Yu.; Schwarz, U. *Z. Kristallogr. NCS* **2011**, 226, 295-296
[5] Harada, M.; Fukuoka, H.; Matsumura, D.; Inumaru, K. *J. Phys. Chem. C* **2012**, 116, 2153-2158
[6] Schwarz, U.; Wosylus, A.; Rosner, H.; Schnelle, W.; Ormeci, A.; Meier, K; Baranov, A.; Nicklas, M.; Leipe, S.; Müller, C.J.; Grin, Yu. *J. Am. Chem. Soc.* **2012**, 134, 13558-13561
[7] Castillo, R.; Baranov, A.; Burkhardt, U.; Grin, Yu; Schwarz, U. *Z. Anorg. Allg. Chem.* **2015**, 641(2), 355-361

Acknowledgments: Support in the preparation by Liudmila Muzica and Nina Straßner is gratefully acknowledged.

S03-05

Polyanions with covalent Si-H, Ge-H and Sn-H bonds in Zintl-phase hydrides

H. Auer[1], R. Guehne[2], M. Bertmer[2], J. Haase[2], H. Kohlmann[1]
[1]Leipzig University, Inorganic Chemistry, Leipzig, Germany
[2]Leipzig University, Felix Block Institute for Solid State Physics, Leipzig, Germany

Zintl phase hydrides gained interest when the first polyanionic hydrides were discovered in 2000. The hydrides show typically two different binding modes: (i) an ionic hydride, that occupies voids of the cationic partial structure or (ii) hydrogen covalently bound to the polyanionic framework (as review see [1]).

Polyanions with group 14 element (tetrel)-hydrogen bonds are rare. A covalent Si-H bond is controversially discussed for $CaSiH_{4/3-x}$ [2,3]. We recently completed the homologue series $AeTtH_y$ (Ae = Ca-Ba, Tt = Si-Sn, 1< y < 2) and described the structures in three related structure types [4,5]. The structures are characterised by hydrogen filled Ae_4-tetrahedra and three-binding tetrel atoms that have two tetrel neighbours forming a zigzag chain. The chain atoms are either saturated by an additional hydrogen atom, or by an additional Tt-Tt bond connecting two chains perpendicular to the chain direction. This leads to three different obtained structural motifs: (i) a single chain, $^1_\infty[TtH^-]$, (ii) two connected chains, $^1_\infty[Tt_2H^{2-}]$ and (iii) three connected chains, $^1_\infty[Tt_3H^{3-}]$. The Tt-H distance clearly indicates a covalent interaction, but there are some inconsistencies within the row of equal group 14 elements (Tab. 1). Furthermore the compounds are non-stoichiometric. The polyanion binding hydrogen site is underoccupied, which can be compensated by π-bonding within the polyanion as shown for the hydrogen free phases [6]. Thus, Rietveld refinement as bulk technique shows only an average position of the tetrel-atom either bound to hydrogen or coordinated by a void. Solid state nuclear magnetic resonance (SSNMR) was applied as a local probe. The magnitude of the quadrupole interaction (C_Q) of deuterium was determined. Under the aid of DFT calculations of idealised, stoichiometric compounds proper bond lengths can be established which are almost equal for like tetrel atoms (Tab. 1). Thus, the quadrupole splitting is a reliable probe for determining Tt-D distances and complement structural studies.

References

[1] U. Häussermann *et al.*, *Struc. Bond.* **2010**, *139*, 143-161.
[2] N. Ohba *et al.*, *Phys. Rev. B* **2005**, *72*, 075104.
[3] H. Wu *et al.*, *Phys. Rev. B* **2006**, *74*, 224101.
[4] H. Auer *et al.*, *Inorg. Chem.* **2017**, *56*, 1061-1071.
[5] H. Auer *et al.*, *Angew. Chem., Int. Ed.* **2017**, *56*, 12344-12347.
[6] I. M. Kurylyshyn *et al.*, *Angew. Chem., Int. Ed.* **2014**, *53*, 3029-3032.

Figure 1

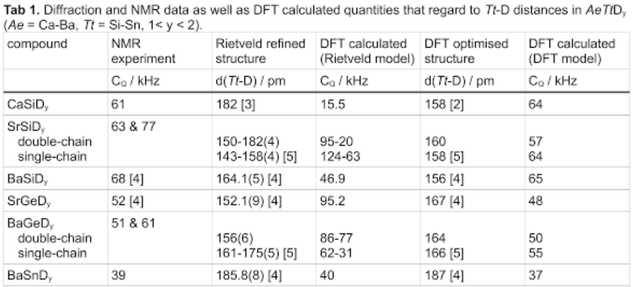

Tab 1. Diffraction and NMR data as well as DFT calculated quantities that regard to *Tt*-D distances in $AeTtD_y$ (Ae = Ca-Ba, Tt = Si-Sn, 1< y < 2).

compound	NMR experiment	Rietveld refined structure	DFT calculated (Rietveld model)	DFT optimised structure	DFT calculated (DFT model)
	C_Q / kHz	d(*Tt*-D) / pm	C_Q / kHz	d(*Tt*-D) / pm	C_Q / kHz
$CaSiD_y$	61	182 [3]	15.5	158 [2]	64
$SrSiD_y$	63 & 77				
double-chain		150-182(4)	95-20	160	57
single-chain		143-158(4) [5]	124-63	158 [5]	64
$BaSiD_y$	68 [4]	164.1(5) [4]	46.9	156 [4]	65
$SrGeD_y$	52 [4]	152.1(9) [4]	95.2	167 [4]	48
$BaGeD_y$	51 & 61				
double-chain		156(6)	86-77	164	50
single-chain		161-175(5) [5]	62-31	166 [5]	55
$BaSnD_y$	39	185.8(8) [4]	40	187 [4]	37

New developments in methods and instrumentation in neutron scattering

S04-01

Energy Research with Neutrons (ERWIN) and installation of a Neutron Powder Diffraction Option at MLZ

M. Heere[1]
[1]KIT/ FRM2, Garching bei München, Germany

The need for rapid data collection and studies of small sample volumes in the range of mm3 are the main driving force for the concept of a high-throughput monochromatic diffraction instrument at the Heinz Maier-Leibnitz Zentrum (MLZ). A large section of reciprocal space will be addressed with sufficient dynamic range and µs time-resolution while allowing for a variety of complementary sample environments. The medium-resolution neutron powder diffraction (NPD) option for "**E**nergy **R**esearch **Wi**th **N**eutrons" (ERWIN) at the research reactor Munich is foreseen to meet future demand. ERWIN will especially be suited for addressing structural studies and its uniformity of energy-related systems and materials by using simultaneous bulk/spatially resolved NPD. A set of useful experimental options will be implemented enabling time-resolved studies, rapid parametric measurements as a function of external parameters or studies of small samples using an adapted radial collimator. The proposed powder diffraction option ERWIN will bridge the gap in functionality between the high-resolution powder diffractometer SPODI and the time-of-flight diffractometers POWTEX and SAPHIR.

S04-04

Structure analysis with hot neutrons and under extreme conditions on HEIDI

M. Meven[1,2], A. Sazonov[1,2], G. Roth[1]
[1]RWTH Aachen, Institute of Crystallography, Aachen, Germany
[2]Forschungszentrum Jülich GmbH, JCNS at MLZ, Garching bei München, Germany

The single crystal diffractometer HEiDi at the 20 MW neutron source Heinz Maier-Leibnitz Zentrum (MLZ) uses hot neutrons for structural studies on various hot topics related to physics, chemistry and mineralogy. Especially in the energy sector and information sector measurements at HEiDi provide users with valuable information about ionic conductors, superconductors and a manifold of magnetic systems by offering high flux, high resolution and large q range respectively, low absorption and high sensitivity for light elements and combining the neutron specific advances with exteme conditions, e.g. in temperature and - in the near future - in pressure.

High temperature studies on Nd2NiO4+δ and Pr2NiO4+δ brownmillerites concerning their oxygen diffusion pathways reveal a double well potential pointing towards the interstitial vacancy sites, creating a quasicontinuous shallow energy diffusion pathway between apical and interstitial oxygen sites (Ceretti et al.). Future studies will use a special mirror furnace which allows temperatures > 1000°C and atmospheres with various oxygen content.

Various multiferroic compounds from the melilite family, e.g. Ba2CoGe2O7 and Ca2CoSi2O7 were studied in order not only to reveal their orthorhombic antiferromagnetic magnetic order structures at low temperature but also the risks of misinterpretation of structural data due to multiple scattering (Sazonov et al.).

Different studies on hydrogen containing silicate and phosphate-based gems like brazilianite, hureaulite and axinite (G.D. Gatta et al.) show the broad variety of hydrogen bonds with different degrees of disorder.

References

[1] M. Ceretti et al.; Journal of Materials Chemistry A (2015), doi 10.1039/c5ta05767a
[2] A. Sazonov et al.; Acta Cryst. B 72 (2016), doi: 10.1107/S2052520615023057.
[3] A. Sazonov et al.; J. Appl. Cryst. 49 (2016), ISSN 1600-5767
[4] G.D. Gatta et al.; American Mineralogist 98 (2013), doi 10.2138/am.2013.4476
[5] G.D. Gatta et al.; Eur. J. Mineral. (2015), doi 10.1127/ejm/2015/0027-2464
[6] G. D. Gatta et al.; Phys. Chem. Min. (2016); doi 10.1007/s00269-015-0798-x.

S04-05

Crystal chirality versus magnetic chirality in CsCuCl3 determined by Neutron Polarization Analysis

V. Hutanu[1], Y. Kousaka[2], K. Ohishi[3], K. Kakurai[3], G. Roth[4]
[1]RWTH Aachen University and Jülich Centre for Neutron Science Heinz Maier-Leibnitz Zentrum, Institute of Crystallography, Garching bei München, Germany
[2]Okayama University, Research Institute for Interdisciplinary Science, Okayama, Japan
[3]Comprehensive Research Organization for Science and Society (CROSS), Neutron Science and Technology Center, Tokai, Japan
[4]RWTH Aachen, Institute of Crystallography, Aachen, Germany

The concept of chirality, meaning left- or right-handedness, plays an essential role in symmetry properties of nature at all length scales from elementary particles to cosmic science. In material sciences, it is very important to understand the chirality in molecules, crystals and magnetic structures both from theoretical and experimental points of view. Chiral helimagnetic ordering, forming only right- or left-handed spiral magnetic structure, has attract much attention in the last time due to unique magnetic textures such as skyrmion and chiral magnetic soliton lattice [1, 2]. Therefore, it is very important to investigate the interplay between crystallographic and helimagnetic chirality. However, only very few experimental results on this interplay are reported up to now, due to the difficulty to synthesize homo-chiral single crystals, which consisting solely of right- or left-handed crystalline domains.

Using novel two-step crystallization technique under stirring we succeeded in obtaining the cm-large ordered homo-chiral single crystals of CsCuCl3 with desired handedness [3]. Circular-polarized synchrotron radiation at SPring 8, J-Park was employed to determine the handedness of the crystal symmetry in different samples [4]. Below 10.5 K a proper-screw magnetic order with propagation vector $k=(1/3,1/3, \pm\delta)$ with ($\delta \sim 0.09$) is formed in CsCuCl3. The magnetic chirality of the homo-chiral crystals was investigated using polarized single crystal diffractometer POLI at MLZ. Our experimental results revealed that the handedness of the magnetic helicity is coupled and directly controlled by the crystallographic lattice chirality [5]. The results could be understood in terms of Dzyaloshinskii-Morya interaction strongly coupled to the lattice, lifting the helix chiral degeneracy.

References

[1] S. Muhlbauer et al., Science 323, 915 (2009).
[2] Y. Togawa et al., Phys. Rev. Lett. 108, 107202 (2012).
[3] Y. Kousaka et al., J.Phys.: Conf. Series 502 012019 (2014).
[4] H. Ohsumi et al., Angew. Chem., Int. Ed. 52, 8718 (2013).
[5] Y. Kousaka et al., Phys. Rev. Materials, 1, 071402(R) (2017)

S04-06

Novel type of neutron polarisation analysis with the multianalyser at PUMA

S. Schwesig[1], O. Sobolev[1], G. Eckold[1]
[1]Georg-August Universität Göttingen, Göttingen, Germany

Introduction

Polarization analysis is one of the most time consuming methods in neutron scattering. One factor for this is the need to spend time measuring both, spinflip and non-spinflip, channels. Utilizing the existing multianalyser system at PUMA with an innovative polarization analysis setup can help saving beam time by allowing a simultaneous detection of both channels.

Objectives

A combination of two deflectors reflecting spin-down and transmitting spin-up neutrons are used to differentiate the neutron beam scattered by the sample (see Fig.1). The separated beam components reach different analyzer blades of the PUMA multianalyser where they are reflected towards different detectors.

Results

First test experiments demonstrated that the spin-up and spin-down components can be measured simultaneously allowing the quantitative determination of the polarization of the scattered neutron beam. Calibration parameters are obtained using McStas simulations as well as analytical calculations. The two different approaches were compared with the results of the test experiments: Incoherent scattering of neutrons polarized by a 3He filter from Vanadium and Bragg scattering from an anti-ferromagnetic hematite (Fe2O3), as well as magnons in cupric oxide (Cu(II)O) sample were analyzed using the presented technique. In the case of the hematite nuclear reflex (006) only the non-spinflip signal was recorded, whereas the anti-ferromagnetic scattering (003) shows both: non-spinflip as well as spinflip intensity. These two signals were clearly distinguishable with our setup and observed simultaneously in a single measurement. The experiment on the cupric oxide showed the potential of this new technique by characterising a more complex sample and applying inelastic scattering.

Conclusion

We demonstrated that the simultaneous measurement of both spin states of the scattered neutrons is possible with good accuracy. The performance of the technique corresponds very well to the expectations based on analytical calculations and McStas simulations. It is assumed that this method will be particularly advantageous for kinetic experiments where it is extremely important to obtain data for different spin states from exactly the same states of the sample [1].

References

[1] Schwesig S, Maity A, Sobolev O, Ziegler F and Eckold G 2018 *Nuclear Instruments and Methods in Physics Research Section A:***877** 124.

Figure 1

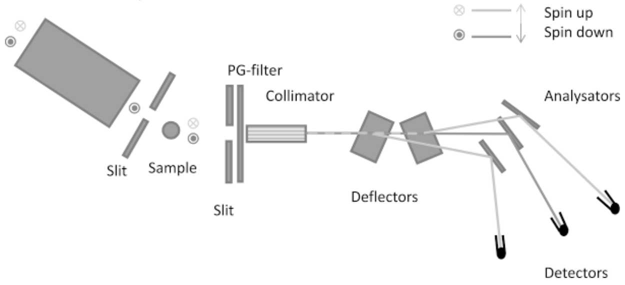

Bio-Crystallography II: Complementation by NMR and EPR

S05-01

Seeing the width of the conformation ensemble

G. Jeschke[1]
[1]ETH Zürich, Department of Chemistry and Applied Biosciences, Zürich, Switzerland

Introduction

Classical structural biology is based on Anfinsen's dogma that sequence encodes a single native conformation, which can be specified at atomic resolution. However, many proteins or their domains are intrinsically disordered. There exists not even a good reason for describing proteins in terms of a dichotomy between well-ordered and disordered domains, which is tantamount to assuming that search space of evolution is restricted to only the extremes of the order-disorder continuum. Crystallography is very well suited to characterize the domains that are ordered at atomic resolution or near-atomic resolution and may inform on weak disorder, but will not usually show moderately or strongly disordered domains.

Several spectroscopic approaches can provide restraints on partially disordered peptide chains, but most of them give only mean values for the conformation ensemble. Such mean values may roughly inform on the extent of disorder, as is the case for NMR chemical shifts, but cannot quantify this extent. Inferring the ensemble width requires distribution restraints. Electron paramagnetic resonance (EPR) combined with site-directed spin labelling yields distance distribution restraints (DDRs). Their range between 15 and about 100 Å matches dimensions of proteins and their complexes.

Objectives

In our structure modelling approach, DDRs from EPR inform on long-range domain arrangement and on locally resolved ensemble width [1]. Restraints from several other techniques can be integrated. Currently, this RigiFlex approach uses atomic-resolution structures of rigid domains from crystallography or NMR spectroscopy together with small-angle scattering curves and crosslink restraints.

Results

The modules of RigiFlex were developed for our experimental projects. The Flex module provided information on the disordered part of the N-terminal domain of plant light harvesting complex LHCII. Determining a rigid-body arrangement from a few DDRs and refining it with SAXS data is demonstrated on the FnIII-3,4 domains of integrin α6β4. First results are shown for a complex consisting of three RNA recognition motifs and an 88-nucleotide long RNA chain.

Conclusion

Information on rigid domains and on the flexibility of less ordered domains is required to a realistically model the dynamic structures of biomolecules.

References

[1] G. Jeschke, MMM: A toolbox for integrative structure modelling, Protein Science, 2017, in press, DOI: 10.1002/pro.3269

S05-02

De novo structure prediction of biomolecules using crystallographic and NMR-derived solvent-accessibility data

C. Hartlmüller[1], C. Göbl[1], J. Günther[1], A. Wolter[2], J. Wöhnert[2], M. Sattler[1], T. Madl[3]
[1]Helmholtz Zentrum München, Institute of Structural Biology, Neuherberg, Germany
[2]Goethe-Universität Frankfurt am Main, Center for Biomolecular Magnetic Resonance (BMRZ), Frankfurt am Main, Germany
[3]Medical University of Graz, Institute of Molecular Biology and Biochemistry, Graz, Austria

Introduction

Since the late 90s, macromolecular modeling software packages, such as Rosetta, have been continuously developed and applied for protein *de novo* structure prediction. Using the protein primary sequence and corresponding short structural fragments from crystal structures deposited to the PDB, protein structure predictions for small proteins less than 100 amino acids can be achieved with reasonable accuracy.

The performance of Rosetta has been improved continuously, for example by including experimental NMR-derived data, and bioinformatics-derived distance restraints based on evolutionary couplings. However, lack of sequence homology and the need for extensive NMR-based experimental data still limits the general applicability of this approach.

Objectives

Here we will present the applicability of NMR-derived surface accessibility data for protein *de novo* structure prediction in the framework of the *de novo* structure prediction package Rosetta. Surface-accessibility data is derived from paramagnetic relaxation enhancements (PRE) obtained from inert and soluble paramagnetic probes – termed solvent PRE (sPRE) - and provide detailed quantitative information about the solvent-accessibility of NMR-active nuclei.

Results

We show that high-quality sPRE data can be obtained in a straightforward manner without modification of the protein. sPRE data improves conformational sampling and scoring of CS-Rosetta, subsequently provides more accurate and better converged structural models, and thereby effectively shifts the size limitations of CS-Rosetta.

Conclusion

We show that sPREs provide a new class of restraints that are easily accessible and applicable to proteins. Our observation that a restricted set of sPRE data is sufficient to improve structural quality indicates that this class of restraints will be particularly powerful for *de novo* structure prediction of larger proteins where complete chemical shift assignments are difficult to obtain. With this respect sPRE data can be used in combination with (sparse) restraints from conventional approaches and offer several benefits over conventional NMR-based approaches

Our approach is open to complementary types of surface accessibility data such as for example bioinformatics and mass spectrometry (cross-linking, radical-mediated protein footprinting) data and will thereby allow integrating different techniques in one program.

S05-03

Resolution and validation of SAS-based structural model

A. Tuukkanen[1,2], G. J. Kleywegt[2], D. I. Svergun[1]
[1]European Molecular Biology Laboratory Hamburg, Hamburg, Germany
[2]European Bioinformatics institute (EMBL-EBI), Hinxton, United Kingdom

The possibility to reconstruct *ab initio* three-dimensional structures from one-dimensional small-angle-scattering (SAS) profiles of particles in solutions was a major breakthrough in the scattering techniques nearly two decades ago, and since then SAS has become a standard method for structural studies of biological macromolecules and their complexes. However, the models generated from SAS data are still reported without quantifying their resolution. This situation contrasts with other structural methods such as X-ray crystallography and electron microscopy. The lack of an objective quality measure for SAS-derived models has limited their validation and further use. We have recently developed a method for resolution assessment of *ab initio* SAS models based on the average variability within a structural ensemble [1]. Here, we shall demonstrate the practical use of the novel measure and discuss the approaches for the validation of SAS-based *ab initio* and hybrid rigid body models. We expect the presented developments to have a significant impact on the archiving of SAS models and on their further use with other structural biology information.

References

[1] Tuukkanen A.T., Kleywegt G.J., Svergun D.I. (2016) Resolution of *ab initio* shapes determined from small-angle scattering. *IUCrJ* **3**: 440-447.

Figure 1

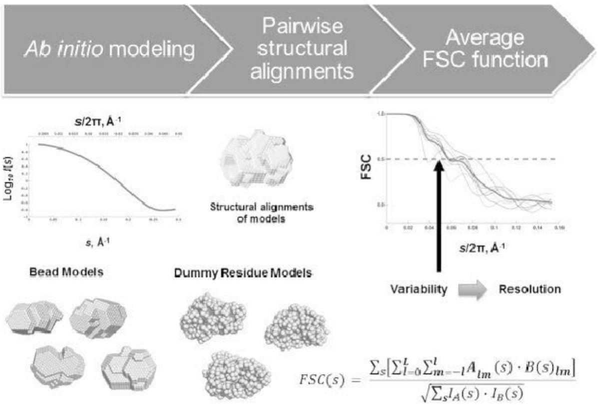

S05-05

Probing protein structure and dynamics by combing X-ray crystallography and EPR spectroscopy of spin labeled protein single crystals

T. Risse[1], P. Consentius[1], B. Loll[1], U. Gohlke[2], M. C. Wahl[1], U. Heinemann[1,2]
[1]Freie Universität Berlin, Institut für Chemie und Biochemie, Berlin, Germany
[2]Max-Dellbrück Zentrum, Berlin, Germany

The line shape of CW EPR spectra of spin labeled proteins has been extensively used to elucidate dynamic information such backbone fluctuations or structural rearrangements under physiological conditions. A detailed analysis of the CW line shape is intricate, because of a lack of sufficient spectral information. In this contribution EPR spectroscopy will be combined with high resolution X-ray crystallography and quantum chemical calculations to unravel additional information concerning the conformational dynamics of the protein, but also into the internal dynamics of the spin label itself.

We will use single crystals of spin labeled T4 lysozyme to show that reversible conformational exchange process of secondary structure elements take place in the single crystal and use a combination of room temperature X-ray crystallography and EPR spectroscopy to determine the structure of the conformational states as well as their thermodynamic properties. The results reveal the importance of entropic contributions which are largely due to the solvent environment. In addition to the conformational dynamics it will be discussed how a combination of high resolution X-ray crystallography, EPR spectroscopy and theory can reveal new insights into the internal dynamics of spin labels.

Crystallography in nanoscience

S06-01

Thickness prediction and elastic strain investigation in single GaAs/(In,Ga)As/GaAs core-shell-shell nanowires using in-plane and out-of-plane X-ray diffraction

A. Al Hassan[1], A. Davtyan[1], H. Küpers[2], R. B. Lewis[2], A. Tahraoui[2], L. Geelhaar[2], U. Pietsch[1]
[1]Universität Siegen, Naturwissenschaftlich- Technische Fakultät, Siegen, Germany
[2]Leibniz-Institut im Forschungsverbund Berlin e.V., Paul-Drude-Institut für Festkörperelektronik, Berlin, Germany

The complex strain state of core-shell nanowires (NW) is encoded along directions perpendicular to the growth axis. Due to fluctuations in the distribution of the growth species on different areas of the substrate, structural parameters such as shell thickness and local indium concenetration may differ between NWs grown on the same substrate. Therefore, structural analysis has to be perfromed on single NWs. The NWs are grown on a patterned Si (111) substrate. In order to access single NWs with incident beam parallel to the surface of the substrate, holes with seperation of 10 µm were drilled by e-beam to form a single line followed by selective molecular beam epitaxy NW growth along [111]. This particular arrangment allowed accessing NW side planes and edges by the x-ray nanobeam realizing x-ray Bragg diffraction within planes perpendicular to the surface of the substrate. Combining nano X-ray diffraction (Fig. 1a,b) and finite element methods (FEM – see Fig. 1c,d), we were able to calculate the strain field and dimension of each layer with high precision (Fig. 1e) in single GaAs/(In,Ga)As/GaAs core-shell-shell NWs in the as-grown geometry from mapping the strain field at directions perpendicular to the NW growth axis, in particular the (2-20) NW side facets and (22-4) NW edges. Moreover, higher strain relaxation at the (In,Ga)As shell was noticed to take place at the side facets compared to the edges. Additional nano-XRD measurements with scatterting vector parallel to the NW growth axis reveal asymmetry in the hexagonal cross-section of single NWs and significant variation in their total thicknesses. More details will be presented in the poster.

Figure 1: (a) and (b) RSMs of the 2-20 and 22-4 Bragg reflections for single NWs. Panels (c) and (d) are FEM simulations of the strain field of 2-20 and 22-4 Bragg reflections. (e) demonstrates the compatibility between XRD and FEM (left) and the predicted NW cross-section from 111 (Black) and 2-20 (colored).

Figure 1

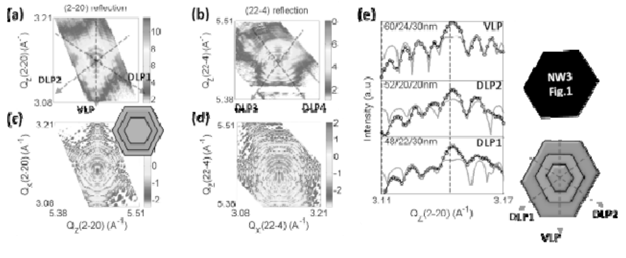

S06-02

Quantum entanglement, Kondo effect, and electronic transport in quantum dots system

S. Babaee Tooski[1]
[1]Azad University, Physics, Malayer, Iran

We present studies of three electrons confined in a triple quantum dot with one of the dots connected to metallic electrodes which is modeled by a three-impurity Anderson Hamiltonian. It is focused on the pairwise quantum entanglement of a three-spin system and its relation to the thermodynamic and transport properties. It is shown that two many-body phenomena compete with each others, the Kondo effect and the inter-dot exchange interactions. In fact, coupling triple quantum dots to the electrodes results a formation of the Kondo singlet which can switch the entanglement due to the interplay between the interdot spin-spin correlations and various Kondolike ground states. The quantum phase transition between unentangled and entangled states is studied quantitatively and the corresponding phase diagram is explained by exactly solvable four spin model. Although the work concentrates on the system of quantum dots, the model is more general and can be applied to the Kondo physics in molecules with a triangular symmetry.

S06-03

Silver-platinum nanoparticles in the miscibility gap: Characterization by X?ray diffraction

V. Grasmik[1], K. Loza[1], O. Prymak[1], M. Heggen[2], M. Epple[1]
[1]Universität Duisburg-Essen, Institut für Anorganische Chemie, Essen, Germany
[2]Forschungszentrum Jülich GmbH, Ernst Ruska-Centre and Peter Grünberg Institute, Jülich, Germany

Metallic nanoparticles (NPs) have a wide range of applications in catalysis[1] or medicine as bactericidal agents.[2] They exhibit distinct solubilities and optical properties compared to the bulk phases.[3] To understand the properties of bimetallic particles it is crucial to carry out a full characterization with different methods. The silver-platinum (AgPt) system is challenging because of conflicting opinions on the existence of nanoalloys[4, 5] due to a large miscibility gap. From the crystallographic point of view, a co-crystallization of silver and platinum should be possible because both metals crystallize in the face-centered cubic system, have similar lattice parameters (Ag: a = 4.0862 Å, Pt: a = 3.923 Å), and atomic radii.
AgPt NPs were synthesized by a seeded-growth method using sodium borohydride as reducing and poly(N-vinylpyrrolidone) as capping agent. X-ray powder diffraction (Fig. 1) was used besides other characterization methods like disc centrifugal sedimentation, UV/vis spectroscopy, atomic absorption spectroscopy, transmission electron microscopy, and scanning transmission electron microscopy (STEM) combined with energy-dispersive X-ray spectroscopy (EDX) (Fig. 2) as tool for probe the alloy character of such AgPt NPs over the whole composition range in steps of 10 at%. Crystallite sizes, micro strain, and lattice parameters were calculated to obtain the crystallinity of the samples and for comparison with the Vegard's law to elucidate the formation of alloys.

Figure 1: Diffraction pattern of AgPt NPs (50:50 mol%) in comparison with the Powder Diffraction Files (PDFs) of pure silver and pure platinum. Lanthanum hexaboride LaB_6 was used as internal standard.
Figure 2: STEM EDX map of a AgPt NP (50:50 mol%).

References

[1] Cui, C.; Gan, L.; Heggen, M.; Rudi, S.; Strasser, P. *Nat. Mater.* **2013,** 12, (8), 765.
[2] Morones, J. R.; Elechiguerra, J. L.; Camacho, A.; Holt, K.; Kouri, J. B.; Ramirez, J. T.; Yacaman, M. J. *Nanotechnology* **2005,** 16, (10), 2346.
[3] Auffan, M.; Rose, J.; Wiesner, M. R.; Bottero, J.-Y. *Environmental Pollution* **2009,** 157, (4), 1127.
[4] Lahiri, D.; Bunker, B.; Mishra, B.; Zhang, Z.; Meisel, D.; Doudna, C. M.; Bertino, M. F.; Blum, F. D.; Tokuhiro, A. T.; Chattopadhyay, S.; Shibata, T.; Terry, J. *J. Appl. Phys.* **2005,** 97, (9), 094304.
[5] Fu, T.; Fang, J.; Wang, C.; Zhao, J. *J. Mater. Chem. A* **2016,** 4, (22), 8803.

Figure 1

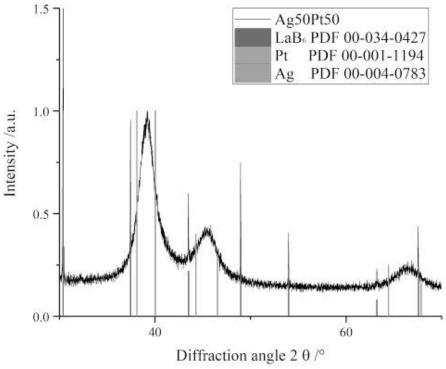

Figure 2

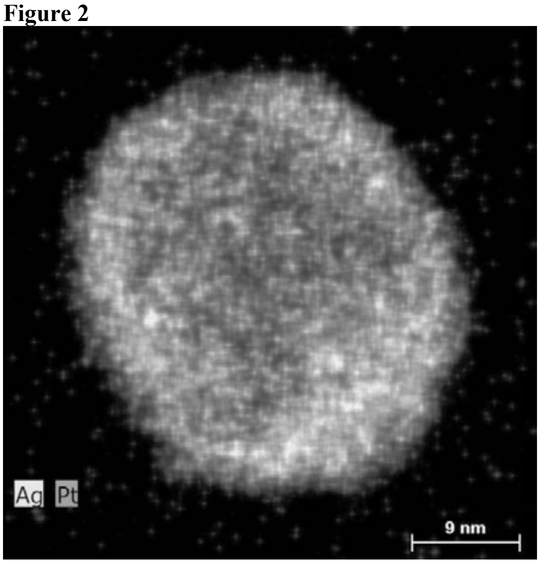

S06-04

Time-resolved *in situ* X-ray nano-diffraction of a single growing GaAs nanowire by self-catalyzed MBE

S. M. Mostafavi Kashani[1], J. Vogel[1], A. Davtyan[1], L. Feigl[2], D. Bahrami[1], J. Jakob[1], P. Schroth[1,3,2], T. Baumbach[3,2], U. Pietsch[1]
[1]Universität Siegen, Solid State Physics, Siegen, Germany
[2]Laboratory for Application of Synchrotron Radiation (LAS), Laboratory for Application of Synchrotron Radiation (LAS), Karlsruhe, Germany
[3]Karlsruhe Institute of Technology (KIT), Institute for Photon Science and Synchrotron Radiation (IPS), Karlsruhe, Germany

Since the beginning of the 21st century, semiconductor NWs have attracted an increasing attention in applications such as optics (e.g. LED, LASER), biological sensing, electronics (e.g. solar-cells, transistors), and fundamental research (e.g. Majorana Fermions, Single Photon Sources) [1]. X-ray nano-diffraction (nXRD) has been reported as a valuable tool for characterization of structure, strain, and size of NWs [2] which are important physical properties that determine the performance of the NWs in device applications [3,4]. For development of reliable NW fabrication processes, in-situ monitoring of NW growth is highly desirable. We here report for the first time monitoring of a single NW growth by in-situ time resolved nXRD. In particular, self-catalyzed GaAs MBE growth onto Si(111) substrate is studied.

The in-situ time-resolved nXRD experiment was performed using a portable MBE [5] growth chamber mounted on the heavy load goniometer at beamline P09 of PETRA III (DESY) synchrotron. Using a set of the compound refractive lenses, the original X-ray beam size of about 0.9 cm decreased to about 1.8x6.0µm² and thus, a X-ray flux of 4·109 Photons·s-1 was achieved. The growth of NWs was performed on a silicon substrate with an oxide covering of about 16nm thickness which was pre-patterned by focused ion beam. Accordingly, epitaxial growth was prevented anywhere but on the defined patterned holes. The spacing of the patterned holes, X-ray beam size, and growth parameters (density of growth) were adjusted interconnectivity which is summarized to resolving diffraction from a single NW. During the NW growth and using 15 keV X-ray (10-4), X-ray scattering was monitored near the (111) Bragg peak of the cubic GaAs NW. With time resolution of 16s the evolution of NW diameter, NW length, and polytype evolution of the growing NW were extracted. At certain time steps, full reciprocal space maps have been recorded (see fig. 1). The characteristics of the grown NW monitored by the X-ray experiments are compared to those measured by SEM.

References

[1] P. Yang, et al., Nano Letters 10, 1529 (2010)
[2] A. Biermanns, X-ray diffraction from single GaAs nanowires, PhD Thesis, Universität Siegen (2012)
[3] M. Heiss, et al., Phys. Rev. B 83, 045303 (2011)
[4] M. Heurlin, et al., Nano Letters 15, 3597 (2015)
[5] T. Slobodskyy, et al., Rev. Sci. Instrum. 83, 105112 (2012)

Figure 1

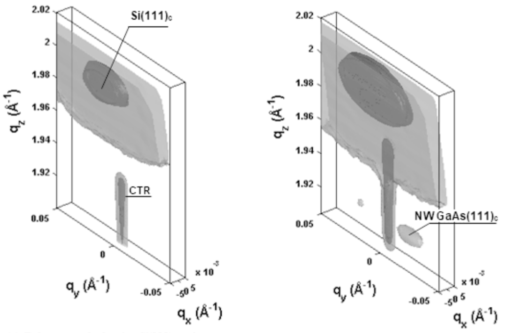

(a) Before growth showing Si(111)c and a cut from the crystal truncation rod (CTR)

(b) After ~55 min of growth showing emerging GaAs NW signal at GaAs(111)c reflection

Figure 1) 3-dimentional diffraction intensity distribution close to the GaAs (111)c reflection. The reciprocal space mapping (RSM) covers a diffused intensity of Si(111)c at q_z close to 2 Å^{-1}. The red and green structures represent iso-intensity surfaces.

S06-05

Fast scanning X-ray diffraction as a strain and orientation microscope at beamline ID01 of the ESRF.

C. Richter[1], G. Chahine[1], T. Zhou[1], M. I. Richard[1], S. Leake[1], M. Zoellner[2], A. Even[3], T. Schulli[1]
[1]European Synchrotron Radiation Facility (ESRF), X-ray Nano-Probe, Grenoble, France
[2]IHP, Frankfurt (Oder), Germany
[3]CEA, LETI, Grenoble, France

The growth of crystalline thin film heterostructures is the basis for modern semiconductor devices, such as optoelectronics (LEDs, laser diodes, solar cells), MOSFETs, etc. Lattice strain due to a mismatch in lattice constants or thermal expansion, is an important consequence of the thin film growth as it influences the band structure and, hence, the optical properties and electron mobility. At the same time, the engineering of strain by geometrical relaxation or constraints is a established tool to tune these properties.

X-ray diffraction is frequently used to determin the unit cell dimensions of the epitaxial layers which allow to derive lattice quality, strain, composition, mosaicity and thicknesses quality in average values over the illuminated area[1]. However, the lack of spatial resolution on the microscopic scale prevents an investigation of the mechanisms behind strain relaxation and reduced lattice quality, and fluctuations of composition can not be resolved. Different techniques (e.g. transmission electron microscopy, Raman spectroscopy) can be used to study these properties microscopically.

In addition, we implemented a non-destructive, sub-um beam, fast scanning X-ray diffraction setup at beamline ID01 which yields all this information simultaneously and allows for model-free data analysis[2]. Imaging of the sample is performed using piezo actuators and a continuous exposure of the area detector with a frame rate of up to 100 Hz. Different kinds of focusing optics allow a spatial resolution of approx. 100 nm based on the X-ray beam size while the probing depth is in the 5...50 µm range. This way, we obtain a 3D reciprocal space for each point on the sample surface that can be used extract lattice parameters and orientation. The mapped strain and tilt fields carry information about defects (e.g. dislocations or point defects) that are even smaller than the beam size.

Here we present different diffraction techniques available for characterization of nano-objects and how to extract the lattice properties from the 5D datasets. Recent results of scanning diffraction microscopy on state of the art light emitting devices based on GeSn and GaN semiconducter materials are highlighted.

References

[1] Moram, M. A. & Vickers, M. E. Reports on Progress in Physics 72, 36502 (2009).
[2] Chahine, G. A. et al. Appl. Phys. Lett. 106, 71902 (2015).

S06-06

Nanoscience crystallography at a high brilliance laboratory X-ray diffractometer: from mesoscopic to atomic length scales

E. Kentzinger[1], U. Rücker[1], A. Qdemat[1], T. Brückel[1]
[1]Forschungszentrum Jülich GmbH, Jülich Centre for Neutron Science, Jülich, Germany

The high brilliance laboratory small angle X-ray scattering instrument GALAXI [1] is used to investigate chemical correlations in bulk materials or between structures deposited on a surface at nanometre and mesoscopic length scales. The instrument is capable to perform GISAXS experiments in reflection at grazing incidence as well as SAXS experiments in transmission geometry. The X-ray flux on sample is comparable or higher than the one obtained at a comparable beamline at a second generation synchrotron radiation source.

Some results of studies on energy and soft mater materials as well as materials for information technology (Fig. 1) will be given. We will also present our project to extend the instrument towards wide-angle scattering for the investigation of interfaces in multilayers and of nanostructures at the atomic length scale, using the techniques of surface diffraction and GIWAXS.

[1] Jülich Centre for Neutron Science. (2016). GALAXI: Gallium anode low-angle x-ray instrument. Journal of large-scale research facilities, 2, A61. http://dx.doi.org/10.17815/jlsrf-2-109

Fig. 1: Left: Scanning electron microscopy image of a patterned silicon substrate used as template for assisted self-assembly of magnetic nanoparticles. Right: GISAXS from this sample obtained on the GALAXI instrument.

Figure 1

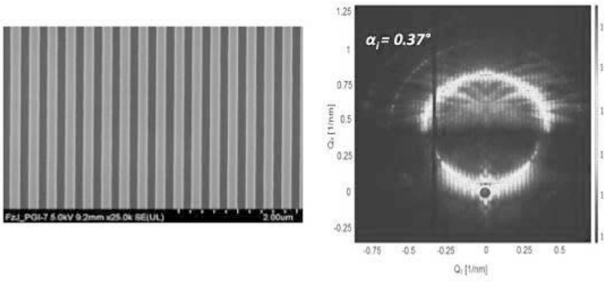

Structure-property-relationships

S07-01

Magnetic properties and proton dynamics in phosphatic oxyhydroxides

S. H. Park[1]
[1]Ludwig-Maximilians-Universität München, Geo- und Umweltwissenschaften, Sektion Kristalllogaphie, München, Germany

Introduction

Geometrically frustrated spin systems comprised of e.g. zig-zag chains, triangles, or pentamers of MO6 (M = 3*d*-metal cations) often show magnetoelectric (ME) coupling effects fundamental in multiferroics. Many phosphatic oxyhydroxides exhibit such interesting moieties of MO6. On the other hand, they contain OH- and HOH-groups in the framework, showing various strengths of hydrogen bonds between OH- and HOH-groups. It is a worthy investigation on a variety of complex magnetic orders and interesting proton dynamic disorder mostly unknown in this structure family.

Objectives

Study of magnetic structures, proton tunnelling and conductivity of the eosphorite-childrenite series AlPO4(OH)2H2O, the rockbridgeite type minerals, (Fe, Mn, Zn)(PO4)3(OH)5, and hureaulite,

Results

The antiferromagnetic structure of the eosphorite-childrenite series Mn0.5Fe0.5AlPO4(OH)2H2O could be uncovered using neutron single crystal diffraction at 3 K with group theoretical representation analysis. The new magnetic structure is described in the magnetic space group **PC**mnb, maintaining the atomistic unit cell size. More interestingly, an anomalous increase in the real part of dielectric response is observed in this mineral while cooling from 300 K to ~70 K. This is addressed to field-induced proton dynamics in a short hydrogen bond of 2.480(3) Å. The absence of discontinuities in heat capacity curves above the Néel temperature (*T*N ≈ 7 K) excludes a paraelectric to antiferroelectric phase transition. Upon application of mild hydrostatic pressures below 1.6 GPa, the maximum in the dielectric response is shifted from 70 K to lower temperatures near ~2 K. This explains a narrow correlation between the proton transfer and the compression of the short hydrogen bond length. Variable-temperature neutron single crystal diffraction in the range 25 K - 475 K strongly indicate a new mechanism for fast proton conduction along the skirt of the of P(OH, O)4-M(OH, O)6 network (Fig. 1-4).

Conclusion

Along with results from the extended study of the eosphorite-childrenite seriesBesides, as aforementioned, we present at DGK 2018 new magnetic structures and a high conductivity at RT in rockbridgeite and hureaulite, based on results from magnetic, dielectric and thermal analysis, quasi-elastic neutron scattering measurements, and structural investigation using neutron and X-ray diffraction.

Figures

Properties of the eosphorite-childrenite series Mn0.5Fe0.5AlPO4(OH)2H2O.

Figure 1

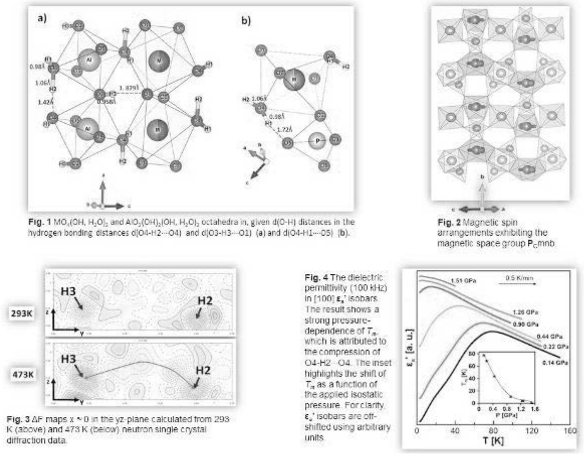

Fig. 1 $MO_4(OH, H_2O)_2$ and $AlO_2(OH)_2(OH, H_2O)_2$ octahedra in, given d(O-H) distances in the hydrogen bonding distances d(O4-H2···O4) and d(O3-H3···O1) (a) and d(O4-H1···O5) (b).

Fig. 2 Magnetic spin arrangements exhibiting the magnetic space group $P_C mnb$

Fig. 3 ΔF maps x ~ 0 in the yz-plane calculated from 293 K (above) and 473 K (below) neutron single crystal diffraction data.

Fig. 4 The dielectric permittivity (100 kHz) in [100] ε_a' isobars. The result shows a strong pressure-dependence of T_m, which is attributed to the compression of O4-H2···O4. The inset highlights the shift of T_m as a function of the applied isostatic pressure. For clarity ε_a' isobars are off-shifted using arbitrary units.

S07-02

Interplay of cation disorder and thermoelastic properties of $MgGa_2O_4$

C. Hirschle[1], J. Schreuer[1], Z. Galazka[2]
[1]Ruhr-Universität Bochum, Bochum, Germany
[2]Leibniz-Institut für Kristallzüchtung, Berlin, Germany

Transparent semiconducting oxides are materials suitable for a wide variety of optoelectronic applications, such as UV-LEDs, Schottky diodes, high voltage transistors and transparent thin film transistors. Spinel structure $MgGa_2O_4$ was recently shown to have an appropriate carrier concentration and bandgap for such applications and it can be grown using various techniques from the melt as relatively large crystals[1]. Furthermore, it has a high chemo-physical stability and its conductivity can be controlled by adjusting the atmosphere during the growth process[1], making it an excellent candidate for future applications. However, both heat capacity[1] and thermal diffusivity[2] of $MgGa_2O_4$ were shown to behave anomalously as a function of temperature, which was interpreted as the result of cation ordering processes.

We studied this issue by direct investigation of the cation ordering of annealed samples using single crystal X-ray diffraction. Additionally, we used push-rod dilatometry and resonant ultrasound spectroscopy to determine thermal expansion and the complete set of elastic constants, respectively, from 103 K to 1673 K to assess correlations between the changing structure and properties.

Thermal expansion and all stiffness coefficients related to shear resistances show a discontinuity in their temperature dependence at about 820 K. Furthermore, the cation disorder is independent of temperature up to about 820 K and increases gradually at higher temperatures. Thus, the cation disorder in $MgGa_2O_4$ is most likely in equilibrium at high temperatures and undergoes a transition to a nonequilibrium state below 820 K, where the disorder cannot relax in laboratory timescales; a glass-transition. This transition is likely also related to the anomalies in heat capacity[1] and thermal diffusivity[2]. Ultrasonic wave attenuation is not affected by the transition.

References

[1] Galazka, Z., Klimm, D., Irmscher, K., Uecker, R., Pietsch, M., Bertram, R., Naumann, M., Albrecht, M., Kwasniewski, A., Schewski, R. and Bickermann, M. (2015): $MgGa_2O_4$ as a new wide bandgap transparent semiconducting oxide: Growth and properties of bulk single crystals. *Phys. Status Solidi A* **212**, 1455–1460.
[2] Schwarz, L., Galazka, Z., Gesing, T. M. and Klimm, D. (2015): On the influence of inversion on thermal properties of magnesium gallium spinel. *Cryst. Res. Technol.* **50**, 961–966.

S07-03

Ordering phenomena in rare-earth oxoborates

M. Münchhalfen[1], J. Schreuer[1], C. Reuther[2], J. Götze[2], E. Mehner[3], H. Stöcker[3]
[1]Ruhr-Universität Bochum, Institut für Geologie, Mineralogie und Geophysik, Bochum, Germany
[2]Technische Universität Bergakademie Freiberg, Institut für Mineralogie, Freiberg, Germany
[3]Technische Universität Bergakademie Freiberg, Institut für Experimentelle Physik Freiberg, Germany

Rare-earth oxoborates $RX_2Z_2O(BO_3)_3$ have been studied for about 25 years because of their promising non-linear optical properties. Recently, these crystal species gathered interest as potential candidates for high-temperature piezoelectric sensing applications, since they combine a high melting point at around 1770 K with no reported phase transitions, high piezoelectric sensitivity and high electric resistivity [1]. The $RCa_4O(BO_3)_3$ structure type offers different possibilities for cation substitution (e.g. X,Z = Ca and R = Y, La, Nd, Sm, Gd, Dy, Er), which in principle allow for tuning of physical properties. The low symmetry of the monoclinic space group Cm results in a high number of degrees of freedom regarding the anisotropy of physical properties.

Large single crystals of $RCa_4O(BO_3)_3$ with R = Gd, Y, La, Er were grown from melt using the Czochralski method. Their relevant thermal and electromechanical properties were studied using a combination of differential scanning calorimetry, dilatometry and resonant ultrasound spectroscopy in the temperature range 100 K – 1500 K. Additionally, ex-situ single crystal X-ray diffraction experiments were conducted employing a 4-circle diffractometer on tempered and quenched samples.

The 13 and 10, respectively, independent components of the elastic and piezoelectric tensors of the investigated crystal species could be determined with high internal consistency. Contrary to the reported lack of phase transitions, all investigated physical properties undergo reproducible discontinuities at around 1000 K. Diffraction experiments on quenched samples indicate a gradual increase of cation disorderstarting roughly at 1000 K. Therefore, a glass-like transition from static to dynamical cation disorder is likely responsible for the observed discontinuities.

References

[1] Yu, F., Hou, S., Zhao, X., Zhang, S. (2014): IEEE Trans. Ultrason., Ferroelect., Freq. Control, **61**, 1344-1356.
[2] Zhang, S., Yu, F. (2011): J. Am. Ceram. Soc. **94**, 3153-3170.

Acknowledgments: The authors gratefully acknowledge financial support of the DFG (PAK921/1, SCHR 761/4: Structure/property relationships and structural instabilities of high-temperature piezoelectrics of the oxoborate family).

S07-04

On the growth mechanism of hetero epitaxial {100} Nickel Titanium shape memory alloy thin films

S. Hahn[1], V. Klemm[2], D. Rafaja[2], S. Kaufmann-Weiß[3], S. Fähler[4], M. F. Wagner[1]
[1]Technische Universität Chemnitz, Institute of Materials Science, Chemnitz, Germany
[2]Technische Universität Bergakademie Freiberg, Institut für Materialwissenschaften, Freiberg, Germany
[3]Karlsruhe Institute of Technology (KIT), Institut für Technische Physik, Karlsruhe, Germany
[4]IFW Dresden, Functional Magnetic Films, Dresden, Germany

Epitaxial Nickel Titanium (NiTi) films have the potential to be used as model systems to provide new insights on phase formations during crystal growth. The orientation relationship of the films investigated here is determined by the {100} single crystalline MgO substrate. Because of the lattice misfit between NiTi and MgO, the as-prepared films are intrinsically stressed; these stresses can be reduced by a 3-step heat treatment routine. The resulting phase in the films and the crystal orientation relative to the substrate is determined by XRD and pole figure measurements. TEM investigations of <100> and <110> cross-sectional FIB lamellae are used for interface studies. We discuss how the microstructure is influenced by the heat treatments. We particularly discuss how forest dislocations and well-defined dislocation networks located in the film influence the film formation itself. Furthermore, we show that forest dislocations can be replaced by misfit dislocations close to the substrate-film interface by changing the heat treatment procedure. These microstructural investigations enable a deeper understanding of microscopic growth mechanisms related to macroscopic observed microstructures in epitaxial NiTi films.

S07-05

Synthesis of all-inorganic double perovskite solar absorbers – How to make a theoretician (un)happy

J. Breternitz[1], S. Schorr[1,2]
[1]Helmholtz-Zentrum Berlin, Structure and Dynamics of Energy Materials, Berlin, Germany
[2]Freie Universität Berlin, Institut für Geologische Wissenschaften, Berlin, Germany

Hybrid perovskite solar absorber materials, with $(CH_3NH_3)PbI_3$ as the signature compound,[1] are undoubtedly regarded as one of the most intriguing fields of research in energy materials at the moment. They do in fact bear very favourable properties for solar cells, such as a well-suited band gap, strong absorption of light and good carrier mobility.[2]

However, severe problems of these materials are their lead content as well as their poor long-term stability,[3] which impede their practical application in commercial solar cells. Therefore, theoretical chemists have tried to address these issues by predicting novel perovskite type materials that neither contain an organic cation, which is a main cause for long-term instability, nor lead as hazardous element. Especially double perovskites $A_2[BB'']X_6$ (A = Cs,Rb B/B" = In,Ag,Cu,Bi and X = Br,I) have caught attention, with a number of compounds, e.g. $Cs_2[AgIn]Cl_6$, predicted to be thermodynamically stable and to have suitable bandgaps.[4] Those double perovskites with Bi have been observed experimentally but they have an indirect bandgap with $E_g > 2$ eV, which makes them unsuitable for solar absorber materials. In contrast, the existence region of double perovskite compounds that do not contain Bi in their respective chemical potential landscapes is typically narrow,[5] which makes their synthesis challenging.

Herein, we report the synthesis of all-inorganic perovskite materials on a mechanochemical route, allowing to reach compositions not normally accessible through different techniques. While our results confirm the existence of these phases and hence demonstrate the accuracy of the theoretical calculations on this aspect, the physical and structural properties of the found materials differs in some points from the predicted values and we will highlight similarities and differences between the calculated and found structures.

References

[1] A. Franz, D. M. Többens, S. Schorr, *Cryst. Res. Technol.*, **2016**, *51*, 534–540.
[2] G. Hodes, *Science*, **2013**, *342*, 317–318.
[3] G. Niu, X. Guo, L. Wang, *J. Mater. Chem. A*, **2015**, *3*, 8970–8980.
[4] Z. Xiao, K.-Z. Du, W. Mang, D. B. Mitzi, Y. Yan, *Angew. Chem. Int. Ed.*, **2017**, *46*, 1–6.
[5] X.-G. Zhao, D. Yang, Y. Sun, T. Li, L. Zhang, L. Yu, A. Zunger, *J. Am. Chem. Soc.*, **2017**, *139*, 6718–6725.

S07-06

Visualisation of Crystalline Structures in Injection Molded Parts

Y. Spörer[1], I. Kühnert[1]
[1]Leibniz-Institut für Polymerforschung Dresden e.V.,, Dresden, Germany

Semi-crystalline thermoplastics are used throughout the world in many different applications, for example in automotive and medical applications or for food packaging. Therefore, to improve the mechanical and optical properties, to reach the stringent requirements for complex molded parts and to develop new application areas, it is of great interest to understand the relationship between the process-induced crystalline structure and properties of the part. Injection molding is one of the most commonly used processes to manufacture complex three dimensional parts. The processing parameters, in particular the processing temperatures and packing pressure have a significant influence on the crystallinity and related properties of molded parts.

In this study microscopy was used to visualize and systematically investigate the crystalline structure of different semi-crystalline materials. Information obtained from Differential Scanning Calorimetry (DSC) measurements about the thermodynamic behavior of the materials was used to observe the crystalline growth in a hot stage experiment under polarized light. The results were used to optimize the temperature profile of the injection molding process. All materials were injection molded with various processing temperatures to evaluate the influence on the skin-core morphology inside tensile test bars.

Under polarized light it was observed that no crystalline structures are visible in the skin region and that the structures become progressively larger closer to the core. The results have shown that the size of the skin region is strongly dependent on the temperature difference between the melt and the mold, respectively the cooling ratio. The process influence on mechanical properties was analyzed and an overview of the maximum tensile strength and elongation of semi-crystalline materials is given.

In conclusion the results help to improve the properties of injection molded semi-crystalline thermoplastics.

In-situ methods

S08-02

In situ Formation and Growth Characterization of Iron Oxide Nanoparticles by Synchrotron X-Ray Scattering Techniques

R. Wendt[1,2], E. Gericke[1,2], A. Lang[2], D. Tatchev[3], G. Greco[1], M. Wollgarten[4], A. Hoell[1], K. Rademann[2], S. Raoux[1,5]
[1]Helmholtz-Zentrum Berlin, Institute for Nanospectroscopy, Berlin, Germany
[2]Humboldt-Universität zu Berlin, Institut für Chemie, Berlin, Germany
[3]Bulgarian Academy of Sciences, Institute of Physical Chemistry, Sofia, Bulgaria
[4]Helmholtz-Zentrum Berlin, Department of Nanoscale Structures and Microscopic Analysis, Berlin, Germany
[5]Humboldt-Universität zu Berlin, Institut für Physik, Berlin, Germany

Solvothermal syntheses are one of the most applied methods in the preparation of crystalline and monodisperse metal oxide nanoparticles [1, 2]. Nevertheless, the drawbacks of this method are long reaction times, expansive autoclaves and difficulties to investigate the nanoparticle growth *in situ*. To overcome this, microwave-assisted solvothermal syntheses (MWASS) techniques have become subject of renewed fundamental and applied interests [3]. Main features of MWASS are distinguished control and exact on-line determination of pressure and temperature inside the sealed reaction vessel which can be understood as an autoclave-type reactor. In contrast to conventional heating, the advantage is the efficient internal volumetric "in-core" heating by directly coupling the MW energy to the reaction solution. It allows high heating rates with small thermal gradients and strongly decreased reaction times based on the Arrhenius law [4]. This work includes an innovative measurement setup which facilitates *in situ* investigations of pressurized colloidal solutions by allowing exact addition of precursor solution into the sealed vessel reactor and withdrawal of colloid solution at any time. Thereby, we are able to investigate and characterize the early stages from molecule to nanoparticle in a time-range of milliseconds by coupling *in situ* UV-Vis spectroscopy, synchrotron based Wide-Angle (WAXS) and Small-Angle X-ray Scattering (SAXS), which is exemplarily shown in Figure 1 for the evolution of microwave-assisted solvothermally synthesized iron oxide nanoparticles. These *in situ* studies are combined with complementary *ex situ* methods, Transmission Electron Microscopy (TEM), Electron Energy Loss Spectroscopy (EELS) and X-ray Absorption Spectroscopy (XAS). By combining these results, we provide concepts for formation and growth mechanisms of iron oxide nanoparticles which were synthesized by microwave-assisted solvothermal routes [1-4].

Figure 1

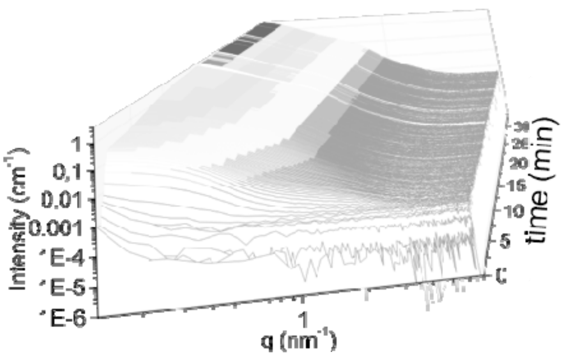

S08-03

In-situ observation of nanoparticle size reduction during laser synthesis in liquids

A. Letzel[1], B. Gökce[1], S. Ibrahimkutty[2], A. Menzel[3], A. Plech[4], S. Barcikowski[1]
[1]Universität Duisburg-Essen, Technical Chemistry I, Essen, Germany
[2]Max-Planck-Institut für Festkörperforschung, Solid State Spectroscopy, Stuttgart, Germany
[3]Paul Scherrer Institute, Coherent X-ray Scattering, Villigen, Switzerland
[4]Karlsruhe Institute of Technology (KIT), Institute for Photon and Synchrotron Science, Eggenstein-Leopoldshafen, Germany

Although nanoparticle synthesis by pulsed laser ablation in liquids (PLAL) is gaining wide applicability, the mechanisms of particle formation, in particular, size-quenching effects by dissolved anions are not fully understood yet. It is known that the size of primary particles (d ≤ 10 nm), secondary particles (spherical particles d > 20 nm) and agglomerates observed ex situ is effectively reduced by the addition of small amounts of monovalent electrolyte to the liquid prior to laser ablation [1]. Furthermore the amount of secondary particles and agglomerates is significantly reduced. As the size distributions of additive-free colloids synthesized by PLAL is complex already inside cavitation confinement, which may compromise the applications of as synthesized nanoparticles, we focus on the particle formation and evolution inside the vapor filled cavitation bubble. This vapor phase is enriched with ions from the afore added electrolyte [2]. By probing the cavitation bubbles interior by means of small-angle X-ray scattering (SAXS), the reaction between nanoparticles and ions is observed. We find that particle size quenching occurs already within the first bubble oscillation (approximately 100 µs after laser impact), still inside the vapor phase. This shows that nanoparticle-ion-interactions during PLAL are in fact a gas phase phenomenon. These interactions include size reduction of both primary and secondary particles and a decreased abundance of the latter as shown by in situ SAXS and confirmed by ex situ particle analysis (e.g. SAXS, TEM). These findings are in compliance with theoretical computations, predicting the formation of a distinct bimodality already a few nanoseconds after laser impact [3].

Figure 1. (Left) Scheme of experimental setup. The interior of the cavitation bubble is probed by SAXS. (Middle) In situ size distributions of gold nanoparticles ablated 100 µs after laser impact in pure water and saline solution obtained from SAXS. (Right) Subtraction of the resulting ex situ TEM-histograms.

References

[1] V. Merk, C. Rehbock, F. Becker, U. Hagemann, H. Nienhaus and S. Barcikowski, Langmuir 30 (2014) 4213.
[2] A. Matsumoto, A. Tamura, T. Honda, T. Hirota, K. Kobayashi, S. Katakura, N. Nishi, K. Amani and T. Sakka, J. Phys. Chem. C 119 (2015) 26506.
[3] C.-Y. Shih, C. Wu, M. V. Shugaev and L. V. Zhigilei, J. Coll. Interf. Sci. 489 (2017) 3.

Figure 1

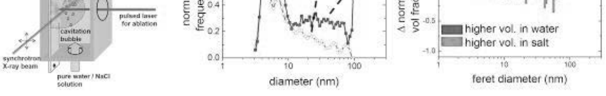

S08-04

In situ/operando powder X-ray diffraction investigations during heterogeneous catalysis of the partial oxidation of acrolein

J. Steffan[1], K. Hofmann[1], S. Knoche[1], H. Vogel[1], B. Albert[1]
[1]Technische Universität Darmstadt, Fachbereich Chemie, Darmstadt, Germany

Cesium salts of vanadium-substituted heteropolyacids with Keggin anions can be used in heterogeneous catalysis to partially oxidize methacrolein or acrolein. There is no detailed knowledge on how the catalyst interacts with the organic molecules and how it is changed during the reaction. To complement other methods that focus on the surface of the catalyst, we designed a set-up to investigate the bulk of a solid catalyst via powder diffraction. The aim was to elucidate how the inorganic substance changes during the oxidation reaction. Acrolein vapour was led through a reaction chamber at the diffractometer. A catalyst of the nominal composition $Cs_2H_2[VPMo_{11}O_{40}]$ was investigated at varying conditions (temperature, water pressure, reaction time). The in situ/operando experiments reveal how the occupation of the different sites reversibly changes during the reaction. The oxygen content of the catalyst was monitored and new conclusions concerning the reaction mechanism were drawn.

Figure 1

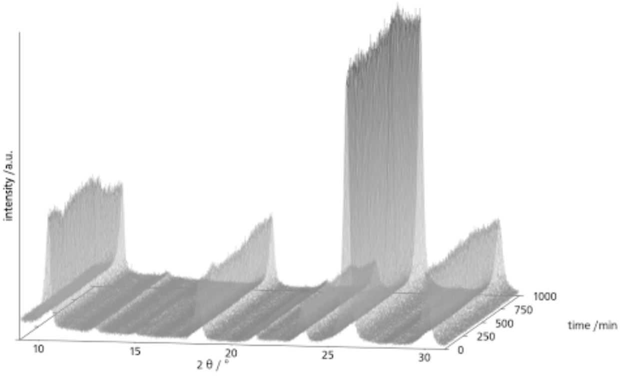

S08-05

New developments using the "in situ" crystallization with a CO2-laser

J. Benet-Buchholz[1], E. C. Escudero-Adán[1], R. Boese[2]
[1]Catalan Institute of Chemical Research ICIQ, X-ray Diffraction Unit, Tarragona, Spain
[2]SciConsult,, Essen, Germany

The "in situ" crystallization method applying a CO2-laser (OHCD-Laser System) has allowed the crystallization and structure determination of several compounds which are difficult to achieve in crystalline form under standard conditions. [1] Main point of such experiments is that the samples under investigation generally need to have a melting point allowing its crystallization when using the "in situ" methodology. The standard procedure to obtain single crystals is to apply a repetitive melting zone, which allows to obtain a high quality cylindrical single crystal filling a part of a quartz capillary. The latest state-of-the-art diffractometers allow obtaining high resolution data (suitable for charge density studies) of excellent quality based on the cylindrical crystal generated in capillaries. As example the charge density studies of toluene is presented.

In order to avoid the known limitations requiring a single-component sample with a sharp melting point, a series of new methodologies have been developed allowing the crystallization of new types of samples. A useful approach to crystallize samples with no sharp melting point or samples which exhibit solid-solid phase transitions, is adding a solvent to the sample in the capillary where the crystallization procedure is performed. As an example the structure of the ordered low temperature phase of cyclopentane obtained by "in situ" crystallization at -181 ºC (solvent: 1-pentene, 30 %) is presented. [2]

The previous procedure can be combined with the addition of crystal seeds, polymers or other compounds. In this case, the capillary used for obtaining the single crystals can be considered as a small crystallization reactor in which different actions, normally applied at laboratory scale, can be performed. For example, the capillary can be filled with mixtures of compounds with the intention to form co-crystals or crystals originating from chemical reactions. The described methodologies are of special interest in the crystallization of polymorphs, salts and co-crystals of pharmaceutical compounds. As example for the application of the developed methodologies, the "in situ" co-crystallization and structure determination of pharmaceutical compound is shown.

References

[1] Boese, R. (2014). *Z. Kristallogr*. **229(9)**, 595.
[2] Torrisi A. et al. (2008). *J. Phys. Chem. B*, **112(12)**, 3746–3758.

Image of a capillary showing the process of seeding of an equimolar mixture of Ibuprofen and Nicotinamide.

Figure 1

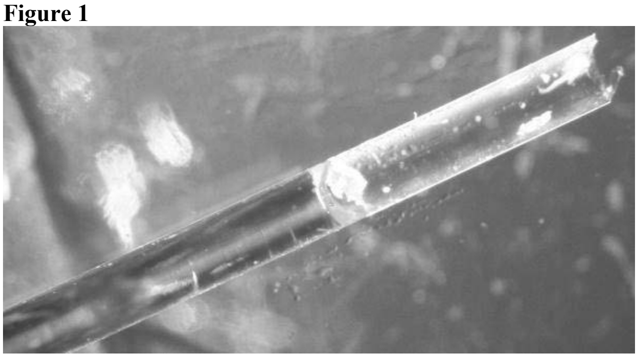

Bio-Crystallography III: Enzymes

S09-02

Structural studies on the substrate and cofactor binding mode of FAD-dependent monooxygenases

J. Kratky[1], R. H. Weiße[1], T. Heine[2], D. Tischler[2], N. Sträter[1]
[1] Leipzig University, Institute of Bioanalytical Chemistry, Leipzig, Germany
[2] Technische Universität Bergakademie Freiberg, Environmental Microbiology, Freiberg, Germany

Introduction and Objectives

Styrene monooxygenases (SMOs) catalyze the enantioselective epoxidation of styrene and structurally related compounds. They are of interest for the development of new biocatalytical production processes for pharmaceuticals and fine chemicals. Our aim is to improve the substrate specificity and enantioselectivity of SMO for such applications. An important step to reach this goal is the use of crystallography to get detailed insight into the binding mode of the substrates and cofactor FADH2.

Substrate epoxidation requires FADH2, provided by an NADH-flavin oxidoreductase component [1]. We used FAD and different substrates for cocrystallization. Crystal structures of the SMO StyA1 in the absence and presence of FAD revealed conformational changes involved in cofactor binding. We will report on challenges in the analysis of the substrate binding mode and our approaches to overcome these problems.

Material and Methods

Diffraction data sets from single crystals of wildtype StyA1 and mutants were collected at the Bessy II beamlines 14.1 and 14.2.

Results

Co-crystallisation of StyA1 with FAD revealed that the occupancy for this cofactor is around 90 %. Based on our results we propose that a chain flip is related to the cofactor binding. First insights into the substrate binding mechanism of SMOs were achieved by co-crystallisation with different substrates like methyl phenyl sulfoxide. For the first time the function of the substrate tunnel and gatekeeper Phe192 could be demonstrated.

Conclusion

Crystallisation studies under anaerobic conditions with FADH2 will be performed to hopefully overcome the low cofactor binding affinity. Different mutations of the gatekeeper were established to create an open binding pocket, which should lead to a free substrate movement from the tunnel into the pocket as well as an increase in activity.

Figure Legends

Figure 1. Binding mode of FAD to StyA1. The 1.8 Å (2mFobs – DFcalc, αcalc) electron density map is shown for FAD and some water molecules at a contour level of 1.0 σ.

References

[1] D. Tischler, R. Kermer, J. A. D. Gröning, S. R. Kaschabek, W. J. H. van Berkel, M. Schlömann (2010): StyA1 and StyA2B from Rhodococcus opacus 1CP. A multifunctional styrene monooxygenase system. In: *Journal of bacteriology* **192** (**19**), pp. 5220–5227

Figure 1

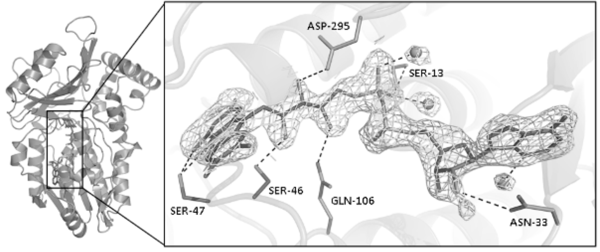

S09-03

Structural and mechanistic investigations on AmbDH3, a bifunctional dehydratase-cyclase domain in ambruticin biosynthesis

K. H. Sung[1], G. Berkhan[2,3], T. Hollmann[2], L. Wagner[2], W. Blankenfeldt[1,4], F. Hahn[2,3]
[1] Helmholtz Centre for Infection Research, Structure and Function of Proteins, Braunschweig, Germany
[2] University of Bayreuth, Fakultät für Biologie, Chemie und Geowissenschaften, Bayreuth, Germany
[3] Leibniz Universität Hannover, Centre for Biomolecular Drug Research (BMWZ), Hannover, Germany
[4] Technische Universität Braunschweig, Institute of Biochemistry, Biotechnology and Bioinformatics, Braunschweig, Germany

Introduction

Hydropyran rings are a common structural motif of reduced polyketides and contribute significantly to their biological activity. However, the mechanism of their biosynthetic formation is not well understood. Ambruticins are antifungal polyketides produced by Myxobacteriales and of interest as lead structures for the development of antifungal agents. Structurally, ambruticins consist of a tetrahydropyranyl ring, a dihydoropyranyl ring and a divinyl cyclopropane ring. They are synthesized by type I polyketide synthase (PKS) containing acyl carrier protein (ACP), ketosynthase (KS), acyltransferase (AT), ketoreductase (KR) and dehydratase (DH) domains. Interestingly, the DH domain of PKS module 3 (AmbDH3) catalyzes both the dehydration and cyclization reactions within the ambruticin biosynthesis [1], but the mechanism behind this dual activity has not been well studied yet. High-resolution structural data is required in order to obtain detailed insight into the mechanism of this bifunctional DH domain.

Methods

The AmbDH3 domain from *Sorangium cellulosum* was overexpressed in *E. coli*, purified to homogeneity and crystallized using sitting drop vapor diffusion. The crystal structure was solved by molecular replacement. In addition, wild-type AmbDH3 and mutants (V173Y, V173A, V173H, V173L) AmbDH3 were used for *in vitro* activity assays.

Results

The crystal structure of AmbDH3 was determined at a resolution of 1.17 Å. It shows the conserved "double hotdog" fold of monofunctional DH domains found in cis-AT PKSs. The structure shows that the conserved catalytic dyad consisting of H51 and D215 catalyzes a dehydration reaction, similar to monofunctional DH domains. In addition, V173 of AmbDH3 seems to be a diagnostic residue for catalysis of the cyclization step, which was reflected by the results of the *in vitro* assay [2].

Conclusions

Our results significantly improve the understanding of the unusual bifunctionality of AmbDH3, and how dehydration and cyclization activities are combined in a single PKS domain. Furthermore, this study lays the groundwork for the development of improved chemoenzymatic syntheses of polyketides and similar natural products containing pyran rings.

References

[1] G. Berkhan, F. Hahn, *ANGEWANDTE CHEMIE INTERNATIONAL EDITION*, **53**, (2014), 14240.
[2] K. H. Sung, G. Berkhan, T. Hollmann, L. Wagner, W. Blankenfeldt, F. Hahn, *ANGEWANDTE CHEMIE INTERNATIONAL EDITION*, 10.1002/anie.201707774.

S09-04

Structural Basis of Regioselectivity Verified by the Structure of the Tryptophan 6-Halogenase Thal.

A. C. Moritzer[1], H. Minges[2], C. Schnepel[2], M. Frese[2], N. Sewald[2], H. Niemann[1]
[1]Universität Bielefeld, Fakultät für Chemie, Strukturbiochemie, Bielefeld, Germany
[2]Universität Bielefeld, Fakultät für Chemie, Bioorganische Chemie, Bielefeld, Germany

Flavin dependent halogenases introduce regio specific halogen substituents into the indole ring, which requires FADH2, a halide ion (Cl- or Br-) and O2. Therefore, halogenases are potentially useful biocatalysts for pharmaceutically relevant natural products like the antibiotics vancomycin and chloramphenicol or the anticancer agent rebeccamycin.

So far, the mechanism of regioselectivity is not fully understood. The crystal structures of tryptophan 7- and 5-halogenases bound to their substrate tryptophan were compared. This led to the hypothesis, that the regioselectivity depends on the orientation of tryptophan within the substrate binding site relative to the catalytic amino acids. But up to now, no crystal structure of a tryptophan 6-halogenase bound to its substrate tryptophan has been determined. We report the crystal structure of the tryptophan 6-halogenase Thal with its substrate tryptophan, and the co-factor FAD. The tryptophan in the substrate binding site is rotated in such a way that its C6 position is presented to the catalytic lysine and glutamate residues and, therefore, adopts the same position as the C5 of tryptophan bound to the tryptophan 5-halogenase PyrH and the C7 of tryptophan bound to the tryptophan 7-halogenase PrnA within 0.17 Å and 0.36 Å, respectively.

Within the tryptophan binding site of Thal five amino acids differ to the tryptophan binding site of the tryptophan 7-halogenase RebH. Mutation of these five amino acids in Thal to the sequence of RebH lead to a complete switch from C6 to C7-tryptophan regioselectivity.

Our data verified the hypothesis, that the regioselectivity of tryptophan halogenases is dependent on the orientation of tryptophan within the substrate binding site.

Figure 1

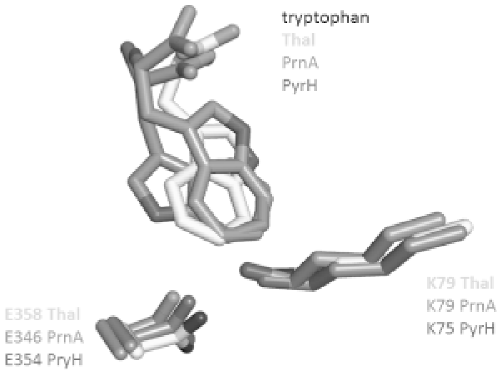

Electron microscopy

S10-01

Elastic and Inelastic Contributions in Electron Diffraction

T. Gorelik[1]
[1]Universität Ulm, Central fascility for Electron Microscopy, Ulm, Germany

Electron diffraction is an attractive method for structure analysis. Numerous examples illustrate the cases when electron diffraction was the only method able to resolve the structure of a material. The interaction of electrons with matter is a complex process resulting in various events, which can be grouped into processes preserving the energy of the incident electrons - elastic scattering, and processes with the loss of energy - inelastic scattering.

The inelastic scattering mainly contributes to the *background* in electron diffraction patterns, therefore can relatively simply be subtracted from Bragg peaks, thus, in principle, not affecting reflections intensity data for structure analysis.

The situation is different for total scattering - here, the whole available range of the scattering angle is used. As a result, there is an unknown contribution of the inelastic scattering in the pair Distribution Function (PDF) of the sample. Generally filtered diffraction data shows better results in PDF analysis [1].

Our aim, however, is not to promote the use of energy filters in PDF analysis, but the deep understanding of the contribution of the inelastic scattering to the electron total scattering data. We present a systematic study of the contribution of the inelastic scattering component in electron diffraction patterns depending on the electron energy and specimen thickens. We correlate the experimental data with the calculated elastic and inelastic cross sections. Finally, the inelastic scattering is the primary reason for the radiation damage in molecular materials. We study the inelastic component in the diffraction of molecular thin films and correlate that with the stability of the films at different electron energies.

References

[1] D. J. H. Cockayne and D. R. McKenzie (1988). Acta Cryst. A44, 870-878.

S10-02

A detailed in-situ and ex-situ TEM study of the carbonization process of electrospun PAN derived fibres

R. Schierholz[1], D. Kröger[1], M. Gocyla[2], H. Tempel[1], H. Kungl[1], R. Eichel[1]
[1]Forschungszentrum Jülich GmbH, Institut für Energie und Klimaforschung, Jülich, Germany
[2]Forschungszentrum Jülich GmbH, Ernst Ruska-Centre and Peter Grünberg Institute, Jülich, Germany

The increasing demand on energy storage for stationary and mobile applications also increases the need for cost-effective alternatives to present Li-ion batteries. Metal air batteries are a promising alternative and can also provide high specific energy density as no storage material is needed on the cathode side [1]. For this application highly porous carbon fiber mats are excellent candidates because those allow the wetting by electrolyte, provide high surface area, are catalytically active for the oxygen reduction reaction and can also serve as supporting material for other catalysts. A suitable and cost-effective route to fabricate nanofibers for energy conversion is electrospinning [2]. Here we apply this method to spin fiber mats of polyacrylnitrile (PAN) which are subsequently carbonized. Before carbonization the as spun fibers are dried at 200 °C and oxidatively stabilized at 250 °C, which is important for the subsequent carbonization process [3]. We studied the fibres ex situ after several carbonization temperatures by transmission electron microscopy (TEM), electron diffraction and spectroscopic methods Electron energy loss spectroscopy and energy dispersive X-ray spectroscopy (EDX), to follow the degree of carbonization and the change in chemical composition. We complete the work with in situ experiments based on MEMS in situ TEM holders (DENSsolutions heating holder). First of all the shrinkage in diameter can be observed on the identical fiber as shown in Figure 1. HRTEM and diffraction reveal increasing ordering of the initially amorphous carbonous structure with temperature. The increasing carbonization can also be traced by the evolution of the plasmon peaks and EELS and EDX allow the quantification of the amount of nitrogen and oxygen in the fibres at each step. Our findings help to understand the carbonization process of PAN fibers and enable the optimization of process parameters towards the application as cathode sheets in metal-air batteries.

Figure 1: TEM images of the same fiber in the uncarbonized state (top) at 100 °C in the TEM and (bottom) after heat treatment up to 1300 °C.

References

[1] J. Christensen *et al. Journal of The Electrochemical Society*, **159** (2) (2012), R1-R30

[2] B. Ding and J. Yu Electrospun nanofibres for Energy and Environmental Applications **ISBN:** 9783642541605

[3] E. Fitzer *et al. Carbon* **13**, 1 (1975), 63

Figure 1

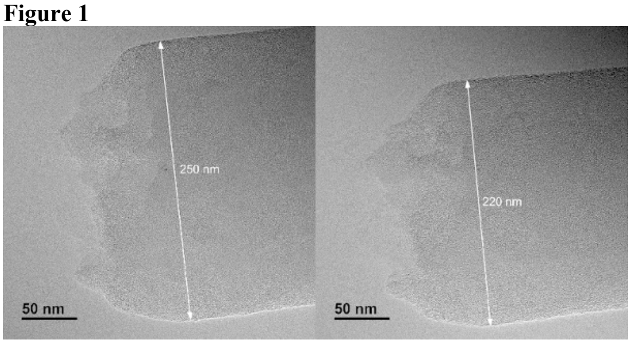

S10-03

Cation disorder in $\mathrm{Ca_{1-x}Li_xAl_{1-x}Ge_{1+x}N_3}$ ($x \approx 0.2$) by STEM-HAADF

L. Eisenburger[1,2], J. Häusler[2], W. Schnick[2], O. Oeckler[1]
[1]Leipzig University, IMKM, Leipzig, Germany
[2]Ludwig-Maximilians-Universität München, Department of Chemistry, München, Germany

Only few nitridogermanates have been discovered and fully characterized including their physical properties. DFT (GGA, HSE) calculations, however, predict interesting optical and electronic properties for this class of compounds. [1] Their lack of thermal stability impedes conventional high-temperature synthesis. Therefore, ammonothermal synthesis represents an intriguing low-temperature approach.

$\mathrm{Ca_{1-x}Li_xAl_{1-x}Ge_{1+x}N_3}$ ($x \approx 0.2$) was obtained from $\mathrm{Ca_3Al_3Ge_2}$ and Li by ammonothermal synthesis. It exhibits an orthorhombic wurtzite type superstructure that was refined using the Rietveld method (space group $Cmc2_1$, a = 9.982, b = 5.776, c = 5.148 Å, Rp = 0.0365, Rwp = 0.0492). The compound is isostructural to $\mathrm{CaAlSiN_3}$.[2] However, EDX and ICP showed a Ge / Al ratio larger than one. Possible ordering of Al and Ge was investigated by means of electron diffraction and Z-contrast imaging (STEM-HAADF). SAED patterns show the superstructure reflections expected from the structure model of $\mathrm{Ca_{1-x}Li_xAl_{1-x}Ge_{1+x}N_3}$. STEM-HAADF along [110] is suitable to differentiate between Ca, Al and Ge columns by *Z*-contrast. The corresponding intensities were compared with three different structure models of $\mathrm{Ca_{1-x}Li_xAl_{1-x}Ge_{1+x}N_3}$ in *translationengleiche* subgroups of $Cmc2_1$ (i.e. $Cm11$, $C1c1$ and $C112_1$). In all models, Al and Ge columns would be clearly separated in projections along [110], resulting in three different intensity profiles along representative lines. The absence of such intensity distributions in favor of a uniform one confirms the absence of cation ordering.

The crystal structure of $Ca_{1-x}Li_xAl_{1-x}Ge_{1+x}N_3$ corresponds to a solid solution between $LiGe_2N_3$ and hypothetical $CaAlGeN_3$.[3] Li / Ca and Al / Ge are disordered on two different Wyckoff positions and coordinated by five and four N atoms, respectively. The three-dimensionally extended network of *sechser* rings is built up from vertex-sharing $(Al/Ge)N_4$ tetrahedra. The compound is stable up to 1000 K.

References

[1] Z.-H. Cai, P. Narang, H. A. Atwater, S. Chen, C.-G. Duan, Z.-Q. Zhu, J.-H. Chu, *Chem. Mater.* **2015**, *27*, 7757-7764.

[2] K. Uheda, N. Hirosaki, Y. Yamamoto, A. Naito, T. Nakajima, H. Yamamoto, *Electrochem. Solid-State Lett.* **2006**, *9*, H22-H25.

[3] J. David, J. P. Charlot, J. Lang, *Rev. Chim. Miner.* **1974**, *11*, 405.

S10-04

TEM-based analysis of the crystal structure of a Ge-rich layer sandwiched between spintronic Fe_3Si

H. Kirmse[1], B. Jenichen[2], E. Willinger[3], X. Huang[3], B. Haas[1], C. T. Koch[1]
[1]Humboldt-Universität zu Berlin, Institut für Physik, Berlin, Germany
[2]Paul-Drude-Institut, Berlin, Germany
[3]Fritz-Haber-Institut, Berlin, Germany

Introduction

The magnetic properties of Fe_3Si make it an excellent candidate for spintronic applications [1]. For a switchable device, two layers of Fe_3Si have to be separated by a thin semiconducting interlayer. Ge was chosen for this interlayer having a nominal thickness of 3 nm only. Sharp interfaces were ensured by solid phase epitaxy [2] which is a two-step approach comprising of layer deposition at 150 °C and recrystallization at 300 °C. From bulk crystals Fm3m space group is expected for Fe_3Si and Fd3m for Ge [3].

Objectives

This work aims at both, crystal structure and composition analysis of the layer stack by transmission electron microscopy (TEM)-based techniques. In particular, nano-beam diffraction (NBD), high-angle annular dark-field atomic-resolution scanning TEM (HAADF ARSTEM) imaging and energy dispersive X-ray spectroscopy (EDXS) were applied for full crystallographic phase analysis.

Results

The generated crystallographic phase of Fe_3Si perfectly corresponds to both, the expected crystal structure and the chemical composition. In contrast to that, superstructure reflections along [001] are observed for the Ge layer. This hints to an ordering along [001]. Moreover, EDXS revealed a composition ratio of about 6:3:1 for Ge:Fe:Si. Both results point to an unexpected crystallographic phase of the interlayer. For gaining real space information, HAADF ARSTEM imaging was performed along [100] and [110] direction (see Fig. 1). Bright spots correspond to atomic columns. The brightness depends on the mean atomic number of the individual column. Both projections consistently reveal ordering along [001]. Brighter spots are dedicated to Ge and weaker spots to Fe columns. Filled interlayers exhibit a larger distance along [001] of $z = 0.52$ compared to $z = 0.48$ for the empty layers.

Conclusion

The semiconductor interlayer is composed of P4mm Ge_2Fe (see Fig. 1 left). The deviation of the position of the atomic columns from the ideal positions at 0.50 and 0.75 is most likely due to the relaxation of strain introduced by the ordering.

References

[1] K. Hamaya et al., Appl. Phys. **113** (2013) 183713.

[2] S. Gaucher et al., Appl. Phys. Lett. **110** (2017) 102103.

[3] B. Jenichen et al., Phys. Stat. Sol. A **206** (2009) 1740.

Fig. 1: Unit cell of Ge_2Fe (left) and HAADF ARSTEM images of the structure along [100] (center) and [110] (right).

Figure 1

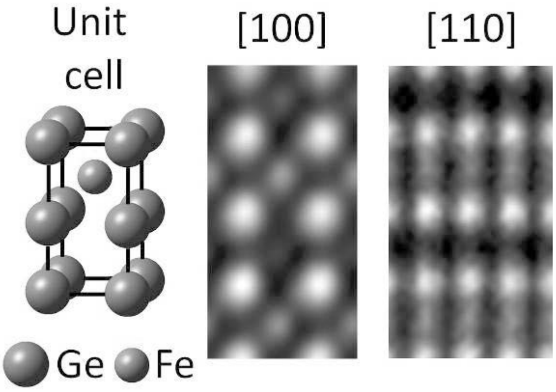

S10-05

Thermal stability of porous iridium nanoparticles by in situ tem heating

K. Loza[1], K. Pappert[1], M. Heggen[2], M. Epple[1]
[1]Universität Duisburg-Essen, Institut für Anorganische Chemie, Essen, Germany
[2]Forschungszentrum Jülich GmbH, Ernst Ruska-Centre and Peter Grünberg Institute, Jülich, Germany

Iridium (Ir) is an important transition-metal catalyst which is used for the catalytic hydrogenation of alkenes, aldehydes and ketones (1,2). Furthermore, Ir-based materials were also studied as anode and cathode electrocatalysts in fuel cells (3,4). The variation of the nanoparticle shape or composition may further increase the Ir mass activity for an efficient oxygen evolution reaction. Herein, we report a wet-chemical synthesis of colloidally dispersed porous iridium nanoparticles with a particle size of a few nanometers. High-resolution transmission electron microscopy (HRTEM) and energy-dispersive X-ray analysis (EDX) measurements were carried out to characterize the morphology, crystal structure and composition of these nanoparticles. The thermal stability was examined by in-situ TEM heating. The work provides a microscopic insight into thermal behavior of porous iridium nanoparticles.

References

[1] J. Dupont, G. S. Fonseca, A. P. Umpierre, P. F. P. Fichtner and S. R. Teixeira, J. Am. Chem. Soc., 2002, 124, 4228-4229.

[2] G. S. Fonseca, A. P. Umpierre, P. F. P. Fichtner, S. R. Teixeira and J. Dupont, Chem. Eur. J., 2003, 9, 3263-3269.

[3] K. Fatih, V. Neburchilov, V. Alzate, R. Neagu and H. Wang, J. Power Sources, 2010, 195, 7168-7175.

[4] T. Ioroi and K. Yasuda, J. Electrochem. Soc., 2005, 152, A1917-A1924.

S10-06

REM and EDX analysis of micro-structured sacrificial anode samples used to combat bacterial adhesion and growth

P. Bellova[1], S. Memar Javid[2], Y. Motemani[2], M. Köller[1], T. A. Schildhauer[1], A. El Arrassi[3], K. Tschulik[3], A. Ludwig[2]
[1]BG Clinic Bergmannsheil Bochum, Surgical Research, Bochum, Germany
[2]Institute for Materials, Faculty of Mechanical Engineering, Bochum, Germany
[3]Micro- and Nano- Electrochemisty and Center for Electrochemical Sciences (CES), Faculty of Chemistry and Biochemistry, Bochum, Germany

Introduction

In recent years, various prevention strategies have been proposed with regard to implant associated infections. An innovative approach consists of micro-structured sacrificial anode samples creating an electrical current of antibacterially active silver ions. Surprisingly, the most potent sacrificial anode pair was found for the combination of silver with iridium (Köller et al. 2017). In this study, electrochemical as well as REM analysis of the samples were undertaken in order to better understand the processes behind the findings

Methods

Bacterial tests with *S. aureus* strains were conducted using a drop-based set up: after incubation, drop fluid was aspirated, diluted and plated for colony counting. Bacterial adherence to the test samples was identified by fluorescence staining.

In order to determine silver ion release, samples were immersed in AMPUWA water for 7 days and subsequently AAS analysis of the supernatants was performed. The samples, after being dried and adequately prepared, were analyzed by SEM (LEO 1530 VP) and EDX elemental mapping analysis was performed. SEM micrographs were also taken of samples which had previously been tested with bacteria (*S. aureus*) Additionally, LSV (linear sweep voltammetry) of the samples was performed before and after immersion

Results

The high antibacterial potential of the iridium-silver sacrificial anode combination could be confirmed by SEM, AAS and LSV findings. SEM-wise, a higher amount of pit corrosion on silver dots could be found, indicating silver ions release- when compared to the other sacrificial anode pairings. According to this finding, the difference in dissolution capacity could be linked to the occurrence of sparingly soluble silver salts, which form a passivation layer, inhibiting the further release of silver ions into the solution (El Arrassi et al. 2017). The latter was a phenomenon primarily observed with platinum and palladium samples, but to a much lesser extent with iridium samples. Indeed, silver salts of different types could be detected in samples that had been previously used for antibacterial and cytocompatibility tests

Discussion

Understanding the dynamics behind the sacrificial anode effects of different metal combinations, the systems can be optimized in order to provide the best possible antibacterial effect while not compromising human tissue.

Figure 1

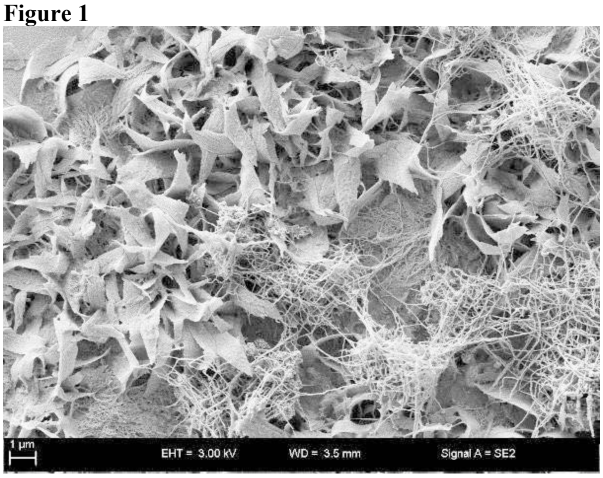

Experimental electron density

S11-01

Charge and spin density in position and momentum space, density matrices, wave functions and energies of periodic systems, from theory or experiments. In one word: Quantum Crystallography

P. Macchi[1]
[1]University of Bern, Chemistry and Biochemistry, Bern, Switzerland

Since the beginning of the quantum era, quantum mechanics and crystallography form an entangled system. The first X-ray diffraction measurements disclosed the structures of solids and molecules, which led to the modern theories on chemical bonding.
This tight interplay concerned not only atomic structures, but also electronic structures of solids, because the X-rays may visualize the accurate distribution of electrons around atoms and the correlation among them. Other radiations (like neutrons) map the spin of electrons. All functions (electron densities, density matrices and wave functions) are representable in position or in momentum space.
These kinds of theoretical and experimental studies are at the heart of the growing field called Quantum Crystallography. Although initially defined by Massa et al. (1999) only for calculations of wave function or density matrices from crystal X-ray diffraction experiments, a broader definition enables to include a large variety of well-established experimental modeling, theoretical calculations and mixed experimental/theoretical modelling (see also Grabowsky *et al.* (2017); Tsirelson (2017) and Genoni *et al.* (2018)).
As for all crystallography, the objects of study are crystalline materials, with two distinct purposes:
a) Investigating properties of condensed matter, in periodically homogeneous systems
b) Using the magnifying effect of a periodic arrangement to visualize fine molecular features
As for quantum mechanics, the paradigm of Quantum crystallography is the probabilistic description of electron distribution and movement, by means of a wave function, its one- or two-electron densities, its density matrices etc. Because electrons possess an intrinsic angular momentum, spin polarized wave functions and densities are necessary. Moreover, all the functions can be represent in momentum or position space.

References

Massa, L. Huang, J. Karle, *Int. J. Quantum Chem.: Quantum Chem. Symp.* **1995**, *29*, 372-384 Grabowsky, A. Genoni, H.-B. Bürgi, *Chem. Sci.* **2017**, *8*, 4159-4176
Tsirelson, *J. Comput. Chem.* **2017**, in the press, DOI: 10.1002/jcc.24893
Genoni, L. Bučinský, N. Claiser, J. Contreras-García, B. Dittrich, P. M. Dominiak, E.Espinosa, C. Gatti, P. Giannozzi, J.-M. Gillet, D. Jayatilaka, P. Macchi, A. Ø. Madsen, L. J. Massa, C. F. Matta, K. M. Merz,P. N. H. Nakashima, H. Ott,, U. Ryde, K. Schwarz, M. Sierka, S. Grabowsky *Chemistry*, **2018**, in the press.

S11-02

Quantum Crystallography: original definition and connections to current research developments

A. Genoni[1]
[1]CNRS and University of Lorraine, Laboratory of Theoretical Physics and Chemistry, Metz, France

In the last few years, discussions around the topic "Quantum Crystallography" started intensifying and heating. This is testified by recent reviews,[1] viewpoint papers,[2] workshops (CECAM Discussion meeting in June 2017: https://qcrystcecam.weebly.com) and future schools dedicated to the subject (e.g., International Erice School in June 2018:
http://crystalerice.org/2018/programme_qc.php).
Although debates on the exact meaning and content of Quantum Crystallography are currently underway among main experts in the field,[2] the "original definition" of Quantum Crystallography dates back to 1990s[3,4] when Massa, Karle and Huang proposed the term to indicate a group of strategies characterized by a simultaneous and strict interplay of the information deriving both from quantum mechanical calculations and crystallographic experiments. The "original definition" actually consists of two main streams: *i)* the *direct definition*,[3] which comprises techniques where the information resulting from the traditional Quantum Chemistry calculations is enhanced by external information intrinsically contained in the experimental crystallographic data, and *ii)* the *converse definition*,[4] which encompasses all those integrated methods that aim at improving crystal structure models with information obtained from tailor-made quantum mechanical computations on the systems under exam.

In this presentation the "original definition" of Quantum Crystallography will be presented in detail, by particularly showing examples of modern techniques (e.g., X-ray constrained wave function approach[5] and Hirshfeld Atom Refinement[6]) that fully belong to it. Furthermore, connections with a future and possibly extended definition of Quantum Crystallography will be also discussed.

References

[1] S. Grabowsky, A. Genoni, H.-B. Bürgi, *Chem. Sci.* **8**, 4159-4176 (2017).
[2] A. Genoni, L. Bučinský, N. Claiser, J. Contreras-García, B. Dittrich, P. M. Dominiak, E. Espinosa, C. Gatti, P. Giannozzi, J.-M. Gillet, D. Jayatilaka, P. Macchi, A. Ø. Madsen, L. J. Massa, C. F. Matta, K. M. Merz, Jr., P. N. H. Nakashima, H. Ott, U. Ryde, K. Schwarz, M. Sierka, S. Grabowsky, *Chem. Eur. J.*, submitted.
[3] L. Massa, L. Huang, J. Karle, *Int. J. Quantum Chem.: Quantum Chem. Symp.* **29**, 372-384 (1995).
[4] L. Huang, L. Massa and J. Karle, *Int. J. Quantum Chem.* **73**, 439-450 (1999).
[5] D. Jayatilaka, *Phys. Rev. Lett.* **80**, 798−801 (1998).
[6] D. Jayatilaka, B. Dittrich, *Acta Cryst. A* **64**, 383- 393 (2008).

S11-03

Accurate treatment of hydrogen atoms using quantum crystallographic techniques

L. A. Malaspina[1], S. Grabowsky[1]
[1]University Bremen, Institut für Anorganische Chemie und Kristallographie, Bremen, Germany

Determining the location of hydrogen atoms as well as their atomic displacement parameters only from X-ray diffraction data is still a challenge. This is due to several factors, which includes lack of available simple methods/software and the nature of the X-ray diffraction experiment itself.

The most widely used model nowadays for structure refinement is the Independent Atom Model (IAM) due to its simplicity, speed/cost and reliability. In the IAM, atoms are considered to be spherical and non-interacting. Consequently, H atom positions (and bond lengths) derived from X-ray IAM are questionable.

The use of more advanced models for structure refinement which include asphericity shifts for atoms in molecules significantly improve the X-H bond lengths compared to those obtained using the regular IAM. [1, 2, 3]

In this work we discuss how to obtain H atom parameters that are comparable to those obtained from neutron data using Hirshfeld Atom Refinement (HAR, [4, 5]) on X-ray data. We will show how HAR uses tailor-made aspherical atomic scattering factors from molecular wavefunction calculations in a regular least-squares refinement procedure and finally compare and discuss different kinds of HAR results based on different approaches of obtaining H atoms ADPs. [6, 7, 8]

Applications to hydrogen atoms in unusual bonding situations will be discussed, e.g. in hydrogen maleates. These results were obtained using high-resolution low-temperature synchrotron X-ray diffraction data and aspherical atomic scattering factors calculated on the fly during the refinement at the HF/def2-TZVP level of theory where the molecule is embedded self-consistently in its own charges and dipoles within a radius of 8 Å.

HAR is now interfaced to the widely used software Olex2 and includes the description of anharmonic motions as a new feature. We will demonstrate how HAR could be routinely used in crystallography in the future.

References

[1] M. Woińska, et.al., *Sci. Adv.*, **2**, e1600192, (2016).
[2] M. Woińska, et.al., *Acta Crystallogr. A*, **70**, 483-498, (2014).
[3] L. A. Malaspina, et.al., *Cryst. Growth Des.*, **17**, 3812-3825, (2017).
[4] D. Jayatilaka and B. Dittrich, *Acta Crystallogr. A*, **64**, 383-393, (2008).
[5] S. C. Capelli, et. al., *IUCrJ*, **1**, 361-379, (2014).
[6] A. Ø. Madsen und A. A. Hoser, *J. Appl. Cryst.*, **47**, 2100-2104, (2014).
[7] A. Ø. Madsen, *J. Appl. Cryst.*, **39**, 757-758, (2006).
[8] B. Dittrich, *et.al., Chem. Eur. J.*, **23**, 4605-4614, (2017).

S11-04

Validation of experimental charge density refinement strategies

R. Herbst-Irmer[1], L. Krause[2], D. Stalke[1]
[1]Georg-August Universität Göttingen, Institut für Anorganische Chemie, Göttingen, Germany
[2]Aarhus University, Department of Chemistry, Aarhus, Denmark

Modern experimental charge density investigations require the most accurate data, the highest possible resolution and an optimized refinement strategy. As stated in the *XD2006* manual the complexity of the model should be increased in a stepwise manner and the final data-to-parameter ratio should not fall below a value of 10. However, following these guidelines does not guarantee a reasonable model or, more precisely, all refined parameters to be reasonable. Common criteria such as residuals of the linear least squares refinement tend to decrease with increasing number of parameters. The statistical method of cross-validation helps to decide whether the addition of parameters increases model quality or introduces bias. This method is well established in macromolecular crystallography, known as the *R*free concept [1]. A fraction of the measured data is excluded from the refinement process and residuals are calculated against the unused data.
In charge density investigations there are two concerns that need to be addressed: Firstly, the changes in R-values are small compared to the precision of the *R*free value. Secondly, the omission of particular reflections can introduce severe bias to the model. Therefore, *k*-fold cross-validation is utilized. The data set is divided into *k* subsets. One set acts as validation set, while the remaining sets determine the model. The refinement is repeated *k* times with each of the subsets serving once as *R*free set [2]. Hence, every single reflection is used for validation. Secondly, the omission of particular reflections may introduce severe bias to the model. This can be monitored by an inspection of the parameter distribution of the *k* refinements, which can additionally be used for further error diagnostics, e.g. to detect erroneously defined parameters or incorrectly determined reflections. Visualisation tools show the variation of the parameters. The different refinements also provide rough estimates for the standard deviation of topological parameters [3]. This approach is automated for charge density refinement procedures using the *XD2006* program suite [3].

References

[1] Brünger, A. T. (1992). Nature 355, 472-475.
[2] Paul, A., Kubicki, M., Jelsch, C., Durand, P. & Lecomte, C. (2011). *Acta Cryst.* **B67**, 365-378.
[3] Krause, L., Niepötter, B., Schürmann, C., Stalke, D. & Herbst-Irmer, R. (2017). *IUCrJ*, **4**, 420-430.

S11-05

The electrostatic potential of dynamic charge densities of α-, γ-boron and boron carbide($B_{13}C_2$)

C. B. Hübschle[1], S. van Smaalen[1]
[1]University of Bayreuth, Laboratory of Crystallography, Bayreuth, Germany

Recently we reported a method to compute the electrostatic potential (ESP) of dynamic-charge-density distributions[1]. Such dynamic density distributions can be computed from a multipole refinement using the PRIOR program [2] which is part of the BayMEM suite[3].

We will present the ESP of dynamic charge densities of α-, γ-boron and boron carbide($B_{13}C_2$)[4],[5].
Figure 1: Electrostatic potential of the dynamic charge density of α-boron mapped on a Hirshfeld surface of a icosahedral structure motif.
Regions involved in two electron two center bonds show positive potential values (violet colors). Regions further away from atoms show negative potential values (red colors).

References

[1] C. B. Hubschle. and S. van Smaalen. J. Appl. Cryst. (2017) 50.
[2] S. Mondal, S. J. Prathapa and S. van Smaalen. Acta Crystallogr.(2012) A68 568-581.
[3] L. Palatinus, S. van Smaalen and M. Schneider. Acta Crystallogr.(2003) A59 459-469.
[4] S. Mondal, E. Bykova, S. Dey, S. I. Ali, N. Dubrovinskaia, L. Dubrovinsky, G. Parakhonskiy, S. van Smaalen. Scientific Reports (2016) 6.
[5] S. Mondal, S. van Smaalen, G. Parakhonskiy, S. J. Prathapa, L Noohinejad, E. Bykova, N. Dubrovinskaia, D. Chernyshov, L. Dubrovinsky. Physical Review (2013) B 88 024118.

Figure 1

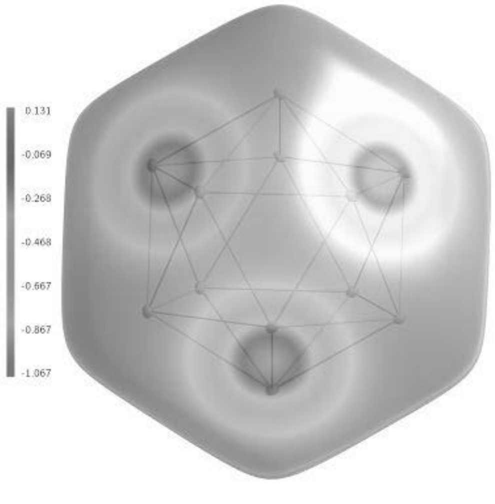

Bio-Crystallography IV: Crystallography in industry

S12-01

Crystal structure of GNIP1Aa, a novel insecticidal protein from *Chromobacterium piscinae*

J. Freigang[1], J. Zaitseva[2]
[1]Bayer AG, Crop Science Division - Research Technologies, Monheim, Germany
[2]Bayer AG, Crop Science Division - Trait Research, Morrisville, United States

Introduction

GNIP1Aa is a novel insecticidal protein with highly selective activity against Western Corn Rootworm (*Diabrotica virgifera virgifera*), one of the most significant pests of corn in the United States. Its sequence shows homology of the N-terminal region to Membrane Attack Complex/Perforin (MACPF) proteins, but the C-terminal region that often is responsible for selectivity in MACPF proteins lacks any similarity to proteins of known structure.

Objectives

We analyzed the crystals structure of GNIP1Aa to understand the molecular details of the insecticidal mode of action and the structural determinants of its remarkable selectivity.

Results

The crystal structure revealed a two-domain architecture of GNIP1Aa: A typical MACPF domain is fused by a flexible linker to a C-terminal domain with a novel fold. The C-terminal domain consists of three similar subdomains that are arranged around a threefold pseudo-axis. Site directed mutagenesis allowed to identify functional important amino acids and putative target recognition sites.

Conclusion

A combination of protein crystallography and site directed mutagenesis demonstrated that the novel C-terminal domain of GNIP1As is the key to its high selectivity, a central feature for its safety.

S12-02

Structure of the Malaria Vaccine Candidate Antigen CyRPA and its Complex with a Parasite Invasion Inhibitory Antibody

P. Favuzza[1,2], G. Pluschke[1], M. G. Rudolph[3]
[1]Swiss Tropical Institute, Molecular Immunology, Basel, Switzerland
[2]The Walter and Eliza Hall Institute of Medical Research, Division of Infection and Immunity, Melbourne, Australia
[3]F. Hoffmann-La Roche Ltd., Chemical Biology, Basel, Switzerland

Malaria is estimated to have caused 214 million clinical cases and 438,000 deaths in 2015. The disease is transmitted by female *Anopheles* mosquitoes and caused by parasitic protozoans of the genus *Plasmodium.* Invasion of erythrocytes by *Plasmodium falciparum* merozoites is a composite process that involves several proteins, among them the **C**ysteine-**R**ich **P**rotective **A**ntigen (CyRPA). Together with the Reticulocyte binding-like Homologous protein 5 (RH5) and the RH5-interacting protein Ripr, CyRPA forms a ternary complex essential for erythrocyte invasion. A structure of CyRPA would delineate surface peptides, against which more potent antibodies could be raised for immunization of patients. Here we present the crystal structure of CyRPA at 2.5 Å and of its complex with the antigen-binding fragment of a parasite growth inhibitory antibody at 4 Å. Phasing of the CyRPA dataset was achieved by placing the Fab in the 4 Å dataset, and then using the unaccounted low-resolution electron density as the "search model" for the CyRPA dataset. CyRPA adopts a 6-bladed β-propeller structure with similarity to the sialidase fold, but possesses no sialidase activity. Thus, CyRPA likely fulfills an adaptor, not an enzymatic function in the ternary complex with RH5 and Ripr. The surface areas recognized by protective antibodies should facilitate design of peptidomimetics that focus the vaccine responses on malaria-protective epitopes. Both, *in vitro* and *in vivo,* anti-CyRPA and anti-RH5 antibodies showed more potent parasite growth inhibitory activity in combination than on their own, supporting a beneficial effect when delivered as a combination of CyRPA and RH5 in vaccines [1].

References

[1] P. Favuzza, E. Guffart, M. Tamborrini, B. Scherer, A. M. Dreyer, A. C. Rufer, J. Erny, J. Hoernschemeyer, R. Thoma, G. Schmid, B. Gsell, A. Lamelas, J. Benz, C. Joseph, H. Matile, G. Pluschke, M. G. Rudolph, Elife 2017, 6.

Figure 2

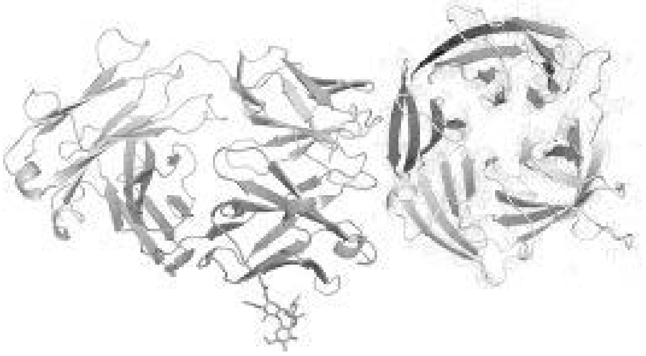

S12-03

GTP Cyclohydrolase I – a target for treating inflammatory and neuropathic pain

Structural Biology, Biophysics and Drug Discovery

H. Nar[1]
[1]Boehringer Ingelheim Pharma GmbH & Co KG, RSG MedChem, Biberach, Germany

GTP Cyclohydrolase I (GTP-CH-I) is a homodecameric protein complex of approximately 250kDa molecular weight.

GTP-CH-I catalyzes the conversion of guanosine triphosphate (GTP) to dihydroneopterin triphosphate (H2NTP). The proposed complex reaction involves the hydrolytic opening of the imidazole ring of GTP and the formation of a formamidopyrimidine intermediate. Release of formate, an Amadori rearrangement of the ribose, and closure of the dihydropyrazine ring affords the product. This reaction is the initiating step in the biosynthesis of tetrahydrobiopterin (BH4) (1).

The function of mammalian GCH1s is regulated by a metabolic sensing mechanism involving a regulator protein, GCH1 feedback regulatory protein (GFRP). GFRP is a pentamer of 9.5kDa subunits whose 6-stranded β-sheet secondary structural elements form a symmetrical five-membered ring similar to β-propellers. GFRP binds to GCH1 to form inhibited or activated complexes dependent on availability of co-factor ligands, BH4 and phenylalanine, respectively.

The BH4 biosynthetic pathway and GCH1 have been identified as promising targets to treat pain disorders in patients (2).

We have studied the structural biology of GCH1 and its regulation by its regulatory protein, GFRP, and, employing biophysical screening methodologies and fragment based screening approaches, we were able to identify chemical starting points to modulate GCH1 function.

References

[1] Nar, H. (2004). GTP cyclohydrolase I, Handbbok of Metalloproteins, John Wiley & Sons Ltd.

[2] Tegeder, I., et al. (2006). "GTP cyclohydrolase and tetrahydrobiopterin regulate pain sensitivity and persistence." Nat Med 12(11): 1269-1277.

Figure 1

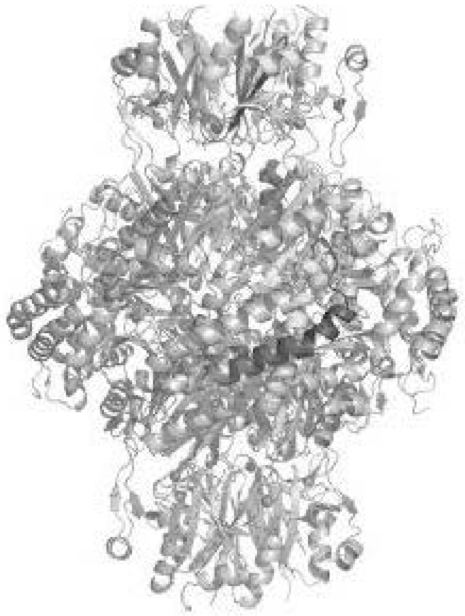

S12-04

Biophysics and Structural Biology in Drug Discovery

R. Hillig[1]

[1]Bayer AG, Structural Biology, Berlin, Germany

Biophysical methods such as the thermal shift assay, isothermal calorimetry, surface plasmon resonance and ligand-observed NMR techniques have become firmly established methods in early drug discovery. Together with structural biology, they enable hit identification via fragment screening and identification of the most promising starting molecules from high-throughput screening hit lists for further optimization. Case studies with relevant oncology targets will be presented.

New crystal structures II

S13-01

New insights in corrosion phenomena of historical art- and craftwork provided by X-ray powder diffraction

S. Bette[1], G. Eggert[2], R. E. Dinnebier[1]
[1]Max-Planck-Institut für Festkörperforschung, X-ray Diffraction, Stuttgart, Germany
[2]State Academy of Arts and Design, Stuttgart, Germany

Introduction

During their storage in museums and collections, historical art- and craftworks are exposed to air, moisture and pollutants like acetic acid, emitted from wooden cabinets, for decades and centuries. This leads to various corrosion phenomena, such as: metal corrosion on the metal-glass interfaces[1] or the growth of efflorescence crystals on the surface of calcareous objects[2]. Corrosion of metal, however, can be used purposefully in order to produce historic pigments, like verdigris, which contains $x\mathrm{Cu(CH_3COO)_2}\cdot y\mathrm{Cu(OH)_2}\cdot z\mathrm{H_2O}$ phases.[3]

Objectives

Profound chemical and structural knowledge on the corrosion products is essential for the development of suitable conservation strategies of historical objects. Both samples from museums and synthesized samples from model experiments were used for the investigations. As corrosion products usually don't occur as single crystals, the crystal structures were solved from XRPD data while employing vibrational spectroscopy, thermal, elemental and EDX analyses and ion chromatography as complementary tools.

Results

$\mathrm{KOH\cdot 2PbCO_3}$ was identified and characterized as one of the products of the corrosion of the lead alloy, induced by the degradation of potash glass, of the lid mounting of a 200 years old beer jug (Fig. 1, a, b).[4] A hitherto unknown efflorescence phase, $\mathrm{Ca_2(CH_3COO)(HCOO)(NO_3)_2\cdot 4H_2O}$, was found on exhibits of 3 different museums (Fig. 1, c, d).[5] Historic verdigris pigments were obtained by chemical synthesis and characterized (Fig. 1, e, f).[6]

Conclusions

The obtained structural and spectral data significantly extent the basis for the identification and the quantitative analysis of the corrosion products and pigments in museums and art collections worldwide.

References

[1] G. Eggert, *Corr. Eng. Sci&Techn.*, 2010, **45**, 414.
[2] L. T. Gibson, et al., *Corrosion Science*, 2010, **52**, 172.
[3] D. A. Scott, et al., *Rev. Conserv.*, 2001, **2**, 73.
[4] S. Bette, et al., *Inorg. Chem.*, 2017, **56**, 5762.
[5] S. Bette, et al., *Corros. Sci.*, 2017, **submitted for publication**.
[6] S. Bette, et al., *Dalton Trans.*, 2017, **in Press**, DOI: 10.1039/C1037DT03288A.

Fig. 1. (a) Glass beer jug (ca. 1800) with corroded lid mounting, (b) motifs in crystal structure of $\mathrm{KOH\cdot 2PbCO_3}$,(c) Attic amphora with white efflorescence crystals, (d) crystal structure of the efflorescence phase, (e) historic vessel containing copper pigments and historic painting © National Gallery London made from copper pigments, (f) crystal of $\mathrm{Cu_3(CH_3COO)_2(OH)_4}$

Figure 1

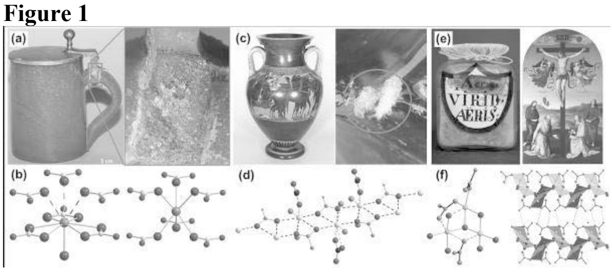

S13-02

Building metal-organic architectures by the design

M. Dakovic[1], M. Borovina[1], C. Aakeroy[2], I. Kodrin[1]
[1]Unviversity of Zagreb, Department of Chemistry, Zagreb, Croatia
[2]Kansas State University, Department of Chemistry, Manhattan, United States

One of the primary challenges of crystal engineering is to deliver solids with a targeted physical property or response. As performance and properties of solid materials can be directly modified by controlling the nature of the 3-D assembly of molecules/ions, the first step towards a targeted property/response requires control over specific structural topologies. Unfortunately, a lack of robust and transferable guidelines for pre-planned synthesis based on non-covalent interactions still stands in the way of predicatable supramolecular assemblies of metal-containing solids.

In this contribution we present our attempts and success in controlling the supramolecular assembly of metal-complexes (of various dimensionalities) via fine-tuning the strength of hydrogen- and halogen-bond donors and acceptors.[1-3] The use of calculated molecular electrostatic potential surfaces for ranking potential donors and acceptors in the system is shown to be a useful method for achieveing the desired supramolecular outcome.

References

[1] M. Kukovec, M. Malik, I. Kodrin, C. B. Aakeröy, M. Đaković, *Cryst. Growth Des.*, 2016, **16**, 7308;
[2] Đaković, Ž. Soldin, B. M. Kukovec, I. Kodrin, C. B. Aakeröy, N. Baus, T. Rinkovec, *IUCrJ*, 2018, **5**, in press.
[3] Borovina, I. Kodrin, M. Đaković, CrystEngComm, 2018, in press.

S13-03

Structural Characterization of an Ultra-High Strength Fe-Cr-Ni Silicide Phase

S. Plana-Ruiz[1,2], Y. Krysiak[1], L. Palatinus[3], D. Bowden[4], M. Preuss[4], U. Kolb[1,5]
[1]Technische Universität Darmstadt, Institut für Angewandte Geowissenschaften, Darmstadt, Germany
[2]Universitat de Barcelona, Electronics and Biomedial Engineering Department, Barcelona, Spain
[3]Czech Academy of Sciences, Institute of Physics, Prague, Czech Republic
[4]The University of Manchester, School of Materials, Manchester, United Kingdom
[5]Johannes Gutenberg-Universität Mainz, Institut für Anorganische Chemie und Analytische Chemie, Mainz, Germany

This study demonstrates the possibilities of the automated diffraction tomography (ADT)[1] technique to structurally characterize complex alloys. These materials usually contain a phase mixture of different intermetallics, thus X-ray diffraction experiments are not suitable to analyse nanoscopic isolated crystals. ADT allows to use an electron beam of 50-200 nanometer size, which opens the door to obtain crystallographic information from such nanocrystals and solve their crystal structure. The tomographic data collection provides reflection intensities allowing an accurate calculation of the Coulomb potential inside the unit-cell using both kinematical[2] and dynamical[3] theory and, therefore, discerning the positions of light and heavy atoms.

This work is focused on the characterization of a new high strength Fe-Cr-Ni silicide, named π-ferrosilicide, which also includes carbon to increase the hardness. A carbon and carbon-free π-ferrosilicide were prepared and measured with ADT to retrieve the structure and specify the carbon distribution. Atomic positions were successfully identified in cubic unit-cell using the non-centrosymmetric space group P213. The possibility to determine the absolute structure using electron diffraction data is discussed as an example case of the applicability of the dynamical theory[4].

Figure 1. RR2450 π-ferrosilicide structure solution obtained by ADT and dynamically refined. Red atoms correspond to interchangeable atomic sites of Fe, Cr and Ni. Green atomic sites correspond to Si positions. VESTA[5] v3.4 is used for display.

References

[1] Kolb, U., Gorelik, T., Kübel, C., Otten, M. T. & Hubert, D. *Ultramicroscopy* **107,** 507–513 (2007).
[2] Mugnaioli, E., Gorelik, T. & Kolb, U. *Ultramicroscopy* **109,** 758–765 (2009).
[3] Palatinus, L., Petříček, V. & Corrêa, C. A. *Acta Crystallographica Section A Foundations and Advances* **71,** 235–244 (2015).
[4] Palatinus, L. et al. *Acta Crystallographica Section B Structural Science, Crystal Engineering and Materials* **71,** 740–751 (2015).
[5] Momma, K. & Izumi, F. *J Appl Crystallogr* **44,** 1272–1276 (2011).

Figure 1

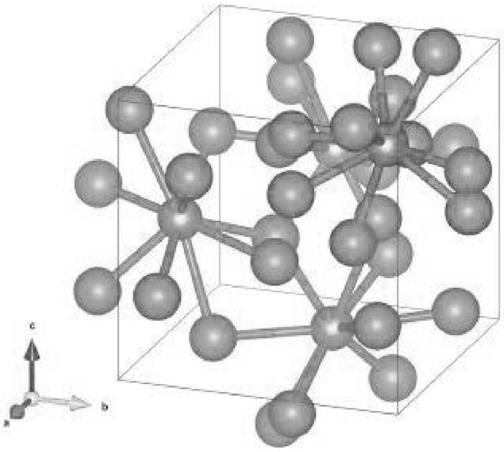

S13-04

From molecular sociology to functional materials

C. Aakeroy[1]
[1]Kansas State University, Manhattan, United States

Co-crystals represent solids where bulk physical properties may be amenable to fine-tuning by making modular and controllable alterations to the crystalline lattice that "houses" an active molecular species. The links between crystal structure and solid-state properties offer opportunities for improving processing, performance and shelf-life of a wide range of specialty chemicals. Consequently, an ability to control and change the crystalline environment of a material without altering molecular properties would be of considerable significance to manufacturers and consumers alike. This presentation will address how supramolecular synthetic strategies based on hydrogen bonds and halogen bonds (1) can be converted to effective crystal engineering in areas of relevance to agrochemicals, drug delivery, and energetic materials (2,3).

References

[1] Gunawardana, C.A., Desper, J., Sinha, A.S., Đaković, M., Aakeröy, C.B., Competition and selectivity in supramolecular synthesis: structural landscape around 1-(pyridylmethyl)-2,2'-biimidazoles, Faraday Discussions, 2017, 203, 371.
[2] Aakeröy, C.B., Is there any point in making co-crystals? Acta Crystallogr. Sect. B, 2015, 71, 387.
[3] Aakeröy, C.B.; Wijethunga, T.K. Desper, J., Crystal engineering of energetic materials: Co-crystals of ethylenedinitramine (EDNA), Chem. Eur. J. 2015, 21, 11029.

S13-05

Boron allotrope with α -Ga structure synthesized at high pressure and high temperature

I. Chuvashova[1,2], E. Bykova[1], E. Bykova[3], V. Prakapenka[4], K. Glazyrin[5], M. Mezouar[1], L. Dubrovinsky[2]
[1]University of Bayreuth, Bayerisches Geoinstitut, Bayreuth, Germany
[2]University of Bayreuth, Laboratory of Crystallography, Bayreuth, Germany
[3]University of Chicago, Center for Advanced Radiation Sources, Argonne, United States
[4]Deutsches Elektronen-Synchrotron DESY, Hamburg, Germany
[5]European Synchrotron Radiation Facility (ESRF), Grenoble, France

Structures of all hitherto known boron allotropes (α-B, β-B, γ-B, δ-B, and ε-B) are based on various arrangements of B12 icosahedra, since three valence electrons of boron are insufficient to form a simple covalent structure. However, theoretical calculations suggest a possibility of the existence of a non-icosahedral boron allotrope with the α-Ga type structure.

We performed the high-pressure high-temperature experiments in diamond anvil cells (DACs) using single crystals of β-boron as a staring material and analyzed the synchrotron *in situ* single-crystal X-ray diffraction data.

At 115(2) GPa the sample color became black and phase transition occurred. The solved crystal structure matches perfectly the one expected for α-Ga-type structured boron, as predicted by Häusserman et al., and has the *Cmce* space group and 8 atoms per unit cell. The following orthorhombic lattice parameters were obtained at 115 GPa: a = 2.7039(10) Å, b = 4.8703(32) Å, c = 2.9697(6) Å. This new HP boron allotrope was denoted as ζ-B.

We compressed the material synthesized at 115 GPa up to 135 GPa. The obtained PV data set of ζ-B was fitted using the second-order Birch-Murnaghan equation of state (EoS) and gave the following EoS parameters: V115 = 39.20(8) Å3, K115 = 575(65) GPa; K′= 4 (fixed); *V*115 is the unit cell volume and *K*115 is the bulk modulus at 115 GPa and room temperature). Therefore, in the studied pressure range (from 115 to 135 GPa) ζ-B is less compressible than any other boron allotropes known so far.

Spectroscopic methods in crystallography

S14-01

X-ray Absorption Spectroscopy for Crystallography at BESSY II

G. Schuck[1], D. M. Többens[1], I. Zizak[1], S. Schorr[1]
[1]Helmholtz-Zentrum Berlin, Abteilung Struktur und Dynamik von Energiematerialien, Berlin, Germany

X-ray absorption spectroscopy (XAS) is increasingly used to study crystallographic problems in a wide range of scientific fields. Its element specificity and sensitivity to the local structure provide high complementarity to X-ray diffraction. Due to the need for radiation with tunable energy it is yet restricted to synchrotron sources. The Berlin Electron Synchrotron BESSY II operates multiple XAS stations for user service, some of which are particularly optimized for crystallographic problems:

mySpot [1] is optimized for mapping experiments with focus spot sizes as low as 1.5 µm. µ-EXAFS and µ-XANES in the energy range 5 - 25 keV can be combined simultaneously with a wide range of other methods. It is especially designed (but not limited to) for the study of hierarchically structured biological samples.

CryoEXAFS at KMC-3 beamline, developed in cooperation with Freie Universität Berlin [2], allows sample temperatures as low as 20 K. Due to the absence of absorption in air, low radiation energies (3.6 - 14 keV) can be used, extending the range of observable light elements.

KMC-2 XANES [3] provides a stable beam in the energy range 4 – 15 keV, microfocus option and a selection of detectors, allowing transmission and fluorescence geometries. The open concept of the station allows the use of a wide range of sample environments, both in-house and user-provided, and flexible movement of the sample.

References

[1] Helmholtz-Zentrum Berlin für Materialien und Energie. (2016). mySpot: a versatile microfocussing station for scanning methods at BESSY II. Journal of large-scale research facilities, 2, A101. doi 10.17815/jlsrf-2-115
[2] H. Dau, Institut für Experimentalphysik, Freie Universität Berlin
[3] Helmholtz-Zentrum Berlin für Materialien und Energie. (2016). KMC-2: an X-ray beamline with dedicated diffraction and XAS endstations at BESSY II. Journal of large-scale research facilities, 2, A49. doi 10.17815/jlsrf-2-65

S14-02

Growth and Physicochemical Properties of Semi-organic NLO crystal Picolinium Taratrate Monohydrate

S. Davidson[1]
[1]Bishop Moore College Mavelikara, Physics, Mavelikara, India

Non-centrosymmetric NLO crystal PTM was synthesized and the structure was confirmed from single crystal XRD analysis and 1H & 13C NMR spectra. The normal coordinate analysis predicts a good agreement between the observed and calculated frequencies and shows that the N29-H30 and hydroxyl O1-H3 stretching vibrations are downshifted due to proton transfer. From AIM analysis, it is evident that these frequency changes are the result of electron density transfer of H-bonding between anion and cation which dominates in the hydroxyl O1...H30 and O12...H3 intermolecular bonds. NBO analysis exposes π conjugative interaction as the prominent charge transfer interaction due to the proton transfer that enables high stabilization energy in the picolinium ring and also predicts the cooperative effect of solvent water molecule N29-H30...O1 and O1-H3...O12 interactions. The photoluminescence spectrum shows a red shift due to the solvent−solute interactions and the intermolecular charge transfer facilitated by the protonation of picolinium moiety affecting the $\pi-\pi^*$ transition, which is responsible for its fluorescence. The self de-focusing nature with high nonlinear refractive index and optical limiting property of PTM crystal, which is reflected from third-order nonlinear optical studies; as well as its SHG efficiency shows that the crystal can be used for second and third-order nonlinear optical applications. The hyperpolarizability calculated by Z-scan measurement and the theoretical value of field dependent second hyperpolarizabilities andare 6.51x10-34, 961.33x10-36 and 338.01x10-36 esu respectively, are in good agreement.

S14-03

Lattice dynamics of $CaCO_3$ and $MgCO_3$

M. Stekiel[1], A. Girard[1], T. Thanh-Nguyen[2], W. Morgenroth[1], A. Bosak[2], B. Winkler[1]
[1]Goethe-Universität Frankfurt am Main, Institut für Geowissenschaften, Frankfurt am Main, Germany
[2]ESRF, Grenoble, France

Calcium and magnesium carbonates are the most abundant carbonates on Earth [1]. They are present in oceanic sediments, from where they can be transported to the Earth interior on subducting slabs [1]. Understanding their physical properties is a key to understand and detect the processes responsible for transportation of carbon into the deep Earth. The lattice dynamics of these compounds govern the thermodynamic and transport properties, from which geoscientifically important parameters can be derived, such as sound velocities, thermal expansion and thermal conductivity [2].

We performed x-ray scattering experiments at ID28 at the ESRF. The side station diffractometer was used to obtain diffuse scattering maps at ambient conditions (Fig. 1). There is strong diffuse scattering in CaCO3 in the (-2.5 0 2) and (-1.5 0 6) points (Fig. 1A). We did not observe such features for MgCO3. Further measurements were conducted with the inelastic x-ray scattering spectrometer. We measured the phonon dispersion relations of CaCO3 and MgCO3 in the Γ-F direction. As has been observed by Dove et al. [3] before, there is a strong softening of the quasi-transverse acoustic phonon, in the case of CaCO3, responsible for the high intensity signal in the diffuse scattering maps. We didn"t observe any softening at the F point in the case of MgCO3.

The observed difference in the lattice dynamics may lead to an explanation of the difference in the stabilities of CaCO3 and MgCO3. The IXS and diffuse scattering data and their interpretation will be presented during the conference.

The study is supported by funding from the German Science Foundation (DFG-Research Unit FOR2125) and through the DFG-ANR project WI1232/41.

References

[1] R. Dasgupta, *Carbon in Earth*, edited by R. Hazen et al., chapt. 7, pp. 1-6, 2013.
[2] M.T. Dove, *Introduction to lattice dynamics*, Cambridge University Press, 1993.
[3] M.T. Dove et al., *J.Phys: Condens. Matter*, vol. 4, pp. 2761-2774, 1992.

Figure 1. Diffuse scattering maps of CaCO3 (A) and MgCO3 (B) in the (H 0 L) plane of the reciprocal space. Strong intensity is observed in the (-2.5 0 2) and (-1.5 0 6) points, that correspond to the F in the Brillouin zone of CaCO3. These features were not observed in the case of MgCO3.
Figure 2. Phonon dispersion relations of CaCO3 (A) and MgCO3 (B) along Γ-F direction. The quasi-T acoustic mode in CaCO3 softens in the vicinity of the F point at $\xi = 0.3$. Such a behavior is not observed in the case of MgCO3.

Figure 1

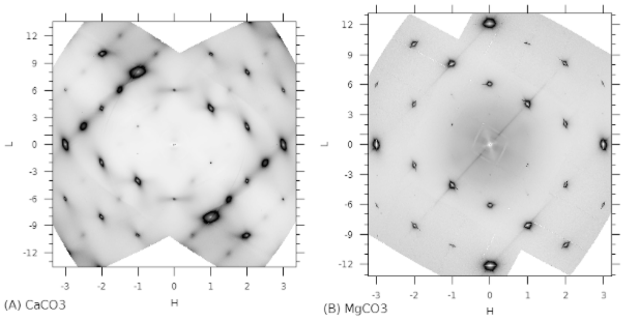

Figure 2

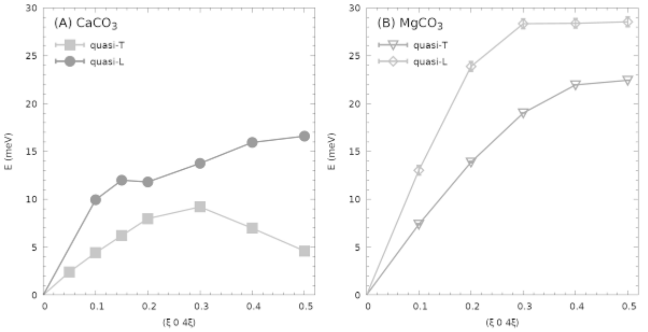

S14-04
Order-disorder phenomena above the Curie temperature in lead titanate

I. Margaritescu[1], K. Datta[1], B. Mihailova[1]
[1]Universität Hamburg, Department of Earth Sciences, Hamburg, Germany

Ferroelectric materials exhibit spontaneous polarization in the absence of an external electric field and have the ability to switch between different allowed orientation states of the polarization under an external electric field. Materials with an ABO_3 perovskite structure constitute one of the most important classes of ferroelectrics, not only because of their large variety of technological applications but also because of their relatively simple structure leading to a deeper understanding of ferroelectricity.

A textbook example of a ferroelectric perovskite is lead titanate ($PbTiO_3$), which exhibits *Pm-3m* symmetry in the paraelectric state above the Curie temperature $T_C \sim 763$ K and *P4mm* in the ferroelectric state below T_C. For a long time, it has been assumed that $PbTiO_3$ undergoes a pure displacive-type phase transition driven by a soft mode. However, recent studies have revealed evidence of order-disorder phenomena above T_C [1][2].

The aim of this study is to analyze in detail the local ferroic distortions of $PbTiO_3$ above the transition temperature by applying in situ Raman spectroscopy to $PbTiO_3$ powder in the temperature range 100 – 1040 K with steps of 10 K and pair-distribution-function (PDF) analysis at four selected temperatures: 300, 500, 700, and 900 K.

The temperature evolution of the anomalous Raman scattering shows that the formation of a ferroelectric phase involves multi-step coupling of small ferroic structural species. Near 980 K distorted BO_6 octahedra begin to couple, as indicated by softening and damping of the BO_6 stretching mode. This process reaches its maximum near 880 K, at which temperature the preexisting off-centred Pb displacements start to couple. At 790 K the latter process is completed and simultaneously, the off-centred Ti displacements couple with the Pb displacements, leading to the formation of polar spatial regions that on further cooling evolve into a ferroelectric long-range order at T_C. Quasi LO modes were detected at 780 K, indicating a net polarization on the length- and time-scale of sensitivity of Raman spectroscopy. The PDF analyses reveal that the average magnitude of off-centred Pb displacements at 900 K > T_C is the same as that at 700 K < T_C and only below 700 K the mean magnitudes start to increase with the temperature decrease.

References

[1] N. Jaouen, A. C. Dhaussy, J. P. Itié, A. Rogalev, S. Marinel and Y. Joly, *Phys. Rev. B* **75**, 224115 (2007)
[2] M. D. Fontana, H. Idrissi and K. Wojcik, *EPL* **11**, 419 (1990)

S14-06
Vibrational study, reinvestigation of the crystal structure of $MgHPO_4.3H_2O$ and calculated IR frequencies for the PO_4^{3-} by isotopic substitutions

M. Belhabra[1], S. Zerraf [1], A. Kheireddine [1], M. Tridane [1,2], H. Moutaabbid [3], M. Moutaabbid [1], M. Radid [1], S. Belaaouad [1]
[1]Ben M'sik University Hassan II Casablanca, Faculty of Science, Casablanca, Morocco
[2]Centre Régional des métiers d'éducation et de formation, Casablanca, Morocco
[3]Sorbonne Universités - UPMC Université Paris, Institut de Minéralogie, de Physique des Matériaux et de Cosmochimie (IMPMC), Paris, France

The monohydrogenomonophosphate trihydrate of magnesium $MgHPO_4.3H_2O$ was reinvestigated by X-ray diffraction, vibrational spectroscopy, nuclear magnetic resonance and calculation of the IR frequencies by using isotopic substitutions. $MgHPO_4.3H_2O$ is orthorhombic, space group Pbca with the following unit-cell parameters: a = 10.0133(2) Å, b= 10.2136(1) Å, c =10.6853(2) Å, Z = 8 and V = 1092.81(3) Å^3. Raman and infrared spectra of $MgHPO_4.3H_2O$ have been recorded and interpreted on the basis of factor group analysis. The occurrence of the four frequencies ν1, ν2, ν3, ν4 in the vibrational spectra confirm the existence of the PO_4^{3-} tetrahedron. The IR and Raman bands observed and the nuclear magnetic resonance for phosphorus in $MgHPO_4.3H_2O$ are in accord with results of reinvestigation of the structure.

Figure 1

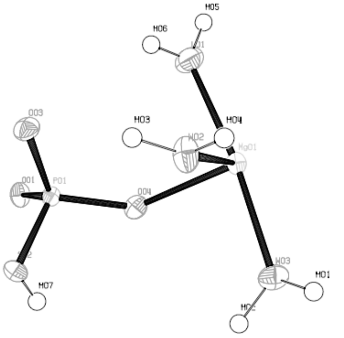

Figure 2

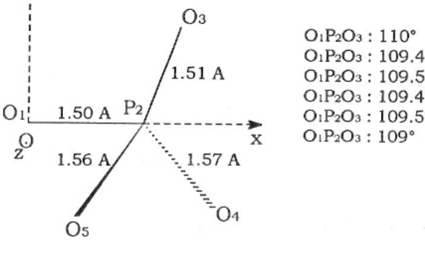

Structurally complex materials

S15-01

Two new incommensurately modulated rare earth metal polytellurides

H. Poddig[1], T. Doert[1]
[1]Technische Universität Dresden, Inorganic Chemistry II, Dresden, Germany

Introduction

Polychalcogenides of the rare earth metals ($REX_{2-\delta}$, X = S, Se, Te; $0 \leq \delta \leq 0.2$) consist of puckered [REX] double layers and planar [X] layers and are structurally related to the ZrSSi type. The compounds adopt different (super)structures according to different chalcogen defects in their planar [X] layers. The defect layer of the polysulfides and polyselenides contain X^{2-}-ions besides X_2^{2-} dianions [1]. For the polytellurides, different ordering patterns including higher polychalcogenide anions have been observed [2,3].

Objectives

We grew single crystals of $PrTe_{1.9}$ and $NdTe_{1.9}$ in alkali halide fluxes and investigated their crystal structures.

Results

Plate like single crystals of $PrTe_{1.9}$ and $NdTe_{1.9}$ were obtained by flux growth. Single crystal diffraction indicated a tetragonal basic unit cell with a ≈ 4.4 Å and c ≈ 9.1 Å and additional satellite reflections. The structures of both compounds could be solved and refined in the superspace group $P4/n(\alpha,\beta,½)00(-\beta,\alpha,½)00$ (No. 85.2.58.2; [4]). Satellites could be indexed with the modulation wave vectors q_1 = (0.25, 0.32, 0.5) and q_2 = (–0.32, 0.25, 0.5) for $PrTe_{1.9}$ and vectors q_1 = (0.26, 0.32, 0.5) and q_2 = (–0.32, 0.26, 0.5) for $NdTe_{1.9}$, respectively, Fig. 1a. The occupancy and displacive modulation mainly affects the Te layers in both compounds.

The modulated Te layer can be described by an array of vacancies, Te^{2-}, Te_2^{2-} and Te_3^{2-} anions, Fig. 1b. The Te–Te distances in the modulated layer range from 2.95 Å to 3.30 Å. The modulation is very similar to those found in the rare earth metal polyselenides $RESe_{1.85}$, (RE = La, Ce, Nd, Sm; [5]), which also display an incommensurate site occupancy and displacive modulation, altough much more pronounced.

Conclusion

Two new rare earth metal polytellurides were obtained by flux synthesis and their incommensurately modulated crystal structures were determined. The structures share similar motives with the known rare earth metal polyselenides.

References

[1] T. Doert, C. J. Müller, *Reference Module in Chemistry, Molecular Sciences and Chemical Engineering*, Elsevier, **2016**.
[2] K. Stöwe, *Z. Kristallogr. - Cryst. Mater.* **2000**, *216, 4*, 215-224.
[3] L. D. Gulay, *J. Alloys Compd.* **2007**, *427*, *1*, 166-170.
[4] H. T. Stokes, B. J. Campbell, S. van Smaalen, *Acta Cryst. A*, **2011**, *67*, 45-55.
[5] C. Graf, T. Doert, *Z. Kristallogr. - Cryst. Mater.* ***2009****, 224, 12, 568-579.*

Fig. 1: Reproduced diffraction pattern of $RETe_{1.9}$. b) Section of the modulated Te-layer in $PrTe_{1.91}$.

Figure 1

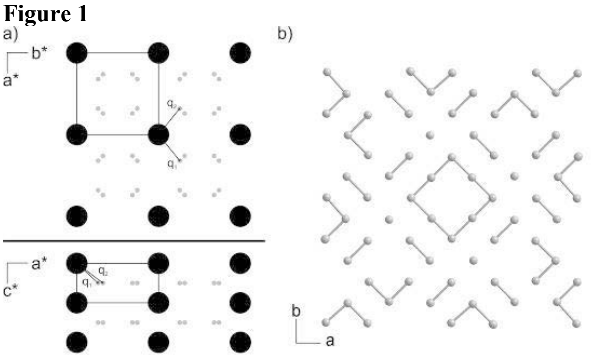

S15-02

Incommensurate modulation of the charge-density wave in CuV_2S_4

S. Ramakrishnan[1], N. Hai An[1], F. Feulner[1], M. Anurova[1], A. Schönleber[1], S. van Smaalen[1]
[1]University of Bayreuth, Laboratory of Crystallography, Bayreuth, Germany

The symmetry of the spinel compound CuV_2S_4 at room temperature is described by the space group *Fd▯ -3m* [1]. At 90 K the diraction pattern shows a charge-density wave (CDW) transition with a modulation wave vector **q** = (3/4, 3/4, 0) [2]. The X-ray powder diraction shows a lowering of the symmetry of the lattice from cubic to tetragonal at temperatures below 90 K [1, 3]. The temperature dependence of the magnetization data report results of the decrease in magnetic susceptibility (χ) at 90 K followed by an upward jump at 54 K [4]. Further phase transitions at lower temperatures were proposed but not characterized. We have studied CuV_2S_4 by single-crystal X-ray direction pattern at temperatures down to 5 K. Here we report the structure at phase transition close to 90 K and the secondary modes used to better describe the model.

References

[1] S. Kawaguchi, H. Ishibashi, N. Tsuji, J. Kim, K. Kato, M. Takata, and Y. Kubota, J. Phys. Soc. Jpn. 82 (2013) 064603.
[2] R. M. Fleming, F. J. DiSalvo, R. J. Cava, and J. V. Waszczak, Phys. Rev. B 24 (1981) 2850.
[3] H. Okada, K. Koyama and K. Watanabe, J. Phys. Soc. Jpn 73 (2004) 3227.
[4] I. Naik, C. S. Yadav, and A. K. Rastogi, Phys. Rev. B 75 (2007) 115122.

S15-03

Mullite Al/Si ordering in superspace revealed by DFT

P. B. Klar[1], X. M. Aretxabaleta[1,2], I. Etxebarria[2], G. Madariaga[1]
[1]Universidad del País Vasco UPV/EHU, Dpto de Física de la Materia Condensada, Bilbao, Spain
[2]Universidad del País Vasco UPV/EHU, Dpto de Física Aplicada II, Bilbao, Spain

The crystal structure of mullite $Al_{4+2x}Si_{2-2x}O_{10-x}$ has a long history of controversial discussions that especially focused on the vacancy ordering. Despite several NMR and neutron diffraction studies, little is known about the relationship between the distribution of Si on the tetrahedral sites and the distribution of vacancies. Commensurate superstructures in the composition range $0.2 \leq x \leq 0.5$ were generated from a superspace model with full vacancy ordering [1]. Symmetry compliant permutations of Al/Si distributions were analysed with force-field methods (FF) and the energetically most promising candidates were then used for DFT calculations.

The objective of this study is to establish the ideal Al/Si ordering scheme for the mullite solid solution range with orthorhombic symmetry.

About 45600 structure models of 5 different compositions were statically relaxed using the GULP package [2]. The results were analysed with respect to the energy and qualitative statements on the Al/Si distribution were derived:

1. $(Si_2O_7)^{6-}$ diclusters are preferably intercalated between two vacancies
2. $(Al_2O_7)^{8-}$ diclusters are avoided (Löwenstein rule)
3. The orientation of $(AlSiO_7)^{7-}$ diclusters influence each other and certain combinations are avoided

DFT calculations confirm that the most stable, ordered mullite structures strictly follow these rules and the energetically best structures with a vacancy concentration $x > 1/3$ are described by the same unified superspace model, which implies the presence of Si atoms in certain triclusters. For $x \leq 1/3$, which includes the 3/2 mullite ($x = 0.25$), the Al/Si ordering pattern is slightly different without Si in triclusters. The steps and the results for the case of the 2/1 mullite ($x = 0.4$) are shown in Figure 1. The model provides a basis to better understand the structurally related disordered, real structure of mullite, that exhibits the same superspace group independent of the vacancy ordering degree ($x \leq 0.5$).

Financial support by FEDER (No. MAT2015-66441-P) and the Basque Government (project No. IT-779-13, PhD grant) is highly appreciated.

References

[1] P.B. Klar et al. (2017), Acta Cryst. **B73**, 377-388
[2] J.D. Gale (2006), Z. Krist., **220**, 552-554

Figure 1: Energies (FF: blue circles, DFT: orange diamonds) for 2/1 mullite. The first data point corresponds to the model suggested in [1]. The structure corresponding to the lowest energy (red circle) is used to define the Al/Si atomic domains for the superspace model (right)

Figure 1

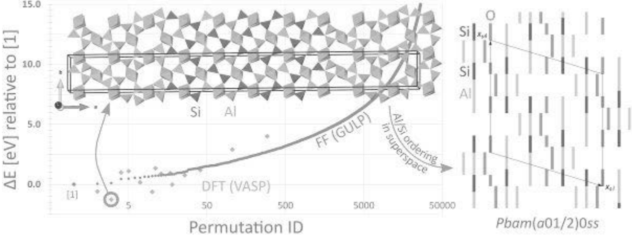

S15-04

Influence of electric field on the room-temperature local structure of (1-x)Na0.5Bi0.5TiO3-xBaTiO3

G. de la Flor [1,2], S. Gorfmann[3], B. Mihailova[2]
[1]University of the Basque Country UPV/EHU, Física de la Materia Condensada, Leioa, Spain
[2]Universität Hamburg, Geowissenschaften, Hamburg, Germany
[3]Tel Aviv University, Faculty of Engineering, Tel Aviv, Israel

Introduction

The ferroelectric solid solution (1-x)Na0.5Bi0.5TiO3-*x*BaTiO3 (NBT-*x*BT) is considered as a promising environmentally friendly replacement for Pb-based ferroelectric materials. This system exhibits a morphotrophic phase boundary (MPB) and a rich composition-temperature (*x*-T) phase diagram, including an antiferroelectric state that cannot be clearly detected by conventional diffraction methods. The latter highlights the importance of ferroic coupling on the mesoscopic scale and calls for the application of methods sensitive to the local structure and dynamics such as Raman spectroscopy. This technique has been proven to be a powerful method for analyzing the mesoscopic-scale transformation processes via following the temperature evolution of phonon anomalies and its renormalization under an external electric field or composition. Very recently, the comprehensive analysis of the zero-field temperature dependencies of the Raman scattering of NBT-xBT revealed the existence of mesoscopic-scale antiferroelecetric and ferroelectric coupling within the A-site-cation subsystem, preceding the temperature of the dielectric-permittivity maximum and the temperature of antiferroelectric-ferroelectric phase transition, respectively [1].

Objective

The aim of this contribution is to study the influence of an external electric field on the room-temperature structural state of NBT-*x*BT across the MPB by in situ polarized Raman spectroscopy. For that purpose, NBT-*x*BT single crystals with x < xMPB (x=0, 0.013), x ~ xMPB x=0.048, 0.053) and x > xMPB (x=0.074) have been studied under different electric fields **E** from 0 to 1 kV/mm applied along the pseudocubic (100) and (110) directions.

Results

The analysis of the collected Raman spectra reveals that all phonon modes below 300 cm-1, which involve mainly cationic vibrations, are rather sensitive to the presence of external **E**. When the direction of **E** is different from the predominant intrinsic direction of coupled cationic polar shifts, the MPB moves away from the zero-field xMPB value.

Conclusion

The Raman scattering experiments under an external electric field give further insight into the atomistic mechanism of polar coupling and shows how one can manipulate the position of the MPB by applying an external electric field.

References

[1] de la Flor et al, Phys. Rev. B 2017, in press

S15-05

Direct observation of polar nanodomains in the incommensurate Phase of $(K_{0.92}Rb_{0.08})_2ZnCl_4$ crystals

C. Kofahl[1], F. Güthoff[1], G. Eckold[1]
[1]Georg-August Universität Göttingen, Institute of Pysical Chemistry, Göttingen, Germany

Introduction

Close to the lock-in transition incommensurate (INC) phases are predicted to consist of an ordered sequence of commensurate (C) nanodomains separated by so-called discommensurations [1,2]. The existence of these domains and the corresponding multisoliton lattice is usually inferred from diffraction experiments. In ferroelectric systems surface charges of the polar domains are expected which should be detectable using scanning force microscopy (SFM). In this contribution, we want to demonstrate that the nanoscaled modulation of the surface can indeed be visualized in Rb-doped K_2ZnCl_4 crystals.

Objectives

Using γ-ray diffraction it was shown that in doped K2ZnCl4 crystals nanodomains can persist at ambient temperature [3] thus facilitating the investigation by SFM under UHV conditions. In order to visualize these polar nanodomains at the surface, we used the well-established Piezo Force Microscopy (PFM) that is sensitive to the polarization of the sample: While a constant force is applied to the cantilever in contact mode the application of AC-voltages of 10 V amplitude leads to deformation at the crystal surface that can be detected with sufficient accuracy even if the piezoelectric coefficient is small.

Results

In Fig. 1, PFM scans are shown which were obtained from a (100)-surface of a $(K_{0.92}Rb_{0.08})_2ZnCl_4$ -crystal. The stripes with a periodicity of about 40 nm perpendicular to the modulation direction ***c*** are clearly visible. This is consistent with the bulk periodicity obtained from diffraction data. Different scan directions exhibit almost the same contrast variation and prove that it is a real effect of the sample rather than an artefact from the experimental setup.

Conclusion

For the first time, to the best of our knowledge, a direct visualization of polar surface structures in incommensurately modulated systems could be achieved. The observed pattern reflects the nanoscaled variation of the surface charge that is associated with the multisoliton lattice of the IC-phase close to the lock-in transition.

References

[1] Janovec V 1983 *Phys. Lett.* **99A** 384.
[2] Kawasaki K 1983 *J. Phys. C: Solid State Phys.* 6911.
[3] Behrendt K and Eckold G 2017 *Phase Transitions* **90** 1049.

Fig 1: PFM-pattern of the polar (100) surface of Rb doped K_2ZnCl_4 obtained from scans along ***b*** (left) and ***c*** (right)(applied force: ~7 nN; applied voltage: 10 V AC).The modulation direction is along ***c*** with a characteristic wavelength of about 40 nm.

Figure 1

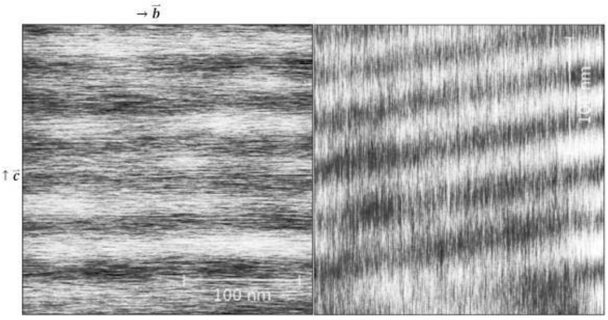

S15-06

Influence of Microstructure on Symmetry Determination of Piezoceramics

M. Hinterstein[1], H. E. Mgbemere[2], M. Hoelzel[3], E. Adabifiroozjaei[4], C. Sorrell[4], M. Hoffmann[1]
[1]Karlsruhe Institute of Technology (KIT), Institut für Angewandte Materialien, Karlsruhe, Germany
[2]University of Lagos, Department of Metallurgical and Materials Engineering, Lagos, Nigeria
[3]Technische Universität München, Heinz Maier-Leibnitz Zentrum (MLZ), Garching bei München, Germany
[4]UNSW Australia, School of Materials Science and Engineering, Sydney, Australia

Frequently symmetry determination in studies is based on the discussion of agreement factors or the quality of the refinements, rather than on the basis of physical arguments. Especially in the field of piezoceramics this can be observed in the discussion whether monoclinic symmetry can be observed or not.

In this study we could show with temperature-dependent high-resolution X-ray and neutron diffraction that based on agreement factors alone the physical origin of observations cannot be revealed. Only in combination with additional electron microscopy and electron probe microanalysis we could elucidate that a segregation of substituents results in a complex reflection splitting and phase coexistence that can be misinterpreted as monoclinic symmetry. This single-phase monoclinic *Pm* model is able to perfectly reproduce the diffraction patterns and is known from literature [1,2]. A model with phase coexistence of two classical orthorhombic *Amm*2 phases can reproduce the diffraction data with equal accuracy.

This demonstrates the need of comprehensive analyses with complementary methods to cover a broad range of length scales as well as considering both average and local structure. The conclusions drawn from this work will have an impact on a broad range of research areas where inhomogeneities cannot be ruled out. The underlying mechanisms of the extraordinary properties of some functional materials originate not just in their structures but also their complex microstructures. Consequently, knowledge of both features of materials may be essential for the exploitation and development of their functionalities as well as improvement of material properties.

References

[1] H. E. Mgbemere, M. Hinterstein, and G. A. Schneider, J. Eur. Ceram. Soc. **32**, 4341 (2012).
[2] L. Liu, X. Ma, M. Knapp, H. Ehrenberg, B. Peng, L. Fang, and M. Hinterstein, Europhys. Lett. **118**, 47001 (2017).

Bio-Crystallography V: Instrumentation and methods

S16-01

P11 at PETRA III: A Versatile Beamline for Serial and High-Throughput Crystallography

A. Burkhardt[1], O. Lorbeer[1], E. Crosas[1], S. Günther[1], T. Pakendorf[1], B. Reime[1], J. Meyer[1], P. Fischer[1], N. Stübe[1], M. Warmer[1], A. Meents[1]
[1]Deutsches Elektronen-Synchrotron DESY, Photon Science, Hamburg, Germany

P11 at PETRA III in Hamburg is dedicated to structural investigations of biological samples at different length scales. The beamline provides two state-of-the-art endstations: a crystallography experiment which is in user operation since 2013 [1] and an X-ray microscope which is currently under construction [2]. In future, a third experimental endstation for serial crystallography will be available.

Basis of beamline design was to make full use of the brilliant source properties of the PETRA III sychrotron and to deliver most of the photons from the source into a very small focal spot at the sample position. The P11 optics concept involves the generation of a secondary source at 65.5 m using three dynamically bendable KB mirrors. A second KB system which is installed further downstream can be used for refocusing the X-ray beam down to $4 \times 9\ \mu\text{m}^2$ (v × h) with full flux from the source (1.3×10 ph/s at 12 keV). Smaller beam sizes down to $1 \times 1\ \mu\text{m}^2$ (v × h) with more than 2×10^{11} ph/s in the focus can be obtained by slitting down the secondary source at the cost of flux.

The flexible X-ray optics allow for tailoring the beam properties to the needs of the experiment: A large parallel beam is available for structure determinations from large unit cell systems [3]. A highly intense microbeam allows for serial crystallography experiments on microcrystals using liquid delivery systems, such as jets or tape-drive [4, 5], or micro-patterned silicon chips for fixed targets [6].
The endstation is equipped with a high precision single axis goniostat with a combined sphere of confusion of less than 100 nm. Crystals can be rapidly exchanged in less than 20 s using a sample changing robot which is equipped with an inhouse-designed sample gripper. In addition, a large capacity storage Dewar provides space for 23 uni-pucks (368 samples). The Pilatus 6M-F detector in place allows for fast data collection with frame rates of up to 25 Hz. A full data set can be typically collected in less than 2 min. These design parameters make P11 ideally suited for screening a large number of crystals in very short time.

References

[1] A. Burkhardt et al., EPJ Plus 131:56 (2016)
[2] A. Meents et al., Proc. SPIE 8851, 88510K (2014)
[3] K. Schulte et al., BMC Biology 14:14 (2016)
[4] F. Stellato et al., IUCrJ 1, 204 (2014)
[5] K. R. Beyerlein, IUCrJ 4, 439 (2017)
[6] P. Roedig et al., Sci. Rep. 5, 10451 (2015)

S16-02

Facilities for Macromolecular Crystallography at the Helmholtz Zentrum Berlin

C. Feiler[1], M. Gerlach[1], R. Förster[1], C. Gless[1], T. Hauss[1], M. Hellmig[1], F. Huschmann[1], A. Kastner[1], P. Malecki[1], K. Röwer[1], L. Schmuckermaier[1], M. Steffien[1], P. Wilk[1], M. Weiss[1]
[1]Helmholtz Zentrum Berlin, Macromolecular Crystallography, Berlin, Germany

HZB operates three beamlines for Macromolecular Crystallography (MX) at the electron storage ring BESSY II [1,2]. Beamlines BL14.1 and BL14.2 are dedicated to multi-wavelength anomalous dispersion (MAD) phasing methods. Operating between 5.5 - 15.5 keV (2.25 to 0.75 Å), absorption edges of most commonly used heavy atom derivatives are covered. State-of-the-art detector technologies, including the PILATUS 6M (BL14.1) and PILATUS3S 2M (BL14.2) detectors (Dectris, Switzerland) enable high quality and rapid data collection.

BL14.1 provides a high degree of automation with a MD2 a mini-kappa axis. Reliable sample changing is realized by a CATS sample changing robot. This beamline also features an *in situ* plate screening option. On beamline BL14.2 an automated sample changer G-ROB, which has a high capacity sample dewar hosting up to 294 samples, supporting both, SPINE and UNIpuck standard allows high sample throughput. Beamline BL14.3 is a fixed energy station operating at 13.8 keV (0.89 Å). This endstation will undergo an upgrade in summer 2018.

Both MAD beamlines are running MXCuBE V2 control software, allowing fast and efficient semi-automated data collection. Collected data is live processed using the data processing expert system XDSAPP [3].

Standard data collection procedures and element identification using an X-ray fluorescence detector are supported on all beamlines. BL14.2 allows ultra high-resolution data collection and is dedicated to long-wavelength due to its minimal detector-sample distance of 56 mm. Further experimental possibilities are e.g. radiation induced phasing experiments using a pulsed UV-laser on BL14.1 and controlled single crystal dehydration using an HC1 device on BL14.3 [4].

Further HZB develops a 1000-compound fragment library since fragment screening e.g. in fragment-based lead discovery, has become a widely used technique. The HZB BioLab, located within closest proximity to the beamlines, supports all steps in the workflow of a campaign. Upgrades, including automated protein purification machines and a liquid handling acoustic transfer system will help to further maximize the sample throughput. The implementation of an automated data analysis pipeline will streamline data output.

References

[1] Mueller, U. et al. (2012). J. Synch. Rad. 19, 442-449
[2] Mueller, U. et al. (2015). Eur. Phys. J. Plus 130, 141
[3] Sparta, K. et al. (2016). J. Appl. Cryst. 49, 1085-1092
[4] Bowler et al. (2015). Cryst. Growth Des., 15 (3), 1043–1054

S16-03

3D printing at the diffraction limit: sample injection for time resolved serial crystallography

M. Heymann[1]
[1]Max Planck Institute of Biochemistry, Molecular and Cellular Biophysics, Martinsried, Germany

Continuous injection using the Gas Dynamic Virtual Nozzle (GDVN) is a proven sample delivery method for biological imaging using X-ray free-electron lasers. However, many important aspects of GDVN functionality have yet to be thoroughly understood and/or refined due to fabrication limitations. We apply 2-photon polymerization as a form of high-resolution 3D printing to fabricate GDVNs with submicron resolution. This allows rapid prototyping of a wide range of nozzle designs from standard CAD drawings to iteratively optimize crucial dimensions for optimal performance. To understand enzyme catalysis and protein conformational changes at the atomic scale, we pioneered mixing-injectors for time-resolved structural biology to record molecular movies of substrate turn-over. We experimentally validate 3D print accuracy, as well as fluid mixing dynamics using X-ray tomographic imaging. We developed mixing-injectors to mix nanocrystals with substrate and to subsequently deliver them into the X-ray interaction region just milliseconds after mixing. This method can determine the structures of transient states and thereby kinetic mechanisms. We will discuss a proof of principle experiment, in which we could follow the catalytic reaction of the M. tuberculosis β-lactamase with the 3rd generation antibiotic ceftriaxone by time-resolved serial crystallography with millisecond to second time resolution at 2Å spatial resolution. We will furthermore present progress on adopting or 3D printed mixing-injection methodology for serial crystallography at synchrotron sources.

S16-04

EMBL beamlines P13/P14 and associated facilities for Macromolecular Crystallography at PETRA III. Status, results, and future plans.

T. R. Schneider[1], G. Bourenkov[1], G. Pompidor[1], I. Bento[1], J. Hakanpää[1], S. Panneerselvam[1]
[1]European Molecular Biology Laboratory Hamburg, Hamburg, Germany

EMBL-Hamburg operates two MX beamlines, P13 and P14, at PETRA III (DESY, Hamburg).

P13 delivers high photon fluxes at energies down to 4 keV. Combining X-rays in the 4-6 keV energy range with beam sizes down to 15 µm diameter while maintaining high photon flux allows to perform full data collections with optimized anomalous signal in less than 5 minutes. S-SAD phasing is achieved routinely; recently the feasibility of MAD-phasing at the Ca K-edge (4.05 keV, 3.1 Å) has been demonstrated. It should be noted that diffraction measurements at low energies on P13 do not require any special preparation of the sample, i.e. a crystal attached to a standard SPINE-pin can be automatically mounted onto the goniostat.

P14 can be run in two modes, one providing a collimated homogeneous beam that can be shaped to any size between 10 and 200 µm (crystal life-time 2-3 minutes at 100 K), the second mode producing micro-focus conditions with a beam size on the 5 µm scale (crystal life-time ~500 ms at 100 K). The collimated beam can be used to illuminate large (50-200 µm) and small crystals homogeneously and/or to resolve diffraction from large (>1000 Å) unit cells. Prominent recent applications of the collimated beam have been the determination of a set of structures of the human 20S proteasome [1] and the phasing of the crystal structure of the mediator complex at 3.4 Å resolution [2]. The micro-focus beam can be used conveniently (fully automated work flows implemented in the MXCuBE-based beamline GUI) for serial crystallographic type of data collections both on cryogenically cooled crystalline suspensions [3] and *in situ* on crystals as grown in CrystalDirectTM crystallization plates. *In situ* structure determinations have been successfully performed from crystals in crystallization drops, in LCP, or as grown in living cells [4].
On P14, a second endstation for time-resolved pump-probe experiments is under construction.

The beamlines are embedded in the Integrated Facility for Structural Biology that offers access to services such as characterization of samples prior to crystallization, high throughput crystallization, crystal harvesting with a CrystalDirectTM Harvester, and a laboratory dedicated to heavy-atom derivatization. For access: smis.embl-hamburg.de

References

[1] Schrader ... Chari (2016) Science 353:594-598.
[2] Nozawa, Schneider, Cramer (2017) Nature 545:248-251.
[3] Gati ... Redecke (2014) IUCrJ 1:87-94.
[4] Collaborative projects, manuscripts in preparation.

S16-05

Facilities for Structural Biology at the ESRF: present and future.

G. Leonard[1]
[1]European Synchrotron Radiation Facility (ESRF), Structural Biology Group, Grenoble, France

A major success story of the European Synchrotron Radiation Facility (ESRF, the European Synchrotron) has been its facilities for Structural Biology [1]. Here, end-stations for experiments in Macromolecular Crystallography, BioSAXS and *in crystallo* spectroscopy have recently been supplemented by the installation and commissioning of a Titan Krios cryo-electron microscope. The very high level of productivity of these end-stations has been driven both by the scientific excellence of the ESRF"s Structural Biology user community and by a very high level of beamline automation which allows experimenters to get the best out of even the most difficult of samples. This talk will provide an overview of the automation currently available, including a completely "hands off" beamline [2] and protocols for the construction of useful, complete diffraction data sets from multi-crystal data collection experiments [3].

December 2018 will see the ESRF temporarily close for the construction of the Extremely Bright Source (EBS) which will have a horizontal emittance of the electron beam in the storage ring ~ 30 times smaller than is currently the case. The proportionate reduction in X-ray beam sizes and divergences will allow the construction of new generation ESRF MX beamlines with flux densities at the sample position up to 5 orders of magnitude higher than at present. This talk will thus also look forward to the possibilities that the ESRF-EBS will afford in the study of structural biology.

References

[1] Mueller-Dieckmann, C., *et al.*, (2015). The status of the macromolecular crystallography beamlines at the European Synchrotron Radiation Facility. *European Physical Journal Plus*, **130(4)**.
[2] Bowler, M.W., *et al.*, (2015). MASSIF-1: a beamline dedicated to the fully automatic characterization and data collection from crystals of biological macromolecules. *Journal of Synchrotron Radiation*, **22**, 1540-1547.
[3] Zander, U., et al., (2015). MeshAndCollect: an automated multi-crystal data-collection workflow for synchrotron macromolecular crystallography beamlines. *Acta Crystallogr.*, **D71**, 2328-43.

S16-06

Data collection at X-ray free-electron lasers and synchrotrons

M. L. Grünbein[1]
[1]Max Planck Institute for Medical Research, Department of Biomolecular Mechanisms, Heidelberg, Germany

High throughput serial crystallography is becoming a highly popular and very efficient way to collect undamaged diffraction data, since it allows spreading the radiation dose over all crystals used for data collection. In particular, this approach allows room temperature data collection from small crystals. Developed initially at X-ray free-electron laser (XFEL) sources using liquid jet injection, serial crystallography is now increasingly used at synchrotron sources as well using high viscosity extrusion (HVE) injection or fixed target approaches to deliver sample into the beam [1-4]. Experience on sample injection both at XFELs and synchrotrons will be discussed.

References
[1] Botha, S., et al., Acta Crystallographica Section D, 2015. 71(2): p. 387-397.
[2] Kovacsova, G., et al., IUCrJ, 2017. 4(4).
[3] Coquelle, N., et al., Acta Crystallographica Section D, 2015. 71(5): p. 1184-1196.
4. Owen, R.L., et al., Acta Crystallographica Section D, 2017. 73(4): p. 373-378.

Acknowledgements to T.R.M. Barends, S. Boutet, R.B. Doak, L. Foucar, A. Gorel, E. Hartmann, M. Hilpert, M. Kloos, G. Nass Kovács, K. Nass, C. Roome, I. Schlichting, R.L. Shoeman, C. Stan and M. Stricker for planning, conducting, discussing and evaluating the presented experiments and results.

Developments in molecular crystallography

S17-01

Modeling bond oriented deformation density in SHELXL

B. Dittrich[1], J. Lübben[1], C. Wandtke[2], C. B. Hübschle[3], G. M. Sheldrick[2]
[1]Heinrich-Heine Universität Düsseldorf, Anorgansiche Chemie und Strukturchemie II, Düsseldorf, Germany
[2]Georg-August Universität Göttingen, Institut für Anorganische Chemie, Göttingen, Germany
[3]University of Bayreuth, Laboratory of Crystallography, Bayreuth, Germany

Features indicative of chemical bonding become more and more apparent
in single-crystal X-ray diffraction, because new detectors lead to improved data quality and facilitate collection of comparably high resolution in ever shorter measurement times. Even in structures measured for connectivity determination residuals frequently show features due to lone pairs and chemical bonds (deformation electron density, DED). Since ignoring such features increasingly becomes a limiting factor in determining structures accurately, a new aspherical scattering factor formalism was implemented in the crystallographic least-squares refinement program SHELXL [1]. The formalism relies on Gaussian functions and can optionally complement the independent atom model (IAM) [2] to take DED into account. Since atomic charges are not required in modeling asphericity, inter- and intramolecular charge transfer is not currently described. Therefore the model is fully backward-compatible with the IAM. Asphericity contributions of the new model were derived from quantum chemical computations on suitable model compounds using density functional theory. Contributions were stored in a database for particular chemical environments, which were defined by the empirical rules of the invariom formalism [3]. In contrast to the Stewart/Hansen/Coppens multipole model (MM) [4], local-atomic coordinate systems are not required anymore. Another important difference to the MM concerns parameter correlation. The MM, which was designed for experimental observation of DED via refinement of multipole parameters, needed to avoid parameter correlation. Since suitable parameterization for each chemical environment within the new model was achieved by metaheuristics rather than by least-squares fitting, parameter correlations are not an issue anymore. SHELXL consequently does not even offer the functionality to adjust these parameters. Still, using pre-calculated scattering factors offers almost similar improvements in the fit to experimental diffraction data and the accuracy/precision of the results than invariom refinement relying on the MM does. Due to a new algorithm atom-type assignment is now fully automated and more user friendly. The new functionality of modeling DED is supported in the SHELXLE graphical user interface [5].

References

[1] Acta Cryst. (2015). C71, 3
[2] Acta Cryst. (1968). A24, 390
[3] Acta Cryst. (2013). B69, 91
[4] Acta Cryst. (1978). A34, 909
[5] J. Appl. Cryst. (2011). 44, 1281

Figure 1

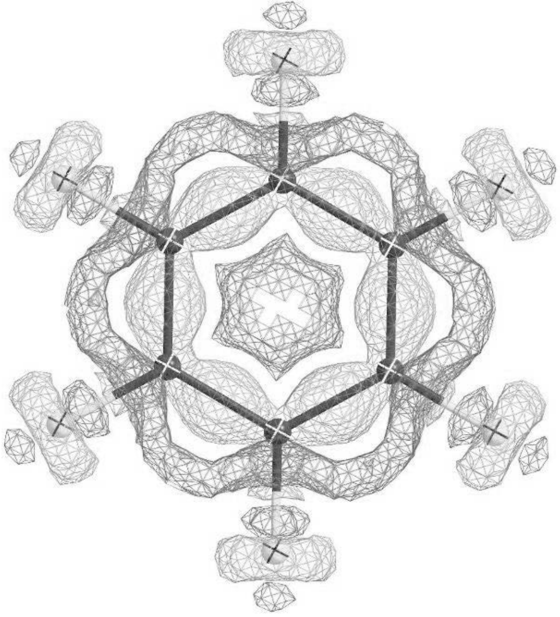

S17-02

Treating residual density in organic molecules using simplified virtual atoms: a technical note

A. Nazarenko[1]
[1]State University of New York, College at Buffalo, Chemistry, Buffalo, United States

The Independent Atom Model (IAM) is based on assumption that the electron density is well described by the spherically averaged density of the isolated atoms. It is a good estimate for the atoms for which the valence electron density is a minor part of the total. IAM is less successful for light atoms: when the quality of structure is reasonably good, you can see areas of bond-related residual positive density located on C-C, C-N and C=O bonds. With resolution better than 0.6-0.5 Å, these peaks can be higher than 0.4 e/Å^3; R-factor and goodness of fit are abnormally large. Controversially, this discourages high resolution measurements!

To reduce the bias coming from bond density, we attempted an empirical approach using usual IAM software (SHELXL-201X, Jana2006). Virtual atoms are placed at calculated positions between C, N, and O atoms, with "occupancies" being different for single, double, aromatic and triple bonds. Scattering is approximated by a single Gaussian which can be possibly justified by small value of correction. These "atoms" are treated as isotropic: multiplication of scattering Gaussian by Debye-Waller factor yields one Gaussian function to describe both effects. The number of introduced parameters can be as low as one (for overall occupancy of pseudo-atom part of the structure). Introduction of virtual atoms makes the effect similar to one hydrogen atom per 4-5 C-C bonds, which is significant enough to justify the effort. Alternatively, each bond can be treated separately (number of additional parameters is roughly equal to the number of bonds). This leads to further improvement. An attempt was made to handle C-H bonds and lone pairs in the same fashion.

A number of structures of various organic and element-organic molecules were tested. Visible improvement of fitting characteristics was achieved, especially for molecules with aromatic fragments.

Some representative examples: Diphenylacetylene, resolution 0.58 Å: before correction R=0.048, S=1.04; after R=0.026, S=1.02. Dimethyl-3,4,5,6-tetraphenylcyclohexa-3,5-diene-1,2-dicarboxylate, 0.80 Å, Cu radiation (!): before R=0.035, S=1.04; after R=0.026, S=1.03. *trans*-[3-(3-nitrophenyl)oxiran-2-

yl](phenyl)methanone, 0.58 Å: before R=0.046, after 0.032. Uncertainties of bond distances are also lower. The quality of the datasets were not sufficient for applying charge density formalism. Nevertheless, the structure improvement can be achieved with minimal effort and using common IAM software.

S17-03

Software development for the P24 "Chemical Crystallography" Beamline at DESY

M. Kremer[1,2], C. W. Lehmann[2]
[1]RWTH Aachen, Institute of Inorganic Chemistry, Aachen, Germany
[2]Max-Planck-Institut für Kohlenforschung, Chemische Kristallographie und Elektronenmikroskopie, Mülheim an der Ruhr, Germany

The new P24 "Chemical Crystallography" Beamline, part of the DESY:PETRAIII storage ring light source, offers a variety of different setups and experimental conditions especially designed for chemical crystallography. To allow users to plan their diffraction experiments, a Graphic User Interface (GUI) was created, with which 3D-Models of the available goniometers can be virtually driven into different positions. This presentation will contain some general information on the P24 Beamline, as well as some useful hints about simple software creation and easy 3D rendering.

Figure 1

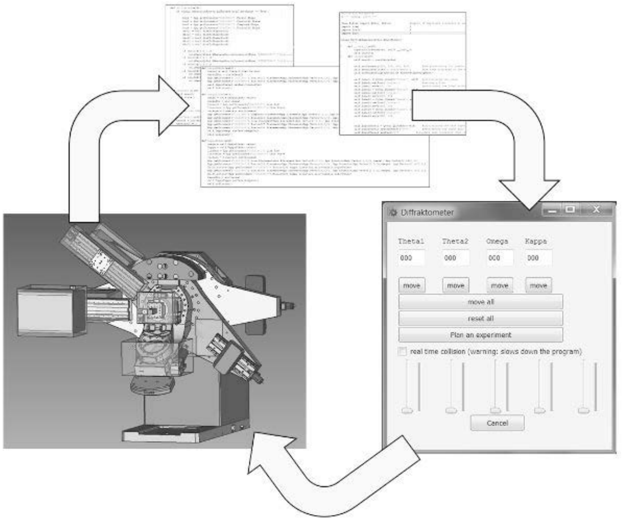

S17-04

StructureFinder

D. Kratzert[1]
[1]Albert-Ludwigs-Universität Freiburg, Institut für Anorganische und Analytische Chemie, Freiburg i. Br., Germany

Every crystallographer at some point has the problem that a measured crystal structure is hard to find in the massive amount of data on modern computers. Presented is a new computer program called StructureFinder. It creates a database of crystallographic structures on a computer or file server and makes them searchable. The program can search for various properties: Unit cell, free text, creation date and included or excluded atom types. To build the database, StructureFinder collects all crystallographic informatio files (cif files) below a certain directory on a hard disk. The containing information is stored into a SQLite database. The database can be accessed by two different interfaces. A stand-alone Qt program (figure 1) to install on a single computer or a web interface (figure 2) to be accesses by a whole work group.
StructureFinder greatly enhances the ability to find old structures in huge collections of crystallographic datasets. The program can easily handle more than 10.000 structures.

Figure 1

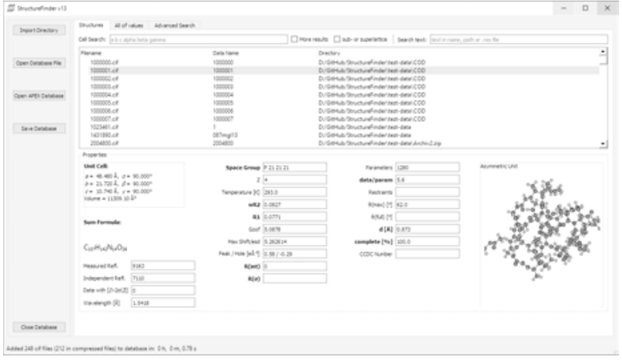

Added 248 cif files (212 in compressed files) to database in: 0 h, 0 m, 0.78 s

Figure 2

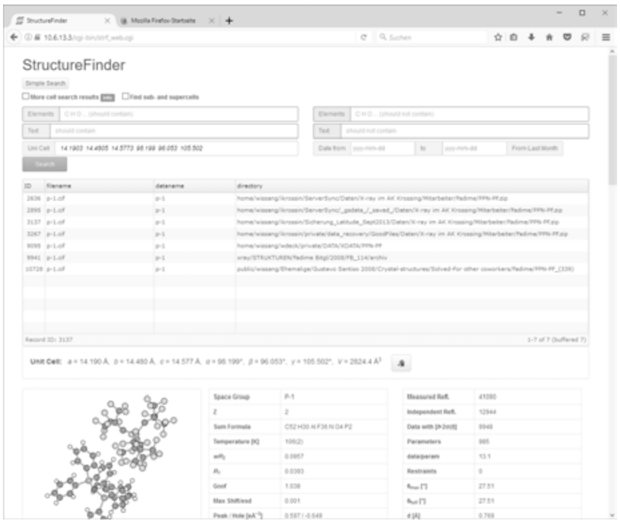

Unit Cell: a = 14.190 Å, b = 14.480 Å, c = 14.577 Å, α = 98.199°, β = 96.053°, γ = 105.502°, V = 2824.4 Å^3

S17-05

Structural modulations in elastically bendable co-crystal of caffeine and 4-chloro 3-nitrobenzoic acid under mechanical stress

S. Dey[1], C. M. Reddy[1], N. Yasuda[2]
[1]Indian Institute of Science Education and Research Kolkata, Department of Chemical Sciences, Mohanpur, India
[2]Sprin-8 synchroton, Beamline BL40XU, Hyogo, Japan

Crystal structure analysis of plastic crystals post mechanical bending has remained elusive till date[1,2] . Recent report on elastically bendable crystal of copper(II) acetylacetonate suggests that structure determination using μfocussed synchroton radiation post mechanical bending is possible because unlike plastic crystals, stress due to mechanical bending is distributed along the length of the elastic ones thus conserving the long range order[3].

Methanol solvated co-crystals of caffeine (CAF) and 4-chloro 3-nitrobenzoic acid (CNB) have been reported to exhibit reversible elastic bending[4]. The compound crystallizes in orthorhombic space group *Fdd*2, asymmetric unit consisting of one CAF and one CNB molecule arranged in dimers via O–H···N and C–H···O hydrogen bonds. It was proposed that upon application of mechanical stress inter-locked packing prevents permanent slippage of molecules as in plastic bending while stretching and contraction of the sheets are allowed by weak C–H···O and van der Waals interactions[4].

To investigate underlying changes in the crystal structure post mechanical bending, space resolved μfocussed X-ray diffraction experiments were performed on a single crystal of dimension 5000 x 12 x 12 μm3 bent into a complete loop [bending face (010)] using radiation λ = 0.78 Å at beamline BL40XU, Spring8, Japan. Using a beam size of 1.63 x 3.50 μm2 diffraction images were collected using ω scans at three positions from outer to inner arc separated by 4 μm at the center of the crystal loop as well as shoulders of the loop.

Data reduction has been performed using *CrysallisPro*. While the lattice parameters do not change significantly as function of the arc at the shoulders, in the mid-region drop in volume of the unit cell is found to be close to 10 % from outer to inner arc. Crystal structures at three points in the center of the crystal loop were solved using *ShelxT* and refined using *ShelxL* and *JANA*2006. Significant changes in both intra- and inter-molecular interactions as function of the arc. The –COOH group gets partially protonated at the outer arc in comparison to the inner arc where the hydrogen bond gets weaker while the center part reveals similar chemistry as the ambient phase.

References

[1]M.K. Panda *et al*. (2015) *Nat. Chem*. **7**, 65–7

[2]S.P. Thomas *et al*. (2017) *Angew. Chem. Int. Ed.* **56**, 8468–8472

[3]A. Worthy *et al*. (2017) *Nat. Chem*. **10**, 65–69

[4]S. Ghosh *et al.* (2012) *Angew. Chem. Int. Ed.* 51, 10319–10203

Figure 1

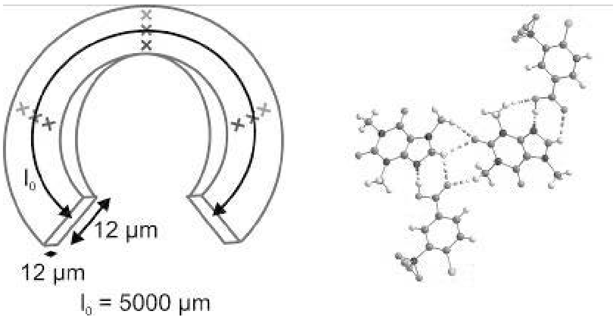

Characterization of defects in crystalline materials

S18-02

Effect of delayed coalescence of nucleation layers on defect structure in HTVPE GaN

M. Barchuk[1], T. Schneider[2], G. Lukin[2], O. Pätzold[2], C. Röder[3], G. Buth[4], E. Yakimov[5], D. Rafaja[1]
[1]Technische Universität Bergakademie Freiberg, Institut für Materialwissenschaften, Freiberg, Germany
[2]Technische Universität Bergakademie Freiberg, Institute of Nonferrous Metallurgy and Purest Materials, Freiberg, Germany
[3]Technische Universität Bergakademie Freiberg, Institute of Theoretical Physics, Freiberg, Germany
[4]Karlsruhe Institute of Technology (KIT), Institute for Photon Science and Synchrotron Radiation, Eggenstein-Leopoldshafen, Germany
[5]Russian Academy of Science, Institute of Microelectronics Technology and High Purity Materials, Chernogolovka, Russian Federation

Gallium nitride (GaN) is extremely promising direct wide bandgap semiconductor material, which is typically grown by heteroepitaxy on foreign substrates. As alternative growth technique to the commonly used metal-organic vapor phase epitaxy (MOVPE), we use high-temperature vapor phase epitaxy (HTVPE) in conjunction with a recently developed vertical reactor [1], which allows a simple control of deposition parameters and low cost production of the GaN layers. In order to achieve a quality of HTVPE GaN layers, which is comparable with the quality of the MOVPE GaN layers having the thickness of several mm, for instance the total density of dislocations of ~ 5×10^8 cm^{-2}, the HTVPE growth mode is permanently improved [2]. In this contribution, we investigate the delayed coalescence of GaN nucleation islands grown on sapphire substrates (Fig. 1 left) that is achieved at low ammonia fluxes as a possible factor influencing the quality of HTVPE GaN layers, in particular the residual stress and the density of screw and edge threading dislocations (TDs).

Fig. 1. (left) - scanning electron micrograph showing the topography of delayed nucleation layer; (middle) – panchromatic cathodoluminescence image of the overgrown layer deposited on GaN template with normal coalescence; (right) – shift of the E_2(high) mode in micro-Raman spectra.

The GaN layers with different thicknesses that were deposited at normal and delayed coalescence of the nucleation islands have been investigated using coplanar and X-ray diffractions, μ-Raman spectroscopy and cathodoluminescence (CL). Panchromatic CL images have shown that TDs are distributed irregularly and that their density is higher at the grain boundaries than in the interior of the grains (Fig. 1 middle). CXRD and GIXRD complemented by Monte Carlo simulations of reciprocal space maps that were performed for correlated dislocation ensemble [3] were utilized to determine the densities of edge and screw TDs. The μ-Raman spectroscopy quantified the residual stresses in the GaN layers and their depth gradients (Fig. 1 right). The results of all methods confirmed bunching of dislocations, reduction of the dislocation density with increasing layer thickness and a positive effect of the delayed coalescence on the quality of the GaN layers grown directly on the sapphire substrates.

References

[1] G. Lukin *et al*., *Phys. Stat. Solidi C* **11** (2014) 491-494.
[2] M. Barchuk *et al*., *Cryst. Res. Tech*., **70** (2017) 1700113.
[3] M. Barchuk *et al*., *J. Appl. Phys,* accepted.

Figure 1

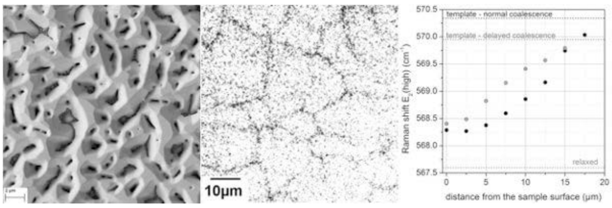

S18-03

Characterizing complex molecular disorder using single crystal diffuse scattering

E. Schmidt[1], R. B. Neder[1]
[1]Friedrich-Alexander-Universität Erlangen-Nürnberg, Physics, Erlangen, Germany

To crystallize modern materials can be quite challenging and many materials show disorder; Orientational disorder is common especially in molecular materials with several molecules in the unit cell. We use single crystal diffuse scattering to characterize the interaction between the various components in such materials.

A complex molecular crystal will usually consist of several components on several sites within the unit cell. Furthermore, a single site may be occupied by molecules in different orientations e.g. a first molecule in orientations A_1, B_1 or C_1 on site 1 and a second molecule in orientations A_2, B_2 and C_2 on site 2, Fig. 1. In such systems short range order is common: On a local scale, the molecules tend to show preferred pair-wise arrangements. Interactions may exist only between equivalent molecules on a given site or include interactions between the different sites. Characterizing this local order enables profound statements about molecular interactions.

With the help of molecular form factors [1] and the theory of diffuse scattering (e.g. Warren [2]), we developed a method that characterizes the local interaction of molecules directly in reciprocal space. For the complex system introduced it is possible to characterize, whether the ordering schemes of the molecules on site one and of the molecules on site two interact, or if the disorder is solely characterized by the interaction of molecules on site one of one unit cell with molecules on site one of neighboring unit cells. This initial analysis in reciprocal space enables the deviation of a qualitative disorder model. On the basis of this model a least squares fit to the diffuse scattering data provides a quantitative measure for the strengths of the interactions.

The method developed for characterizing complex molecular disorder using single crystal diffuse scattering is a powerful tool to understand and model molecular interactions in disordered crystals. As the method treats data directly in reciprocal space and enables least squares fitting of disorder models, calculations can be performed on desktop computers without the excessive use of computation time.

References

[1] Schmidt, E., & Neder, R. B.(2017). Acta Cryst. A,73,231.
[2] Warren, B.E. (1969). X-ray Diffraction. Courier Corporation.

Figure 1: (a) Schematic representation of a complex disordered unit cell. (b) Example for diffuse scattering for a complex disordered system.

Figure 1

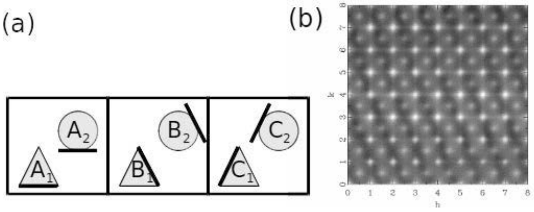

S18-04

Structural incorporation of Mo^{6+} into akaganéite (β-FeOOH) and its microbial reduction by *Shewanella loihica* PV-4

R. M. Bolanz[1], C. Grauer[1], R. Cooper[2], J. Göttlicher[3], R. Steiniger[3], S. Perry[4], K. Küsel[2]
[1]Friedrich Schiller Universität Jena, Institut für Geowissenschaften, Jena, Germany
[2]Friedrich Schiller Universität Jena, Aquatic Geomicrobiology, Jena, Germany
[3]Karlsruhe Institute of Technology (KIT), ANKA Synchrotron Radiation Facility, Karlsruhe, Germany
[4]Harwell Science and Innovation Campus, Diamond Light Source Ltd, Didcot, United Kingdom

Among all natural iron oxides, akaganéite (β-FeOOH) possesses one of the most unconventional structural setups and scavenges for large quantitates of molybdenum (Mo^{6+}). The exact mechanisms for Mo^{6+} incorporation into the akaganéite crystal structure are poorly understood and the ability of dissimilatory Fe^{3+}-reducing microorganisms to reduce pure akaganéite is not well characterized. In this study, we investigated the short-range order around Mo^{6+} in akaganéite and the fate of Mo^{6+} under microbially-mediated Fe^{3+}-reducing conditions. Akaganéite can incorporate up to 14.11 ± 0.22 wt% Mo, while the Fe content decreases from 59.70 ± 0.31 to 40.40 ± 0.24 wt%, which indicates a loss of 2–3 Fe atoms for each Mo incorporated. At the same time, the unit cell parameters a, b and c decrease, while β increases with increasing Mo content. Dissolution of akaganéite by *Shewanella loihica* PV-4 showed higher dissolution rates of Mo-akaganéite compared to its Mo-free counterpart. Moreover, the reduction of Mo^{6+} within the crystal structure of akaganéite is most likely microbially-induced ($Fe^{3+} \rightarrow Fe^{2+}$, $Mo^{6+} + 2Fe^{2+} \rightarrow Mo^{4+} + 2Fe^{3+}$). Furthermore, X-ray absorption spectra collected at the Mo L_3-edge show a peak-splitting of the white line with a splitting gap of 2.7 eV and an increased amplitude for the first peak. This observation indicates Mo_{6+} is octahedrally coordinated by oxygen, assuming a strongly distorted MoO_6-octhaedron. Fitting of the X-ray absorption spectra of the short-range order around Mo^{6+} in akaganéite supports the presence of a strongly distorted MoO_6-octahedron in a coordination environment similar to the Fe position in akaganéite and the formation of Fe-vacancies close to the newly incorporated Mo^{6+}.

S18-05

γ -Al_2O_3 – a defect stabilized phase

M. Rudolph[1], M. Motylenko[1], D. Rafaja[1]
[1]Technische Universität Bergakademie Freiberg, Freiberg, Germany

The γ-alumina (γ-Al_2O_3) belongs to the metastable phases and is frequently used for functionalization of surfaces, as it possesses a large surface and high catalytic activity. Recently, γ-Al_2O_3 was suggested to be employed as a functional coating for filtration of molten aluminum and steel alloys. Such melts contain nanoscopic inclusions of metastable alumina phases, which are believed to anchor more easily on related material than on a conventional (non-functionalized) filter surface.

However, γ-Al_2O_3 is only stable below 700 °C. At higher temperatures, it transforms over the metastable phases δ-Al_2O_3 and θ-Al_2O_3 to the thermodynamic stable α-Al_2O_3. For applications at higher temperatures, γ-Al_2O_3 must be stabilized. A prerequisite of a targeted stabilization is the understanding of the role of microstructure defects for the consecutive phase transition that requires a reliable and parametrized structure model of γ-Al_2O_3.

In this contribution, a new microstructural model of γ-Al_2O_3 derived from crystalline boehmite will be introduced that is based on a 3D network of antiphase boundaries (APBs). In this model, the APBs tessellate the spinel-type γ-Al_2O_3 nanocrystallites, but keep their cubic close packed anion sublattice intact. It will be shown that this microstructure model is capable of describing a strongly anisotropic broadening of diffraction lines that is observed both in selected electron diffraction (SAED) and in X-ray diffraction (XRD) patterns. The SAED and XRD patterns calculated using our structural model are in excellent agreement with the respective experimental diffraction patterns. The adjustment of the simulated diffraction patterns on the measured ones revealed fundamental parameters of the microstructure model like the mean size of the domains that are constrained by the APBs and the ordering of structural vacancies in the spinel-like structure of γ-Al_2O_3. Finally, the effect of these microstructure defects on the thermal stability of γ-Al_2O_3 and on the formation of a tripled supercell, which is associated with the formation of δ-Al_2O_3, will be discussed.

Bio-Crystallography VI: Protein - nucleic acid complexes

S19-01

The mechanism of negative DNA supercoiling by gyrase: dissecting structure, function and dynamics by single-molecule FRET and X-ray crystallography

A. Gubaev[1], D. Weidlich[1], S. Hartmann[1], M. G. Rudolph[2], D. Klostermeier[1]
[1]Universität Münster, Münster, Germany
[2]F. Hoffmann-La Roche Ltd, Chemical Biology, Basel, Switzerland

Gyrase is a bacterial DNA topoisomerase that introduces negative supercoils into DNA in an ATP-dependent reaction. The two-fold symmetric heterotetrameric enzyme is formed by two GyrB and two GyrA subunits. According to the strand-passage mechanism, gyrase negatively supercoils DNA by cleaving both strands of a DNA duplex and passing a second DNA duplex through the gap. To catalyze strand passage and supercoiling, three protein-protein interfaces, termed N-gate, DNA-gate and C-gate, need to open and close in a temporally coordinated manner.

Using single-molecule FRET and X-ray crystallography, we have generated structural models for key intermediates in the catalytic cycle of gyrase, and have delineated a cascade of DNA- and nucleotide-driven conformational changes of gyrase/DNA complexes that drive the supercoiling reaction (reviewed in Ref. 1, Figure). DNA bound at the DNA-gate, close to the catalytic tyrosines that act as a nucleophile in DNA cleavage, is distorted in a process coupled to cleavage. Flanking DNA regions establish contacts with the C-terminal domains (CTDs) of GyrA that then move away from the gyrase body. Wrapping of longer DNAs around the CTDs induces a narrowing of the N-gate, formed by the GyrB subunits. The N-gate closes on ATP binding, fixing a second DNA segment above the first in the correct geometry for strand passage. Strand passage then requires opening of the DNA-gate, and the transported DNA duplex leaves the enzyme through the open C-gate. Crystal structures demonstrate that the DNA-and C-gates can open in principle (2, Figure), but their opening has not been observed in real time. Recent biochemical studies show that gyrase can also catalyze negative supercoiling in the absence of strand passage, following a nicking-closing mechanism (3). It is unclear whether this pathway is widely explored or constitutes a back-up mechanism. Gyrase is a common drug target for therapeutics against infections. Mechanistic knowledge paves the way for the identification of novel, mechanism-based gyrase inhibitors.

References

[1] Gubaev, A., D. Klostermeier, DNA Repair 2014, 16: 23-34.
[2] Rudolph, M.G., D. Klostermeier, J. Mol. Biol. 2013, 425(15): 2632-2640.
[3] Gubaev, A., D. Weidlich, D. Klostermeier, Nucleic Acids Res. 2016.

Figure 1

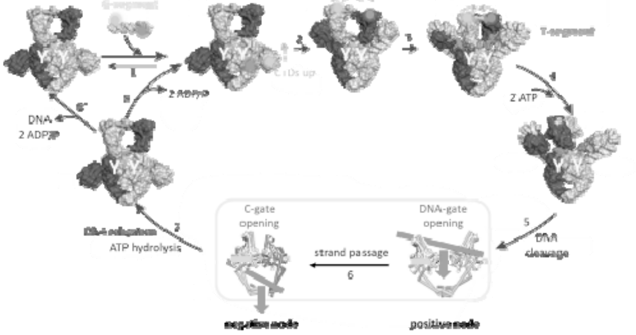

S19-02

Structure and conformational dynamics of type I-Fv CRISPR-Cas mediated DNA interference

P. Pausch[1], W. Steinchen[1], H. Müller-Esparza[2], D. Gleditzsch[2], F. Altegoer[1], L. Randau[2], G. Bange[1]
[1]Philipps University Marburg, Chemistry, Marburg, Germany
[2]MPI for Terrestrial Microbiology, Marburg, Germany

Question

CRISPR-Cas systems are prokaryotic immune systems against invading nucleic acids. Type I CRISPR-Cas systems employ highly diverse, multi-subunit surveillance Cascades facilitating duplex formation between crRNA and complementary target DNA for R-loop formation, retention and DNA degradation by the subsequently recruited nuclease Cas3. Typically, the large subunit recognizes *bona fide* targets through the protospacer adjacent motif (PAM) and the small subunit guides the non-target DNA strand (NTS). However, the subtype I-F variant (I-Fv) does not feature small and large subunit homologs and it is unclear how it compensates for the essential functions of PAM dependent recognition of foreign DNA and NTS guiding.

Methods

X-ray Crystallography, Small Angle X-ray Scattering (SAXS), Hydrogen-Deuterium Exchange Mass Spectrometry (HDX-MS), in vivo DNA Interference Assay by Efficiency of Transformation (EOT)

Results

X-ray crystallography reveals apo- and target DNA-bound structures of the type I-F variant (I-Fv) Cascade lacking the small and large subunits. Large and small subunits are functionally replaced by the 5′-terminal crRNA cap Cas5fv and the backbone protein Cas7fv, respectively. Cas5fv facilitates PAM recognition from the DNA major groove site, in contrast to all other hitherto described type I systems. Comparison of I-Fv with the related anti-CRISPR protein vulnerable I-F Cascade, reveals that type IFv Cascade differs substantially at the anti-CRISPR protein target sites and might therefore be resistant to viral Cascade interception. Conformational dynamics analysis by HDX-MS of the interference stages confirms the interpretation derived from the crystal structures and reveals that the Cas3fv nuclease is recruited to the NTS after R-loop formation for processive degradation of foreign DNA.

Discussion

Analysis of the structure and conformational dynamics of the effector complex suggests a model for type I-Fv mediated DNA interference that involves the following stages: PAM searching by Cas5fv; Seed-bubble formation initiated by Cas5fv; R-loop propagation and locking along Cas7fv; Cas3fv association and NTS nicking; processive degradation of the NTS for DNA interference.

References

[1] Pausch et al. (2017) Structural Variation of Type I-F CRISPR RNA Guided DNA Surveillance. Molecular Cell
[2] Gleditzsch et al. (2016). Modulating the Cascade architecture of a minimal type I-F CRISPR-Cas system. Nucleic Acids Research

S19-03

Canonical and novel non-canonical cold shock-domains of UNR interact with lncRNA roX2 and MLE during roX2 remodelling

N. M. Hollmann[1], P. Masiewicz[1], L. J. Sweetapple[1], S. von Buelow[1], P. K. A. Jagtap[1], J. Hennig[1]
[1]EMBL Heidelberg, Structural and Computational Biology, Heidelberg, Germany

Upstream of N-ras (UNR) is a cold shock-domain (CSD) containing RNA binding protein. In *Drosophila melanogaster* it has an important role during the early steps of dosage compensation. It promotes the assembly of the male-specific lethal (MSL) complex, which achieves two-fold hypertranscription of male X-linked genes (1). The current hypothesis describes UNR to bind to stemloops of lncRNA roX2 in concert with MLE to remodel the RNA and prime it for incorporation into the MSL complex via MSL2 (2, 3). In order to obtain detailed mechanistic insights into RNA remodelling and complex formation, structural knowledge is paramount.

Hitherto, only the structure of the first of five predicted CSD of UNR has been solved (4). Hence structure determinations of the other CSDs and the full-length dUNR, as well as CSDs bound to parts of RNA and MLE are necessary.

Our biochemical and structural studies of UNR and its interactions with MLE revealed surprising novel features. We solved a triple cold shock domain crystal structure validated by SAXS data, which unveiled as of yet undiscovered non-canonical cold-shock domains and domain interactions critical for architecture and stability. Further, we were able to determine domains of UNR responsible for promoting the interaction with MLE and roX2 by EMSA and filter binding assays. Nuclear magnetic resonance (NMR) data provide further CSD structures and insight into their RNA binding preference. Integrating X-ray crystallography, NMR and small-angle X-ray and neutron scattering drives the structure determination of the full-length complex.

References

[1] Militti et al. 2014. Nat Commun. 5, 4762
[2] Maenner et al. 2013. Mol Cell. 51, 174-84
[3] Ilik et al. 2013. Mol Cell. 51, 156-73
[4] Hennig et al. 2014. Nature. 515, 287-290

S19-04

Structural and Functional Characterization of the Spliceosomal Protein Prpf39

F. De Bortoli[1], B. Loll[2], M. C. Wahl[2], F. Heyd[1]
[1]Freie Universität Berlin, Biochemie, Berlin, Germany
[2]Freie Universität Berlin, Structural Biochemistry, Berlin, Germany

Introduction

Splicing is an essential step in RNA processing. It is catalyzed by the spliceosome which consists of five core components, the U1, U2, U4, U5 and U6 snRNPs. The spliceosome is assembled in a stepwise manner and must accurately recognize each splice site as a single mistake can result in the production of a nonfunctional protein. This complex process needs to be finely regulated and to this purpose many additional proteins are involved.

Prpf39 is a largely unstudied protein that came to our attention because it is alternatively spliced in a differential manner in murine naive vs memory T-cells. Earlier studies in yeast have shown that Prp39 is necessary for binding of the U1snRNP to its pre-mRNA substrate and has been proven to be essential in cell lines. Prp39 has been shown to be associated with the yeast U1snRNP forming a heterodimer with Prp42.

Objectives

The objective of this project was, to analyze mammalian Prpf39 on both a structural and functional level to further increase understanding of how this protein is involved in the splicing cycle. Interestingly, outside of the yeast system there is no prp42 homolog which could act as a dimerization partner leading to the question of how Prpf39 is associated with the spliceosome in higher eukaryotes. Furthermore, understanding the functionality of Prpf39 could help us understand its connection to T-cell differentiation states.

Results

Here we present the crystal structure of murine Prfp39 at 3.3 Å resolution. The protein is largely α-helical and the structure shows the protein to be organized as a dimer with three distinct subdomains. The dimerization is also observed in solution with SEC-MALS and the mode of dimerization shows significant similarity to the yeast Prp39/Prp42 heterodimer. The dimerization interface shows a high conservation in its residues implying a functional relevance for the Pprf39 homodimerization. Based on this, structurally guided point mutations were made to disrupt the dimer. The mutation of just one of the 665 residues of Prpf39 is enough to completely disrupt the dimer giving us a basis for further functional studies exploring the impact of Prpf39 dimerization on splicing.

Conclusion

Prpf39 is an essential protein that is involved in splicing. Here we contribute to a further understanding of its role through elucidation of its structure. We have inserted structure guided mutations that disrupt the dimer and are now testing the functionality of the dimer.

S19-06

Building atomic models into electron-microscopy maps with ARP/wARP

G. Chojnowski[1], J. Pereira[1,2], P. Heuser[1], V. Lamzin[1]
[1]European Molecular Biology Laboratory Hamburg, Hamburg, Germany
[2]Max Planck Institute for Developmental Biology, Tübingen, Germany

The number of experimentally determined structures of nucleic acid–protein complexes is rapidly increasing, reflecting discoveries and a growing interest in the biological functions exerted by nucleic acids beyond their protein-coding capacity. Recent examples include the CRISPR surveillance complex [1] and intron lariat spliceosome [2] that were determined to help elucidate mechanisms of bacteriophage resistance and splicing. Interestingly, both these structures were determined using cryogenic Electron Microscopy (cryo-EM), demonstrating a broadening relevance of this method, in particular for the studies of large macromolecular samples that may be difficult to crystallise.

The ARP/wARP software project [3] has, for over twenty years, provided tools for macromolecular X-ray crystallographic structure determination. Here we present recent developments of ARP/wARP that enables *de novo* building of atomic models of protein structures and protein-nucleic acid complexes into cryo-EM maps at a resolution better than 3.5 Å. The input maps are automatically pre-processed to account for possible over-sharpening. The main-chain tracing routines for proteins and nucleic acids have been advanced to yield more reliable models with improved local stereochemistry [4]. A new protein sequence-docking algorithm has been developed based on the Fragmentation Tree concept [5] and on the graph theory method and which provides better performance at low resolution. Finally, the implementation of a new method for building poorly defined loops has enabled a significant reduction in the fragmentation of the built model.

Initial tests on deposited cryo-EM maps have been particularly encouraging. One example is the automatic construction of a 70%

complete model of the 70S ribosome (PDB code 5mdv) in a 3.0 Å resolution EM map in less than 48 hours on a single core.

References

[1] Xiao Y *et al.* (2017). *Cell.* **170**, 48-60.
[2] Wan R *et al.* (2017). *Cell.* **171**, 120-32.
[3] Langer *et al*. (2008). *Nature Protoc.* **3**, 1171-1179.
[4] Pereira J, Lamzin VS. (2017). *IUCrJ* **4**, 657-670.
[5] Langer *et al*. (2012). *J Mol Biol*. **419**, 211-222.

New Crystal structures and properties

S20-01

Structure variations within certain rare-earth disilicides

M. Nentwich[1], M. Zschornak[1,2], M. Sonntag[1], R. Gumeniuk[1], S. Gemming[2,3], T. Leisegang[1,4], D. C. Meyer[1]
[1]Technische Universität Bergakademie Freiberg, Insitut für Experimentelle Physik, Freiberg, Germany
[2]Helmholtz-Zentrum Dresden-Rossendorf, Institute of Ion Beam Physics and Materials Research, Dresden, Germany
[3]Technische Universität Chemnitz, Institute of Physics, Chemnitz, Germany
[4]Samara National Research University, Samara Center for Theoretical Materials Science, Samara, Russian Federation

By evaluating almost 300 articles with 430 structure reports of hexagonal AlB_2- and tetragonal $ThSi_2$-like compounds (R is an alkaline earth metal, rare earth metal or actinoide, T is a transition metal), we gained an overview of the various structure reports on RSi2 and $R_2T\mathrm{Si}_3$ compounds. We summarized composition, lattice parameters a and c, ratios c/a, formula units per unit cell, and structure types in an extensive table and analyzed the structural relationships geometrically and within a group-subgroup scheme.

As a result, we identified a typical occupational pattern within the Si/T sublattice of AlB_2-like compounds occurring in all structure types with Si/T ordering. We further studied possible Si/T ordering for tetragonal compounds by means of geometry, double bonds distribution, and Bader analysis considerations. In addition, we performed DFT calculations on carefully chosen, not yet reported $R\mathrm{Si}_2$ and $R_2T\mathrm{Si}_3$ compositions to evaluate their stability and predict a potential synthesis.

Finally, we discuss peculiarities of symmetry distribution among the $R\mathrm{Si}_2$ and $R_2T\mathrm{Si}_3$ compounds and several correlations related to structural parameters. We found that the thermal treatment has a tremendous effect on the formation of superstructures. Furthermore, we identified the origin of Si-T bond length variations as electronic interplay between R element and Si/T sublattice rather than the rare-earth radius.

S20-02

Hydrothermal Synthesis of M3Sb4O6F6 (M = Zn, Fe etc.), FeSbO2F2 and their Characterization.

S. I. Ali[1], M. Johnsson[2]
[1]Moyna College, Vidyasagar University, Department of Chemistry, Tamluk, India
[2]Stockholm University, Department of Materials and Environmental Chemistry, Stockholm, Sweden

Non-centrosymmetric materials (NCS) are of interest due to their interesting physical properties such as magnetic frustration and nonlinear optical second harmonic generation.[1-3] Transition metal oxo-fluorides containing p-block elements with a streochemically active lone-pair often have a tendency to form NCS materials. The p-block elements prefer to bond to oxygen while transition metal cations bond to both oxygen and fluoride ions in such an environment, which leads to form non-centrosymmetric compounds often. The objective is to find out new transition metal oxo-fluorides of M – Sb – O – F -type (M = Transition metal) by hydrothermal techniques and then investigate their physical properties. Single crystals of the new compounds M3Sb4O6F6 (M = Zn, Fe etc.) and FeSbO2F2 were successfully synthesized at relatively low temperature by using hydrothermal techniques. The new compounds M3Sb4O6F6 crystalizes in the non-centrosymmetric P-43m space group where a = 8.1291 (10) Å for M = Zn. The crystal structure is made up of corner sharing [MO2F4] octahedra that connect exclusively via fluorine. Trigonal pyramidal [SbO3] units form [Sb4O6] groups that are located in the voids of the [MO2F2]n network. Powder second-harmonic generation (SHG) measurements using 1064 nm radiation on Zn3Sb4O6F6 indicate an SHG intensity of approximately 40 × α-SiO2.[4] FeSbO2F2 crystallizes in monoclinic symmetry with $C2/c$ space group with a = 11.9129(15) Å, b = 4.9605(5) Å, c = 5.5000(6) Å, β = 103.897(7)°. It consists of [FeO2F2]n sheets and [SbO2]n chains. Magnetic susceptibility and heat capacity measurements indicate long-range antiferromagnetic ordering below a Néel temperature of ~175 K. [5]

References

[1] Hu, S. et al. (2014). Chem. Mater. 26, 3631.
[2] Hu, S. et al. (2012). *Dalton Trans.* 41, 12786.
[3] Yu, H. et al. (2016). *Cryst. Growth Des.* 16, 1081.
[4] Ali, S. I. et al. (2017). *J. Solid State Chem.* 256, 158.
[5] Ali, S. I. et al. (2017). *Inorg. Chem.* 56, 4662.

S20-03

Structural and molecular spectroscopic behaviour of the Mg-Ni kieserite solid solution, (Mg,Ni)$SO_4\cdot H_2O$, with relevance to icy satellites of Jupiter and Saturn

D. Talla[1], M. Wildner[1]
[1]Universität Wien, Institut für Mineralogie und Kristallographie, Wien, Austria

The investigation of the presence of sulfates in our solar system receives growing attention, as these compounds significantly influence melting equilibria on the icy moons of Saturn and Jupiter, leading to the existence of subsurface oceans and even cryovolcanism (Kargel 1991, McCord et al. 2001). Although higher-hydrated sulfates such as epsomite and mirabilite dominate on their surfaces, it is not excluded that low-hydrated Mg-sulfates, such as kieserite, are also present, as indicated by the results of high-pressure experiments (Kargel 1991, Nakamura and Ohtani 2011). Given the probable intermediate Mg/Ni composition of kieserite and other sulfates on the icy moons (Burgess et al. 1991), the relationship of structural and spectroscopic properties along the entire Mg-Ni kieserite solid-solution range is of particular interest, especially in view of the known differences between both endmembers.

We hereby present first results on structural and lattice parameter changes from powder X-ray diffraction data of hydrothermally synthesized material with variable Mg/Ni ratio. Respective FTIR and Raman spectra reveal a significant decrease in the wavenumber positions of the vibrational modes of the H2O molecule as the Ni/Mg ratio progresses towards Ni-dominant compositions. The entire Mg-Ni kieserite solid solution shows Vegard-type behaviour, i.e. lattice parameters as well as spectral band positions change along linear trends with increasing Ni content (a = 6.914(2) - 6.837(2), b = 7.621(2) - 7.593(2), c = 7.642(2) - 7.471(3) Å; β = 118.05(2) - 117.82(2)° from the Mg- to the Ni-endmember). The changes in wavenumber position observed for the H2O absorption features in the IR spectra enable to roughly estimate the Ni/Mg ratio in extraterrestric kieserite from present and future IR remote sensing data as well as in-situ measurements.

References

[1] Burgess R, Wright IP, Pillinger PT (1991) Determinations of sulphur-bearing components in C1 and C2 carbonaceous chondrites by stepped combustion. Meteoritics 26, 55-64
[2] Kargel JS (1991) Brine volcanism and the interior structures of asteroids and icy satellites. Icarus 94, 368-390
[3] McCord TB, Hansen GB, Hibbits CA (2001) Hydrated salt minerals on Ganymede's surface: Evidence of an ocean below. Science 292, 1523-1525
[4] Nakamura R, Ohtani E (2011) The high-pressure phase relation of the MgSO4–H2O system and its implication for the internal structure of Ganymede. Icarus 211, 648-654

S20-04

Structural phase transitions of copper(I) phosphide $Cu_{3-x}P$

T. Doert[1], A. Wolff[1], J. Hunger[1]
[1]Technische Universität Dresden, Chemistry and Food Chemistry, Dresden, Germany

Introduction

Two different modifications of the metal phosphide $Cu_{3-x}P$ have been reported in literature. At ambient temperature, $Cu_{3-x}P$ crystallizes in the acentric hexagonal space group $P6_3cm$ ($a = 695.9$ pm, $b = 714.3$ pm, *anti*-La_3F type).[1] Upon heating, to 200 °C the compound undergoes a phase transition to adopt the Na_3As type (trigonal space group $P\text{-}3m1$; $a = 409.2$ pm, $b = 718.6$ pm at 560 °C).[2] It is of particular interest how the substoichiometry of this compounds manifest itself in partially occupied copper positions, as Cu vacancies seems to be responsible for plasmonic absorption features.[3]

Objectives

We grew single crystals of $Cu_{3-x}P$ and investigated the crystal structure at different temperatures.

Results

The room temperature modification of $Cu_{3-x}P$ (*anti*-La_3F type) as reported by Oloffson can structurally be subdivided into layers.[1] Two of the four unique copper atoms are located on the nodes of a honeycomb net parallel (001). Each of these copper atoms is bonded to a phosphorus atom. Two copper sites are located between the honeycomb nets and are only partially occupied, as evidenced by the structure refinement and density functional theory calculations.[1,3] Upon cooling single crystals of $Cu_{3-x}P$ to 80 K, two further structural phase transitions are observed. Additional reflections indicate a doubling of the *a* and *b* axes of the trigonal unit cell below 250 K and a structure model an fourfold isomorphic superstructure of the RT structure could be deduced. Further reflections emerge below 200 K and point towards an additional tripling of the *c* axis.

Conclusion

Upon cooling two hitherto unknown phase transitions of $Cu_{3-x}P$ were observed and the crystal structure at 200 K could be determined.

References

[1] O. Oloffson, *Acta Chem. Scand.* **1972**, *26*, 2777–27871
[2] H. Schlenger, H. Jacobs, R. Juza, *Z. Anorg. Allg. Chem.* **1971**, *385*, 177–201.
[3] L. De Trizio, R. Gaspari, G. Bertoni, I. Kriegel, et al., *Chem. Mater.* **2015**, *27*, 1120–1128.

Figure 1: Precession images of $Cu_{3-x}P$; reconstructed *hk*0 layers at RT (left) and at 100 K (right).

Figure 1

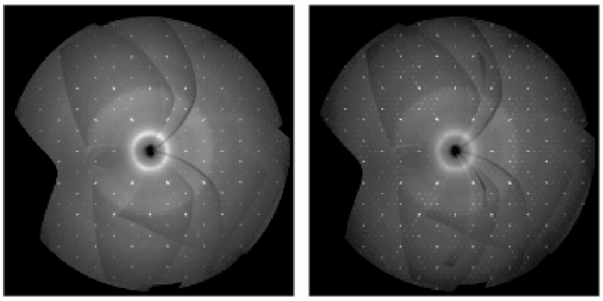

S20-05

Crystal, electronic structure, optical and electrical studies of new 2D hybrid perovskite [(CH2)n(NH3)2]MX4 ; X= Cl, Br; M= Co, Mn; n= 4-9 promising for photovoltaic applications

S. K. Abdel-Aal[1], A. Seham[1]
[1]Cairo University, Physics, Giza, Egypt

Great attention has been devoted to the preparation and characterization of organic-inorganic hybrid perovskites (OIHs). These advanced materials can provide low cost materials for self assembly quantum well applications, fuel, solar cells, batteries, electronic and optoelectronic applications. Diammonium halide perovskite hybrids [NH3(CH2)nNH3]MClxBr4-x ; x= 0, 2, 4; M= Co, Mn; n= 4-9 allow mixing of organic and inorganic components in one molecule which possesses a property that may not exist in either of the parent components. Possibilities could elaborate hybrid materials in terms of processing new chemical and physical properties according to the application needed. Single crystals were prepared by slow evaporation. The complete structure information as well as lattice parameters for Co series n= 4-9 are provided, and for n = 5-6 for Mn hybrid. Differential thermal analysis DSC shows reversible order - disorder transition for both the Co and Mn hybrids. Permittivity studies confirm the phase transition. The optical properties of Co series show strong absorption in the visible range from 500 to 700 nm. The calculated band gap energy using Kubelka-Munk equation ranges from 1.75 eV for [NH3(CH2)9NH3]CoCl4 denoted C9CoCl to 1.73 eV for [NH3(CH2)5NH3]CoCl2Br2 denoted C7CoCB. These values are very promising for lead free hybrid perovskite solar cell.

Fig.1. Visible spectra and band gap energy of Co-OIHs (left panel), Crystal structure of [NH3(CH2)4NH3]CoCl4, XPS raw spectra of [NH3(CH2)9NH3]CoCl4

Electronic structure and chemical bonding in Co, Mn OIHs were studied by X-ray (XPS) photoemission spectroscopy. All elements of Co and Mn organic-inorganic hybrid perovskites were found in XPS spectra and can be related to the peaks of N1s, C1s, Co2p, Mn2p and Cl2p. Wide peak of C1s spectra was related to the chemically unequivalent C atoms in the compounds. The spectrum of the N1s level with binding energies of 401.2 eV was assigned to NH3-group. The analysis of Co2p states in Co OIHs compounds shows the divalent state of Co with a typical satellite structure.

Figure 1

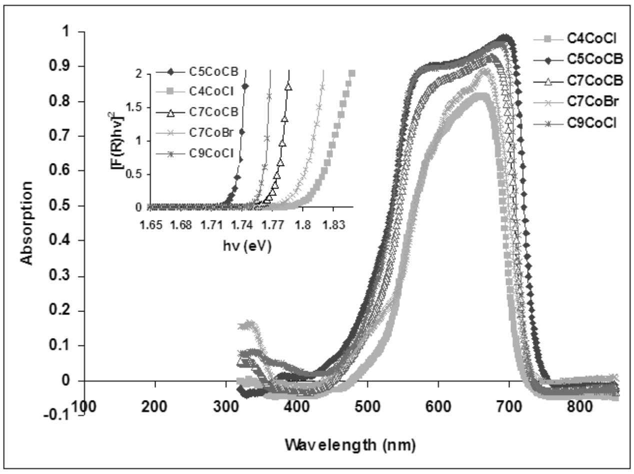

Figure 2

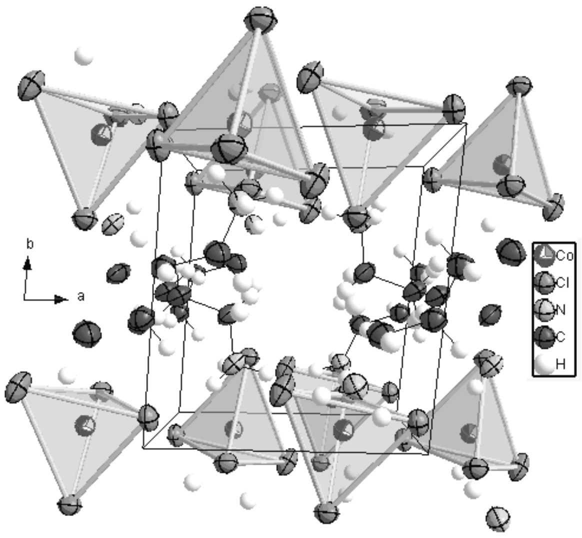

S20-06

Pure gyrotropic phase transitions in the arcanite related materials PbMGeO4 (M = Ba, Sr)

M. Schreyer[1], G. Nénert[1], D. Opper[2]
[1]Malvern Panalytical, Almelo, Netherlands
[2]Malvern Panalytical, Almelo, Netherlands

Gyrotropic phase transitions are characterized by the appearance of spontaneous optical activity [1]. The appearance of such activity is very common in ferroelectric materials. In such materials, the optical activity is a secondary order parameter and is coupled to the primary order parameter, the electrical polarization. However, only very rare examples are known of a purely gyrotropic phase transition. Among those, one can cite $BiFeO_3$ under strain [2] and $(C_5H_{11}NH_3)_2ZnCl_4$ as a function of temperature [3]. In both cases, the transition exhibits a change from Pnma to $P2_12_12_1$ symmetry.

In this contribution, we have investigated two materials belonging to the BaNdGaO4 structural type, namely $PbMGeO_4$ (M = Ba, Sr) using powder X-ray diffraction as a function of temperature. While $PbBaGeO_4$ exhibits a first order phase transition with a large temperature of phase coexistence, similarly to $(C_5H_{11}NH_3)_2ZnCl_4$, $PbSrGeO_4$ shows a 2nd order type phase transition towards a Pnma structure with a metrically hexagonal phase.

Figure 1: Temperature dependence study of $PbSrGeO_4$

This work shows that both materials are purely gyrotropic materials and identify the $BaNdGaO_4$ structural type as a novel source of new purely gyrotropic materials.

References
[1] C. Konak, V. Kopsky, F. Smutny; J. Phys. C: Solid State Physics 11, 2493 (1978)
[2] S. Prosandeev, I. A. Kornev, L. Bellaiche; Phys. Rev. Lett. 107, 117602 (2011)
[3] A. Gomez Cuevas, J. M. Perez-Mato, M. J. Tello, G. Madariaga, J. Fernandez, L. Echarri, F. J. Zuniga, G. Chapuis; Phys. Rev. B 29, 2655 (1984)

Figure 1

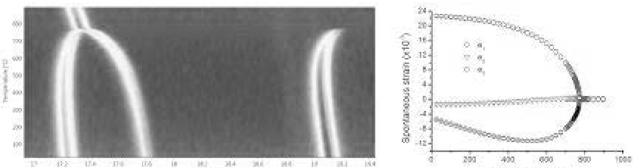

Powder diffraction / PDF

S21-01

On the robustness of atomic pair distribution function (PDF) models

S. Billinge[1]
[1]Columbia University + Brookhaven Lab, Applied Physics and Applied Mathematics, New York, United States

Modern materials under study for next generation technologies, such as for energy conversion and storage, environmental remediation and health, are highly complex, often heterogeneous and nano-structured. A full understanding of the structure requires us to go beyond crystallography and to study the local aperiodic components of the structure, which is a major experimental challenge. Among these tools are total scattering at atomic pair distribution function (PDF) methods which use diffuse and Bragg scattering to give information about short and intermediate range structure in nanomaterials and bulk materials. These methods involve a significant amount of signal averaging and information loss due to limited structural coherence and non-ideal samples. Nonetheless, they are critical for understanding nanomaterials and are growing in popularity. I will introduce these methods and discuss some of the uncertainties associated with modeling and uncertainty estimation and quantification.

S21-02

Crystallographic investigation of silver-gold nanoparticles in situ: Crystallite size and thermal expansion

O. Prymak[1], V. Grasmik[1], K. Loza[1], M. Heggen[2], M. Epple[1]
[1]Universität Duisburg-Essen, Institut für Anorganische Chemie, Essen, Germany
[2]Forschungszentrum Jülich GmbH, Ernst Ruska-Centre and Peter Grünberg Institute, Jülich, Germany

Metallic nanoparticles represent a well-established part of nanoscience today. Alloyed metal nanoparticles enable a combination of their physico-chemical properties, e.g. in catalysis and biomedicine. Inspired by the antibacterial effects of silver (Ag) and the easy covalent functionalization of gold (Au) we have wet-chemically synthesized PVP-coated alloyed silver-gold nanoparticles with the molar ratios of Ag:Au in the full concentration range. Microscopic methods (scanning transmission electron microscopy; STEM) and colloid-chemical methods (disc centrifugal sedimentation; DCS) methods showed spherical and monodisperse nanoparticles with a diameter of 7-10 nm. UV-vis spectroscopy, energy-dispersive X-ray spectroscopy (EDX) and atomic absorption spectroscopy (AAS) confirmed a homogenous distribution of the elements inside the nanoparticles (Fig. 1, left) with the actual molar metal compositions very close to the theoretical values. By an extended crystallographic investigation by X-ray powder diffraction (XRD) and powder diffraction *in situ*, a precise determination of the lattice parameters and the crystallite size was performed by Rietveld refinement. The results showed that the nanoparticles in the whole composition range were polycrystalline with a calculated crystallite size of about one third of the particle size observed by TEM and DCS. Based on the *in situ* diffraction measurements up to 800 °C (Fig. 1, right), the thermal expansion of the alloyed AgAu nanoparticles was investigated.

Figure 1: Representative STEM EDX map at room temperature (left) and Rietveld refinement (right) at 800 °C of Ag50Au50 nanoparticles. The AgAu fcc-phase is additionally labelled; other sharp diffraction peaks belong to the tantalum sample holder (as indicated) and to LaB6 added as internal crystallinity standard.

Figure 1

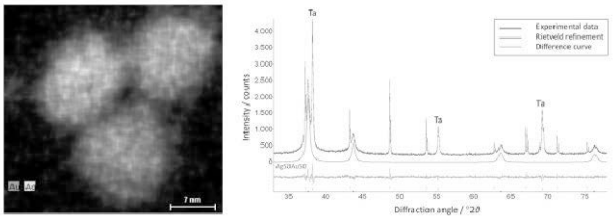

S21-03

New insights into morphotropic phase boundaries of ferroelectric solid solutions from pair distribution function analysis

K. Datta[1], R. B. Neder[2], J. Chen[3], J. Neuefeind[4], B. Mihailova[1]
[1]Universität Hamburg, Department of Earth Sciences, Hamburg, Germany
[2]Friedrich-Alexander-Universität Erlangen-Nürnberg, Department of Crystallography and Structure Physics, Erlangen, Germany
[3]University of Science and Technology Beijing, School of Metallurgical and Ecological Engineering, Beijing, China
[4]Oak Ridge National Laboratory, Chemical and Engineering Materials Division, Oak Ridge, United States

Morphotropic phase boundary (MPB), which refers to the structural-crossover region in a composition-driven phase diagram, is a key topic in materials science since materials often exhibit anomalous properties at the MPB. Although there have been extensive studies on many ferroelectrics to understand the underlying structure-property relations, there is still no rigorous structural model at the atomic level to describe categorically the state of local polarization and the roles of individual cations across an MPB. Here we report our results from pair distribution function (PDF) and Raman scattering analyses on $x\mathrm{BiMg_{1/2}Ti_{1/2}O_3}$-(1-$x$)$\mathrm{PbTiO_3}$ exhibiting an MPB at $x = 0.63$. The study reveals unique structural characteristics depicted by enhanced orientation disorder of the polar shifts for all ferroelectrically active cations along with a strong dynamical coupling between the A-site and the B-site cations of a perovskite-type structure. In addition, solid correlations can be drawn from the observed variation of the composition-driven orientation disorder and the reported physical properties. Altogether these manifest new experimentally-derived models, exclusively based on the local structural phenomena, which in general should be the atomistic driving force for the enhanced properties often seen around an MPB in similar perovskite-based solid solutions.

Reference

[1] K. Datta, R. B. Neder, J. Chen, J. Neuefeind and B. Mihailova, "Atomic-level structural correlations across the morphotropic phase boundary of a ferroelectric solid solution: $x\mathrm{BiMg_{1/2}Ti_{1/2}O_3}$-(1-$x$)$\mathrm{PbTiO_3}$" Scientific Reports, **7**, 471 (2017).

S21-04

Detailed X-ray diffraction and pair distribution function study on the layered compound $\mathrm{CrTe_3}$

A. L. Hansen[1], B. Dietl[1], M. Etter[2], R. Kremer[3], D. C. Johnson[4], W. Bensch[1]
[1]Christian-Albrechts-Universität zu Kiel, Institut für Anorganische Chemie, Kiel, Germany
[2]Deutsches Elektronen-Synchrotron DESY, Hamburg, Germany
[3]Max-Planck-Institut für Festkörperforschung, Stuttgart, Germany
[4]University of Oregon, Department of Chemistry, Eugene, United States

Introduction

Among transition metal chalcogenides, $\mathrm{CrTe_3}$ is the only crystalline group VI trichalcogenide, crystallizing in a complex layered structure (space group $P2_1/c$; a = 7.88 Å, b = 11.22 Å, c = 11.56 Å and β = 118.41°) built up by layers of $\mathrm{CrTe_6}$ octahedra stacked along the crystallographic a axis. The octahedra within each layer are arranged in clusters of edge sharing $\mathrm{Cr_4Te_{16}}$ rhombi like tetramers. Cr is in the oxidation state +III. An ionic notation would therefore be $[Cr^{3+}]_2[Te]^{2-}[Te_2]^{2-}[Te_3]^{2-}$, illustrating the polymeric mixed valent anion network.

Objectives

While the Cr–Te phase diagram and $CrTe_3$ homogeneity range were first investigated over three decades ago, important questions concerning the stability of $CrTe_3$ still remain open.[1] It was proposed that a peritectical decomposition into an unknown polytelluride phase and elemental Te takes place at elevated temperatures. Additionally, it was mentioned after annealing single crystals for several months it was not possible to eliminate tiny residues of elemental Te.[2] These observations and the open questions concerning the exact stoichiometry inspired us to investigate the low and high temperature behavior of this unique polytelluride. Our analysis provides insights why it is apparently impossible to prepare phase pure $CrTe_3$.

Results

Our investigations evidence a short range structural distortion of one of the two crystallographically independent $CrTe_6$ octahedra. Between 100 and 754 K a pronounced anisotropic expansion of the lattice parameters is observed which can be explained on the basis of anisotropic changes of the geometric parameters of the Cr_4Te_{16} structural building units. Upon cooling, an abrupt structural distortion occurs at about 250 K which persists down to 100 K.

Conclusion

Our results evidence that $CrTe_3$ is an inherently inhomogeneous compound. Two major unique features could be elucidated. First our data suggests that the occurrence of an amorphous Te phase is inevitable. The Te starts to crystallize at low temperatures and certainly melts in the temperature region where previously a peritectic decomposition was reported. Secondly, the discrete distortion of one of the two unique $CrTe_6$ octahedra, caused by the higher mobility of one Te ion, was discovered.

References

[1] K. O. Klepp, H. Ipser, *Monatsh. Chem.* **1979**, *110*, 499–501.
[2] H. Ipser, K. L. Komarek, K. O. Klepp, *J. Common Met.* **1983**, *92*, 265–282.

Lightning talks I

LT1-01

High pressure properties of Bi_2SiO_5 from synchrotron powder diffraction and first principle calculations

G. Adrien[1], S. Michal[1], M. Wolfgang[1], T. Hiroki[2], B. Alexei[3], W. Björn[1]
[1]Goethe-Universität Frankfurt am Main, Institut für Geowissenschaften, Frankfurt am Main, Germany
[2]Materials and Structures Laboratory, Yokohama, Japan
[3]European Synchrotron Radiation Facility (ESRF), Grenoble, France

Currently, there is a considerable interest in ferroelectric lead-free oxide materials with high transition temperatures. In this context, Bi2SiO5 (BSO) has emerged as a promising lead-free oxide, after the finding of high temperature ferroelectricity with a transition temperature from the *Cc* to *Cmcm* phase at TC = 670 K [1]. The ferroelectricity in BSO is primarily driven by the tilt of the SiO4 units within the 1D tetrahedral chains, characteristic for this structure (Fig. 1A). These findings have triggered numerous experimental and theoretical studies making BSO a benchmark system for ferroelectrics based on polymerized tetrahedra as an alternative to perovskite-type ferroelectrics. In contrast to the efforts devoted to the understanding of the ferroelectric properties of BSO at ambient pressure, its high-pressure properties remain unreported so far.

We report a high-pressure study of BSO based on *in situ* powder synchrotron experiments and density functional theory (DFT). We describe the compression mechanisms of the ferroelectric *Cc* structure and the pressure dependence of the 1D tetrahedral chains, responsible for the ferroelectric properties of BSO and the large polarization along the *c*-axis of BSO (Fig. 1B). The compression involves a rotation of the SiO4 units and change of the tilt angles in the 1D tetrahedral chains, and is associated with a change in the coordination of the Bi ion. Finally, we address the adaptation of stereochemically active lone electron pair of the Bi ion up to 50 GPa (Fig. 2). These results provide insights into the complex compression mechanisms of the structure of BSO.

The study is supported by funding from the German Science Foundation (Projects Wi1232 and DFG Research Unit FOR2125) and the BMBF (grants 05K16RFA and 05K16RFB).

References

[1] Hiroki Taniguchi *et al*, Ferroelectricity driven by twisting of silicate tetrahedral chains. Angewandte Chemie - International Edition, 52(31):8088–8092, 2013.

Figure 1: A. Structure of BSO and B. Evolution of the kink angle with pressure. Inset: 1D chains of SiO4 tetrahedral units.
Figure 2: Calculated electron localization function at *p* = 50 GPa.

Figure 1

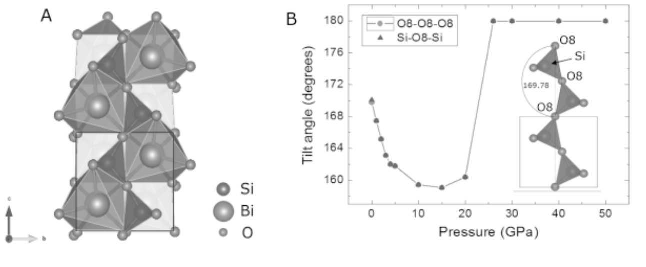

Figure 2

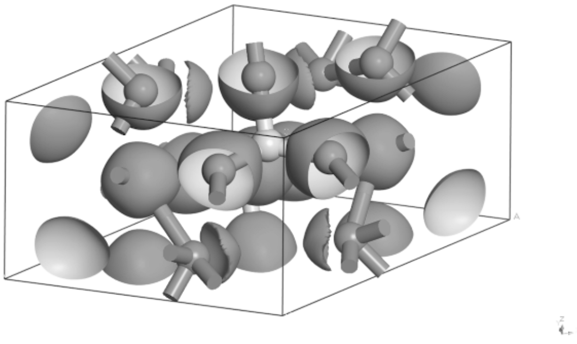

LT1-02

A Study on the Growth, Structural, Optical, Photoluminescence Properties of Dye doped L-Arginine Diphosphate Single crystals

R. Ittyachan[1]
[1]Sacred Heart College, Chalakudy, Kerala 680307, India, Physics, Chalakudy, India

In recent years, the need for fast data retrieving, amplifying, modulating, transforming and transmitting a signal by optical techniques has inspired many researchers to grow new nonlinear optical (NLO) materials with exceptionally high optical transparency in the ultraviolet to near IR spectral range[1,2]. In this work, we have reported the effect of crystal violet dye doping on the structural (powder XRD), spectral (FTIR), optical (UV–vis–NIR, PL), and nonlinear optical (SHG) properties of the grown l-arginine diphosphate crystal(LADP) crystals.

The comparison between the PXRD patterns of grown crystals of pure and dye doped LADP with the simulated single crystal XRD spectral patterns revealed that exact identities of the grown pure and dye doped LADP crystallize in the orthorhombic system with non-centrosymmetric P212121 space groups. The lattice parameters were evaluated as a=7.0692Å, b=9.6321Å, c=21.7281Å, α=β=γ=900 for LADP and a=7.0663Å, b=9.6388Å, c=21.74636Å, α=β=γ=900 for dye doped LADP [3]. A single broad peak was obtained in pure LADP which blue shifted to with dye doping. For pure LADP, blue green emissions cantered at 413 nm were observed. For CV doped samples, a shift in blue green emissions with peaks centered at 430 nm was observed. This shift arises from lattice defects, created in the form of interstitials because of the CV dye which is devoid of Phosphor. Moreover, because of dye doping, the effective band gap increases which resulted in comparatively high energy values for the emitted photons. Hence, these high energy photons give photoluminescence peaks at shorter wavelength as evident from the PL spectra. The decreased luminescence broadness of dye doped crystals with increasing concentration indicates the usefulness of these crystals for developing coherent sources in applications that require violet-blue light.

LT1-03

Solvent-controlled molecular self-assembly: From alkoxoiron(III) wheels to coordination networks

K. N. Truong[1], H. Gildenast[1], H. Crützen[1], A. Nellessen[1], J. Lange[1], L. Ferres[2], U. Englert[1]
[1]RWTH Aachen, Institute of Inorganic Chemistry, Aachen, Germany
[2]RWTH Aachen, Institute of Physical Chemistry, Aachen, Germany

Coordination polymers provide a huge playground, both for basic research in structural chemistry and for applied materials science.[1-4] These coordination polymers consist of metal cations interconnected via organic linkers. The synthesis of coordination networks incorporating two different (or more) cations in a one-pot reaction is associated with synthetic challenges. A stepwise procedure on the other hand allows for a higher degree of control: in the first reaction, a secondary building unit (SBU) based on one kind of metal cation is formed. In the second step, these SBUs are cross-linked with a second type of cation via the alternative coordination site of the ligand. Following this strategy, well-ordered mixed-metal systems can be obtained.[5-7] Here, we report compounds starting from an iron(III) complex, [Fe(acacCNen)3], with properties in-between inertness and lability. Depending on the reaction partners and solvent systems, partial degradation or inclusion of the SBUs as synthesized may occur. In case of a partial degradation, an alkoxo-bridged multinuclear iron complex is formed. This occurs only if methanol is used as co-solvent. These overall heptanuclear clusters have the "Anderson-type" structure motif in which six iron(III) cations are located on the rim with the second cation in the center. Depending on the reaction partner, we have observed an inclusion of either silver(I) or sodium(I). These compounds may reveal magnetic behaviour and are currently under investigation. The reaction of the iron(III) SBUs with silver hexafluorophosphate in methanol/chloroform reveals a 2D cross-linking network with the heptanuclear complex as central part. Using other solvents than methanol shows the formation of bimetallic systems in various dimensions with inclusion of the SBUs as synthesized. Similar reaction behaviours of related SBUs have been observed in earlier studies.[8,9] The ditopic ligand 4-acetyl-5-oxohexanenitrile, HacacCNen, exists as enol tautomer in the solid state. The ethyl bridge between the acetylacetone and the nitrile moiety imparts flexibility, which can lead to high degrees of conformational freedom and, thus, interesting structures (see Scheme 1). The enol form has been experimentally established in the crystal and in solution − how about the geometry of the molecule in the gas phase? Quantum chemical calculations were carried out to answer this question. Scheme 1: Synthesis and composition of the bimetallic Al(III)-Ag(I) networks. Two different types of network structures are observed: inclusion of SBUs as synthesized (left), and partial degradation (right) are formed depending on the solvent system (cocrystallized solvent molecules have been omitted for clarity).

Figure 1

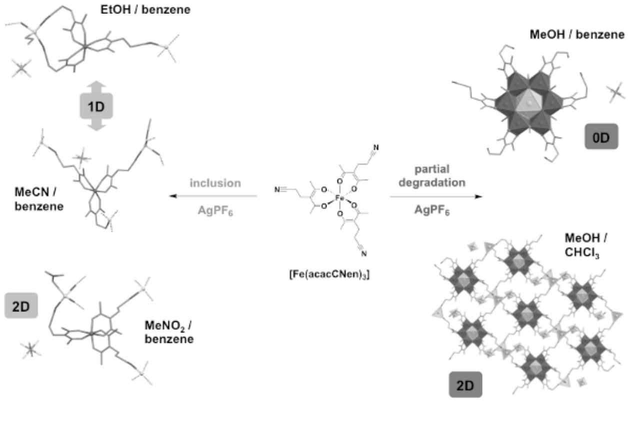

References

[1] U. Müller, M. Schubert, F. Teich, H. Pütter, K. Schierle-Arndt, P. Pastre, *J. Mater. Chem.* **2006**, *16*, 626-636.
[2] K.A. Williams, A.J. Boydston, C.W. Bielawski, *Chem. Soc. Rev.* **2007**, *36*, 729-744.
[3] W. Lin, W.J. Rieter, K.M.L. Taylor, *Angew. Chem. Int. Ed.* **2009**, *48*, 650-658.
[4] A.D. Burrows, *CrystEngComm* **2011**, *13*, 3623-3642.
[5] Q. Guo, U. Englert, *Cryst. Growth Des.* **2016**, *16(9)*, 5127-5135.
[6] C. Merkens, K.-N. Truong, U. Englert, *Acta Cryst.* **2014**, *B70*, 705-713.
[7] K.-N. Truong, C. Merkens, U. Englert, *Acta Cryst.* **2017**, *B73*, 981-991.
[8] A.D. Burrows, K. Cassar, M.F. Mahon, J.E. Warren, *Dalton Trans.* **2007**, *24*, 2499-2509.
[9] C. Merkens, N. Becker, K. Lamberts, U. Englert, *Dalton Trans.* **2012**, *41*, 8594-8599.

LT1-05

In Situ Powder Diffraction Measurements of a High-Yield Microwave Synthesis of Silver Nanoparticles using Synchrotron Radiation

K. Pappert[1], L. S. Germann[2], M. Etter[3], R. E. Dinnebier[2], M. Epple[1]
[1]Universität Duisburg-Essen, Institut für Anorganische Chemie, Essen, Germany
[2]Max-Planck-Institut für Festkörperforschung, Stuttgart, Germany
[3]Deutsches Elektronen-Synchrotron DESY, Beamline P02.1, Hamburg, Germany

Silver nanoparticles (AgNP) show a wide range of practical and possible applications due to their physical and antimicrobial properties.[1,2] For those applications, a reliable synthesis with high yield is required. A polyol reduction-based microwave synthesis that was developed by Helmlinger et al.[3] was studied using *in situ* powder diffraction on Beamline P02.1 at the DESY facility (Hamburg, Germany). This was done to establish the proof of principle of *in situ* microwave experiments and to further investigate the crystallographic behaviour during the reaction. The crystallite size, growth behaviour and lattice parameters were determined. After the *in situ* synthesis, the particles where purified by ultracentrifugation and characterized by electron microscopy and dynamic light scattering.

Fig. 1.: 3D-powder pattern plot of the performed in situ measurements of AgNP synthesized in a microwave by a polyol process at 160 °C. Frames where taken every 20 seconds (total number of frames 97, corresponding to a reaction time of 32.3 min.).

References

[1] X. Chen and H. J. Schluesener, *Toxicol. Lett.*, **2008**, 176, 1–12.
[2] J. Helmlinger et al., *RSC Adv.*, **2016**, 6, 18490-18501.
[3] J. Helmlinger et al., *RSC Adv.*, **2015**, 5, 92144-92150.

Figure 1

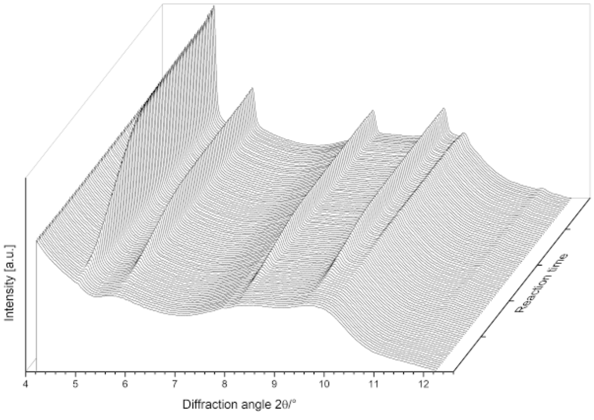

LT1-07

Treatment of wastewater by adsorption on raw ore graphite (deposit point 214-area sidi bouothmane-marrakech)

S. Sabir[1]
[1]Ben M'sik University Hassan II Casablanca, Faculty of Science, Casablanca, Morocco

This work has allowed us to study the adsorption phenomenon of BM methylene blue on raw ore graphite (deposit point 214 SIDI BOUOTHMANE region MARRAKECH).

At the beginning of this work, we conducted a series of experiments to study this phenomenon methylene blue playing on a number of parameters, namely: The pH of the medium, the particle size, the mass of graphite, the concentration of methylene blue, the main results of this study are:

The adsorption is done in a first time in a monolayer when the initial concentration of methylene blue does not exceed 10mg / l. Once this concentration limit is outdated, a new multilayer adsorption phenomenon began to appear according to the concentration put out.

Otherwise, the saturation of a monolayer of 1 g of GP214 with 10mg of (BM) has confirmed by two models (Langmuir, Freundlich)

We are planning into perspective to continue our trials multilayer adsorption subject to try to discover the farthest upper boundary layer of the support and which could result in improvement, the adsorption capacity of the GP214 natural material.

LT1-08

In situ XRD studies on the hydrogenation of Ti thin films

Z. Balogh-Michels[1], E. Hadjixenophontos[2], L. Michalek[2], M. Roussel[2], M. Hirscher[3], G. Schmitz[2]
[1]Empa, Swiss Federal Laboratories for Materials Science and Technology, Center for X-ray Analytics, Dübendorf, Switzerland
[2]Universität Stuttgart, Chair of Materials Physics, Stuttgart, Germany
[3]Max Planck Institut für Intelligente Systeme, Stuttgart, Germany

Introduction

Understanding the reaction of Ti with H is interesting for many aspects nowadays. Both in beneficial processes, such as hydrogen [1] or thermal energy storage [2] as well as in the unwanted embrittlement of Ti components [3].
Hydrogen is first intercalated in Ti which is followed by a chemical reaction to form the hydrides (see the phase diagram in Ref. [4]). In-operando studies are highly useful for studying kinetic processes at intermediate stages. In this work we present the results of in situ hydrogenation experiments carried out in a purpose built reaction chamber attached to a Bruker D8 diffractometer [5].

Objectives

In this work we studied the reaction between Ti and hydrogen both in the intercalation and the hydride formation phase. A mixture of H_2:N_2 with different compositions as well as different temperatures were used. On the qualitative level, we were interested on the rate controlling process (gas absorption, diffusion, phase transition).

Results

Figure 1 shows the evolution of the diffractogram in the 35-39° range at 450 °C at 0.5:0.5 H_2:N_2. First shifts (0002) Ti peak to lower angles due to the intercalation, later on this peak disappears and the corresponding TiH peak grows. During the intercalation stage the peak width of the Ti (0002) remains constant and is shifted linearly with the time (Fig 2a). This indicates an efficient redistribution of the H-atoms and that the diffusion is much faster than the absorption step.

During the phase transition the position of the Ti peak remains stable (Fig. 2a). The peak area of the Ti peak decreases linearly while the TiH grows linearly. This again indicates a reaction control, though from these results it cannot be said whether the absorption or the formation of the TiH controls the process.

Conclusions

Our results indicate that both the intercalation and the phase transition is reaction controlled. For the intercalation the reaction step is at the absorption of the gas through the surface oxide, while for the phase transition the Ti→TiH phase transition can also play the role of the reaction bottleneck.

References

[1] M. Ma, Int. J. Hydrogen Energ., 40 (2015) 8926–8934.
[2] C. Corgnale, Renew. Sust. Energ. Rev., 38 (2014) 821–833.
[3] D. Setoyama et al., J. Alloy Compd., 381 (2004) 215–220.
[4] E. Königsberger et al., J. Alloy Compd., 299 (200) 148-152.
[5] Z. Balogh-Michels et al., J. Appl. Phys., 122 (2017) 025111.
Fig. 1; Fig. 2

Figure 1

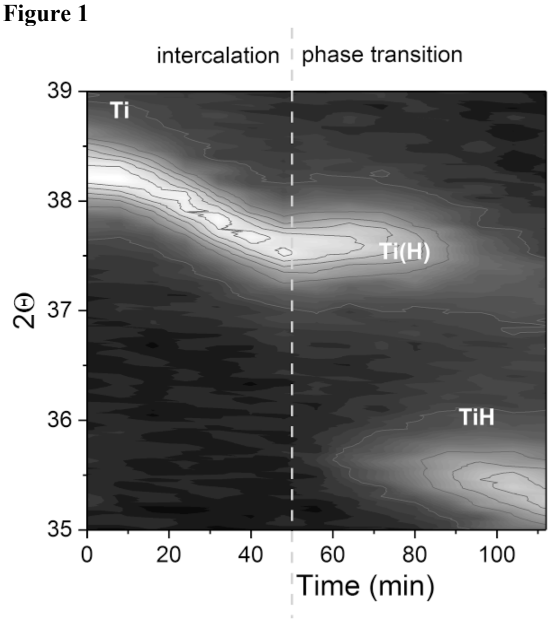

Figure 2

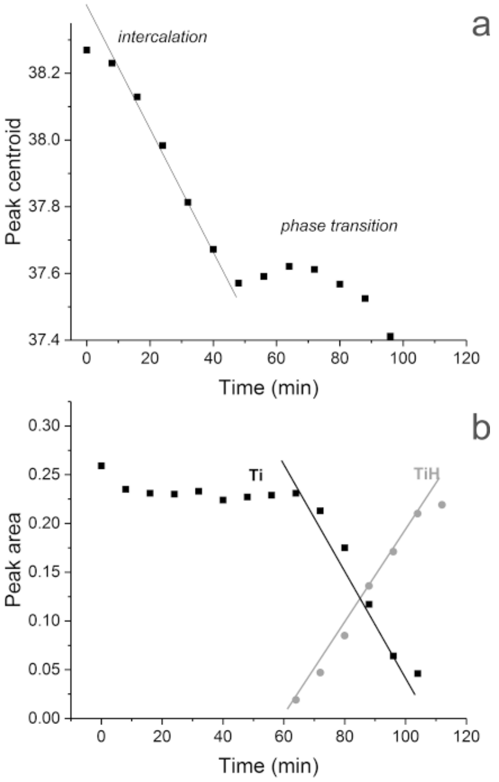

LT1-09

Investigation of illuminated manuscripts by micro-diffraction using an aircooled X-ray microfocus source

B. Hasse[1], J. Wiesmann[1], F. Vanmeert[2], K. Janssens[2]
[1]Incoatec GmbH, Geesthacht, Germany
[2]University of Antwerp, Department of Chemistry, Antwerp, Belgium

In recent years the interest in the non-destructive investigation of cultural heritage objects has risen strongly. Besides infrared and optical imaging and spectroscopic methods, X-ray methods like X-ray fluorescence, X-ray diffraction, X-ray radiography and X-ray imaging (e. g. tomography) are often used for the analysis of paintings and books.

Using XRF analysis of paintings generally provides information about the possible presence of elements on the surface of art-objects due to pollution (e.g. sulphur or chlorine), about the elements and pigments used by the artist, about previous restored areas detected by the presence of "modern" elements like titanium or zinc, and identification of fraudulent submission. In combination with X-ray diffraction (XRD) also the crystallographic composition of the used pigments could be characterized. A study about the alteration involved the oxidation of cadmium yellow (CdS) to $CdSO_4 \cdot 2H_2O$ under the influence of light, oxygen and moisture is an example of the use of this technique in the investigation of paintings.

In the study shown here a medieval book painting was investigated using XRF and XRD-techniques simultaneously. While with XRF the elemental composition of the used pigments are analyzed, with XRD crystallographic information could be revealed. Using both methods, the chemical composition of the pigments could be analyzed. Here an X-ray microfocus source with Mo radiation and a focusing optics was used. The XRD patterns were recorded with a CCD-detector in transmission geometry, XRF signals were measured with an energy dispersive detector arranged in 90° to the beam direction. A sample area of about 130 µm x 130 µm was illuminated with the X-ray beam. Using this setup, XRD frames were recorded within 30 seconds exposure time, the XRF measurement was done simultaneously. In an overnight-scan (approx. 18 hours) an area of several square millimeter and a resolution of 150 µm could be investigated.

This study shows, that it is possible to obtain high quality results even with a quite simple setup. The air-cooled microfocus source IµS, the sample and the XRD-detector were just aligned on an optical bench while the XRF-detector was just placed on a shelf in a suitable position.

Some further examples of customized solutions with the IµS demonstrate new experimental possibilities for the measurement of sensitive materials with methods like microdiffraction, crystallography and small angle scattering.

LT1-10

Flexibility *vs.* Rigidity: Linker Extension Influence on MOF Formation and Porosity

D. Sensharma[1], F. W. Steuber[1], P. Wix[1], L. Macreadie[1], W. Schmitt[1]
[1]Trinity College Dublin, School of Chemistry, Dublin, Ireland

Metal-Organic Frameworks (MOFs) are promising materials with a variety of applications resulting from their porosity and chemical tunability. Isoreticular synthesis relies on the extension of organic linkers with the aim of retaining the topology of a framework with larger voids and lower densities. Yet, with the extension of linkers come about new degrees of freedom, such as rotational flexibility of the linker and the ability for the net to interpenetrate itself. The removal of steric constraints can lead to new topologies, which has important implication for MOF design.[1] Both the acetylene and *p*-phenylene moieties are commonly used to extend linkers, with the former providing uninhibited rotational freedom.[2,3] Recently, we showed that using the extended tritopic linker 1,3,5-benzenetrisethynylbenzoic acid (BTEB) with dinuclear copper(II) secondary building units (SBUs) yields MOFs with rare in addition to "default" topologies.[4]

In an effort to explore MOFs with rare topologies we utilised cadmium(II) together with BTEB, and the more rigid linker 4,4',4''-(benzene-1,3,5-triyl-tris(benzene-4,1-diyl))tribenzoic acid (BBC). Moreover, mixed ligand synthesis with 4,4'-azobipyridine (azopy) was explored.

Here we present three trinuclear cadmium(II) MOFs: $[Cd_3(BTEB)_2(DMF)_3(H_2O)]\bullet 2.5DMF\bullet 0.5H_2O$ (**1**) forms a doubly interpenetrated **sit** net, $[Cd_3(BTEB)_2(DMF)_3(azoPy)_{0.5}]\bullet 1.75DMF$ (**2**) in which two **sit** nets are connected by azoPy into one net with point symbol $\{4.6^2\}_4\{4^2.6^{10}.8^9\}_2\{8\}$, as well as $[Cd_3(BBC)_2(DMF)_3(H_2O)]\bullet 0.3DMF$ (**3**) with point symbol $\{4^3.6^{12}\}\{4^3\}_2$, in which azoPy could not be incorporated. While their composition is quite similar, the flexibility of BTEB in **1** and **2** leads to a barely porous packing, whereas hexagonal channels with a diameter of 15.6 Å are present in **3**.

In summary, we have shown that in isoreticular synthesis a linker should not necessarily be simplified to its geometry but flexibility can have great influence on the porosity of the resulting framework.

References

[1] D. Frahm, F. Hoffmann, M. Fröba, Cryst. Eng. Comm. 2013, 15, 9429.
[2] B. F. Hoskins, R. Robson, J. Am. Chem. Soc. 1990, 112, 1546.
[3] I. M. Hauptvogel, V. Bon, R. Grünker, I. A. Baburin, I. Svenskova, U. Müller, S. Kaskel, Dalton Trans. 2012, 41, 4172.
[4] N. Zhu, D. Sensharma, P. Wix, M. J. Lennox, T. Düren, W. Y. Wong, W. Schmitt, Eur. J. Inorg. Chem. 2015, 1939.

LT1-11

Synthesis and compressibility of iridium borides

C. Neun[1], B. Petermüller[2], L. Bayarjargal[1], W. Morgenroth[1], D. Zimmer[1], K. Wurst[2], H. Huppertz[2], B. Winkler[1]
[1]Goethe-Universität Frankfurt am Main, Institut für Geowissenschaften, Frankfurt am Main, Germany
[2]Leopold-Franzens University Innsbruck, Institute of General, Inorganic and Theoretical Chemistry, Innsbruck, Austria

Transition metal borides are a group of potentially high-performance materials, of which the binary compounds have attracted considerable interest [1]. In the system Ir-B, there are six binary phases, some of which have been investigated due to their high hardness [2-8]. Other physical properties are still unknown.
We investigated the bulk moduli of iridium borides and elemental iridium in order to correlate the composition with the elastic behavior. We synthesized hexagonal and orthorhombic Ir_4B_{3-x}, Ir_5B_4 and α-Ir_4B_5 by arc melting and found a new phase named β-Ir_4B_5, which we synthesized in a multi-anvil press. We determined the bulk moduli by pressure-dependent synchrotron powder diffraction in diamond anvil cells up to pressures of at least 30 GPa at the Extreme Conditions Beamline P02.2 at PETRA III.

The bulk moduli vary between $B_0(\alpha\text{-}Ir_4B_5) = 249(3)$ and $B_0(\text{hexagonal } Ir_4B_{3-x}) = 320(6)$ GPa. Iridium borides therefore are not as incompressible as diamond (443 GPa), OsB (431-453 GPa) or Re_7B_3 (391(5) GPa), but their elastic behavior rather resembles that of TaB_2 (341(7) GPa), RuB (261-275 GPa) and RuB_2 (242-303 GPa) [9, 10].

All iridium borides show a higher compressibility than the pure metal ($B_0(Ir) = 326(3)$ GPa) and the phases become more compressible with increasing boron content. This is in contrast to systems such as Os-B or Re-B [9, 10], where the bulk moduli increase upon boron incorporation. In order to understand why boron incorporation can lead to either a decrease or an increase of the compressibility of binary transition metal borides relative to the pure metal, a better understanding of the bonds in these systems is now required.

Funding by the DFG (WI 1232/40), the FWF (I 1636-N19), and the BMBF (project 05K16RFB) is gratefully acknowledged.

References

[1] Chung *et al., Science* ***316*** *(2007)*
[2] Rogl, P. *et al.*, *Monatshefte für Chemie* **102** (1971)
[3] Aronsson B. *et al.*, *Acta Chem. Scand.* **14** (1960)
[4] Aronsson, B., *Acta Chem. Scand.* 17 (1963)
[5] Zeiringer, I. *et al.*, *Science China Materials* **58** (2015)
[6] Xie, Z. *et al.*, *J. Solid State Chem.* **233** (2016)
[7] Latini, A. *et al.*, *J. Appl. Mater. Interfaces* **2** (2010)
[8] Rau, J.V., and Latini, A., *Chem. Mater.* **21** (2009)
[9] Gu, Q. *et al.*, *Adv. Mater.* **20** (2007)
[10] Neun, C. *et al.*, in preparation

Figure 1: Compression behavior of the normalized unit cell parameters of α-Ir4B5 up to 37 GPa.
Figure 2: Compression behavior of the normalized unit cell parameters of β-Ir4B5 up to 40 GPa.

Figure 1

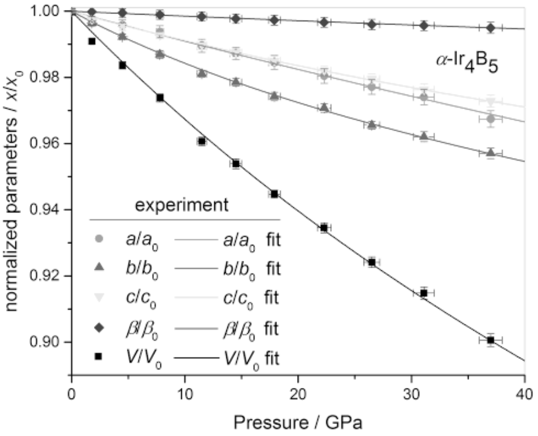

Figure 2

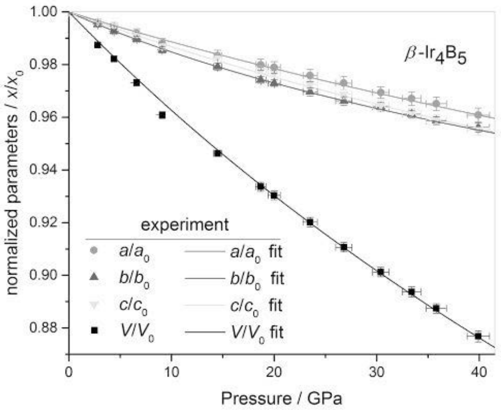

LT1-12

Single crystal structure investigation of $Cu(C_{10}H_{20}O_5)Br_2 \cdot 2H_2O$ and analysis of physical properties

N. van Well[1,2], C. Eisele[1], A. Biffin[2], C. Rüegg[2,3], S. van Smaalen[1]
[1]University of Bayreuth, Laboratory of Crystallography, Bayreuth, Germany
[2]Paul Scherrer Institute, Laboratory for Neutron Scattering and Imaging, Villigen, Switzerland
[3]University of Geneva, Department for Quantum Matter Physics, Geneva, Switzerland

This study aims to investigate the equation of the state and the development of the structure complex 1,4,7,10,13-Pentaoxacyclopentadecane with copper (II) bromide: $Cu(C_{10}H_{20}O_5)Br_2 \cdot 2H_2O$ (1). This composition (1) has been prepared, to investigate the low dimensional spin system of compounds with a comparable flexibility based on crown ethers. Currently, the following structure of this compound was published: it has a monoclinic crystal structure with space group $P2_1$ and a=8.698(4)Å, b=13.740(7)Å, c=8.019(4)Å and β=116.31(3)°. We have crystallised this compound from solution with the evaporated method. To compare the structure parameters with the published ones, we have prepared a single crystal diffraction experiment. The results show new superstructure reflections, which leads to a new structure determination. We will present this of compound (1). Furthermore we have investigated the compound of the complex 1,4,7,10-Tetraoxacyclododecan with copper(II) chloride: $Cu(C_8H_{16}O_4)Cl_2$ (2). For both compounds we will present the results of the magnetic susceptibility measurements.

LT1-13

An integrative approach to study the conformation of the *Yersinia* type-III-effector protein YopO and its activation by actin in solution

G. Hagelueken[1], A. Tuukkanen[2], A. Selsam[1], C. Heubach[1], D. Marx[1], F. Duthie[1], D. I. Svergun[2], O. Schiemann[1]
[1]University of Bonn, Institute for Physical & Theoretical Chemistry, Bonn, Germany
[2]European Molecular Biology Laboratory Hamburg, Hamburg, Germany

Yersinia pestis is the causative agent of plague and has caused several pandemics in human history. During infection, the bacterium is able to avoid innate immune defenses, e.g. phagocytosis, by utilizing a syringe-like type-three-secretion-system (T3SS). This molecular needle injects a set of six Yop proteins (*Yersinia outer proteins*) into attacking phagocytes. After injection, the Yops interfere with several important cellular processes [1]. One of the effector proteins, YopO (also known as YpkA), is subject of this study. When injected into the host cell, YopO specifically interferes with the regulation of the actin cytoskeleton in at least three different ways: 1) The C-terminus of YopO binds to Rac1 GTPases and acts as a guanidine nucleotide dissociation inhibitor. 2) YopO binds to monomeric actin, forming a stable 1:1 complex. This interaction leads to autophosphorylation and activation of the N-terminal kinase domain of YopO, which then, in turn, phosphorylates various cellular targets that are involved in cytoskeletal dynamics [2, 3].

Question

A recent crystal structure of the YopO/actin complex revealed how the bound actin molecule is used as a bait to recruit cellular proteins for phosphorylation [3], however, some questions remained unanswered: It is for example completely unclear, how YopO is activated by actin binding.

Method

To answer this question, we have conducted PELDOR distance measurements on spin-labeled apo YopO and the YopO/Actin complex. Additionally, we have investigated the structure of YopO and the YopO/Actin complex by small-angle X-ray scattering experiments.

Results

Overall, the PELDOR measurements are in agreement with the crystal structure of the YopO/Actin complex [3]. However, they also indicate that compared to the complex, apo YopO must have a significantly different and more flexible structure. This flexibility is likely the reason why apo YopO has proved recalcitrant to our crystallization attempts. So, in order to produce a structural model of apo YopO with an alternative approach, the PELDOR distance data and SAXS measurements were simultaneously used as restraints for integrative structural modeling.

Conclusions

In this way, we were for the first time able to deduce a structural model for the apo state of YopO. The apo structure gives important clues concerning the activation mechanism of this intriguing protein.

LT1-14

Total scattering and pair distribution function characterization of disordered polymer structures

M. Terban[1], B. Hinrichsen[2], R. E. Dinnebier[1]
[1]Max-Planck-Institut für Festkörperforschung, X-ray diffraction, Stuttgart, Germany
[2]BASF, Ludwigshafen, Germany

The detailed characterization of polymeric structures from diffraction methods is difficult due to their intrinsically disordered nature. Structure determination typically relies on extra sample treatments to maximize crystallinity, in addition to assumptions made on data of poor quality or limited information. These can lead to ambiguities in the structure models reported. It is therefore important to develop experimental and structure refinement protocols to determine structures in their as-manufactured state.

Here, we apply total x-ray scattering methods towards the analysis of chain polymers such as thermoplastic polyurethanes and nylons, in the as-manufactured state. Pair distribution function (PDF) analysis allows for a higher resolution determination of local chain conformation, orientation, packing of chains, domain size, and relative quantification of ordered and disordered phase contributions. Constraints from reciprocal-space refinement and molecular knowledge are explored to obtain more accurate and robust refinements, moving toward structure determination of disordered polymers using small-box models. The results are contrasted with the variety of previously proposed models.

LT1-16

All You Can Diffract: Elucidating the Commensurately Modulated Structure of $HfTaO_{4.5}$

D. Wiedemann[1], T. Lüdtke[1], L. Palatinus[2], M. J. Mühlbauer[3], E. Willinger[4], M. Willinger[4]
[1]Technische Universität Berlin, Institut für Chemie, Berlin, Germany
[2]Czech Academy of Sciences, Institute of Physics, Prague, Czech Republic
[3]Technische Universität München, Heinz Maier-Leibnitz Zentrum, München, Germany
[4]Fritz-Haber-Institut der Max-Planck-Gesellschaft, Department of Inorganic Chemistry, Berlin, Germany

High-temperature polymorphs of ZrO_2 stabilized with low-valent oxides (CaO, Y_2O_3) are used as oxygen-conducting electrolytes. Solid solutions of zirconia or hafnia substituted with higher-valent oxides (*e.g.*, Ta_2O_5 or Nb_2O_5), on the other hand, exhibit an anion excess compared to the binary oxides. Albeit showing similarities to the α-PbO_2 type, their crystal structures are unexpectedly complex[1]—especially at low substituent concentrations—and have been subject to research since the 1950s[2].

Exploring the system HfO_2–Ta_2O_5, we have synthesized a phase with the composition $HfTaO_{4.5}$. Initial powder X-ray diffractometry suggested a structure of the α-PbO_2 type. This is, however, incompatible with the composition $(Hf,Ta)O_{2+0.25}$ because of a lack of space for additional anions. Trying to elucidate the position of the extra ions (or confirm cation deficiency), we recorded a powder neutron diffractogram. Originally, we were unable to index the reflections and thus to deduce a structural model.

Transmission electron microscopy (TEM) showed the powder to be nanocrystalline (grain diameter: 20–50 nm) and, at atomic resolution, yielded critical information (see Fig. 1): the structure is modulated as seen in direct (periodically larger gaps, positional waves) and reciprocal space (satellites). Using electron diffraction, we could solve and refine the commensurately modulated structure with $\boldsymbol{q} = (0, 0, 1/5)$ in (3+1)-dimensional superspace. The resulting preliminary model shows three distorted modes of cation coordination (see Fig. 2): six- (octahedron), seven- (augmented triangular prism), and eightfold (biaugmented triangular prism). The latter gives rise to positions for the additional oxide ions. According to first refinements, the model agrees very well with the X-ray and neutron data acquired before.

This work is based upon experiments performed at the high-resolution neutron powder diffractometer SPODI at the Heinz Maier-Leibnitz Zentrum (MLZ), Garching, Germany.

References

[1] J. G. Thompson, R. L. Withers, J. Sellar, P. J. Barlow, B. G. Hyde, *J. Solid State Chem.* **1990**, *88*, 465–475.
[2] R. S. Roth, L. W. Coughanour, *J. Res. Natl. Bur. Stand. (U. S.)*. **1955**, *55*, 209–213.

Fig. 1. High-angle annular dark-field (HAADF) image with atomic resolution oriented along the [100] zone axis; Hf/Ta positions as bright dots. Inset: FFT pattern of the image.

Fig. 2. Crystal structure of $HfTaO_{4.5}$ (preliminary supercell model) .

Figure 1

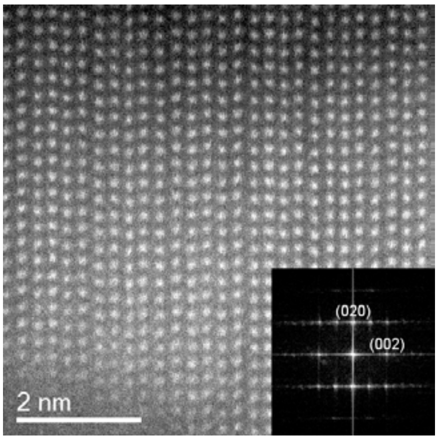

Figure 2

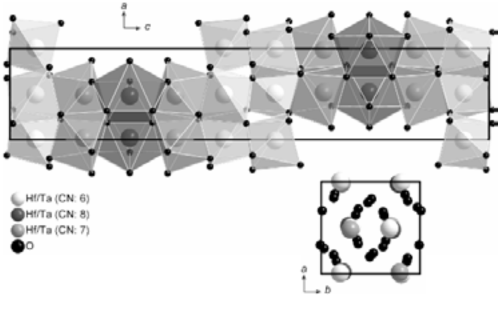

Lightning talks II

LT2-01

STD-NMR as a tool to identify (and characterize) weakly binding ligands for protein crystallography

B. Blaum[1]
[1]Universität Tübingen, Interfakultäres Institut für Biochemie, Tübingen, Germany

Crystal structures of weak protein-ligand complexes are sometimes hard to come by. Shallow binding pockets on the protein side can be involved in crystal contacts which may be favored over complex formation, leading to apo structures even in the presence of high ligand concentrations. Weakly binding ligands can even get lost during cryo protection. In particular, if several potential ligands exist screening for hits by crystallography can thus become tedious. A complementary technique that can help to firmly identify potential ligands (also from mixtures) and delineate a common binding epitope from a set of ligands prior to soaking or co-crystallization experiments is saturation transfer difference (STD-)NMR. Upon successful crystallization, the method can serve to compare the crystallographic interaction of interest with complex formation in solution, to scrutinize potential bias by crystal contacts, and to refine the bound ligand conformation with hybrid protocols. Another beautiful aspect of the STD-NMR experiments is the fact that, unless in protein-detected NMR, there is no requirement for isotope labeling and no size limit on the protein side. STD-NMR can, therefore, also serve to extend findings from crystallography to more complex systems that are not or hardly amenable to crystallography, such as large flexible proteins, viruses, even live cells. I will report on our experience of STD-NMR as a complement to protein crystallography in the field of protein-glycan interactions, which are often multivalent but generally of low affinity (with K_d-values in the mM range). Examples from research on polyomaviruses, which use glycans as attachment factors or functional receptors, and complement factor H, a 20-domain protein with a particular taste for sialylated glycans, will serve to underline the complementarity of protein crystallography, STD-NMR, and, in one case, MD simulations.

LT2-02

Na3ZrCo(SiO4)2(PO4) as an electrolyte material for sodium-ion batteries.

A. Loutati[1]
[1]Ben M'sik University Hassan II Casablanca, Faculty of Science, Casablanca, Morocco

The Na+ super-ionic conductor Na3Sc2(SiO4)2(PO4), known as the original NASICON material, is a promising solid-state electrolyte that can be used for sodium batteries. A solution-assisted solid state reaction (SA-SSR) method has been developed for its synthesis. In an attempt to investigate the structure, the corresponding space group and lattice vibrational modes of Na3Sc2(SiO4)2(PO4) phosphate, a sample of this compound was studied by X-ray diffraction and Raman spectroscopy. A comparison of powders and ceramics prepared by the Pechini and SA-SSR methods was carried out. Scanning electron microscopy, X-ray diffraction and impedance spectroscopy were used to investigate the products of both synthesis routes and the possible reasons of the high quality of SA-SSR samples are discussed.

LT2-03

Structure-optimized ProM scaffolds address Ena/VASP as a possible antimetastatic target

M. Brone[1], M. Müller[1], S. Chiha[2], U. Heinemann[3], H. G. Schmalz[2], R. Kühne[1]
[1]Leibniz-Forschungsinstitut für molekulare Pharmakologie, Drug Design, Berlin, Germany
[2]Universität zu Köln, Chemie, Köln, Germany
[3]Max-Delbrück-Center for Molecular Medicine, Berlin, Germany

Metastasis is the major lethal attribute of cancer. However, the lack of antimetastatic drugs and the limited progress of metastasis-directed drug development efforts make new approaches essential in drug design. Despite being a marker of breast carcinogenesis and signature of invasive cancer progression, potent inhibitors against the actin regulatory protein family Ena/VASP remained elusive.

Recently, we showed that interfering with Ena/VASP causes significant reduction in breast cancer cell invasion. We designed and evaluated di-proline mimicking scaffolds, coined ProM, to inhibit the proline-mediated protein-protein interaction of the Ena/VASP EVH1 domains with a non-toxic, selective and cell-membrane-permeable inhibitor (see image). However, the moderate affinity of the initial inhibitor will restrict the validation in future animal studies. We therefore optimized the affinity of this inhibitor by using structural informations and *in silico* docking studies based on 18 Ena/VASP EVH1 crystal structures. For the first time, we solved the binding mode of the elongated peptide of the actin assembly-inducing protein (ActA) of *Listeria monocytogenes*. We mimicked the newly found interactions of ActA with new scaffolds and developed a 734 Da compound with nanomolar affinity, which serves as novel starting point for *in vivo* studies. We conserved the structural simplicity, low-molecular weight and pharmacological properties of the inhibitor while drastically increasing the affinity of the scaffolds against the flat protein surface.

The herein presented structure-affinity relationship study demonstrates the powerful modular architecture of our scaffold toolbox and paves the way for future in vivo studies. Structure-optimized ProM scaffolds might represent a novel class of antimetastatic drugs acting at the very end of converging receptor kinase signaling and integrin pathways.

Figure 1

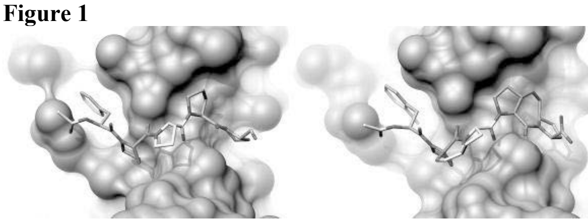

LT2-04

High temperature in-situ PDF study on TiO2 nanoparticle growth

S. Diez[1]
[1]Friedrich-Alexander-Universität Erlangen-Nürnberg, Erlangen, Germany

Our latest research concentrates on keeping track of the structural evolution during the growth of TiO2 nanoparticles. These investigations deal with Anatase as one of the four naturally occurring polymorphs of TiO2. Herein, the challenge is to in-situ grow phase-pure Anatase particles without the occurrence of other polymorphic phases (such as Brookite) at any stage of the synthesis. In order to access phase-pure particles we have developed a synthesis which can be carried out in 2-3 hours and runs at 90°C in an aqueous solution.

The elevated temperature setup allows us to observe the synthesis from the nucleation stage to an apparent presence of fully developed nanoparticles. By tuning temperature accordingly we can accelerate the particle growth rate and subsequently monitor the synthesis with various XRD techniques at the second timescale.

Fig. 1: In-situ synthesis of Anatase at 90°C in aqueous solution a) Peak intensities above solvent background in in-situ XRD measurements b) Time resolved PDFs plotted against time illustrating the nucleation and cluster phase (particles of less than 1nm size within the first 10 minutes) up to the appearance of aged particles of 3 nm size.

PDF as well as SAXS data analysis illustrates how the particle formation takes place. By setting the temperature just below the boiling point of water, nucleation and subsequently the radial growth of the nanoparticles to sizes of up to 5 nm can be studied. The data of both mentioned techniques suggests that right after the nucleation phase, spherical particles are formed. By adding merely traces of heavy metal ions, however, the kinetics of the syntheses are considerably decelerated in comparison to a pure synthesis at identical condition. Elongated morphologies and often TiO2 nanorods are reported in multiple studies and explained owing to differences in growth velocity resulting of interactions on nanoparticle surfaces. Yet, metal impurities or dopants have not been found to change the habit of the nanoparticles. We suppose that metal impurities in low percentage concentrations influence growth velocities and should be considered as reason for morphology changes in sol-gel processes. In order to investigate those hypotheses we apply various modelling strategies and track the transformation of polynuclear clusters towards nanoparticles by simultaneously tracing effects from incorporation of metal ions, structural healing processes and morphology transitions.

Figure 1

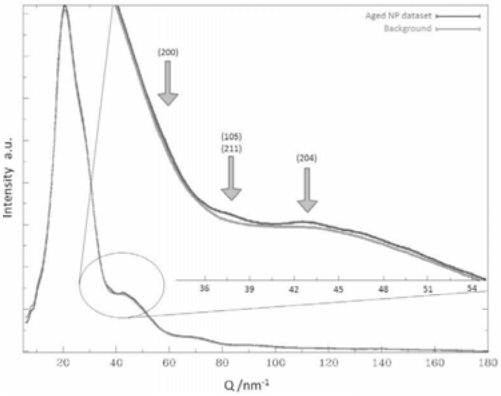

Figure 2

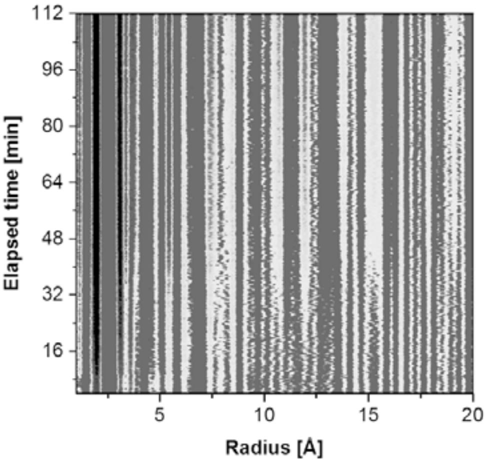

LT2-06
Serial synchrotron crystallography at EMBL PETRA III beamline P14

J. Hakanpää[1], G. Bourenkov[1], I. Karpics[1], G. Pompidor[1], I. Bento[1], T. Schneider[1]
[1]European Molecular Biology Laboratory Hamburg, Hamburg Unit, Hamburg, Germany

Serial synchrotron crystallography (SSX) combines X-ray images taken from randomly oriented crystals, passed through the beam using diverse delivery methods, into a single dataset. The method requires a high-brilliance synchrotron source with a beam size similar to the sample size, an appropriate sample delivery method, a detector with sufficient frame rate and a data processing pipeline. SSX can act as a pre-screening method for XFEL experiments or a stand-alone experiment when crystal growth to larger size cannot be achieved, e.g. *in vivo* grown crystals. Proof of principle experiments (1) have shown the feasibility of the method.

Our SSX setup at the EMBL beamline P14 (PETRA III, DESY Hamburg) utilizes the tools of conventional crystallography, minimizing setup time and sample consumption. *In situ* experiments can be done in CrystalDirect^{TM} plates, also *in meso*. Cryo-samples are mounted in loops or harvested from plates with the CrystalDirect^{TM} Harvester. Generally, the sample size is a few microns. Data collection runs as series of helical line scans, typically a dataset is collected in a few minutes, depending on the size of the region of interest. Progression of the data collection is monitored throughout the experiment as on-the-fly calculated heat map, displaying the diffraction scores as estimated by program DOZOR (2).

The acquired diffraction images are sorted and bunched into sub datasets according to the DOZOR score. The sub datasets are process in parallel with XDS and scaled using XSCALE. We have demonstrated the feasibility of the pipeline using 5 µm lysozyme and insulin crystals as test objects. Using an Eiger4M detector, a data set of 65120 images was collected at P14 in 3 minutes as an *in situ* experiment of 5 micron lysozyme crystals grown and presented to the beam in a CrystalDirect^{TM} plate. About 2000 sub dataset, each containing 5-10 diffraction images, were integrated and scaled to yield complete data to 1.7 Å resolution. The structure could be solved by molecular replacement and electron density maps were of good quality. Beamtime for SSX experiment can be applied for through the EMBL user program at https://smis.embl-hamburg.de.

References

[1] Gati G., Bourenkov G., Klinge M., Rehders D., Stellato F., Oberthür D., Yefanov O., Sommer B.P., Mogk S., Duszenko M., Betzel C., Schneider T.R., Chapman H.N., Redeckec L. (2014) *IUCr J.* **1** 87-94
[2] Popov, A. & Bourenkov, G. (2015). DOZOR. European Synchrotron Radiation Facility, Grenoble, France

LT2-07
Phase transition of tetragonal copper sulfide Cu_2S at low temperatures

D. Zimmer[1], J. Ruiz-Fuertes[2], L. Bayarjargal[1], E. Haussühl[1], B. Winkler[1], J. Zhang[3], C. Jin[3], V. Milman[4], E. Alig[5], L. Fink[5]
[1]Goethe-Universität Frankfurt am Main, Institut für Geowissenschaften, Frankfurt am Main, Germany
[2]Universitat de València, Departament de Física Aplicada, Valencia, Spain
[3]Chinese Academy of Sciences, The Institute of Physics, Beijing, China
[4]Dassault Systèmes Biovia, Cambridge, United Kingdom
[5]Goethe-Universität Frankfurt am Main, Institut für Anorganische und Analytische Chemie, Frankfurt am Main, Germany

Cu_2S-based solar cells have been studied intensively due to their potentially favorable price-performance ratio. Unfortunately, the limited phase stability of the dominant copper sulfide phase in these cells, monoclinic α-chalcocite (Cu_2S) [1], led to a cancellation of further developments and the industrial production of Cu_2S-based cells [2]. However, a recent study on the stability of nanoparticles of copper sulfides [3] suggests that tetragonal Cu_2S [4], a high-pressure-high-temperature polymorph, might be a possible substitute for the monoclinic phase. The current knowledge about the properties of this polymorph is rather limited and inconsistent. Therefore we investigated tetragonal copper sulfide at ambient and low temperatures [5].

The low-temperature behavior of tetragonal Cu_2S was investigated by XRD, resistance measurements and calorimetry. The experiments were complemented by DFT-based calculations and optical absorption (OA) measurements at ambient conditions.

Our heat capacity and powder XRD measurements confirm previous findings [6], showing a temperature-induced phase transition at ~202 K with a hysteresis of about ±21 K. The temperature dependence of the heat capacity is asymmetric on cooling and shows a double peak on heating, indicating that the transition is not a single process (Fig. 1). The structure of the low-temperature polymorph was solved here (space group: *Pna*21) (Fig. 2) [5].

The electrical resistance is strongly correlated with the structural transition and changes by several orders of magnitude across the transition. For tetragonal and orthorhombic Cu_2S an activation energy of the conductivity of 0.15(2) and 0.22(1) eV was determined, respectively. From the interpretation of the DFT-based calculations combined with the results of OA measurements a direct band gap of 1.04(2) and 0.98 eV was derived for the tetragonal and the orthorhombic phase, respectively [5].

The authors gratefully acknowledge financial support by the DFG (Wi 1232).

Figure 1: Excess heat capacity of tetragonal *Cu_2S* on heating
Figure 2: Crystal structure of orthorhombic Cu_2S

References
[1] H. T. Evans (1971). *Nature Phys. Sci.* **232**, 69.
[2] K. L. Chopra & S. R. Das (1983). Thin Film solar cells, Plenum, New York.
[3] T. Machani *et al.* (2011). *Chem. Mater.* **23**, 5491.
[4] A. Janosi (1964). *Acta Crystallogr.* **17**, 311.
[5] D. Zimmer *et al.* (2017). *Phys. Rev. B* **96**, 054108.
[6] S. Stølen *et al.* (1990). *J. Chem. Thermodynamics* **22**, 1035.

Figure 1

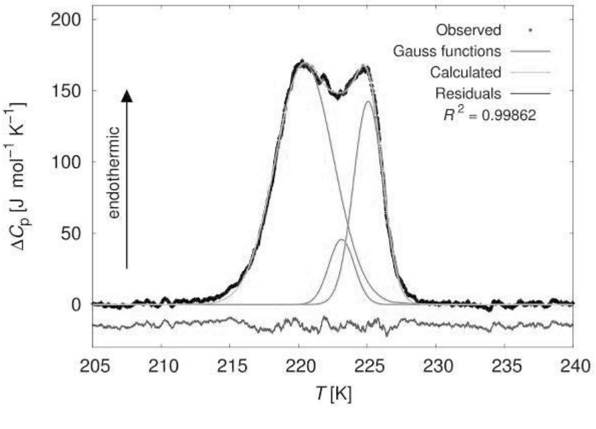

Figure 2

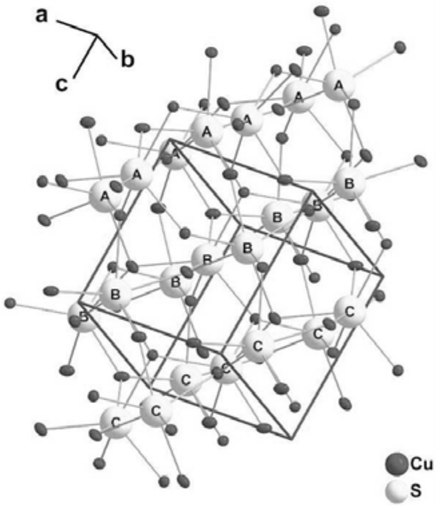

LT2-08
In situ Studies of Dislocations in GaAs with Synchrotron White Beam X-ray Topography

P. Fritsch[1], M. P. Kabukcuoglu[1,2], S. Haaga[1,2], T. Baumbach[2,3], A. N. Danilewsky[1]
[1]Albert-Ludwigs-Universität Freiburg, Kristallographie, Freiburg i. Br., Germany
[2]Karlsruhe Institute of Technology (KIT), Institute for Photon Science and Synchrotron Radiation (IPS/ANKA), Karlsruhe, Germany
[3]Karlsruhe Institute of Technology (KIT), Laboratory for Application of Synchrotron Radiation (LAS), Karlsruhe, Germany

Studies in the past on Si showed that defects on wafer surfaces and edges during heat treatment produces dislocations and slip bands. These defects contribute significantly to the performance of an electronic device [1]. In this work the formation and dynamics of dislocations and slip bands are observed in undoped GaAs having a cellular dislocation network. These defects can be observed by means of synchrotron white beam x-ray topography (SWBXT). The measurements were performed at the test facility and synchrotron radiation source in the TopoTomo beamline at IPS. For this work (001) GaAs wafers of 400 µm thickness were cut into 2x2 cm² samples and indented. The samples received a heat treatment in the double ellipsoidal mirror furnace up to a temperature of 590°C while in situ SWBXT was performed and recorded with a CCD-camera setup (PCO4000) on the 220 reflection. Ex situ topographs on photographic films were taken before and after the heat treatment for additional Burgers vector analysis. Fig. 1(a-c) shows images from the 220 reflection taken in the in situ SWBXT experiment. Fig. 1a displays the sample before the heat treatment with its cellular network and the strain field of the indent marked by a circle. In fig. 1b the development of the strain field can be observed while the sample is heated up, also marked by a circle. Fig. 1c reveals the sample after the heat treatment with the final slip bands. The main propagation direction of the glide planes are [-110] and [-1-10] with a velocity of 12 µm/s and 11 µm/s respectively which was directly taken from the digitally acquired footage of the 220 reflection. In the area, where the slip bands developed during the heat treatment, 120 section scans were recorded with the PCO4000 and afterwards 3D reconstructed to observe the orientation and composition of the glide planes. The segments show a 54.7° angle relatively to the (001) surface as a result of a glide in a {111} glide plane. The dynamical development will be shown in the SWBXT movie.

References

[1] A.N. Danilewsky, J. Wittge, A. Cröll, D. Allen, P. McNally, P. Vagovic, T. dos Santos Rolo, Z. J. Li, T. Baumbach, E. Gorostequi-Colinas, J. Garagorry, M. R. Elizalde, D. Jaques, M. C. Fossati, D. K. Bowen and B.K. Tanner., **J. Crystal Growth** 318 (2011) 1157-1163

Figure 1

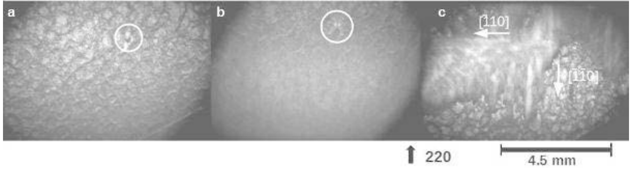

LT2-09

Analysis of aluminum conductivitiy in high-valent transition metal oxides with Bond-Valence-Site-Energy calculations

M. Rothenberger[1], F. Meutzner[1,2], T. Nestler[1], T. Leisegang[1,2], D. C. Meyer[1]
[1]Technische Universität Bergakademie Freiberg, Institut für Experimentelle Physik, Freiberg, Germany
[2]Samara National Research University, Samara, Russian Federation

Since the utilization of renewable energy carriers such as wind and sun is environmentally benign, they are interesting sustainable alternatives to fossil fuels. However, due to their fluctuating availability, they may not match the demand and offer of the energy grid. Electrochemical storage technologies offer high achievable energy densities, which can counterbalance this irregularity.

Still, such energy storage systems need a large amount of active mass in order to store considerable quantities of energy. Since Li shows a low abundance in the earth"s crust, we propose the application of higher-abundant elements like Al to increase the availability of energy storage systems in the future.

Furthermore, increased energy density, decreased cost of energy storage systems, and reduced dependence on critical elements for utilized materials are important parameters. Al is a valid candidate since it is the most abundant metal in the earth"s crust and offers a high theoretical capacity due to its high valence. Still, it is not yet incorporated in working battery technologies as an active ionic species. Solid-state ionic conductors and cathode materials are necessary to provide corresponding materials.

We have applied two theoretical approaches to the ICSD to identify promising materials for Al-ion conduction. The first rating concerns geometrical aspects and is carried out using high-throughput Voronoi-Dirichlet partitioning. The materials found this way possess structure-immanent interconnected void-systems suitable to favor Al-ion conduction. The second step consists of crystal-chemical calculations based on bond-valence site-energies to find continuous paths for Al-ion conduction and to assess respective activation energies in the potential materials found.

In order to support prior searches within at least Al and O-containing compounds, we have analyzed high-valent transition metal oxide materials described without any Al in their structure in order to expand the range of chemical compositions and thus increase the amount of analyzed materials. If these materials can be produced by either adding Al to the synthesis of the transition metal oxides or a subsequent Al-intercalation, we hope to identify materials with potentially high Al-ion diffusivity for the future.

The work was performed within the joint-research project R2RBattery, financially supported by the German Federal Ministry of Education and Research (BMBF: 03SF0542A).

LT2-10

Beamline P02.1: A Workhorse for High-Resolution Powder Diffraction & Total Scattering Experiments at PETRA III, DESY

M. Wharmby[1], M. Etter[1], J. Bednarcik[1], J. C. Tseng[1], M. Wendt[1], S. Wenz[1], A. Ehnes[1], H. P. Liermann[1], O. Seeck[1]
[1]Deutsches Elektronen-Synchrotron DESY, FS-PE, Hamburg, Germany

Powder diffraction is a standard tool for characterisation in a wide range of fields across the physical sciences: from materials science and metallurgy, to chemistry and solid state physics. Third generation synchrotron sources provide high fluxes of X-rays at higher energy than laboratory sources. These characteristics open the door not only to rapid data collection for high spatial-resolution structural studies, but also to time-resolved *in situ*/*in operando* measurements of functional materials under real conditions, thanks to high energy X-rays being able to penetrate operating environments. Furthermore, the use of high energy X-rays increases the region of reciprocal space which may be studied in an experiment, facilitating improved spatial resolution in total-scattering measurements.

Beamline P02.1 (PETRA III, DESY, Hamburg, Germany) is almost unique amongst high-resolution powder diffraction instruments in operating at a fixed energy of 60 keV. This energy is particularly well suited to the collection of powder diffraction data for Rietveld refinement (especially for high-Z materials, where absorption is a problem at lower energy) and for collection of total-scattering data (the high energy facilitating Q_{Max} of at least 20 $Å^{-1}$), which may be interpreted by Pair Distribution Function (PDF) analysis. Currently two detectors are available on the beamline (a two-dimensional Perkin Elmer XRD1621 and an in-house developed 10-channel Multi-Analyser Detector), whilst additional devices are available from a shared detector pool (including a Dectris Pilatus3 CdTe 2M designed for high-energy data collection).

In addition to ambient temperature capillary measurements, P02.1 offers a range of standard sample environments (e.g. hot-air blower – RT-1100 K; cryostream – 90-500 K; cryostat – 10-300 K) whilst a number of others are under development (e.g. low pressure gas adsorption cell) or are maintained by the PETRA III sample environment group. Moreover the enormous amount of free space around the diffractometer, compared to many other powder diffraction beamlines, allows easy integration of complicated sample environments which are brought to the beamline by our users.

We report here the latest developments at P02.1 including planned changes to detector configurations, new sample environments, updates to the control software and possible remote access schemes.

LT2-11

Investigations on crystal structures and planar defects of heavily stacking faulted honeycomb iridates

S. Bette[1], R. E. Dinnebier[1], T. Takayama[1], H. Takagi[1]
[1]Max-Planck-Institut für Festkörperforschung, X-ray Diffraction, Stuttgart, Germany

Introduction

Iridates having a honeycomb like structural motif recently attracted interest as promising candidates for a topological quantum spin liquid described by Kitaev model.[1, 2] $Ag_3LiIr_2O_6$ and $H_3LiIr_2O_6$, modified honeycomb iridates, were visited as candidates and the latter one was discovered to exhibit a spin liquid ground state.[3] To clarify the reason why quantum spin liquid can be stabilized in $H_3LiIr_2O_6$, a detailed structural understanding, including the microstructural effects like stacking faults, which are a common phenomenon in layered alkali- and earth alkali metal iridates[4, 5], is necessary.

Objectives

The ideal crystal structure of the iridates was solved by using XRPD-data and PDF-analysis (Fig. 1, a), defects were derived from the structural model and investigated by systematic *DIFFaX* simulations. A Rietveld compatible approach[6, 7] was used to determine the real structure, i.e. the degree of faulting by using a supercell approach. The obtained superstructure was confirmed by PDF-analysis.

Results

$Ag_3LiIr_2O_6$ and $H_3LiIr_2O_6$ reveal almost identical $LiIr_2O_6^{3-}$-layers that include $Ir_6O_{18}^{12-}$ honeycombs (Fig. 1, b). The stacking order is governed by the linear coordination sphere of the silver ions and by interlayer O···H-O contacts, respectively. Accordingly distinct stacking vectors can be derived (Fig. 1, c). The hexagonal lattice symmetry is broken by the slight preference of one stacking vector.

Conclusions

The approach for the determination of the faultless, ideal crystal structure and the kind and amount of faulting, i.e. the real crystal structure, presented in this study[8] should pave a way to determine the crystal structure and the degree of stacking faulting of other layered materials of interest, e.g. $Cu_3LiIr_2O_6$, $Cu_3NaIr_2O_6$[9].

References

[1] A. Kitaev, *Ann. Phys. (Amsterdam, Neth.)*, 2006, **321**, 2.
[2] T. Takayama, et al., *Phys. Rev. Lett.*, 2015, **114**.
[3] K. Kitagawa, et al., *Nature*, 2017, **submitted for publication**.
[4] D. C. Wallace, et al., *J. Solid State Chem*, 2015, **224**, 28.
[5] D. C. Wallace, et al., *Dalton Trans.*, 2015, **44**, 20344.
[6] S. Bette, et al., *J. Appl. Crystallogr.*, 2015, **48**, 1706.
[7] A. Kudielka, et al., *J. Mater. Chem. C*, 2017, **5**, 2899.
[8] S. Bette, et al., *Dalton Trans.*, 2017, DOI: 10.1039/c7dt02978k.
[9] J. H. Roudebush, et al., *Dalton Trans.*, 2016, **45**, 8783.

Fig1. (a) Low r-region of the measured PDF-curve of $H_3LiIr_2O_6$, (b) stacking of the $Ir_6O_{18}^{12-}$-honeycombs (c) alternative stacking order.

Figure 1

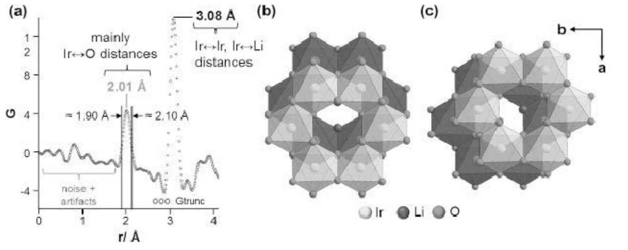

LT2-12
Towards the structure of TRAP transporters with an integrative approach of crystallography and PELDOR

M. F. Peter[1], J. Glaenzer[1], G. H. Thomas[2], G. Hagelueken[1]
[1]University of Bonn, Institute for Physical and Theoretical Chemistry, Bonn, Germany
[2]University of York, Department of Biology, York, United Kingdom

The tripartite ATP-independent periplasmic (TRAP) transporters are secondary membrane-transporters, which are widespread in bacteria and archaea but absent in eukaryots (1). Since their first description in 1997, many different substrates for TRAP transporters were identified, illustrating the importance of these transporters for prokaryotic cells. The best studied TRAP transporters are specific for *N*-acetylneuraminic acid and play an essential role in infections of humane-pathogenic bacteria like *Haemophilus influenzae* and *Vibrio cholerae* (2). All TRAP transporters consist of three different domains, a small and a large membrane domain and a periplasmic substrate-binding protein. While the structure and function of the substrate-binding protein has been well-characterized with different approaches, the membrane domains are less well studied (3). There is currently no experimental information about their 3D-structure as well as about the dynamics and interaction between all three domains during the transport.

To study the TRAP transporter membrane domains with X-ray crystallography and pulsed electron-electron double resonance spectroscopy (PELDOR), large amounts of pure protein are needed. Here we present, how the expression and purification procedure of the membrane domains were optimized to get sufficient yields. At the same time, different extraction methods like polymer-bounded nanodiscs were tested, to analyse the behaviour of the membrane domains not only in different kinds of detergents but also in lipid-environments. For the co-crystallization of all three domains the formation of the tripartite complex was investigated to find optimal complex-forming conditions.

We use PELDOR spectroscopy to analyse the dynamics of the membrane protein in solution and to study the interaction between the substrate-binding protein and the membrane domains. Due to the diamagnetic characteristics of the TRAP transporter, it was necessary to introduce spin labels like MTSSL via cysteine site-directed spin labelling (SDSL) into the proteins. We present how surface accessible native cysteines were identified and how the labelling procedure was optimised.

References

[1] Mulligan, C.; Fischer, M.; Thomas, G. H. *FEMS Microbiol. Rev.* **2010**, 35, 68-86.
[2] Severi, E.; Hood, D. W.; Thomas, G. H. **2007**, 153, 2817-2822.
[3] Glaenzer, J.; Peter, M. F.; Thomas, G. H.; Hagelueken, G. *BiophysJ*, **2017**, 112, 109-120.

LT2-13
New crystal structures of two zirconium metal-organic frameworks

H. Zhao[1], S. Leubner[2], T. Rhauderwiek[2], N. Stock[2], U. Kolb[1]
[1]Johannes Gutenberg-Universität Mainz, Institut für Anorganische Chemie and Analytische Chemie, Mainz, Germany
[2]Christian-Albrechts-Universität zu Kiel, Institut für Anorganische Chemie, Kiel, Germany

Automated electron diffraction tomography (ADT) provides a three-dimensional electron diffraction reciprocal space from single nanocrystals.[1] In comparison with X-ray powder diffraction, electron crystallography shows its strong power and successful applications in structure analysis of nano crystalline materials with extra-large lattice parameters, detecting light scattering atoms (e.g. Li), pseudo-symmetry, small crystalline domains, multiple phases, superstructure and disorder.[2–4] Metal-organic framework (MOFs) compounds, one type of porous materials, are of increasing interest particularly due to its potential applications in catalysis. These highly beam sensitive materials were investigated at liquid nitrogen temperature using a cryo-transfer tomography holder in order to reduce electron beam damage.

We present two new crystal structures of ZrMOFs studied by tomographic electron diffraction. The crystal morphologies were observed by scanning transmission electron microscopy (STEM). Crystallographic information including unit-cell parameters and crystal symmetry were obtained from the three-dimensional reconstruction of ADT datasets. The *ab initio* structure solutions based on ADT data delivered well-resolved Fourier potential maps (Fig.1). The crystal structures were refined against X-ray powder diffraction data. High-resolution TEM imaging was applied to confirm the solved structures.

References

[1] E. Mugnaioli, T. Gorelik and U. Kolb, *Ultramicroscopy*, 2009, **109**, 758–765.

[2] M. Feyand, E. Mugnaioli, F. Vermoortele, B. Bueken, J. M. Dieterich, T. Reimer, U. Kolb, D. de Vos and N. Stock, *Angew. Chem. Int. Ed.*, 2012, **51**, 10373–10376.

[3] M. B. Mesch, K. Bärwinkel, Y. Krysiak, C. Martineau, F. Taulelle, R. B. Neder, U. Kolb and J. Senker, *Chem. Eur. J.*, 2016, **22**, 16878–16890.

[4] H. Zhao, Y. Krysiak, K. Hoffmann, B. Barton, L. Molina-Luna, R. B. Neder, H. J. Kleebe, T. M. Gesing, H. Schneider, R. X. Fischer and U. Kolb, *J. Solid State Chem.*, 2017, **249**, 114–123.

Figure 1: Fourier potential map of ZrMOF derived from ADT data overlaid with the atomic framework model viewed in [001] direction.

Figure 1

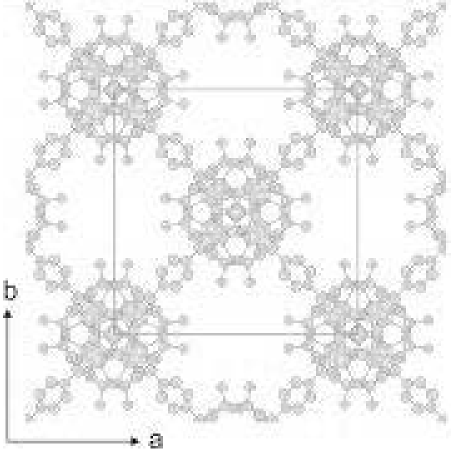

LT2-14

In-situ small-angle X-ray scattering (SAXS) and powder X-ray diffraction (PXRD): Complementary tools to investigate the structural behaviour and the composition of mono- and bimetallic nanoparticles

A. Rostek[1], K. Loza[1], O. Prymak[1], P. R. A. Garcia[2], C. L. Oliveira[2], M. Heggen[3], M. Epple[1]
[1]Universität Duisburg-Essen, Institut für Anorganische Chemie, Essen, Germany
[2]University of São Paulo, Institute of Physics, São Paulo, Brazil
[3]Forschungszentrum Jülich GmbH, Ernst Ruska-Centre for Microscopy and Spectroscopy with Electrons, Jülich, Germany

Introduction

X-ray diffraction methods are widely used to investigate the structural behaviour of metals, alloys, and steels in metallurgy and industry. In addition to well-established colloid-chemically and microscopic methods for the characterisation of nanoparticulate systems, small-angle X-ray scattering (SAXS) and powder X-ray diffraction (PXRD) represent complementary tools to investigate the structural behaviour and composition of mono- and bimetallic nanoparticles.

Objectives

Au, Pd, and Pd/Au core-shell nanoparticles (5-10 nm) were wet-chemically prepared, stabilised with poly(N-vinylpyrrolidone) and characterised with colloid chemically and spectroscopic methods. Studying the structural behaviour during the synthesis, *in-situ* SAXS was carried out. The composition of mono- and bimetallic nanoparticles of gold and palladium was determined by PXRD. Furthermore, high-resolution transmission electron microscopy (HRTEM) and element-specific methods like high-angle annular dark field (HAADF) microscopy, and energy-dispersive x-ray spectroscopy (EDX) were performed.

Results

In-situ SAXS measurements were performed to follow the particle formation during the synthesis. From the modelling of the time-resolved SAXS data it is possible to follow the evolution of the particle diameter (Fig. 1) which showed that the Pd seeds are almost immediately formed. An increase in size is observed when Au is added to the solution (at *t*=50 min). The diameters correspond very well to the values determined by analytical disc centrifugation, dynamic light scattering, and from TEM. Under consideration of the phase diagram and Vegard"s law, the present Pd/Au core-shell nanoparticles show a molar Au:Pd ratio of 43:57 at% as determined by PXRD with subsequent Rietveld refinement. This value is in agreement with the EDX data (molar Au:Pd ratio 41:59 at%).

Conclusions

In-situ SAXS and PXRD are useful methods to study the ultra- and microstructure as well as the composition of bimetallic nanoparticles and give insights into particle formation during the synthesis. They are complementary to the established spectroscopic and microscopic methods and represent additional tools for the investigation of the structural behaviour.

Figure 1

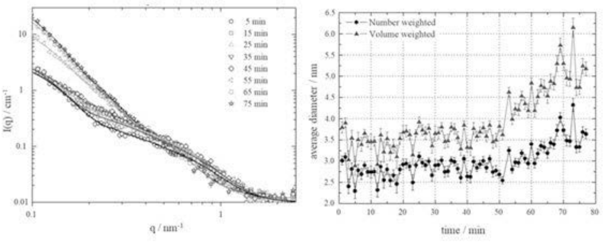

Fig. 1: Scattering intensity data from *in-situ* SAXS measurements (left) and time-resolved evolution of the average diameter of Pd/Au core-shell nanoparticles (right).

LT2-15

How does the crystal structure influence the final composition of the Au-Fe alloy nanoparticles generated via pulsed laser ablation in liquids?

A. Tymoczko[1], M. Kamp[2], C. Rehbock[1], U. Schürmann[2], O. Prymak[1], L. Kienle[2], S. Barcikowski[1]
[1]Universität Duisburg-Essen, Center for Nanointegration, Essen, Germany
[2]Christian-Albrechts-Universität zu Kiel, Technische Fakultät, Kiel, Germany

Nanostructure of the alloy nanomaterials are of high importance, as the composition defines the properties of the new generated nanoparticles. Alloy nanomaterials, particularly those composed of iron gold, are highly interesting not only for industrial application but also in medical area. In catalysis systems composed of a gold core and an iron shell were shown to exhibit advanced photocatalytic activity in low temperature oxidation of carbon monoxide and combustion of organic compounds [1]. For applications in biomedicine a reversed core shell ultrastructure, composed of an iron core and a gold shell is more relevant, where the magnetic properties of the core can be combined with the plasmonics of the shell e.g. during MRI /optical-dual imaging [2]. In this work we applied pulsed laser ablation in liquid to generate gold-iron core shell nanoparticles directly from bulk iron-gold alloy targets. Laser ablation in liquid is an established technique [3] which allows generation of highly pure nanoparticles without any organic surfactants and stabilizers. The main focus of our work lies in a detailed understanding of the formation mechanism of the Fe@Au nanoparticles, generated by pulsed laser ablation in liquid media. The influence of the composition of the target on ultrastructure of nanoalloys is investigated. Analysis of the results are established by X-Ray diffraction (XRD) and compared to High Resolution transmission electron microscopy (HR-TEM).It could be shown that during NP generation from the elements Fe and Au, which obey Hume-Rothery rule, the composition as well as the phase structure in the target material defines if phase segregation takes place in the resulting nanoparticles. We could conclusively proof that for Au rich targets containing FCC-Fe & FCC-Au predominantly solid solution nanoparticles with ideal miscibility of the elements in the solid state are formed. On the other hand, for Fe rich targets with iron contents exceeding 50% and deviating crystal structures BCC-Fe & FCC-Au in the target, phase segregation was observed in the fabricated nanoparticles. Here particles with an iron rich core surrounded by a gold rich shell were predominantly found. Furthermore, we observed a correlation between the size of the nanoparticles and the crystal structure. Experimental data supported by theoretical calculations revealed that core shell structures with FCC-Au and BCC-Fe are solely found when the diameter of the particles exceeds 10 nm.

Figure 1

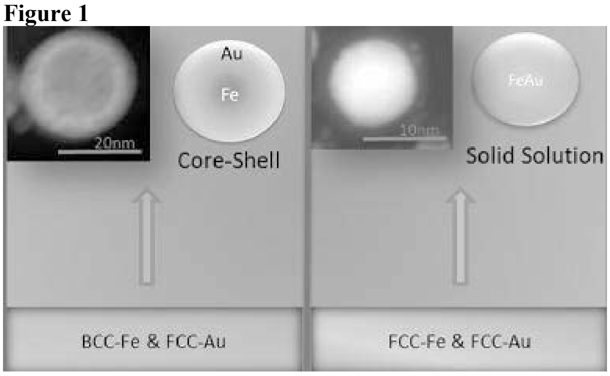

LT2-16

Crystal structure of the human lysosomal mTORC1 scaffold complex

G. Shivalingaiah[1], M. E. G. de Araujo[1], A. Naschberger[1], B. G. Fürnrohr[1], T. Stasyk[1], T. Dunzendorfer-Matt[1], S. Lechner[1], S. Welti[1], L. Kremser[1], H. H. Lindner[1], M. Offterdinger[1], L. A. Huber[1], K. Scheffzek[1]
[1]Innsbruck Medical University, Department of Biological Chemistry, Innsbruck, Austria

mTORC1 plays a pivotal role in regulating cellular growth and metabolism in response to nutrient condition. This nutrient dependent activation, in other words amino acid dependent activation of mTORC1 is regulated via hetero dimeric Rag GTPases that are anchored on lysosomes through the pentameric LAMTOR complex, also known as "Ragulator," thereby controlling the activity of mTOR complex 1 (mTORC1) on the lysosome. Recently we have elucidated the crystal structure of LAMTOR that consists of two heterodimers LAMTOR2/3 and LAMTOR4/5 both displaying same dimerization mode, wrapped and held together by LAMTOR1, which is largely helical in structure and stabilizes the heterodimers by forming a U shaped belt around them. We have identified three areas of contact regions between LAMTOR1 and LAMTOR3, 4 or 5 contributing to increased affinity between the subunits. In addition to this, we have also shown that the carboxyl-terminal domains of Rag guanosine triphosphatases (GTPases) is sufficient for associating with pentameric LAMTOR complex and revealed the binding regions between carboxyl-terminal domains of Rag GTPases to the region of LAMTOR2 and LAMTOR3 with additional contact surfaces provided by LAMTOR1, providing an idea on how mTORC1 might bind to and interact with this complex. In our in vitro experiments, absence of LAMTOR1 during protein reconstitution did not form a complete LAMTOR complex, which marked the importance of LAMTOR1 for the complete assembly of the complex and furthermore site directed mutagenesis in the predicted interaction regions of LAMTOR1 with other components defined the importance of LAMTOR1 in maintaining the accuracy of mTORC1 signaling.

Reference

Crystal structure of the human lysosomal mTORC1 scaffold complex and its impact on signaling" Mariana E.G. de Araujo*, Andreas Naschberger*, Barbara G. Fürnrohr* et al, SCIENCE, 2017

LT2-17

Structure determination of 2-(4-(6-Fluoropyridin-3-yl)phenyl)quinoxaline

D. V. Geetha[1], K. B. Harsha[2], M. A. Sridhar[1], K. S. Rangappa[2]
[1]University of Mysore, Department of Studies in Physics, Mysuru, Karnataka, India
[2]University of Mysore, Department of Studies in Chemistry, Mysuru, Karnataka, India

Introduction

The title compound 2-(4-(6-Fluoropyridin-3-yl)phenyl)quinoxaline (C38H24F2N6) belongs to a quinoxaline group. Quinoxaline is a aromatic benzene ring fused with pyrazine ring. It is also called as benzopyrazine. Quinoxaline derivatives show wide spectrum of biological properties viz., antibacterial, antifungal, antimalarial, anticancer, anti-depression, antitubercular etc [1]. They also serve as basis for many insecticides, herbicides, and fungicides. Besides this, quinoxaline derivatives have also been reported for their efficiency in making dyes, electroluminescent materials, organic semiconductors and DNA cleaving agents [2]. The diverse range of biological applications of quinoxaline derivatives has rised an interest to characterize the title compound.

Experimental methods

For X-ray diffraction study a block of single crystal with approximate dimensions 0.23 × 0.22 × 0.21 mm was used. X-ray data were collected on Bruker CCD diffractometer equipped with CuKα radiation of wavelength 1.54178 Å. Data were collected in the θ range 2.69° to 64.74° at temperature 296 K. For data reduction of all the measured reflections and absorption corrections *APEX*2 package [3] was ued. Crystal structure was solved by direct methods using *SHELXS*-97 [4] and refined by full matrix least squares against *F*2 using *SHELXL*-97. All the non-hydrogen atoms were refined anisotropically. The hydrogen atoms were placed at geometrically acceptable positions and were allowed to ride on their parent atoms. A total of 416 parameters were refined with 4689 unique reflections. After the final refinement the residual value R converged to 4.09 %. The crystal data, data collection and structure refinement details are given in **Figure1**.

Results and discussions

The compound C38H24F2N6 crystallizes in the monoclinic crystal system in the space group . The unit cell parameters are a=12.6878(4)Å, b= 6.8467(2)Å, c= 33.0184(10)Å, β=95.813(2)°; V=2853,45(15)Å^3 . The asymmetric unit of the compound has two crystallographically independent molecules. All the rings in the structure are Sp^2 hybridized. Both quinoxaline ring and fluoropyridine rings lie out of plane from the central phenyl ring plane. The fluoropyridine ring is almost planar with a maximum deviation of 0.006(1) Å for C5A. The dihedral angle between C14A-C13A-C18A-N3A = 180.0(1)° , C19A-N3A-C18A-C17A = 178.7(1)° , N2A-C13A-C18A-C17A = −178.8(1)° , and C16A-C17A-C18A-N3A = −179.3(1)° indicates that quinoxaline ring is coplanar. The torsion angles between the atoms C3A-C4A-C6A-C7A = 37.8(2)° indicates that fluoropyridine and phenyl rings are in syn-clinal conformation. In the crystal structure molecules are linked by C-H...cg interactions forming the three dimensional network. There are no classic hydrogen bonds have been found in the structure. The *ORTEP* diagram of the compound is shown in the **Figure2**.

References

[1] Joana A. P., Ana M. P., M. Natália D. S. C., Rúben F., Cristina P., João P. N., Mónica V.,
European Journal of Medicinal Chemistry, xxx, **2014**, 1–9.
[1] Ashutosh Kumar P., Jeyakandan M., Ashok Kumar M., Selvam G., *International Journal of PharmTech Research*, 3, **2011**, 386–392.
[1] Bruker, *APEX*2, SAINT, SADABS, 2009, Bruker AXS Inc, Madison, Wisconsin, USA.
[1] Sheldrick G. M., *SHELXS*-97, A program for crystal structure determination, Univ. of Göttingen, **2008**, Germany.

Figure 1

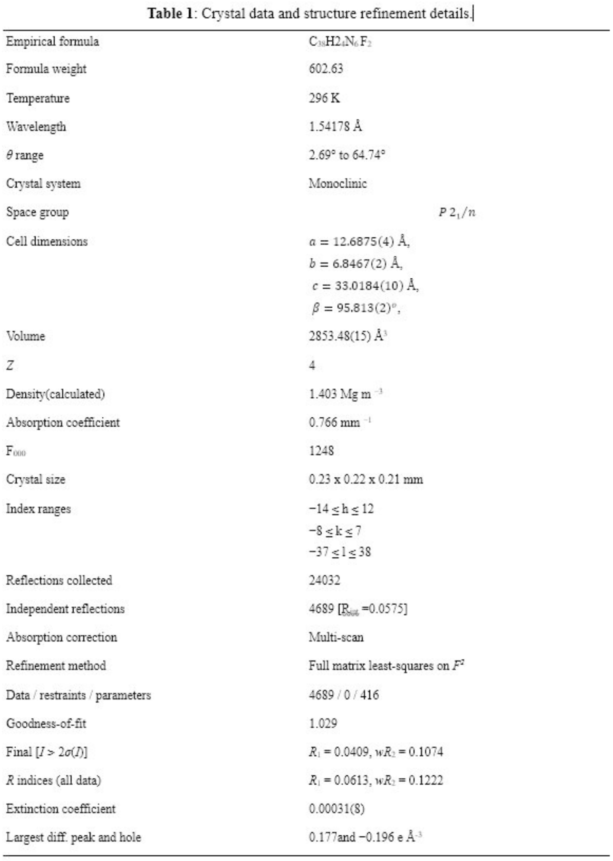

Table 1: Crystal data and structure refinement details.

Empirical formula	$C_{38}H2_{4}N_{6}F_{2}$
Formula weight	602.63
Temperature	296 K
Wavelength	1.54178 Å
θ range	2.69° to 64.74°
Crystal system	Monoclinic
Space group	$P\,2_1/n$
Cell dimensions	$a = 12.6875(4)$ Å, $b = 6.8467(2)$ Å, $c = 33.0184(10)$ Å, $\beta = 95.813(2)°$,
Volume	2853.48(15) $Å^3$
Z	4
Density(calculated)	1.403 Mg m^{-3}
Absorption coefficient	0.766 mm^{-1}
F_{000}	1248
Crystal size	0.23 x 0.22 x 0.21 mm
Index ranges	$-14 \leq h \leq 12$ $-8 \leq k \leq 7$ $-37 \leq l \leq 38$
Reflections collected	24032
Independent reflections	4689 [R_{int} =0.0575]
Absorption correction	Multi-scan
Refinement method	Full matrix least-squares on F^2
Data / restraints / parameters	4689 / 0 / 416
Goodness-of-fit	1.029
Final [$I > 2\sigma(I)$]	$R_1 = 0.0409$, $wR_2 = 0.1074$
R indices (all data)	$R_1 = 0.0613$, $wR_2 = 0.1222$
Extinction coefficient	0.00031(8)
Largest diff. peak and hole	0.177and −0.196 e $Å^{-3}$

Figure 2

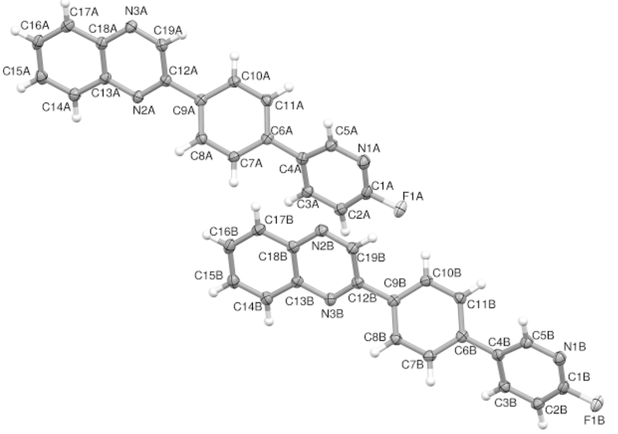

This work is funded by the BMBF (R2RBattery: 03SF0542A), Russian Megagrant (14.B25.31.0005), and RSF (16-13-10158).

Bio-Crystallography I: Hot new structures

P001

Crystal Structure of the most prominent phospholipase PlaB, a hemolytic virulence factor from *Legionella pneumophila*

M. Diwo[1], W. Michel[2], K. Kuhle[2], J. Krauße[3], A. Flieger[2], W. Blankenfeldt[1]
[1]Helmholtz-Centre for Infection Research, Structure and Function of Proteins , Braunschweig, Germany
[2]Robert Koch Institut, Bakterielle darmpathogene Erreger und Legionellen , Wernigerode, Germany
[3]Technische Universität Braunschweig, Institute for Plant Biology, Braunschweig, Germany

Legionella pneumophila is a parasitic pathogen causing legionnaires' disease as a lung infection upon inhalation of contaminated aerosols. *L. pneumophila* survives intracellularly by replicating in macrophages, but is also able to enter various epithelial cells. Numerous virulence factors of *L. pneumophila* are known, such as lipopolysaccharides, toxins or hemolytic enzymes. The ability of *L. pneumophila* to lyse membranes and trigger pore formation for vacuolar escape upon intracellular replication is likely related to a number of phospholipases A (PLA). The PLAs of *L. pneumophila* count at least 15 members, clustered in three families. PlaB, the first member of a new PLA family, comprises an outer membrane associated virulence factor with the most prominent PLA activity in *L. pneumophila* combined with an additional hemolytic activity. Concentration dependent PlaB dimer formation leads to PLA activity inhibition, pointing towards a conjectural mechanism for self protection. Though PlaB lacks structural characterization, it is known that the N-terminal domain contains the catalytic triad Ser85/Asp203/His251, which is mandatory for PLA as well as hemolytic function. Hemolytic activity is further dependent on fifteen C-terminal residues as indicated by reported truncation mutants. Interestingly, a 170 amino acid long region in the C-terminal domain has not been assigned to any function yet. Therefore structural elucidation is important in order to increase functional and mechanistic understanding of PlaB.

Expression and purification of PlaB was successfully performed. However, reproducibility of crystal growth was one of the main obstacles. Seeding techniques helped to achieve well diffracting crystals of a SeMet derivative. Those crystals were used to solve the structure of full length PlaB by single-wavelength anomalous dispersion. PlaB shows an N-terminal α/β-hydrolase fold, which has been previously proposed by sequence-based analysis. The C-terminal domain of unknown function comprises a β-sandwich fold. A stretch of 20 residues at the C-terminus seems to be necessary for homo dimer formation by interacting with the N-terminal domain of a second PlaB molecule.The structure does support the hypothesis of a likely connection between state of oligomerisation and hemolytic activity of PlaB. Further characterization and substrate identification is needed to fully understand PlaB's mode of action.

Figure 1

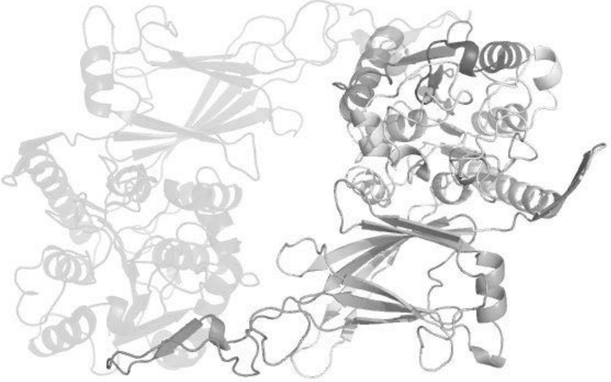

P002

Structural and functional analysis of the TSC2 GAP-Domain

P. Hansmann[1], S. Kiontke[2], D. Kümmel[1]
[1]Universität Münster, Institute of Biochemistry, Münster, Germany
[2]University of Osnabrück, Biology/Chemistry, Osnabrück, Germany

Small GTPases of the Ras superfamily are molecular switches and control various pathways within the cell. They exist in two different forms, a GTP bound form, which is considered as active and a GDP bound form, which is the inactive one. Due to the low hydrolytic activity, small GTPases need GTPase Activating Proteins (GAPs) as accessory protein to hydrolyze GTP to GDP and for their inactivation.

The Ras-like GTPase Rheb is an upstream regulator of the mTORC1 complex, a master regulator of cellular growth. Rheb requires TSC2, part of the TSC-Complex, as GAP for its regulation. Defects and mutations of the TSC complex are linked to the genetic disease tuberous sclerosis complex. This disease leads to the formation of benign tumors in heart, kidney, lung and brain that ultimately cause organ failure.

We here present the crystal structure of the TSC2 GAP domain and compare it to the structure of the homologous protein RapGAP. We provide a model of the active TSC2GAP/Rheb complex that suggests a conserved catalytic mechanism involving an Asn-thumb residue at the active site.

Bio-Crystallography II: Complementation by NMR and EPR

P004

Towards understanding of *Hunchback* mRNA translation suppression in early embryonic development

J. Macosek[1], J. Foot[1], S. Winter[1], P. Masiewicz[1], B. Simon[1], I. Loedige[1], J. Hennig[1]
[1]EMBL Heidelberg, Structural and Computational Biology, Heidelberg, Germany

One of the most crucial processes during development is the establishment of the anterior-posterior axis. In *Drosophila* embryos, the axis is established by a gradient of Hunchback protein. *Hunchback* (*hb*) mRNA is uniformly distributed throughout the embryo, thus the protein gradient results from spatially restricted suppression of mRNA translation at the posterior. The translation of *hb* mRNA is suppressed by a complex comprised of three proteins – Pumilio (Pum), Nanos (Nos) and Brain tumor (Brat)1. Nos is expressed in an opposing gradient to *hb* mRNA providing spatial information, whereas uniformly expressed Pum and Brat are RNA binding proteins (RBPs) that specifically recognize *hb* mRNA.

The structures of the Brat-NHL domain bound to RNA, Pum-HD domain bound to RNA and of the complex of Pum-HD, Nos-ZnF domains and RNA have been published. However, the architecture of the full quaternary complex of Brat, Pum, Nos and the RNA together as well as the mechanism how these multiple RBPs recognize a single RNA together remains enigmatic.

To elucidate the architecture of the complex we use X-ray crystallography and modelling based on SAS data combined with the information from published high resolution structures and additional restraints from NMR and crosslinking-mass spectrometry. The data are further complemented and validated by various *in vitro* assays such as EMSA and ITC. Ultimately, we aim to obtain a high-resolution structure or an accurate hybrid model of the full quaternary translation repression complex, thus explaining the mechanistic details of one of the most fundamental developmental processes.

Bio-Crystallography III: Enzymes

P006

Antimetabolite biosynthesis in *Pseudomonas aeruginosa*

Y. Xiao[1], C. Calderone[2], R. Müller[3,4], W. Blankenfeldt[1,5]
[1] Helmholtz Center for Infection Research, Structure and Function of Proteins , Braunschweig, Germany
[2] Carleton College, Department of Chemistry, Northfield, United States
[3] Helmholtz Institute for Pharmaceutical Research Saarland, Department of Microbial Natural Products , Saarbrücken, Germany
[4] German Centre for Infection Research Association , , Braunschweig, Germany
[5] Technische Universität Braunschweig, Institute of Biochemistry, Biotechnology and Bioinformatics, Braunschweig, Germany

AMB (L-2-amino-4-methoxy-trans-3-butenoic acid) is a γ-substituted vinylglycine that was identified in 1971 as an inhibitor of pyridoxal 5"-phosphate dependent enzymes, resulting in antibiotic activity. Recent studies indicate that the gene cluster *ambABCDE* is responsible for AMB biosynthesis in *Pseudomonas aeruginosa*. Among the proteins of this gene cluster, AmbC and AmbD, two α-ketoglutarate-dependent oxygenases are involved in the modification of L-glutamate as substrate for AMB synthesis. AMB is then synthetized from one modified glutamate and two alanine moieties condensed to a tripeptide by the non-ribosomal peptide synthetases (NRPS) AmbB and AmbE. However, exact timing of the tailoring reactions remains unclear so far and our research thus primarily focuses on AmbC and AmbD. Additionally, we aim at determining structures of unknown NRPS domains in AmbB and AmbE to gain information on their function in AMB synthesis.

We mainly employ X-Ray crystallography to obtain structures of targeted proteins, combined with mass spectrometry (MS) experiments to provide a model for biosynthesis of AMB in *Pseudomonas aeruginosa.*

By now, we determined the structures of AmbD and AmbC in the native state as well as in the ligand-bound state complex with the co-factor α-ketoglutarate analog N-oxalylglycine (NOG). We sought to obtain crystals of the substrate-bound state which would provide insights into timing of the reaction. Additionally, we determined the structure of an uncharacterized domain of AmbE, which exhibits structural elements of a condensation domain, while an essential conserved HHxxxDG motif is absent.

We now aim at combining the structural information with results from ongoing MS experiments to gain information on function of these proteins as well as on timing of the tailoring reactions.

P007

Towards the structural investigation of an RNA-cleaving deoxyribozyme

M. Mieczkowski[1], C. Höbartner[2,3], V. Pena[1]
[1] Max Planck Institute for Biophysical Chemistry, Macromolecular Crystallography Group, Göttingen, Germany
[2] Georg-August Universität Göttingen, Institut für Organische und Biomolekulare Chemie, Göttingen, Germany
[3] Julius-Maximilians-Universität Würzburg, Institut für Organische Chemie, Würzburg, Germany

DNA enzymes, also known as deoxyribozymes, are synthetic single stranded DNA molecules able to catalyze chemical reactions. There are two main reasons for studying deoxyribozymes: their practical value in various applications, and for understanding the complex properties, such as folding and catalysis, of a biopolymer that is of central importance for life. Compared to ribozymes, the DNA enzymes have a higher potential value as tools for industrial or therapeutic applications, owing to their easier and more cost-effective synthesis, as well as the higher stability.

The first crystal structure of a deoxyribozyme demonstrated that DNA possesses the intrinsic ability to adopt complex tertiary folds that support catalysis, and unveiled the active site of a DNA enzyme in the post-catalytic state (Ponce Salvatierra et al). Although this work represented a major breakthrough in the field, basic questions about deoxyribozymes remain unanswered. We still do not know whether deoxyribozymes use metal ions for catalysis, or in what respects their folds and active centers differ and/or share common features.
To address some of these questions, we decided to investigate an RNA-cleaving deoxyribozyme, which is also of interest as a tool for the selective inactivation of genes. Here, we show the synthesis, crystallization and preliminary crystallographic analysis of this deoxyribozyme in complex with the substrate.

P008

Structural insights into phosphoryl transfer mechanism of ADP-dependent glucokinase from Methanocaldococcus jannaschii

P. Tokarz[1,2], M. Wisniewska[2], M. M. Kaminski[3], G. Dubin[1,2], P. Grudnik[1,2]
[1] Jagiellonian University in Krakow, Faculty of Biochemistry, Biophysics and Biotechnology, Krakow, Poland
[2] Jagiellonian University in Krakow, Malopolska Center of Biotechnology, Krakow, Poland
[3] St. Jude Children's Research Hospital, Department of Immunology, Memphis, United States

Introduction
ADP-dependent glucokinase (ADPGK) has been described for the first time in hyperthermophilic Archaea. In contrast to classical ATP-dependent hexokinases, ADPGK utilizes ADP as a phosphoryl group donor to perform glucose phosphorylation in the glycolytic pathway. Recently ADPGK involvement in the modified bioenergetics of activated T cells was postulated and its elevated expression was reported in various cancer tissues, however, the detailed physiological role of ADPGK remains unknown.

Objectives
The main aim of the study was to uncover the mechanism of ADP-dependent glucose phosphorylation by determining the molecular architecture of ADPGK from hyperthermophilic Archaeon Methanocaldococcus jannaschii in complex with substrate and inhibitor.

Results
Here, we present the high-resolution crystal structure of ADPGK from archaeon Methanocaldococcus jannaschii. Our structure reveals the protein in a complex with an inhibitor [5-iodotubercidin (5ITU)], D-glucose, inorganic phosphate and a magnesium ion bound at the active site. Moreover, using a model system of T-cell-activation-induced ROS generation and gene expression, we have tested the inhibitory effect of 5ITU on these phenomena.

Conclusion
Our study reports the first structure of ADP-dependent glucokinase (ADPGK) from Methanocaldococcus jannaschii in a complex with a pan-kinase inhibitor 5-iodotubercidin. Presented data confirm the previously proposed glucose phosphorylation mechanism and the role of the conserved arginine residue in this process. Moreover, since human ADPGK is involved in the regulation of T cell activation, the study lays the foundation for the future development of ADPGK-specific inhibitors to be used in immunology research.

References
[1] Tokarz P. Wisniewska M., Kaminski M.M., Dubin G. and Grudnik P. 2018 Prot Sci in press
[2] Kaminski MM, Sauer SW, Kaminski M, Opp S, Ruppert T, Grigaravicius P, Grudnik P, Grone HJ, Krammer PH, Gulow K 2012, Cell Rep 2:1300-1315.

P009

Control of methylglyoxal synthesis in Bacillus subtilis: Structural basis for the regulatory interaction of the methylglyoxal synthase MgsA with the carbon flux regulator Crh

J. Arens[1], A. Dickmanns[1], C. Zschiedrich[2], J. Gundlach[2], R. Hofele[3,4], P. Neumann[1], H. Urlaub[3,4], B. Goerke[2,5], J. Stülke[2], R. Ficner[1]
[1]Georg-August Universität Göttingen, Abteilung für Molekulare Strukturbiologie, Göttingen, Germany
[2]Georg-August Universität Göttingen, General Microbiology, Göttingen, Germany
[3]Max Planck Institute for Biophysical Chemistry, Bioanalytical Mass Spectrometry Group, Göttingen, Germany
[4]University Medical Center Goettingen, Institute for Clinical Chemistry, Göttingen, Germany
[5]Universität Wien, Microbiology, Immunobiology and Genetics, Wien, Austria

The methyl glyoxylate pathway is essential for various prokaryotic organisms, where an increased glucose uptake can lead to the accumulation of the toxic intermediate methylglyoxal and therefore this pathway needs to be tightly regulated. In many gram positive organisms, the histidine protein (HPr) tightly regulates the expression of proteins involved in the central carbon catabolite cycle [Warner et. al. 2003]. In Bacillus subtilis one anchor point of this regulation is the methylglyoxal synthase (MgsA) and the paralog of HPr the catabolite repression HPr-like protein (Crh), which fulfills a similar role of regulation via a direct MgsA interaction [Landmann et. al. 2012].

Here we structurally and functionally investigated how MgsA is regulated via its interaction partner. The crystal structure at 2.34 Å demonstrates that MgsA is a hexamer (trimer of dimers), whereas in solution an equilibrium between the hexameric and dimeric state can be observed. Hence, the biological active form of MgsA is the hexamer and the arrangement of the individual subunits results in six active centers. In the crystal structure of the hexamer two alternative dimers can be distinguished, though only one seems to prevail in solution. Mutational analysis showed which of the two possible dimers is formed in solution and therefore is supposed to form the stable oligomer, which is not disrupted at low concentrations. Further in vitro crosslinking studies and docking experiments revealed, that the regulatory protein Crh interacts with the N-terminal helices of MgsA. This binding leads to inactivation MgsA most likely due to an active site deformation, which is consequently no longer accessible for the substrate molecules.

References

[1] Warner, J.B., and Lolkema, J.S., (2003) CcpA-dependent carbon catabolite repression in bacteria. Microbiol. Mol. Biol. Rev. 67, 475-490
[2] Landmann, J. J., Werner, S., Hillen, W., Stülke, J., and Görke, B. (2012) Carbon source control of the phosphorylation state of the Bacillus subtilis carbon-flux regulator Crh in vivo. FEMS Microbiol. Lett. 327, 47-53

P010

Halogenase crystals in space group $P3_2$ and in P1 with a non-crystallographic pseudo 3_2 axis harvested from the same drop

C. Widmann[1], M. I. F. Ismail[1]
[1]Universität Bielefeld, Biochemie IV, Bielefeld, Germany

Aryl halides are important intermediates in chemical and pharmaceutical industries as they can be modified by nucleophilic substitution or metal-catalyzed cross-coupling reactions. Their chemical production has various pitfalls such as harsh reaction conditions and potentially poor regioselectivity. The use of flavin-dependent halogenases enables the regioselective introduction of halogen substituents into electron-rich substrates.
During structure determination of a *Xanthomonas campestris* halogenase via X-ray crystallography, an intriguing observation was made. Crystallization had taken place in a Na/K-Tartrate condition buffered with MES or Hepes. While some data sets could be indexed in space group $P3_2$ with one dimer per asymmetric unit, others taken from the same or similar crystallization conditions could only be indexed in space group P1 (with 3 dimers per asymmetric unit). The structure exhibited the same symmetry, however, it was non-crystallographic as two of the dimers had a slightly changed position relative to those in the $P3_2$ crystals.
This effect was recurring with no obvious systematics to it. It seemed to be independent of buffer, pH and cryoprotectant.

P011

Specific allosteric regulation of protozoan sugar-activating nucleotidyltransferases as a new approach to antimicrobial treatments

O. Zeymer[1], J. Cramer[1,2], J. Führing[2], F. Routier[2], A. C. Lamerz[2], J. Lieske[1,2], P. Baruch[3], H. J. Knölker[4], R. Gerardy-Schahn[2], R. Fedorov[1,3]
[1]Hannover Medical School, Institute for Biophysical Chemistry, Hannover, Germany
[2]Hannover Medical School, Institute of Clinical Biochemistry, Hannover, Germany
[3]Hannover Medical School, Research Division for Structural Biochemistry , Hannover, Germany
[4]Technische Universität Dresden, Department of Chemistry, Dresden, Germany

Protozoan pathogens have major negative impacts on public health worldwide and represent a significant healthcare burden. To date, there are no vaccines or effective drugs against these pathogens. Several reports highlight the importance of the central nucleotide sugar UDP-glucose (UDP-Glc) in the growth of trypanosomatid parasites. Suppressing the biosynthesis of UDP-galactose (UDP-Gal) leads to the cessation of the parasites" growth. The enzymes involved in UDP-Gal/UDP-Glc biosynthesis are thus potential drug targets in these organisms. UDP-Glc is synthesized by the UDP-glucose pyrophosphorylase (UGP) that catalyzes the reversible conversion of glucose-1-phosphate (Glc-1-P) and UTP to UDP-Glc and pyrophosphate. In addition, Leishmania parasites and several other protists possess an unspecific UDP-sugar pyrophosphorylase (USP), which is also able to synthesize UDP-Glc. The double knockout of both UGP and USP genes is lethal for Leishmania parasites. Both UGP and USP belong to the superfamily of nucleotidyltransferases (NTs) involved in many vital biological processes. NTs adopt a common fold and active site structure. These similarities suggest that targeting active sites of UGP and USP may result in unspecific inhibition and misregulation of important biological processes through cross-reactivity. Solution to this problem can be provided by employing allosteric effects in the drug-design strategy, utilizing the conformational control by non-conserved residues located far from the catalytic center.

In our work, we cloned, functionally and structurally characterized UGPs from the human pathogen *Leishmania major* (LmUGP) and the host (hUGP). Combining kinetics with structural and theoretical chemistry, we explored the molecular movements of enzymes during the reaction cycle. Comparative analysis of allosteric activation mechanisms in host vs. pathogen UGPs helped us identify an allosteric site on the surface of LmUGP that can be used as a target for developing specific inhibitors. The potential of this site for LmUGP inhibition was confirmed by mutagenesis experiments, and specific allosteric inhibitor targeting this site was developed. This study also revealed mechanisms of allosteric regulation common in NTs including, in particular, the mechanical control of the chemical reaction in the active site. The presented approach can be extended to other pathogens of the Trypanosomatidae family including *Trypanosoma brucei*, *Trypanosoma cruzi*.

Bio-Crystallography IV: Crystallography in industry

P012

Industrial applications at beamline P11 at PETRA III

E. Crosas[1], O. Lorbeer[1], S. Guenther[1], J. Meyer[1], P. Fischer[1], B. Reime[1], T. Pakendorf[1], N. Stübe[1], A. Meents[1], A. Burkhardt [1]
[1]Deutsches Elektronen-Synchrotron DESY, Hamburg, Germany

Beamline P11 is located at PETRA III, the high brilliance 3rd generation synchrotron radiation source at the Deutsches-Elektronen Synchorotron DESY in Hamburg, Germany. P11 is dedicated to imaging and diffraction experiments of biological samples, with a special focus on protein crystallography. The high photon flux (1.3×10^{13} ph/s at 12 keV) provided at the sample position allows for structure determination from weakly diffracting microcrystals and serial crystallography experiments (Stellato et al., 2014; Roedig et al., 2015; Beyerlein et al., 2017). The P11 crystallography endstation can be operated between 5.5 keV and 25 keV and provides full SAD/MAD capability. The X-ray beam size at the sample position can be freely chosen between 4×9 μm^2 and 200 μm^2 ($v \times h$). Energy and beam size changes can be easily realized within a few minutes. The crystallography endstation is equipped with a high-precision single axis goniostat, a rapid automatic sample changer, a large capacity storage Dewar and a fast Pilatus 6M detector, which allows to collect a data set within 2 – 3 min and offers excellent conditions for high-throughput crystallography and fast crystal screening (Burkhardt et al., 2016). Together with a user friendly software and an automatic data processing pipeline, P11 is ideally suited for industrial applications, providing rapid acquisition of high quality data.

References

[1] Beyerlein K.R., Dierksmeyer D., Mariani V., et al. Mix-and-diffuse serial synchrotron crystallography. IUCrJ. 2017;4(Pt 6):769-777.
[2] Burkhardt, A., Pakendorf, T., Reime, B., et al. Status of the crystallography beamlines at PETRA III. Eur. Phys. J. Plus. 2016;131:56.
[3] Roedig P., Vartiainen I., Duman R., et al. A micro-patterned silicon chip as sample holder for macromolecular crystallography experiments with minimal background scattering. Sci Rep. 2015;5:10451.
[4] Stellato F., Oberthuer D., Liang M., et al. Room-temperature macromolecular serial crystallography using synchrotron radiation. IUCrJ. 2014;1(Pt 4):204-212.

Bio-Crystallography V: Instrumentation and methods

P013

Ctrl-D, a tool for diffraction data analysis

F. Dall'Antonia[1], T. R. Schneider[1]
[1]European Molecular Biology Laboratory, Hamburg Unit, Hamburg, Germany

In crystal structure determination of macromolecules, the stages of raw diffraction data processing and subsequent solution of the phase problem with its context-specific methods (Molecular Replacement and/or experimental phasing) are well-established and offer users the choice among various mature software.

In between, the analysis of processed observations of reflection intensities might receive insufficient attention, unless twinning or other crystallographic problems are suspected. However, with rising popularity of native SAD and rapidly evolving serial crystallography approaches both at cryogenic and ambient temperature, the careful analysis of measurements is vital.

We are developing a software tool, based based on the CCTBX framework [1], that provides quick access to typical decision-relevant data statistics. First, prior to the averaging of multiple symmetry-equivalent intensity observations, information about their time/dose coordinate allows for radiation damage analysis and the monitoring of other frame-based pathologies. Second, in the presence of combined and scaled data from multiple crystals, the comparison of frame-intensity profiles between runs as well as their merged-data cross-correlation serve as a means to filter observation subsets of inappropriate quality.

Here, we present some aspects of the current implementation of these ideas and highlight the importance of such analyses, including data filtering, for the performance of experimental phasing. Our tool Ctrl-D will also be embedded to the HKL2MAP-GUI [2], which is free for academics.

References

[1] R. W. Grosse-Kunstleve, N. K. Sauter, N. W. Moriarty & P. D. Adams (2002). *J. Appl. Cryst.* **35**, 126-136.
[2] T. Pape & T. R. Schneider (2004). *J. Appl. Cryst.* **37**, 843-844.

P014

Automating the D8 VENTURE to improve the productivity of home-lab crystallography

M. Adam[1], M. Mrosek[1], V. Smith[1]
[1]Bruker AXS GmbH, SC-XRD, Karlsruhe, Germany

The past five years has seen the introduction of innovative new technologies the D8 VENTURE home-lab X-ray diffractometers that have significantly increased the variety of measurements that can be successfully conducted. Bruker is the first company to introduce large area CPAD detectors. Thanks to mixed mode readout the PHOTON III large active area detector has no dead-time and single-photon sensitivity. Novel X-ray sources such as the METALJET and the ImS DIAMOMD deliver smaller X-ray beams up to an order of magnitude brighter than achievable with traditional rotating anode generators. Entirely air-cooled systems contribute to reducing downtime and operating costs. Bruker has introduced various accessories to automate sample handling and data collection, further increasing the effectiveness of the D8 VENTURE:

Sample centring has increasingly become a weak point in home-lab systems. Manual goniometer heads make centering of small, translucent crystals time-consuming and inaccurate. The AGH enables two-click or fully automated centering of crystals. In addition, the AGH features X-ray centering which is able to centre samples on the diffraction hotspot. This makes the D8 VENTURE effective at working with tiny crystals or crystals *in meso* which can be impossible to visualize optically.

SCOUT is a system for the automated mounting of crystals under cryogenic conditions. Automated sample mounting can vastly increase the available "beamtime" enabling well diffracting crystals to be identified much more rapidly. Crystals can be scored and data-collection performed automatically.

The ISX STAGE is an easy-to-mount accessory to facilitate the automated *in situ* screening of an entire crystallization plate. *In situ* screening of crystals and data collection at room temperature is becoming increasingly useful as more challenging projects are tackled. Such cases might include crystals sensitive to cryo-conditions, crystals too small to harvest, or fragile crystals damaged by manipulation.

Examples on how these new developments improve every day in-house productivity will be given.

Figure 1

P015

Improved home lab productivity without downtime - an old dream comes true

V. Smith[1], M. Mrosek[1], M. Adam[1]
[1]Bruker AXS GmbH, SC-XRD, Karlsruhe, Germany

It is now over forty years since rotating anodes generators (RAGs) became stable enough for use in X-ray diffraction experiments. Crystallographers quickly recognized their potential for protein structure investigations combining RAGs with X-ray film or first generation online detectors. Researches also quickly recognized their shortfalls. Particularly, the fast deterioration of the X-ray beam intensity, regular down time for maintenance and consequently high costs of ownership prevented the general use of rotating anode generators but also drove the search for more reliable alternatives.

Only a few month ago the ImS DIAMOND has become available, delivering higher average X-ray intensity than state-of-the-art microfocus RAG. The high stability of the ImS DIAMOND X-ray output over time is significantly greater. This new X-ray source features an advanced diamond hybrid cooling, taking advantage of diamond"s five times higher heat conductivity compared to Copper, traditionally used as a heat sink. The new technology brings down maintenance costs, and essentially eliminates downtime.

Not only does the new ImS DIAMOND have extremely low cost of ownership it also has an impressively footprint. The ImS DIAMOND presents the possibility ofcurrent RAG"s becoming redundant within a short period of time. This holds even more since, as compared to the 80s, also at the X-ray detector end, time did not stand still. Modern CPAD detectors with a large active area, such as the PHOTON III, thanks to mixed mode detection technology deliver noise-free data with shortest experiment times.

We will present a number of data sets - including examples obtained from very small crystals, and with large unit cell axes - suitable to illustrate the radical change in in-house data collection. All data sets have been measured on a D8 VENTURE equipped with the ImS DIAMOND.

Figure 1

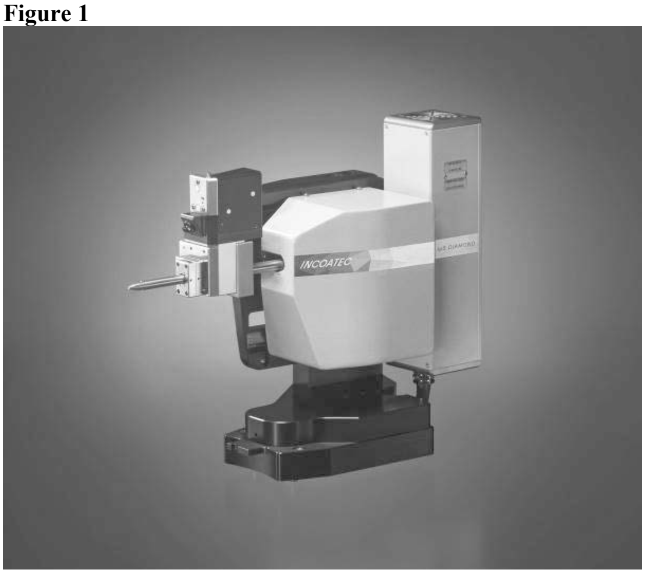

P016

Solving structures with native native SAD on laboratory X-ray sources

A. Förster[1], C. Schulze-Briese[1]
[1]DECTRIS Ltd., Baden-Dättwil, Switzerland

With synchrotrons producing ever more brilliant radiation, concern about radiation damage is increasingly pressing. While ways exist to mitigate damage at synchrotrons, it can also be tackled at the source. For a given photon energy, the absorbed energy and with it the damage sustained by the crystal are proportional to the incident photon flux. Laboratory X-ray sources with their limited flux are thus excellent environments to develop data collection strategies unlimited by radiation damage.

Radiation damage is of particular detriment to experimental phasing where highest accuracy is required to measure the small differences between the structure factors of anomalous pairs. Here, we show how strong anomalous data can be collected on standard laboratory equipment even at room temperature. Not only does this result in structures of macromolecules as close to their physiological state as protein crystallography can provide, it also increases throughput in the laboratory by eliminating the time-consuming screening of cryo-conditions.

Solving structures by native SAD is the gentlest approach to data collection. It requires no soaking with heavy metal and no labeling with Se atoms. As long as the diffraction data are measured with the highest accuracy, e.g. on EIGER R series detectors, doses as low as 30 kGy prove sufficient to obtain the multiplicity and intensity for successful experimental phasing, though sometimes careful alignment of the crystal or an inverse-beam protocol is required.

It is ironic that in times of abundant beamtime at synchrotron facilities and a quest for ever brighter beams, the humble home source proves such a powerful instrument. Phasing of native macromolecular crystals at room temperature is routinely achievable with noise-free Hybrid Photon Counting detectors.

P017

Shine Bright Like a Diamond: Microfocus X-ray Sealed Tube Sources with Hybrid Diamond Anode Technology

J. Graf[1], T. Stürzer[2], H. Ott[2], P. Radcliffe[1], J. Wiesmann[1], C. Michaelsen[1]
[1]Incoatec GmbH, Geesthacht, Germany
[2]Bruker AXS GmbH, Karlsruhe, Germany

Diamond exhibits several unique properties, such as high thermal conductivity, low thermal expansion, extreme hardness, chemical inertness and a fairly high transmission coefficient for X-ray radiation. The thermal conductivity of diamond is about 5 times higher than that of copper and the highest known conductivity of all bulk materials. Therefore, diamond, being a non-toxic material, is increasingly replacing traditional materials for the thermal management in challenging application where a high local heat load needs to be dissipated, such as in heat sinks for high-power microelectronic devices.

The high transmission coefficient, even at low X-ray energies, fosters the use of diamond in X-ray components such as carrier membranes in X-ray lithography or X-ray windows. In X-ray sources, diamond can be used as a transparent heat sink directly coupled to the anode material, improving the heat dissipation considerably and allowing for an increase in tube brilliance by applying a higher power load on the anode.

The IμS DIAMOND, is a new type of microfocus sealed tubes using a unique anode technology, the diamond hybrid anode. It contains a bulk industrial diamond as heat sink that is coated with a layer of the target material (e.g. Cu). The diamond hybrid anode takes advantage of the exceptional high thermal conductivity of diamond, making the heat dissipation in a diamond hybrid anode more efficient. Consequently, the IμS DIAMOND can accept a higher power density in the focal spot on the anode without damaging the surface of the target layer. The balanced heat management in the source assures that the intensity loss over time is only a few percent over 10,000 h of full power operation, which is significantly lower than in microfocus rotating anode sources. As a consequence, the intensity of the IμS DIAMOND is about 20% higher than the average intensity output of a modern microfocus rotating anode.

The IμS DIAMOND establishes a new class of X-ray sources, combining an intensity output that exceeds the intensity of a microfocus rotating anode with all the comfort and lifetime of a standard IμS with a bulk Cu anode. In this presentation, we will be discussing the main features of the IμS DIAMOND and presenting selected results to demonstrate the impact of this new class of microfocus sealed tube X-ray sources on the data quality for applications, such as protein crystallography or absolute structure determination.

P018

Macromolecular Neutron Diffraction at the FRM II Neutron Source

A. Ostermann[1], T. E. Schrader[2], M. Monkenbusch[3], B. Laatsch[4], P. Jüttner[1], W. Petry[1], D. Richter[3]
[1]Technische Universität München, Heinz Maier-Leibnitz Zentrum (MLZ) , Garching bei München, Germany
[2]Forschungszentrum Jülich GmbH, Jülich Centre for Neutron Science JCNS , Garching bei München, Germany
[3]Forschungszentrum Jülich GmbH, Institute for Complex Systems ICS, Jülich, Germany
[4]Forschungszentrum Jülich GmbH, Engineering and Technology (ZEA-1), Jülich, Germany

Neutron single crystal diffraction provides an experimental method for the direct location of hydrogen and deuterium atoms in biological macromolecules, thus providing important complementary information to that gained by X-ray crystallography. At the FRM II neutron source in Garching near Munich the neutron single crystal diffractometer BIODIFF, a joint project of the Forschungszentrum Jülich and the FRM II, is dedicated to structure determination of proteins. Typical scientific questions address the determination of protonation states of amino acid side chains, the orientation of individual water molecules and the characterization of the hydrogen bonding network between the protein active centre and an inhibitor or substrate. This knowledge is often crucial towards understanding the specific function and behaviour of an enzyme. BIODIFF is designed as a monochromatic diffractometer and is able to operate in the wavelength range of 2.4 Å to about 5.6 Å. This allows to adapt the wavelength to the size of the unit cell of the sample crystal. Data collection at cryogenic temperatures is possible, allowing studies of cryo-trapped enzymatic intermediates. Some recent examples will be presented to illustrate the potential of neutron macromolecular crystallography.

P019
MX Data collection strategies at EMBL-Hamburg beamlines P13 & P14

S. Panneerselvam[1], G. Bourenkov[1], G. Pompidor[1], J. Hakanpää[1], I. Bento[1], I. Karpics[1], T. Schneider[1]
[1]European Molecular Biology Laboratory Hamburg, Hamburg, Germany

EMBL-Hamburg is operating two beamlines for macromolecular crystallography at PETRA III (DESY, Hamburg). Both beamlines are fully tunable and provide various possibilities for data collection from serial crystallography to extremely long wavelength phasing. High flux X-ray beams with adjustable dimensions between 5 and 200 µm are available in the energy range between 4.0 and 17.5 keV on P13 and between 6 and 30 keV on P14. Both beamlines are equipped with fast sample changers with high capacity dewars to enable high through-put data collection. A large variety of data collection strategies are available:

Long wavelength data collection, e.g. for S-SAD phasing, using 4.5 keV X-rays and a helium-cone on P13.
High-resolution data collection using short wavelength and a theta-offset of the detector at P13.

Optimized data collection for large (>20 µm) crystals using a CRL-collimated X-ray beam with a "top-hat" profile at P14.
Serial crystallography data collection under cryogenic conditions and at room temperature at P14.

Pump-probe experiments on P14.

Screening and *in situ* data collection in CrystalDirect^{TM} plates at P14.

Please check the following link for more details about beamlines and for beam time proposal procedures.

http://www.embl-hamburg.de/services/mx/index.html

P020
Size and stability analysis in nano-scaled systems

B. Arlt[1]
[1]Anton Paar Germany GmbH, Nanostrukturanalyse, Ostfildern, Germany

Nanoparticles are key applications of the current research and development. Emulsions, colloids, suspensions, dispersions and protein solutions can be found among others in the chemical and pharmaceutical industries. We will focus on protein-like nanoparticles.

Particle size, shape and stability of these systems are important parameters for the application, the process, transport and storage.

As a first remark, we are going to present, how small angle X-ray scattering (SAXS) can be used for the determination of protein characteristics, such as size, folding properties and structures. Additionally, the molar mass can be extracted from SAXS data.

Secondly, we introduce the latest technology of light scattering (LS) devices. LS is a modern tool for determining particle size, stability, transparency and molar mass of nano-scaled systems. Advantages are non-invasive, simple and quick measurements. Agglomeration behavior, mono- and polydispersity are measured; as well as temperature, pH and concentration dependencies.

The latest technology from Anton Paar combines 6 measuring principles in one instrument. A special focus was set on the analysis of biological samples.

Bio-Crystallography VI: Protein – nucleic acid complexes

P024

A conserved structural element in the RNA helicase UPF1 regulates its catalytic activity in an isoform-specific manner

M. Gowravaram[1], F. Bonneau[2], V. Maciej[1], F. Fiorini[3], J. Kanaan[3], S. Raj[4], V. Croquette[4], H. Hir[3], S. Chakrabarti[1]
[1]Freie Universität Berlin, Institut für Chemie und Biochemie , Berlin, Germany
[2]Max Planck Institute of Biochemistry, Structural Cell Biology, Martinsried, Germany
[3]IBENS, Département de Biologie, Paris, France
[4]PSL Research University, Département de physique de l'ENS, Paris, France

The RNA helicase UPF1 is a key component of the nonsense mediated mRNA decay (NMD) pathway. Previous X-ray crystal structures of UPF1 elucidated the molecular mechanisms of its catalytic activity and regulation. In this study, we examine features of the UPF1 core and identify a structural element that adopts different conformations in the various nucleotide- and RNA-bound states of UPF1. We demonstrate, using biochemical and single molecule assays, that this structural element modulates UPF1 catalytic activity and thereby refer to it as the regulatory loop. Interestingly, there are two alternatively spliced isoforms of UPF1 in mammals, which differ only in the lengths of their regulatory loops. The loop in isoform 1 (UPF11) is 11 residues longer than that of isoform 2. We find that this small insertion in UPF11 leads to a two-fold increase in its translocation and ATPase activities. To determine the mechanistic basis of this differential catalytic activity, we have determined the X-ray crystal structure of the helicase core of UPF11 in its apo-state. Our results point towards a novel mechanism of regulation of RNA helicases, wherein alternative splicing leads to subtle structural rearrangements within the protein that are critical to modulate enzyme movements and catalytic activity.

Measurements and syntheses under extreme conditions

P026

High pressure lattice dynamics of aragonite and $CaCO_3$ –VII up to 45 GPa

L. Bayarjargal[1], C. J. Fruhner[1], N. Schrodt[1,2], B. Winkler[1,2]
[1]Goethe-Universität Frankfurt am Main, Abt. Kristallographie, Frankfurt am Main, Germany
[2]HuK Umweltlabor, Wenden-Hünsborn, Germany

Due to their scientific and economic importance, $CaCO_3$ phases have extensively been studied. Specifically, the phase stabilities of $CaCO_3$ polymorphs at high pressures and temperatures have been a focal point of numerous studies, as this knowledge is a prerequisite for understanding the carbon cycle in the deep Earth and the presence of carbonates in diamond inclusions.

At ambient temperature, aragonite has been suggested to be stable up to 50 GPa from X-ray diffraction, Raman and infrared spectroscopy experiments [1-3]. Litasov et al. [4] demonstrated that aragonite is the stabile phase up to 29 GPa and up to 1600 K. Liu et al. [5] observed that $CaCO_3$-VI was stable between 16 GPa and 53 GPa. The crystal structures of two new phases ($CaCO_3$-VII and aragonite-II) were predicted by Gavryushkin et al. [6] using density functional theory and were confirmed using X-Ray diffraction. Both phases coexisted after laser heating at 35 and 50 GPa. Up to now, no further studies of aragonite-II and $CaCO_3$–VII have been reported.

The aim of this study was the exploration of phase stabilities of aragonite and $CaCO_3$–VII at high pressures and temperatures using Raman spectroscopy. KCl was used as a thermal insulator in laser heated diamond anvil cells. Ne or Ar was employed as a pressure transmitting medium. Theoretical Raman intensities were calculated with DFT-based model calculations and were in excellent agreement with experimental observations. The frequencies of most modes in $CaCO_3$-VII increased linearly with pressure, while the frequencies of the out-of-plane bending mode and of a low frequency lattice mode decreased with pressure. In contrast to $CaCO_3$–VII the pressure-induced shifts of some of Raman modes of aragonite show a quadratic dependence on pressure. Similar to $CaCO_3$-VII, two soft modes have been found in aragonite. A more detailed description of the lattice dynamics and the stabilities derived from the Raman data will be presented at the conference.

The authors gratefully acknowledge financial support by the DFG (FOR 2125 "CarboPaT", BA4020/2-1 and RA2585/1-1)

References

[1] S. E. Palaich, et al., Am. Mineral. **101**, 1651 (2016)
[2] J. Santillan and Q. Williams, Am. Mineral. **89**, 1348 (2004)
[3] P. Gillet, et al., Phys. Chem. Miner. **20**, 1 (1993)
[4] K. D. Litasov et al., Phys. Earth Planet. Inter. **265**, 82 (2017)
[5] J. Liu et al., Am. Mineral. **101**, 2723 (2016)
[6] P.N. Gavryushkin et al., Cryst. Growth Des. (2017)

P027

High pressure physical properties of lead stannate, Pb_2SnO_4

W. Morgenroth[1], D. Zimmer[1], D. Spahr[1], M. Stekiel[1], L. Bayarjargal[1], B. Winkler[1]
[1]Goethe-Universität Frankfurt am Main, Frankfurt am Main, Germany

Rare earth element doped stannates, M_2SnO_4:X with M = Ca, Sr, Ba, have been studied extensively, as they are employed in numerous technological applications, e.g. as long afterglow phosphors (e.g. [1]). In contrast, their structure-property relations have not been investigated extensively. As a representative for this family of compounds we chose lead stannate (Pb_2SnO_4, [2]), which shows interesting electronic properties. It has a stereochemically active lone electron pair localized on the lead atom.

We will present results on X-ray diffraction and electrical resistance measurements as a function of pressure. Preliminary results of resistance measurements based on the 2-point probe method are shown in Fig. 1. Further experiments using the 4-point probe method are in progress. The set-up is shown in Fig. 2. The electrical resistance of Pb_2SnO_4 changes by more than seven orders of magnitude when the pressure is raised to 15 GPa, indicating an insulator-semiconductor transition (Fig. 1). The closing of the band gap with increasing pressure is accompanied by a change of color, where the Pb_2SnO_4 sample, which is colourless at ambient pressure, becomes dark brown (Fig. 2).

Funding by the BMBF (05K16RFB) and DFG (Wi1232, RA2585/1-1) is gratefully acknowledged.

References

[1] Stanulis et al., Opt. Mater., 36:1146-1152, 2014.
[2] Gavarri et al., J. Solid State Chem., 36:81-90, 1981.

Figure 1. Logarithm of the electrical resistance as a function of pressure for Pb_2SnO_4.
Figure 2. 4-point probe set-up for measurement of the electrical resistance of Pb_2SnO_4 in a diamond anvil cell at 1.8(1) GPa with a transparent sample (left) and at 11.2(6) GPa (right) where the sample is now dark brown.

Figure 1

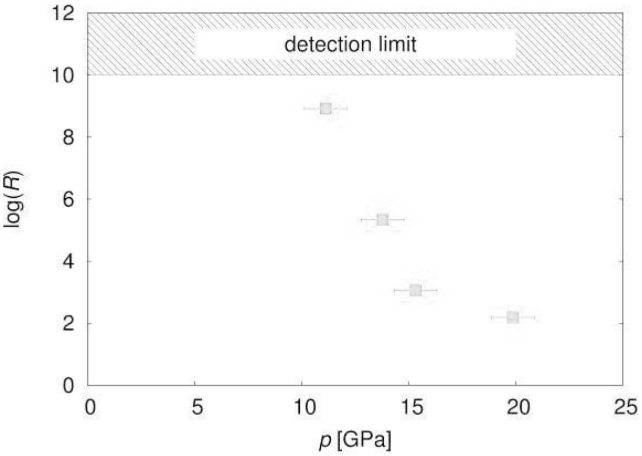

Figure 2

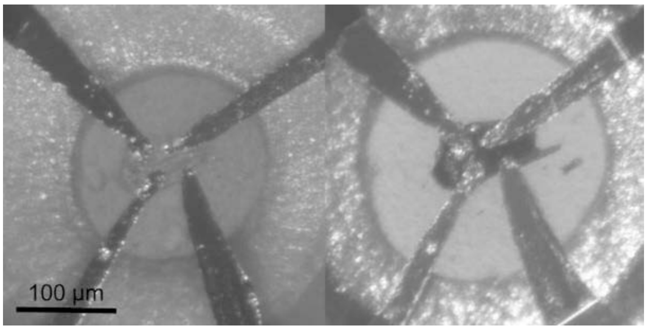

P028

Femtosecond diffraction of solid flame reactions at HED at European XFEL

W. Morgenroth[1], L. Bayarjargal[1], B. Winkler[1], D. Varentsov[2], K. Appel[3], U. Zastrau[3]
[1]Goethe-Universität Frankfurt am Main, Frankfurt am Main, Germany
[2]GSI Helmholtzzentrum für Schwerionenforschung GmbH, Darmstadt, Germany
[3]European XFEL, Schenefeld, Germany

Self-propagating high-temperature synthesis (SHS) allows the synthesis of a very large variety of compounds and new materials in an energy-efficient way [1]. They have therefore been extensively studied. SHS reaction fronts propagate with 1 – 150 mm/s, reach temperatures up to 4 500 K and the heating rates vary between 1 000 and 100 000 K/s. Many SHS reactions have been well characterized with respect to the underlying equilibrium thermodynamics. In contrast, the characterization of the transient processes before, in, and after the reaction fronts have not been characterized yet due to the extreme reaction rates, temperatures and heating rates.

The European XFEL in Schenefeld will be operated at a repetition rate of 10 Hz. The number of electron bunches per pulse can be as high as 2700. The pulse length will vary between a few and 100 fs and bunches are separated by 220 ns. The number of photons per pulse is in the order of 1012. Due to these beam characteristics, diffraction experiments with approx. 25 keV photon energy and femtosecond time resolution will become possible.

Our goal is to contribute to the infrastructure for time resolved diffraction experiments in the femtosecond region including an appropriately fast radiometric pyrometry at the High Energy Density Science (HED) instrument [2]. The SHS experiments will be carried out in a small chamber located in the interaction area 2. For the temperature determination, a fast pyrometer built by the HED group of GSI has been adopted [3] and examples of temperature determination will be presented. First experiments during commissioning of the instrument will include the formation of silicides [4], and will focus on structural changes before, in, and after the reaction front.

The authors gratefully acknowledge financial support by BMBF (project 05K16RFB).

References

[1] Merzhanov, A. and Averson, A. The present state of the thermal ignition theory: An invited review. Combustion and Flame, Elsevier, 1971, 16, 89-124
[2] https://www.xfel.eu/facility/instruments/hed/index_eng.html
[3] Ni, P. et al. Pyrometric system for temperature measurements of HED matter generated by intense heavy ion beams. Journal de Physique IV (Proceedings), EDP Sciences, 2006, 133, 977-980
[4] Bernert, T. Dissertation, Goethe-Universität Frankfurt, 2014

P029

First evidence of a displacive transformation in $MgSO_4 \cdot H_2O$ under high pressures

M. Ende[1], J. Meusburger[1], D. Talla[1], R. Miletich[1], M. Wildner[1]
[1]Universität Wien, Institut für Mineralogie und Kristallographie, Wien, Austria

Although the terrestrial occurrence of the low-hydrated magnesium sulphate kieserite ($MgSO_4 \cdot H_2O$) is mostly restricted to marine evaporates, this phase has been discovered on Mars [1] and seems to play a role in the sulphur cycle and for surface processes on Mars and other extra-terrestrial environments [2]. At ambient conditions, the lattice parameters of kieserite are larger than expected from both the respective ionic radii and the octahedral Mg–O bond lengths [3]. On the other hand, data for low-temperature or high-pressure conditions have not been reported yet. The objective of this study was to investigate synthetic kieserite single crystals by means of in-situ high-pressure X-ray diffraction at 298 K using an ETH-type diamond-anvil cell. Single crystal samples were studied on a STOE-StadiVari diffractometer system with a Dectris Pilatus 300K pixel detector for the standard single-crystal and the in-situ high-pressure single-crystal X-ray diffraction studies in a hydrostatic pressure regime between 0.2 and 4.1 ± 0.1 GPa. The measurements were performed using a sample-detector distance of 60 mm and a 50 W (at 1000 µA) molybdenum air-cooled Incoatec IµS micro-focus (110 µm FWHM) source with high-brilliance 2D-focussing Quazar multilayer mirrors.

The preliminary crystal-structure investigations at high-pressure conditions using one sample crystal per DAC revealed that kieserite undergoes a compression-induced change of symmetry from monoclinic to triclinic, associated with a structural phase transition somewhere between 2 and 4 GPa. The space group changes directly from *C*2/*c* (No. 15) into *P*-1 (No. 2). Both, the SO_4 tetrahedra and the MgO_6 octahedra, reveal tilting at higher pressure, and the previously symmetrically hydrogen bonded H_2O molecule forms a shorter (stronger) and a longer (weaker) hydrogen bond in the high-pressure polymorph (Fig. 1).

Fig. 1: Corresponding sections of the crystal structures of monoclinic and triclinic $MgSO_4 \cdot H_2O$.

References

[1] Arvidson, R.E., Poulet, F., Bibring, J.P., Wolff, M., Gendrin, A., Morris, R.V., Freeman, J.J., Langevin, Y., Mangold, N., Bellucci, G. (2005): Science, 307, 1591-1594.
[2] Wang, A., Freeman, J.J., Jolliff, B.L. (2009): J. Geophys. Res., 114, E04010.
[3] Bechtold, A., Wildner, M. (2016): Eur. J. Mineral., 28, 43-52.

Figure 1

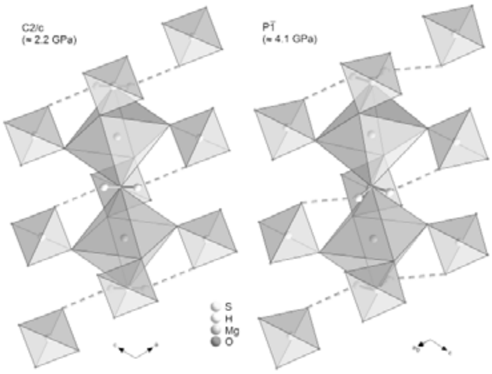

P030

Hydrogen bonding in natrochalcite under hydrostatic pressure

M. Ende[1], G. Giester[1], R. Miletich[1]
[1]Universität Wien, Institut für Mineralogie und Kristallographie, Wien, Austria

Natrochalcite and its isotypic compounds exhibit hydrogen-bond lengths that are among hydrogen-bearing minerals the shortest bond lengths reported so far [1]. However, data for low-temperature or pressure-dependent hydrogen bonds have not yet been reported. Although, this can give rise to the formation of an even shorter single-well no-barrier hydrogen bond (NBHB) known for example from $K_3H(SO_4)_2$ below 100 K [2].

O-H···O bonds are normally very strong when involving two identical molecules or chemical groups. The strengthening of these bonds is associated with a parallel lowering of the proton transfer barrier. Therefore, short bonds of this type are also known as low-barrier H-bonds (LBHB) [3]. One symmetrical bond of this type can be found in natrochalcite ($NaCu_2(SO_4)_2(OH)\cdot 2H_2O$) [4, 5]. Single-crystal samples were used on a STOE-StadiVari diffractometer system with a Dectris Pilatus 300K pixel detector. The in-situ high-pressure X-ray diffraction studies were taken with an ETH-type diamond anvil cell in a hydrostatic pressure regime between 0.2 and 10 GPa. The intensity data collections were performed with a 50 W molybdenum air-cooled Incoatec IμS micro-focus source.

The experimental study revealed that there is neither any evidence of a structural transformation nor an apparent change of space-group symmetry *C*2/*m* within the investigated pressure range. Therefore, the NBHB of natrochalcite between O4 and O4 shrinks linearly with pressure (Fig. 1). At ambient conditions the dynamically disordered hydrogen positions are shifted each only about 0.13(2) Å [3] from the corresponding centred position. The measured $O_{acceptor}$-O_{donor} bond distance at 10 GPa of around 2.372(9) Å is shorter compared to $K_3H(SO_4)_2$ below 100 K and the formation of a NBHB is quite likely. Furthermore, with loosing 0.171(15) Å in length the hydrogen bond between O4 and O2 at 10 GPa can be classified as LBHB as well.

Fig. 1: Pressure-dependent hydrogen O-O distances found in natrochalcite. Grey bars with dashed lines represent typically maximal O_{donor}-$O_{acceptor}$ distances for LBHB and NBHB after [3].

References
[1] Krickl, R., Wildner, M. (2007) Eur. J. Mineral., 19, 805-816.
[2] Perrin, C. L., Nielson, J. B. (1997) Annu. Rev. Phys. Chem., 48, 511-544.
[3] Garret, R. H., Grisham, C. M. (2012) Brooks/Cole, Cengage Learning, 1169p.
[4] Giester, G., Zemann, J. (1987) Z. Kristallogr., 179, 431-442.
[5] Chevrier, G., Giester, G., Zemann, J. (1993) Z. Kristallogr., 206, 7-14.

Figure 1

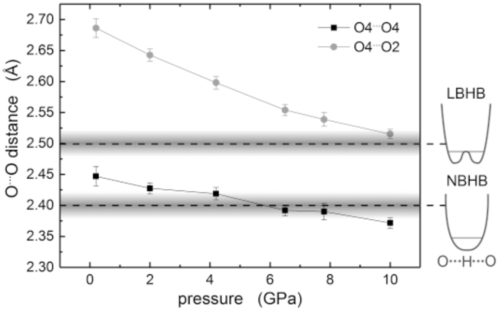

P031

Synthesis of Co-Cl- and Ni-Cl boracite crystals in hydrothermal solutions

T. Setkova[1], V. Balitsky[1], T. Bublikova[1], D. Khanin[1]
[1]Institute of Experimental Mineralogy RAS, Chernogolovka, Russian Federation

Boracites are large crystal family with more than 20 isomorphous compounds have unique ferroelectric and magnetic properties [1]. The general formula is M3B7O13X, where M=Mg, Cr, Mn, Fe, Co, Cu, Ni, Zn or Cd, and X= Cl, Br, I or F. In nature boracites formed by dehydration of the original magnesium borates. In laboratory conditions, the crystals of Co-Cl and Ni-Cl boracites were synthesized at temperatures of 600-1000 ° C in the gas phase in N2 atmosphere [2].

In this work, the crystals of Co-Cl- and Ni-Cl boracite were obtained in hydrothermal conditions. The experiments were conducted in an autoclave made of titanium alloy (B8) at a temperature of 400-450 ° C and a pressure of 60-100 MPa using crystallohydrate of cobalt and nickel chloride solutions in presence of boric acid. The crystals of Co-Cl- boracite (up to 3 mm in size, space group R3c, a = 8.5418(3), c = 20.9517(8) Å) are characterized by a bright crimson color of varying intensity and have a cubic (pseudocubic) habitus, with mostly developed facets of the tetrahedron, cube and rhombic dodecahedron (Fig.1a). Smaller crystals of Ni-Cl (up to 0.02 mm in size) are formed in the octahedron habitus (Fig.1b).

Fig.1. SEM images of Co-Cl (a) and Ni-Cl (b) boracite crystals.

References
[1]. V. A. Shuvaeva, K. A. Lysenko, and M. Yu. Antipin. Crystallog. Rep. **2011**, 56, 6, 1004–1006.
[2]. D. Li, Z.J. Xu, Z.H. Wang et al. Alloys and Comp. **2003**, 351, 235–240.

Figure 1

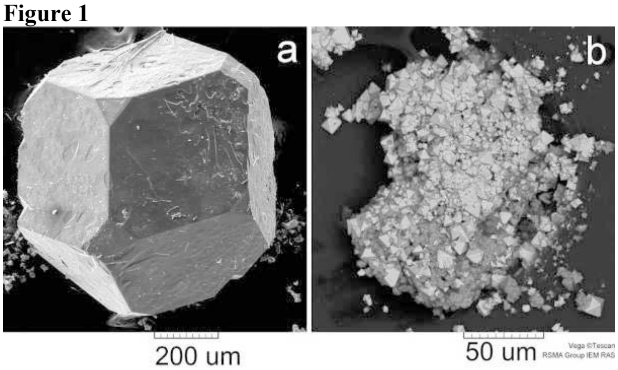

P032

High-pressure behaviour of $SrSO_4$

D. Spahr[1], M. Stekiel[1], L. Bayarjargal[1], W. Morgenroth[1], V. Milman[2], N. Schrodt[1], B. Winkler[1]
[1]Goethe-Universität Frankfurt am Main, Institut für Geowissenschaften, Frankfurt am Main, Germany
[2]Dassault Systèmes Biovia, Cambridge, United Kingdom

The high-pressure behaviour of $SrSO_4$ has not been unambiguously determined so far. Based on Raman and X-ray diffraction data using a methanol-ethanol mixture, Chen et al. [1, 2] concluded that a first phase transition occurs at 10-12 GPa, and a second at ~25 GPa. Later, it was shown that the transition pressure in sulfates strongly depends on the pressure medium [3]. For the isostructural $BaSO_4$ an experiment using helium gave a transition at ~27 GPa [3], in contrast to a value of 6 GPa obtained by Chen et al. [2]. Isostructural compounds should show a similar sequence of phase transitions, which should appear at lower pressures in the higher homologue [4].

Synthetic $SrSO_4$ (Johnson Matthey, 99.7% purity) was used in our studies. High-pressure experiments were carried out using diamond anvil cells in Boehler-Almax design [5] and neon as pressure medium. Pressure-dependent Raman spectra were acquired up to 30 GPa and X-ray powder diffraction data up to 60 GPa on beamline P02.2 at PETRA III. The pressure dependence of the lattice parameters was obtained using Le Bail refinements [6]. Experimental Raman and diffraction data were complemented by calculations based on density functional theory (DFT) using the CASTEP package [7].

The experimentally determined Raman spectra are in good agreement with earlier study (e.g. [8]) and our DFT calculations (Fig. 1). The compression behaviour is shown in Fig. 2. Our experiments do not reveal any phase transition. The bulk modulus was obtained from the experimental data using the program EOSFit7 [9] and is B = 69(4) GPa.

Acknowledgements
Funding by DFG (WI1232/44, WI1232/41, RA2585/1), DFG-Research Unit FOR2125, BMBF (05K16RFB) and Adolf Messer Stiftung is gratefully acknowledged.

References
[1] Y. H. Chen et al., *Physica B Condens Matter*, **405**:4386, 2010.
[2] Y. H. Chen et al., *Solid State Commun.*, **149**:2050, 2009.
[3] D. Santamaría-Pérez et al., *Phys. Rev. B*, **84**:054102, 2011.
[4] A. Neuhaus, *Chimia,* **18**:93, 1964.
[5] R. Boehler, *Rev. Sci. Instrum.*, **77**: 115103, 2006.
[6] A. Le Bail et al., *Mat. Res. Bull.*, **23**:447, 1988.
[7] S. J. Clark et al., *Z. Kristallogr.*, **220**:567, 2005.
[8] T. Kloprogge et al., *Mineral. J.*, **5**:334, 2001.
[9] J. Gonzalez-Platas et al., *J. Appl. Crystallogr.*, **49**:1377, 2016.

Fig. 1: Raman spectra at from 0 GPa to 31(2) GPa.
Fig. 2: Pressure-dependent behaviour of the lattice parameters.

Figure 1

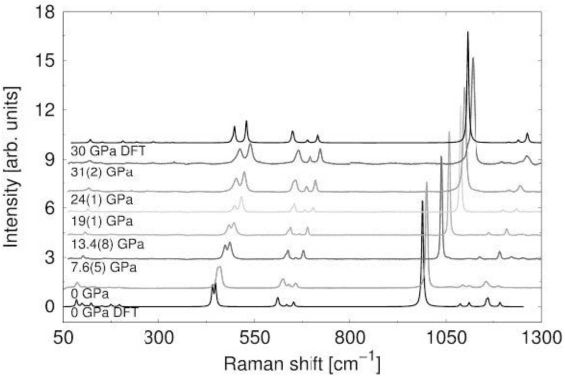

Figure 2

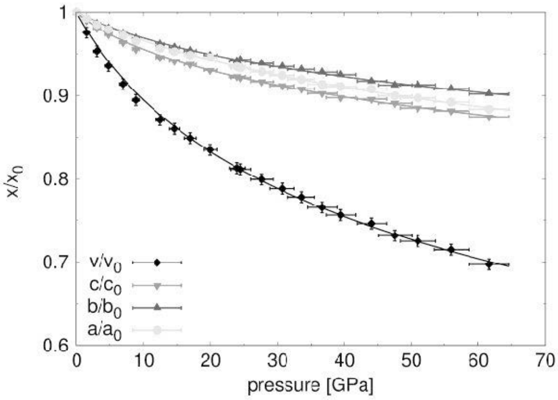

P033

High-pressure–high-temperature synthesis, hardness and magnetic properties of the metastable ferromagnet ε-Fe_2MnN

W. P. Clark[1], K. Guo[2], D. Rau[1], U. Burkhardt[2], M. Bobnar[2], R. Castillo[2], L. Akselrud[2], R. Niewa[1], U. Schwarz[2]
[1]Universität Stuttgart, Institut für Anorganische Chemie , Stuttgart, Germany
[2]Max-Planck-Institut für Physik fester Stoffe, Dresden, Germany

Investigations into iron substitutions of ε-$Fe_3N_{1\pm x}$ have seen limited success,[1] due in part to the metastability of the products. In recent years,[2, 3] the ternary nitrides Fe_2CoN, Fe_2NiN and $Fe_2IrN_{0.24}$ have been synthesized using a high-pressure-high-temperature technique. This technique has now been used to produce ε-Fe_2MnN, by reacting ζ-Fe_2N and Mn at 15(2) GPa and 1573(200) K in a Walker-type multi-anvil device.

Powder X-ray diffraction investigations showed that the product has lattice parameters very similar to ε-$Fe_3N_{1.08}$. EDXS confirms the presence and homogeneous distribution of both Fe and Mn in the sample, with an atomic metal ratio of Fe : Mn = 2.06(1) : 0.94(1). Analysis of various samples suggests there is a significant homogeneity range for ε-Fe_2MnN.

Thermal investigations at ambient pressure showed that the ε-Fe_2MnN phase is metastable. Upon heating to roughly 800 K an exothermic signal, coupled with a decrease in mass, was observed. This transition is suspected to correlate with the formation of a γ'-nitride phase, which has been previously observed in ε-Fe_2NiN.[4] Further heating results in the exothermal decomposition of this γ'-nitride to a fcc (Fe, Mn):N phase, which was characterized with X-ray powder diffraction.

Hardness measurements were conducted, giving an average value of 636 ± 21 HV (6.2(2) GPa). This value is slightly lower than that found for ε-$Fe_3N_{1\pm x}$ (7.4(10) GPa),[4] but still in the typical range of nitrided steels. SQUID measurements revealed a magnetic phase transition from ferromagnetism to paramagnetism above 400 K. Both the magnetic moment and Curie-temperature are lower than those of ε-$Fe_3N_{1\pm x}$.

References
[1] (a) Gajbhiye, N. S.; Ningthoujam, R. S.; Bhattacharyya, S. *Hyperfine Interact*. **2005**, *164*, 17. (b) Gajbhiye, N. S.; Bhattacharyya, S. *Mater. Chem. Phys*. **2008**, *108*, 201. (c) Gajbhiye, N. S.; Bhattacharyya, S.; Sharma, S. *PRAMANA − J. Phys*. **2008**, *70*, 367. (e) Mishra, P. P.; Raja, M. M.; Panda, R. N. Mater. Res. Bull. **2016**, *75*, 127.
[2] Guo, K.; Rau, D.; Toffoletti, L.; Müller, C.; Burkhardt, U.; Schnelle, W.; Niewa, R.; Schwarz, U. *Chem. Mater*. **2012**, 24, 4600.
[3] Guo, K.; Rau, D.; Schnelle, W.; Burkhardt, U.; Niewa, R.; Schwarz, U. *Z. Anorg. Allg. Chem*. **2014**, *640*, 814.
[4] Niewa, R.; Rau, D.; Wosylus, A.; Meier, K.; Hanfland, M.; Wessel, M.; Dronskowski, R.; Dzivenko, D. A.; Riedel, R.; Schwarz, U. *Chem. Mater*. **2009**, *21*, 392.

New crystal structures

P035

Organic-Inorganic Hybrid Materials from Divalent Metal Cations and Expanded N,N'-Donor Linkers

M. Zahedi[1], U. Englert[2]
[1]University of Tabriz, , Tabriz, Iran
[2]RWTH Aachen, Aachen, Germany

Coordination polymers continue to attract enormous interest not only because of their intriguing variety of architectures and topologies but also for applications in the fields like magnetism, luminescence and catalysis [1-3]. The topology of a coordination polymer depends on various factors such as the versatile coordination geometries of the metal nodes, the enormous variability of the organic linkers, counter ion, and solvent [4]. It may be affected by weak non-covalent supramolecular interactions, for example by hydrogen bonding or π–π interactions.

In this contribution, The rod-shaped linker N,N'-(3,3'-dimethyl-4,4'-biphenyldiyl)bis[1-(3-pyridinyl)methanimine] (L)(scheme 1) is exploited for the first time in the synthesis of extended structures. Four new coordination polymers $\{[\mathrm{ZnL(OAc)_2}]\cdot\mathrm{EtOH}\}_n$ **(1)**,$\{[\mathrm{CdL(OAc)_2}]\cdot\mathrm{MeOH}\}_n$ **(2)**, $\{[\mathrm{Cu_2L(OAc)_4}]\cdot\mathrm{CH_2Cl_2}\}_n$ **(3)** and $[\mathrm{MnL(N_3)_2}]_n$ **(4)** have been structurally characterized and the effect of metal cations and the anionic ancillary ligands as pivotal roles on the topology of these compounds have been investigated. In the crystalline reaction products of Zn(II), Cd(II) and Cu(II) acetate with the organic linker, the acetate anions connect two neighbouring cations to dinuclear $[\mathrm{M_2(OAc)_4}]$ subunits. These SBU are further crosslinked by the N,N'-donor ligand leading to the 1-D ladder-like or simple chain structures **1**, **2** and **3**. A different topology has been seen in **4**: end to end bridging mode of the $\mathrm{N_3^-}$ groups lead to infinite chains. These are crosslinked by L in perpendicular direction, and the layer structure is obtained. Natural bond orbital (NBO) analyses revealed information on the basis of orbital interactions about the coordination environments of the metal ions. Thermogravimetric measurements indicate the highest thermal stability for **2**. Strong antiferromagnetic coupling within the dinuclear subunits of **3** is observed as a consequence of superexchange *via* the acetato bridges.

Reference

[1] P. Bhowmik, S. Biswas and et al., *Dalton Trans*, 43 (2014) 12414-12421.
[2] Y.-Y. Liu, R. Decadt and et al., *J. Phys. Chem*., 117 (2013) 11302-11310.
[3] D. Bansal, S. Pandey, G. Hundal, R. Gupta, *New J. Chem*, 39 (2015) 9772-9781.
[4] J. Yang, G.D. Li, J.J. Cao, Q. Yue, G.H. Li, J.S. Chen, *Chem. Eur. J.*, 13 (2007) 3248-3261.
[5] H.R. Khavasi, B.M.M. Sadegh, *Dalton Trans,* 44 (2015) 5488-5502.

Figure 1

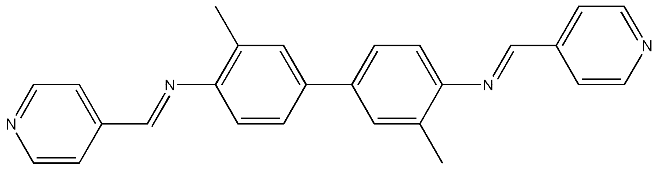

P037

pinB-SiMe$_2$Ph: A Versatile Reagent with Diverse Structures

C. Kleeberg[1]
[1]Technische Universität Braunschweig, Institut für Anorganische und Analytische Chemie , Braunschweig, Germany

Question

The silylborane pinB-SiMe$_2$Ph (**1**, pin: pinacolato (OC(Me)$_2$C(Me)$_2$O)) was first reported by *Ito* and coworkers in 1996 and became a widely used reagent in various silylation and silylboration reactions developed by *Oestreich*, *Suginome*, *Ito* and many others since a convenient synthetic protocol was reported by *Ito* and *Suginome* in 2000.[1,2] For the synthesis of **1** several protocols have been described employing either the reaction of a silyldiaminoborane with pinacol or, more convenient, the reaction of a boric acid ester with the respective silyl lithium derivative, but **1** is also commercially available.[1,3] In all reports **1** was reported to be a colourless liquid with a boiling point of 82–99 °C at 0.13 mbar, however, no melting point was reported.[1,3a]

Methods

In course of our investigation on copper catalysed silylation reactions employing the silylborane **1**, we found that **1** is in pure form a crystalline solid at ambient temperature. However, crystallisation of **1** does only occur below room temperature. Following this observation we investigated the solid state structures and the thermal behaviour of **1** in greater detail, employing single crystal X-ray diffraction and DSC methods.

Results & Conclusions

In conclusion, two ambient condition polymorphs of the silylborane **1** were identified and their crystal structures were determined in detailed, temperature dependent, X-ray diffraction studies. Polymorph *A* crystalizes in a space group *P*–1 with four molecules in the asymmetric unit (Z = 8, Z" = 4) and polymorph *B* in a space group *Fdd*2 with three molecules in the asymmetric unit (Z = 48, Z" = 3). However, while both polymorphs are stable at room temperature, crystallisation was only observed at lower temperatures.

Figure: Structural formula and views of the asymmetric unit of the polymorphs A (left) and B (right) of **1**.

References

[1] (a) M. Suginome, H. Nakamura, Y. Ito, *Chem. Commun.* **1996**, 2777–2778. (b) M. Suginome, T. Matsuda, Y. Ito, *Organometallics* **2000**, *19*, 4647–4649.
[2] For recent reviews, see: (a) T. Ohmura, M. Suginome, *Bull. Chem. Soc. Jpn.* **2009**, *82,* 29–49. (b) M. Oestreich, E. Hartmann, M. Mewald, *Chem. Rev.* **2013**, *113*, 402–441.
[3] (a) Sigma-Aldrich, Product Number: 683434, 9.10.2017. (b) ABCR, Product Number: AB440348, 9.10.2017.

Figure 1

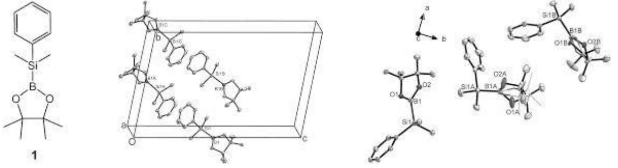

P038

$K_7[Fe^{II/III}S_2]_4$ - a new 'reduced' sulfido-ferrate with a commensurate superstructure

P. Stüble[1], K. Köhler[1], M. Schwarz[1], C. Röhr[1]
[1]Albert-Ludwigs-Universität Freiburg, Institut für Anorganische und Analytische Chemie, Freiburg i. Br., Germany

The new sulfido ferrate $K_7[FeS_2]_4$ (*Aba*2, $a = 5252.19(11)$, $b = 1364.03(3)$, $c = 2487.41(8)$ pm, $Z = 36$, $R1 = 0.07$) containing buckled and linear SiS_2-analogous anionic chains expands the series of 'reduced' alkali chalcogenido ferrates [1,2]. In the system K-Fe-S, it completes the set of chain ferrates by adding the compound with the lowest Fe^{III} ratio and therefore the largest average bond lenth $d_{Fe\text{-}S}$:

chain ferrate	lit.	Fe^{II} [%]	Fe^{III} [%]	$d_{Fe\text{-}S}$ [pm]
$K[FeS]_2$	[3]	0	100	223.8
$K_7[FeS_2]_5$	[4]	40	60	228.8
$K_3[FeS_2]$	[5]	50	50	231.3
$K_7[FeS_2]_4$		**75**	**25**	**234.2**

$K_7[FeS_2]_4$ was obtained by reacting pyrite with a slight excess of potassium in corundum crucibles under an argon atmosphere ($T_{max} = 800$°C, $K:FeS_2 \approx 19:10$). Even though its existence and composition was assumed correctly in a previous work [6], the actual crystal structure remained unclear. However, a convincing structure model was finally obtained from single crystal X-ray diffraction data: An orthorhombic *C*-centered lattice with commensurate superstructure requiring a nine-folding of the *c* axis of the subcell was observed. As a side effect of the enlarged axis, overlapping of strong subcell reflections with neighbouring superstructure reflections occured due to the crystals mosaicity (*cf. Fig. 1*), resulting in the falsification of intensities of (partly extinct) satellite reflections and leading to comparatively high *R*-values. Nevertheless, the structure of $K_7[FeS_2]_4$ is self-consistent and fits in nicely with related compounds.

The chains $^1_\infty[Fe^{II/III}S_2]^{1.75-}$ running along the *c* axis form a hexagonal rod packing. Nearly linear chains can be found at $x = 1/4$ and 3/4, whereas buckled chains are located at $x = 0$ and 1/2 (*cf. Fig. 2*). As discussed recently [2], the chains' distinct geometry is essentially a result of the overall composition and the local K^+ coordination, varying strongly in case of the buckled chains. Consequently, the latter exhibit a high variation of bond lengths and angles with remarkable maxima and minima, but common averaged values (*cf. Fig. 2*).

Figure 1

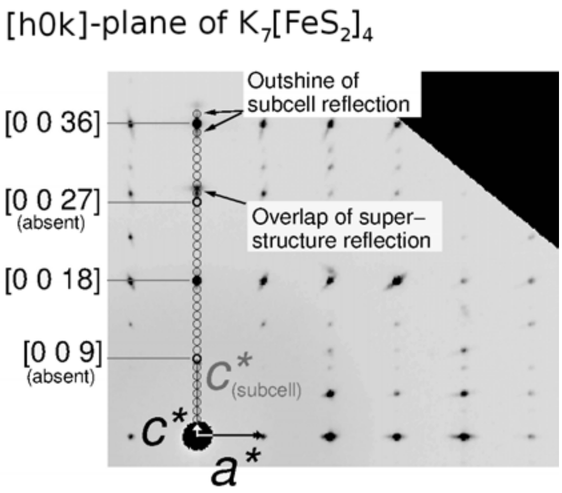

Figure 2

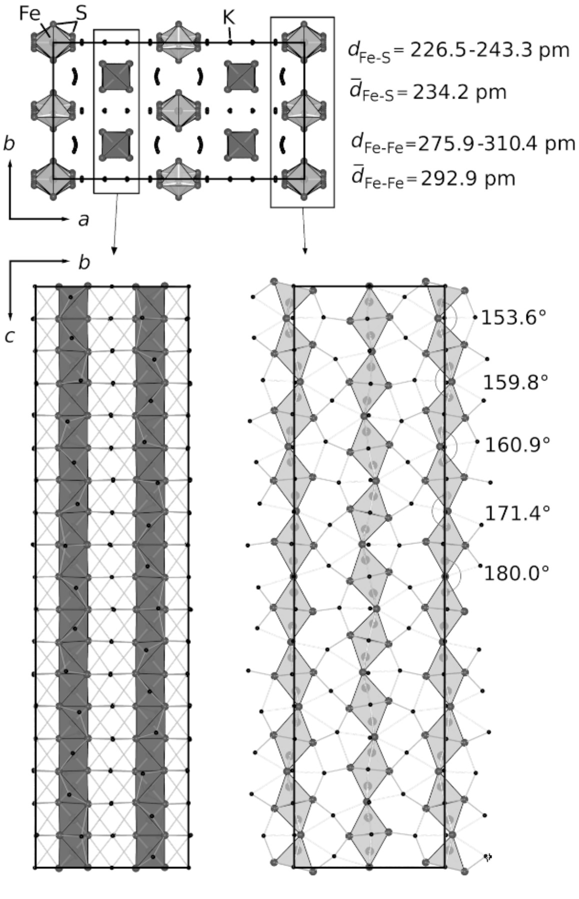

References

[1] P. Stüble, S. Peschke, D. Johrendt, C. Röhr. *J. Solid State Chem.* **in press.**
[2] P. Stüble, C. Röhr, *Z. Anorg. Allg. Chem.* **643**, 1462-1473 (2017).
[3] J. W. Boon, C. H. Mac Gillavry. *Rec. Trav. Pays-Bas*. **61**, 910-920 (1942).
[4] M. Schwarz, M. Haas, C. Röhr. *Z. Anorg. Allg. Chem.* **639**, 360-374 (2013).
[5] W. Bronger, U. Ruschewitz, P. Müller. *J. Alloys Compd.* **218**, 22-27 (1986).
[6] M. Schwarz, Dissertation, Universität Freiburg (2015).

P039

New Hg-rich mercurides in the systems K-Hg-In and Rb-Hg-In

M. Wendorff[1], C. Röhr[1]
[1]Albert-Ludwigs-Universität Freiburg, Institut für Anorganische und Analytische Chemie, Freiburg i. Br., Germany

Binary and somewhat electron-richer ternary (+*M*: Ga, In, Sn) Ba mercurides Ba(Hg/M)$_x$ exhibit a rich crystal chemistry, especially for x=4-7 [1-5]. Due to the isotypism of $BaHg_6$/KHg_6 [5,6], Ba_7Hg_{32}/K_7Hg_{32} [7,8] and $BaHg_{11}$/KHg_{11} [9] we extend our synthetic, crystallographic and bond-theoretical investigations to the respective alkali compounds. Studies of the x=4 and x=6 sections of the title systems reveal two structure typs with no analogs among binary border phases nor among ternary Ba compounds. KHg_3In crystallizes in a new structure type (*Cmcm*, a=943.6(2), b=902.6(1), c=632.9(1) pm, R1=0.0486), in which KM_{18} polyhedra (Fig. 1: yellow) and trigonal prisms (green) tile the space. The structure is crystallographically related (Fig 1, left) to the common $BaAl_4$-type. The pyramid layers (running perpendicular a) are undulated along b, which results - besides the Hg(2)-Hg(2) tip bonding - in additional bonds between the pyramid's bases. In KHg_3In_3 and $RbHg_{3.5}In_{2.5}$ ($SrAu_3In_3$-type [10], *Pmmn*, a=489.5(2)/495.9(1), b=803.5(4)/808.7(2), c=9.610(4)/961.3(2) pm, R1=0.0661/0.0333). RbM_{20} polyhedra and distorted empty M_8 cubes fill the space (Fig. 2). Therewith, the structures are closely related to binary and ternary $A^{II}M_{6/7/8}$ mercurides. In addition, the Hg->In substitution (e.g. the electronic stability range) of Rb_3Hg_{20} [8] and the $BaHg_{11}$-type phases [9] has been elucidated. The electronic structures of all compounds show a strong Hg/In *p* bonding inside the polyanion (Fig. 2 right), in which Hg carries the negative *Bader* charge.

References

[1] M. Wendorff, C. Röhr, Z. Naturforsch. 67b, 893 (2012).
[2] M. Wendorff, C. Röhr, Z. Naturforsch. 68b, 307 (2013).
[3] M. Wendorff, M. Schwarz, C. Röhr, J. Solid State Chem. 203, 297 (2013).
[4] M. Wendorff, C. Röhr, Z. Naturforsch. 69b, 388 (2014).
[5] M. Wendorff, C. Röhr, J. Alloys Compds 546, 320 (2013).
[6] F. Tamborino, C. Hoch, J. Alloys Compds 618, 299 (2015).
[7] M. Wendorff, C. Röhr, Acta Cryst. A 72, s311 (2016).
[8] E. Todorov, S. C. Sevov, J. Solid State Chem 149, 419 (2000).
[9] E. Biehl, H. J. Deiseroth, Z. Anorg. Allg. Chem. 625, 1073 (1999).
[10] I. R. Muts, F. M. Schappacher, W. Hermes, V. I. Zaremba, R. Pöttgen, J. Solid State Chem. 180, 2202 (2007).

Fig. 1: Crystal structure of KHg_3In and it's group-subgroup relation to the $BaAl_4$-type structure (left)
Fig. 2: Crystal structure of $RbHg_{3.5}In_{2.5}$ (left) and calculated t/p-DOS of KHg_3In_3 (right).

Figure 1

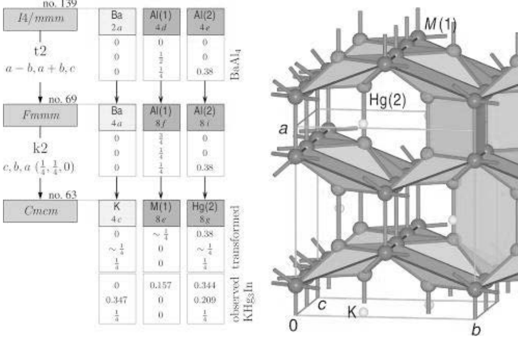

Figure 2

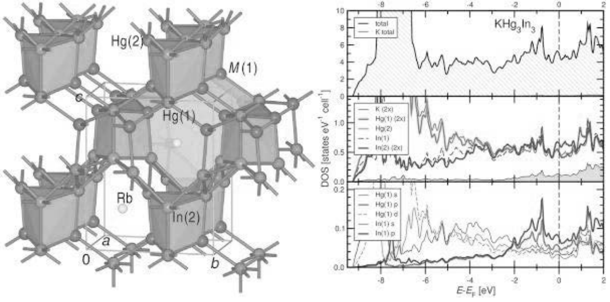

P040

Synthesis and crystal structure of new alkali-chalcogenido-manganates A_6MnQ_4.

M. Langenmaier[1], C. Röhr[1]
[1]Albert-Ludwigs-Universität Freiburg, Institut für Anorganische und Analytische Chemie, Freiburg i. Br., Germany

Until now alkali-rich chalcogenido-metallates A_6MQ_4 [1-5] (M=Mn/Fe/Co/Zn; Q=S/Se/Te) are only known for the lighter alkali elements sodium and potassium. These ortho salts with isolated $[TMQ_4]^{6-}$ tetrahedra crystallize in the Na_6ZnO_4-type structure [5].

The new compounds Rb_6MnS_4, Rb_6MnSe_4, Rb_6MnTe_4, Cs_6MnS_4, Cs_6MnSe_4 and Cs_6MnTe_4 were obtained during the systematic studies on the crystal chemistry of chalcogenido manganates [6]. The crystals differed vastly in shape and colour, from platelike to xenomorph and from yellow to darkred and were obtained by heating stoichiometric mixtures of the elements or binary phases at T_{max}= 1100 K.

All compounds are isotypic and crystallize in the hexagonal spacegroup $P6_3mc$, with lattice parameters from a=1021.9(7) and c=796.2(5) pm (Rb_6MnS_4) to a=1173.3(7) and c=906.3(5) pm (Cs_6MnTe_4). The crystal structure, which was determined by means of X-ray single crystal diffraction, contains two A, one Mn and two Q sites. The Q atoms [Q(1), 2b, 3m; Q(2), 6c, m; red spheres in fig. 1 and 2] form a hexagonal close-packing with slightly undulated hexagonal layers due to Q(1) being slightly out of the plane.The Mn(II) ions (2b, 3m) are located in nearly ideal Q-tetrahedra (grey polyhedra in fig. 1) and occupy 1/8 of the vacancies. These isolated tetrahedra are the key characteristic of the structure and are uniformly oriented along [001]. The A(1) ions (6c, m) take 3/8 of tetrahedral intersticies (green polyhedra in fig. 2) and share three common edges with the aforementioned [MnQ_4] tetrahedra. The second type of A^+ ions (A(2) 6c, m) are octahedrally coordinated (golden polyhedra in fig. 2) by six Q^{2-} anions. These octahedra share common edges with themselves as well as common faces with both kinds of tetrahedra. Both the [AQ_4] tetrahedra and the [AQ_6] octahedra are considerably more distorted than the [MnQ_4] tetrahedra. The remaining 1/4 of octahedra voids remain empty and are connected via common faces, thus forming chanals along the c axis.

References

[1] K. Klepp, W. Bronger, *Rev. Chim. Miner.*, **20**, 682 (1983).
[2] K. Klepp, W. Bronger, *Z. Naturforsch.* **38b**, 12 (1983).
[3] W. Bronger, H. Balk-Hardtdegen, *Z. Anorg. Allg. Chem.*, **574**, 89 (1989).
[4] W. Bronger, H. Balk-Hardtdegen, U. Ruschewitz, *Z. Anorg. Allg. Chem.*, **616**, 14 (1992).
[5] P. Kastner, R. Hoppe, *Z. Anorg. Allg., Chem.*, **409**, 69 (1974).
[6] M. Langenmaier, C. Röhr, *Z. Kristallogr. Suppl.*, **37**, 113 (2017)

Figure 1

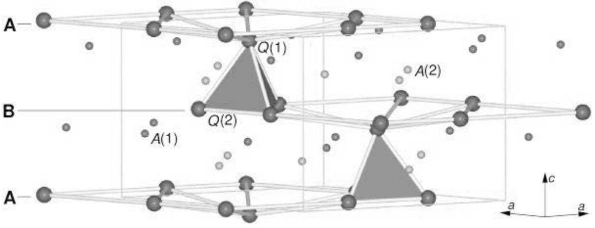

Figure 2

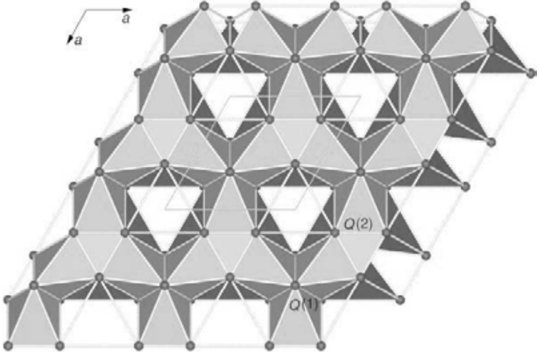

P041

Paving the way to new Organic-Inorganic Hybrid Perovskites containing derivatives of Azobispyridine

S. Schmitz[1], C. Wallerius[1], A. Klein[1]
[1]Universität zu Köln, Institut für Anorganische Chemie, Köln, Germany

Reactions of derivatives of Azobis(*n*-pyridine) (azpy) in the presence of HX (X = Cl, I) with divers di- and trivalent transition metal salts were carried out to obtain perovskite-like structures such as $(azpyH_2)M(II)I_3$ or $(azpyH_2)M(III)I_4$ by crystallization from corresponding mixtures. Besides the new 1-D pseudo-perovskite structures (4,4'azpy)$^{1}\infty$[CuI4] and (2,2'azpy)$^{1}\infty$[CuI2] a variety of different structures was obtained including polyiodide-containing Structures such as $(4,4'azpyH)_2{}^{1}\infty[Cu_2(I_4)(I_8)]$ and $(4,4'azpyH_2)_2[BiI_6]I_3$, but also the non-metal containing pentaiodide $(2,2'azpyH_2)I_5$ and the hydrochloride and -iodide $(azpyH_2)Cl_2$ and $(azpyH_2)I_2$. In comparison, these and further already reported or non-satisfactorily solved crystal structures give an interesting impression on possible stable structures as pitfalls along the way to new organic-inorganic hybrid perovskites.

P042

Functional coordination polymers

A. Kochel[1]
[1]University of Wroclaw, Faculty of Chemistry, Wroclaw, Poland

Coordination polymers raise interest as potential ionoselective absorbents or catalytic, porous materials, also for non-linear optics [1]. Coordination polymers also have many interesting properties, which the chemist can fan explore. All these reasons are playing a big role within the subject of crystal engineering. In particular coordination polymers can playing an important role in the accumulation of gases such as H_2, O_2, CO, NO, CH_4. In my research, which I am going to present hew the complex compounds of chosen transition metals are received as well as the use of solvothermal method. This method is used to receive the compounds of magnetic materials. It is generally one-stage method and makes possible to obtain the complexes with high purity in crystalline state. All reactions were synthetized by using Berghoff"s pressurized reactors. The solvothermal method allows to obtain a very good repeatability of synthesis and stable conditions of a reaction. Organic ligands are most common used in synthesis. Reactions are usually conducted at temperature from 100°C to 300°C. Temperature selection of the reaction depends on a number of factors. The most important are ligand"s melting temperature and temperature level above which the ligand is decomposed. It is possible several types of complexes from the same reactants, with proper selection of reactants, that is closely related to temperature at which the synthesis is conducted. Construction of pressure apparatus allows to conduct the reaction under an inert gas atmosphere, thus change in oxidation number of metal during the reaction is prevented. An additional advantage of reactor usage is a possibility of slow cooling of reaction mixture, which allows a slow growth of crystals. The crystals are characterized by very high quality and purity, which causes them to be suitable for X-ray diffraction measuring.

All polymers were characterized by X-ray diffraction studies, IR spectra, elemental analysis, TGA, magnetic properties measurements and analysis of the electron density. The new coordination polymers with a new aminocarboxylates as a ligand will be presented.

[1] (a) M. Lahav, I. Weissbuch, Chem. Rev., 111 (2011) 3236, (b) M. Gingras, Che. Soc. Rev., 42 (2013) 1051, (c) Y. Liu, W.M. Xuan, Y. Cui, Adv. Mater., 22 (2010) 4112, (d) C.B. Aakeröy, N.R. Champness, C. Janiak, CrystEngComm, 12 (2010) 22, (e) C. Janiak, J.K. Vieth, New J. Chem., 34 (2010) 2366.

P043

Simple and Superstructure Ternary Indium Variants of K_2Ga_3

M. Falk[1], C. Röhr[1]
[1]Albert-Ludwigs-Universität Freiburg, Institut für Anorganische und Analytische Chemie, Freiburg i. Br., Germany

Alkali gallides and indides show a fascinating structure diversity, reaching from simple intermetallics to complex cluster compounds [1]. There are three known binary compounds crystallising in the Cs_2In_3-type structure (tetragonal, *I*4/*mmm*): Cs_2In_3 [2], Rb_2In_3 [3] and K_2Ga_3 [4]. Two ternary variants, $K_2Ga_{2.32}In_{0.68}$ [5] and K_2InGa_2 [6] were reported, the latter crystallising in a superstructure derivative. In systematic experimental, crystallographic and bond theoretical studies, the "coloring" of the polyanions in the Cs_2In_3-type structure has been examined, i. e. the influence of the different size and electronegativity of Ga and In. In the investigations, a substitution up to 87 % of Ga by In was observed as well as the appearance of the superstructure in several compounds (27–44 % In).

K_2M_3 contains two K and two *M* positions. Four *M*(1) and two *M*(2) atoms form distorted M_6 octahedra, which are connected via *M*(1)-*M*(1) exo-bonds to form layers perpendicular [001]. The superstructure can be described in the space group $P4_2/ncm$ with a split up *M*(1) position, leading to slightly tilted octahedra. The structures are related by two k2 group-subgroup relations, the transformed *a* axis is the diagonal of the unit cell base of the aristotype. In all compounds, In occupies the octahedra tips [*M*(2)] preferably. This position has a larger negative Bader charge, but also a much larger volume than *M*(1). The "coloring" of the polyanion is therefore not determined by electronegativity (Ga: 1.82, In: 1.49), but by geometrical factors (covalent radii: Ga: 126 pm, In: 144 pm).

Fig. 2 shows the deviation of Vegard's law for the series of compounds. This can be explained by the fact that In occupies the octahedra tips [*M*(2)] first, which mainly increases the *c* axis. Further In occupation of the base positions expands the octahedra plane and thus increases *a*, but the inter-layer distance and therewith *c* shrinks unexpectedly. Similar trends also apply to all ternary Rb and Cs analogues [7].

References

[1] M. Falk, C. Meyer, C. Röhr, *Z. Anorg. Allg. Chem.* (in press).

[2] S. P. Yatsenko, K. A. Tschuntonow, A. N. Orlow, Y. P. Yarmolyuk, Y. N. Grin, *J. Less-Common Met.* **108**, 339 (1985).
[3] C. S. Sevov, J. D. Corbett, *Z. Anorg. Allg. Chem.* **619**, 128 (1993).
[4] R. W. Henning, J. D. Corbett, *Inorg. Chem.* **38**, 3883 (1999).
[5] V. Müller, PhD thesis, TH Darmstadt (1995).
[6] P. Hofmann , PhD thesis, ETH Zürich (1997).
[7] M. Falk, C. Röhr, *Z. Kristallogr. Suppl.* **36**, 81 (2016)

Figure 1

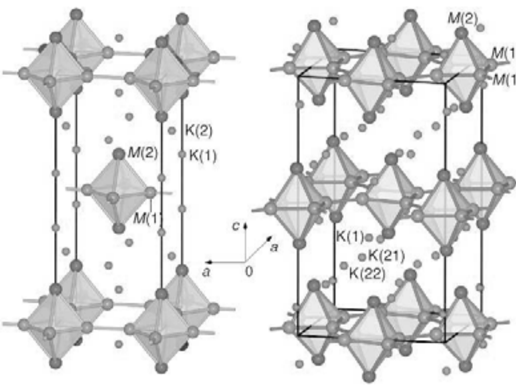

Figure 2

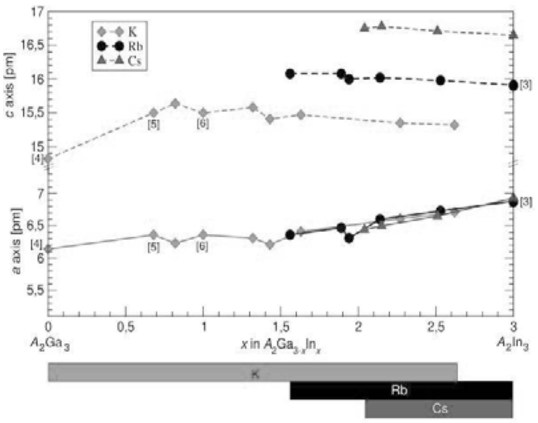

P044

The role of magnesium in zinc-rich ternary phases of the system Ca-Mg-Zn:

Systematic experimental, crystallographic and bond theoretical studies

K. Köhler[1], C. Röhr[1]
[1]Albert-Ludwigs-Universität Freiburg, Institut für Anorganische und Analytische Chemie, Freiburg i. Br., Germany

Mg-based alloys, known as lightweight materials, show some interesting properties. Amongst others, biodegradable implants are of interest [1]. Some regions of the Ca-Mg-Zn phase diagram have been investigated to find appropriate alloys, but only a few ternary compounds are reported just by powder data yet [2]. These phases could now be reproduced and structurally characterized for the first time. Their crystal chemistry is closely related to a series of *Ln*-Mg/Zn compounds e.g. [3] and also to recently investigated complex hexagonal and cubic mixed Sr-Zn/Cd phases [4]; Sr takes the role of Mg, compared to binary and ternary Mg-Zn/Cd phases. In the above-named type of compounds, Mg can either take the role of the alkaline-earth elements or of Zn. Two new ternary phases were obtained (starting from elements, weighed under argon atmosphere in tantalum-tubes, T_{max}=900°C).

$CaMgZn_5$ (*Pnma*, a=867.48(3), b=530.37(5), c=1104.45(9) pm) (structure shown in fig. 1) is an ordered variant of the orthorhombic $CeCu_6$-type structure, where Mg occupies the same position as In, Sn, Ag or Au in the numerous ternary compounds $LnXCu_5$ of this type e.g. [5]. Mg is part of a three-dimensional covalent bonded network, but carries, however, an even more positive Bader charge than Ca.

The ordered phase $CaMgZn_{10}$ ($I4_1/amd$, a=1082.66(6), c=688.95(5) pm) (structure shown in fig. 2) crystallizes as a ternary derivative of the tetragonal $BaCd_{11}$-type structure, which is formed by the binary border phase $CaZn_{11}$ as well. The appearance of this ordered phase is explained by the fact that the Cd position, occupied by Mg in the ternary phase, differs considerably in a crystal-chemically view from the remaining Cd sites. Eye-catching features of the $CaMgZn_{10}$ structure are the channels along the c direction, built up by a highly condensed Zn tetrahedral network. The Ca and Mg atoms alternating occupy the centre of these channels. This behaviour can also be observed in other ternary phases such as $KNaCd_{10}$ [6].

References

[1] B. Zberg, P. J. Uggowitzer, J. F. Löffler, *Nat. Mater.* **8**, 887 (2009).
[2] Y. Zhang, D. Kevorkov, F. Bridier, M. Medraj, *Sci. Technol. Adv. Mater*. **12**, 025003 (2011).
[3] K. Sugiyama, K.Yasuda, T. Ohsuna, K. Hiraga, *Z. Kristallogr.* **213**, 537 (1998).
[4] M. Schwarz, M. Wendorff, C. Röhr, *Z. Kristallogr.* **232**, 515 (2017).
[5] V. Zaremba, V. Hlukhyy, J. Stępień-Damm, R. Troć, *J. Alloys Compd.* **321**, 97 (2001).
[6] V. Mihajlov, C. Röhr, *Z. Anorg. Allg. Chem.* **636,** 1792 (2010).

Figure 1

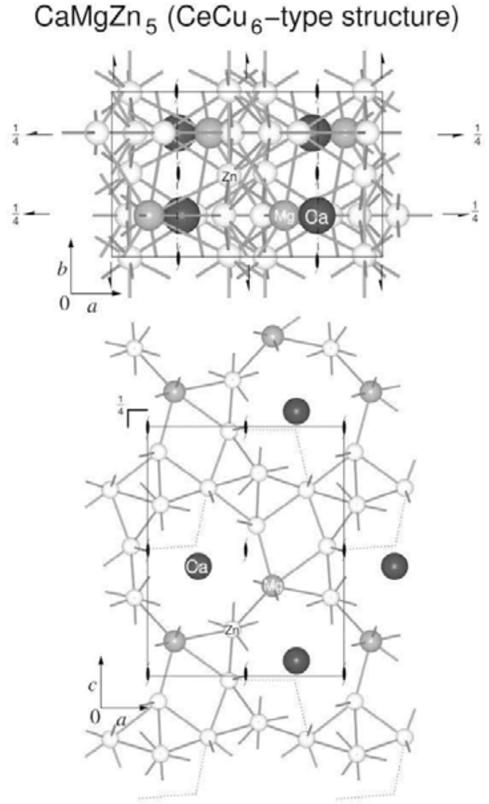

Figure 2

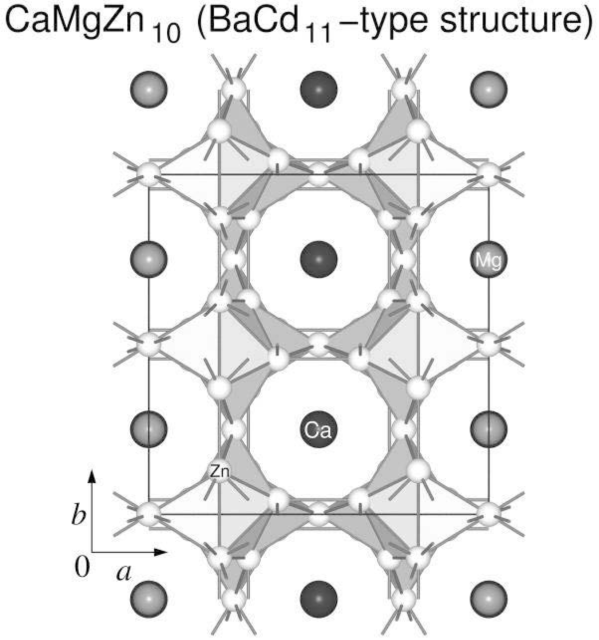

P045

Intermediate compounds in Ca*REE*$_x$Al$_{2-x}$O$_4$ (0 ? x ? 2)

C. Otgonbayar[1], H. Pöllmann[1]
[1]Martin-Luther-Universität Halle Wittenberg, Institut für Geowissenschaften, Halle (Saale), Germany

Luminescent materials based on Ca*REE*AlO$_4$ (*REE* = Rare Earth Elements) as host lattice are gaining more interest due to their smooth emission spectra and long lasting phosphorescence. Yb-doped CaGdAlO$_4$ is well known for its continuous emission spectrum (from 990 to 1080 nm) and a relatively high thermal conductivity.

The abstract reports on the results concerning the sol-gel preparation of intermediate compounds Ca*REE*AlO$_4$ (R = Yb, Y, Dy, Eu, Sm, Nd, La). The synthesised compounds are studied by powder X-ray diffraction analysis, IR, TG, REM, calorimetry and fluorescence spectrometry.

The following intermediate compounds could be synthesised in pure by Pechini method (Table 1).It employs complexing of cations using citric acid in an aqueous-organic medium and makes use of low cost precursors resulting in a homogenous ion distribution at the molecular level. The gels were prepared using stoichiometric amounts of analytical-grade Ca(NO$_3$)$_2$·4H$_2$O, Al(NO$_3$)$_3$·9H$_2$O and R*EE*$_2$O$_3$ (*REE* = Yb, Y, Dy, Eu, Sm, Nd, La). The annealing temperature was between 1000 and 1500 °C.

Table 1: Synthesised Ca*REE*AlO$_4$and unit cell parameters, refined by Pawley method

The intermediate compound has tetragonal structure. Calcium and rare earth element atoms are statistically distributed over the sites of the C$_{4v}$ symmetry. For this phase the similar ionic radii of calcium and rare earth elements are essential.

The unit cell parameters are plotted against lanthanide ionic radius in Figure 1. As expected, the unit cell volume contracts with decreasing lanthanide ionic radius from La to Yb, and are in good agreement with the data from literature.

Table 2: Comparison of Ca*REE*AlO$_4$ unit cell parameters with lanthanide radius

The present study demonstrates the synthesis of monophasic Ca*REE*AlO$_4$ (R = Yb, Y, Dy, Eu, Sm, Nd, La)using the Pechini method. Compared to usual solid state synthesis the applied method shows advantages of lower synthesis temperatures and shorter synthesis times.

In compounds Ca*REE*AlO$_4$ (*REE* =Yb, Y, Dy, Eu, Sm, Nd, La) calcium and rare earth metals share the same atomic position.The unitcell volumesas well as lattice constants decrease with decreasing ionic size of rare earth elements.

References

[1] Ricaud, Jaffres et al., Opt. Lett. **36**, 4134 - 4135 (2011)
[2] Oudalov et al., *Bull. Soc. Chim. Fr.*, 3408, (1970)
[3] Pajaczkowska, A., *J. Phys.Chem. Solids*, **52**, 1043, (1991)
[4] Lehmann, U., *Z. Anorg. Allg. Chem.*, **447**, 47, (1978)
[5] Choisnet, J., et al *Eur. J. Solid State Inorg. Chem.*, **30**, 619, (1993)

Table 1

Compounds	Unit cell parameter		
	a [Å]	c [Å]	V [Å]
CaLaAlO$_4$	3,715(1)	12,338(3)	170,29(0)
CaNdAlO$_4$	3,679(9)	12,149(2)	164,52(0)
CaSmAlO$_4$	3,670(5)	12,061(4)	162,50(6)
CaEuAlO$_4$	3,663(6)	12,025(0)	161,40(4)
CaDyAlO$_4$	3,647(7)	11,909(4)	158,47(2)
CaYAlO$_4$	3,641(0)	11,888(4)	157,60(7)
CaYbAlO$_4$	3,643(3)	11,756(2)	156,05(1)

Table 2

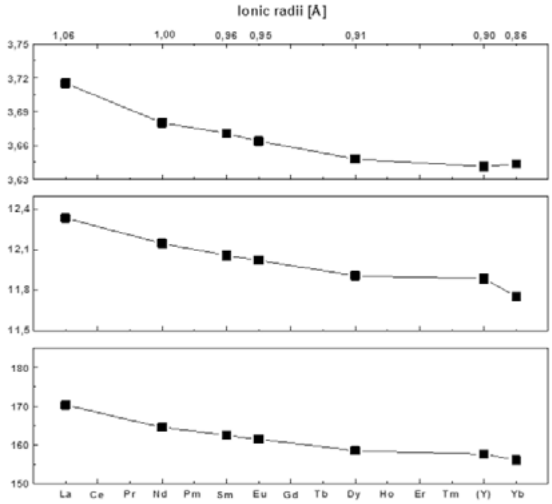

P046

Reconstruction of Individual Isomers from Disordered Average Structure

E. Peresypkina[1], A. Virovets[1], I. S. Bushmarinov[2], M. G. Medvedev [3], B. Krämer[1], M. Scheer[1]
[1]University of Regensburg, Chemie und Pharmazie, Regensburg, Germany
[2]Institute of Organoelement Compounds RAS, Moscow, Russian Federation
[3]Zelinsky Institute of Organic Chemistry RAS, Moscow, Russian Federation

Single crystal X-ray diffraction being one of the most informative methods of establishing molecular structure. If mutual displacement of structural fragments varies from one cell to another, the crystal structure shows static disorder. In the vast majority of the cases, it does not preclude revealing the structure of an individual molecule or ion. It is not always so in the structures of giant supramolecules.

Since 2003, we have been investigating the supramolecular chemistry of pentaphosphaferrocene, $[Cp^{R}Fe(\eta^5\text{-}P_5)]$ ($Cp^R = \eta^5\text{-}C_5R_5$, R = Me, CH_2Ph, PhC_4H_9). Phosphorus atoms of planar P_5-rings coordinate Cu^+ and Ag^+ cations resulting in self-assembled spherical supramolecules of 2.1 – 4.6 nm [1]. The self-assembly of the pentaphosphaferrocene $Cp^{Bn}Fe(\eta^5\text{-}P_5)$ (**1**) with Cu(OTf) ($OTf^- = CF_3SO_3^-$) leads to a supramolecule $[\{\mathbf{1}\}_{12}\{Cu(OTf)\}_{19.6}]$ with icosidodecahedral inorganic core (Fig. 1a,b) [2]. Thirty vertices of icosidodecahedron are statistically occupied by 20 Cu atoms with occupancy factors varying in the range from 0.2 to 0.9 (Fig. 1b). To interpret this complicated static disorder and to reveal the structure of individual supramolecule we modeled all theoretically possible 10,015,005 isomers and excluded all repetitions and structurally meaningless configurations. As a result, two pairs of enantiomers with point symmetries D_5 and D_2 have left (Fig. 1c,d). DFT geometry optimizations at the EDF1/SBKJC level were performed resulting in the difference in energy of only 2.5 kcal/mol. Therefore, both D_5 and D_2 isomers should be equally stable and able to co-exist in the solid state.

We thank ERC grant AdG339072-SELFPHOS for support. The research was partly done on the P11 beamline at the light source PETRA III at DESY (Hamburg).

References

[1] E. Peresypkina, C. Heindl, A. Virovets, M. Scheer (2016) *Structure and Bonding* (2016) **174**, 321
[2] C. Heindl, E.V. Peresypkina, A.V. Virovets et al (2017) *Angew. Chem. Int. Ed.* **56**, 13237

Figure 1

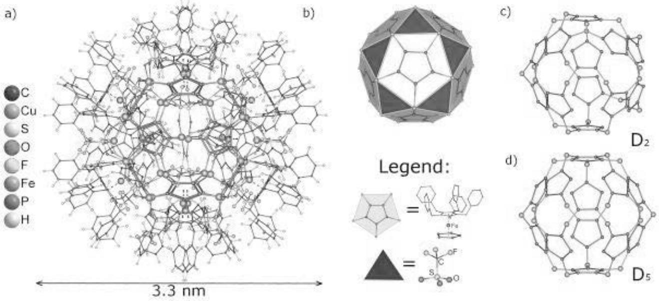

P047

Layered inorganic-organic hybrid materials: crystal engineering with sodium methanesulfonate and "simple" inorganic halides

F. Thoelen[1], W. Frank[1]
[1]Heinrich-Heine-Universität Düsseldorf, Lehrstuhl für Material- und Strukturforschung, Düsseldorf, Germany

The combination of short-chained alkanesulfonates and metal acids was shown to generate layered inorganic-organic hybrid materials[1,2]. We here present two new substances, which can be formally described as double salts of sodium methanesulfonate with sodium chloride or sodium bromide. Platelets of **1** and **2** were synthesized by mixing the corresponding hydrohalogenic acid with an aqueous solution of sodium methanesulfonate, followed by the isothermal evaporation of the solvent. The compounds are isotypic, crystallizing in the monoclinic space group type *P*2/*c*. $Na_4(CH_3SO_3)_4 \cdot NaCl \cdot H_2O$ (**1**) $a = 17.3660(7)$ Å, $b = 5.4860(1)$ Å, $c = 21.3685(9)$ Å, $\beta = 100.867(3)$ °, $Z = 4$, $R_1 = 0.0542$, $wR_2 = 0.1282$. $Na_4(CH_3SO_3)_4 \cdot NaBr \cdot H_2O$ (**2**) $a = 17.3043(7)$ Å, $b = 5.5097(1)$ Å, $c = 21.9907(9)$ Å, $\beta = 99.798(3)$ °; $Z = 4$, $R_1 = 0.0645$, $wR_2 = 0.1208$. The formulation as double salts $Na_4(CH_3SO_3)_4 \cdot NaX \cdot H_2O$ (X = Cl, Br) is justified at least to some extent. The halide ion in **1** and **2** is connected to one sodium centre only, with a Na–X distance of 2.673(4) Å (**1**) and 2.842(5) Å (**2**), respectively. These values range between the Na–X distances in the NaCl type structures and the distances in monomeric NaX, so that **1** and **2** can be described as double salts of sodium methanesulfonate with the respective sodium halides[3]. However, the description as a layer-like structure is in our feeling more suitable, *i. e.* both compounds feature a hierarchic layered structure, which reminds on the structure of anhydrous sodium methanesulfonate[4]. In both compounds tenside-like bilayered arrays are given, consisting of $\{(Na_5[CH_3SO_3]_4)^+\}_n$ cations, containing hydrophobic and hydrophilic layered regions. The hydrophobic layers, formed by the methylgroups of the methanesulfonate anions, are disrupted alternately by both halide anions and water molecules, which coordinate to single sodium cations. The alternate sequence of water molecules and halide anions results in chains of hydrogen bonds. In both compounds strong hydrogen bonds are present ((**1**) O–H···Cl type, D···A distances from 2.688(2) Å to 2.766(5) Å, (**2**) O–H···Br type, D···A distances from 2.693(8) Å to 2.754(6) Å).

References

[1] V. Verheyen. W. Frank, *Z. Kristallogr. Suppl.* **2009***, 29*, 41.
[2] F. Thoelen, W. Frank, *Z. Kristallogr. Suppl.* **2017**, *37*, 118.
[3] M. Hargittai, *Coord. Chem. Rev*, **1988**, *91*, 35-88.
[4] C. H. Wei, B. E. Hingerty, *Acta Crystallogr.* **1981**, B*37*, 1992.

Fig. 1: Packing diagram of **1**.
Fig. 2: Packing diagram of **2**.

Figure 1

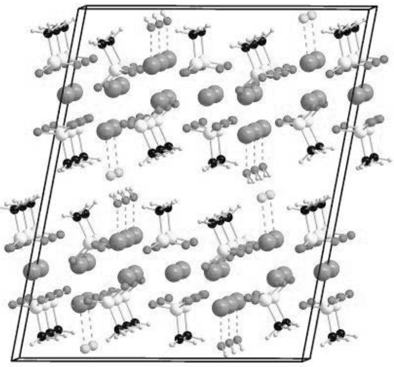

Figure 2

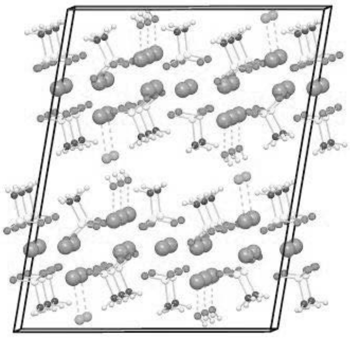

P048

Molecular Structures of a pH-Dependent, Mechanically Interlocked Switch: Organometallic [2]Rotaxane vs. Organic [3]Rotaxane

A. Pöthig[1], P. J. Altmann[1]
[1]Technische Universität München, München, Germany

The molecular structure of the first [2]rotaxane featuring a functional organometallic host was determined by single crystal X-ray diffraction and is presented.[1] The structure as well as the reactivity of the Ag8 pillarplex host is fully retained within the assembly, as is exemplified by the first transmetalation in a rotaxane framework to provide the respective Au8 analogue. The transformation under acidic conditions yields a purely organic [3]rotaxane, whose molecular structure is also presented. This reaction is fully reversible by adding an adequate base, which renders the system a pH-dependent molecular switch.

References

[1] P. J. Altmann, A. Pöthig*, *Angew. Chem., Int. Ed.*, **2017** *accepted*. DOI: 10.1002/anie.201709921

Figure 1

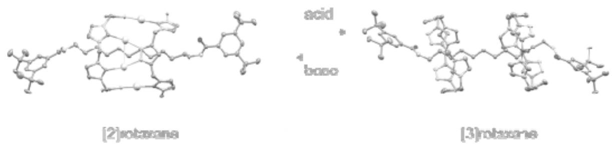

P049

Crystal structure analysis as an essential tool in the characterisation of organometallic compounds: solid state structures of two unusual bismuth-manganese compounds

C. M. Bianga[1], W. Frank[1]
[1]Heinrich-Heine-Universität Düsseldorf, Institut für Anorganische Chemie und Strukturchemie II, Düsseldorf, Germany

In previous investigations of the reaction system bismuth(II) trifluoroacetate/dimanganese decacarbonyl a few compounds composed of $[(O_2CCF_3)_2BiMn(CO)_5]$ units were obtained.[1, 2] These substances are characterised by their rare bismuth─manganese bonds. In further studies we were able to synthesise two new compounds of unusual composition by reaction of bismuth(II) trifluoroacetate and dimanganese decacarbonyl in either mesitylene or trifluoroacetic acid anhydride:

$[(1,3,5\text{-}(CH_3)_3C_6H_3)Bi_4O_2(O_2CCF_3)_9]_2[(1,3,5\text{-}(CH_3)_3C_6H_3)Mn(CO)_3]_2 \cdot 2\ \{1,3,5\text{-}(CH_3)_3C_6H_3\}$ (**1**)

and $[Bi_2Mn(O_2CCF_3)_{10}\{Mn(CO)_5\}_2]_n$ (**2**).

For the analysis of such complex compounds the crystal structure determination proves to be essential.

1 crystallises in the monoclinic space group $P2_1/n$ with the unit cell parameters $a = 14.273(3)$ Å, $b = 14.066(3)$ Å, $c = 35.520(7)$ Å, $\beta = 98.98(3)°$ and $Z = 4$. It is composed of $[Bi_4O_2(O_2CCF_3)_9]^-$ anions, cationic $[(\eta^6\text{-mesitylene})Mn(CO)_3]^+$ fragments and embedded mesitylene molecules (Figure 1). The anionic units consist of four bismuth atoms which are bridged by both, oxygen atoms and trifluoroacetato ligands (*Z,Z*-type bidentate and tridentate chelating[3]). In addition, one of the bismuth atoms is η^6-coordinated by a mesitylene molecule which completes the coordination sphere of this bismuth atom. These tetranuclear units form dimers *via* tridentate bridging trifluoroacetato ligands. In the solid state of **1** the fragments build polymolecular layers with alternating anionic and cationic sections along the *a*-axis.

2 crystallises in the triclinic space group *P*-1 with the unit cell parameters $a = 10.826(2)$ Å, $b = 11.683(2)$ Å, $c = 12.189(2)$ Å, $\alpha = 104.39(3)°$, $\beta = 95.87(3)°$, $\gamma = 110.00(3)°$ and $Z = 1$. Within the solid of **2** (Figure 2) the bismuth and manganese atoms are also bridged by both, *Z,Z*-type bidentate and tridentate chelating[3] trifluoroacetato ligands, forming a chain. The $Mn(CO)_5$ fragments are bound to the bismuth atoms *via* *Z,E*-bridging bidentate[3] trifluoroacetato ligands. The orientation of the $Mn(CO)_5$ units is alternating with respect to the backbone of the chain (viewing direction: *b*-axis).

References

[1] A. Atatrah, *Dissertation*, Heinrich-Heine-Universität Düsseldorf (Düsseldorf) **2007**.
[2] V. Verheyen, *Polymorphie und supramolekulare Assoziation von Bismut(II)-trifluoracetat*, Shaker Verlag, Herzogenrath, **2014**.
[3] A. Ouchi, Y. Suzuki, Y. Ohki, Y. Koizumi, *Coord. Chem. Rev.* **1988**, *92*, 29-43.

Figure 1

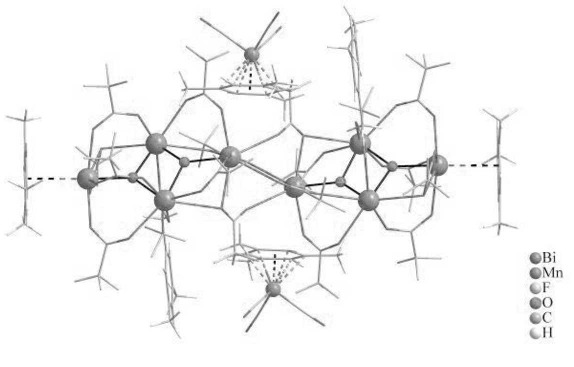

Figure 2

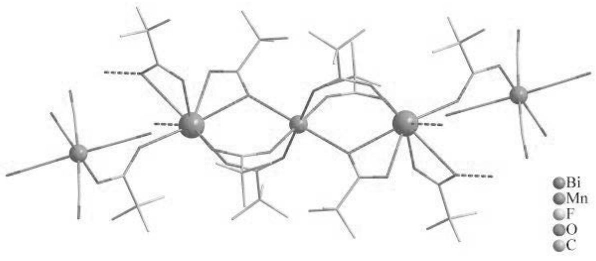

P051

Electron-poor ternary representatives of the $BaAl_4$-type structure: a combined crystallographic and bond theoretical study

C. Meyer[1], M. Kledt[1], C. Röhr[1]
[1]Albert-Ludwigs-Universität Freiburg, Institut für Anorganische und Analytische Chemie, Freiburg i. Br., Germany

The $BaAl_4$-type (fig. 1) is the most frequent structure of binary [1] and mixed ternary [2] alkaline-earth tetratrielides. The structure is formally electron precise for 14 v.e./f.u..

Geometric and electronic aspects of the stability range have already been discussed for many transition metal containing trielides [e.g. 3]. For the Ba-based binary Al, Ga and In compounds the substitution of the triel element by Zn and Cd allows the investigation of electronic aspects on the one hand and the influence of size criteria on the other hand. Changes in lattices parameters, interatomic distances and the coloring [4] of the anionic network (i.e. site preferences) are discussed for the three cases $BaZn_xAl_{4-x}$, $BaCd_xAl_{4-x}$ and $BaCd_xGa_{4-x}$.

In order to understand the distribution of the transition metals and triels on the two different *M* sites (fig. 1), DFT bandstructure calculations, including a Bader analysis, were performed. Computed Bader charges allow the interpretation of the coloring, calculated densities of states (DOS) make a discussion of the electron deficiencies reasonable.

Starting from $BaAl_4$ two electronpoor single crystals $BaZn_xAl_{4-x}$ (x=0-1.5, 14-12.5 v.e./f.u.) could be obtained.
The slightly smaller but more electronegative Zn shows a clear preference to occupy the apical position M_a (fig. 2). The Al substituiton by Cd could only be realized to a very small extent (x=0-0.6, 14-13.4 v.e./f.u.). In these ternary compounds lattice parameters and interatomic distances are enlarged. Cd containing $BaAl_4$-type compounds show a different coloring scheme: the larger Cd prefers to take the basal position M_b. In structures of the general composition $BaCd_xGa_{4-x}$ (x=0-2, 14-12 v.e/f.u.) [5] all lattice parameters increase, the larger and less electronegative Cd shows a clear preference to occupy the basal M_b position, which is again consistent with the calculated Bader charges.

References

[1] U. Häussermann, S. Amerioun, L. Eriksson, C.-S. Lee, G.J. Miller, *J. Am. Chem. Soc.* **124**, 4371-4383 (2002).
[2] M. Falk, C. Meyer, M. Kledt, *Acta Crystallogr.* **A 72 Suppl.** s253-s254 (2016).
[3] M. Wendorff, C. Röhr, *Z. Naturforsch.* **69b**, 388-408 (2014).
[4] G. J. Miller, *Eur. J. Inorg. Chem.* **5**, 523-536 (1998).
[5] T. Friedrich, PhD thesis, TH Darmstadt (1993).

Figure 1

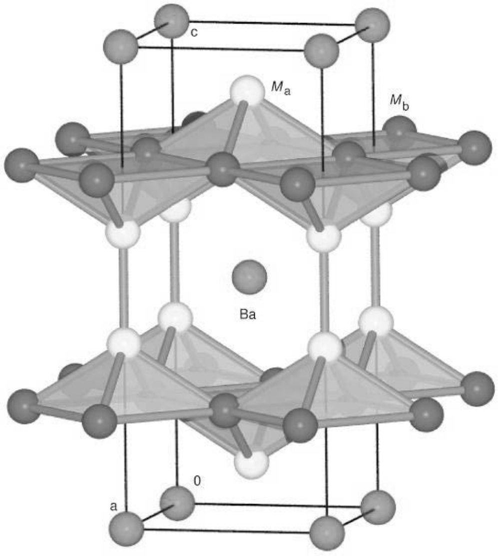

Figure 2

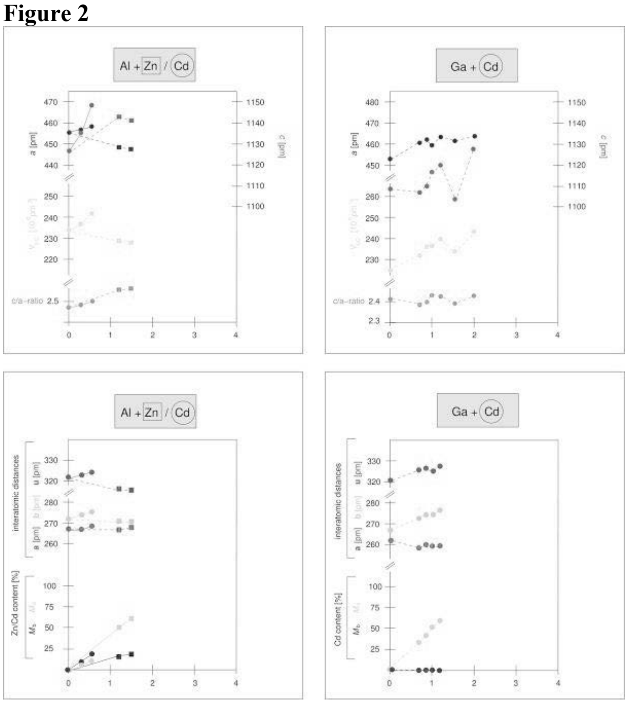

P052

$Sr_4RECl_3[SeO_3]_4$ (*RE* = Y and Yb): New Strontium Rare-Earth Metal(III) Chloride Oxoselenates(IV) with Layer Structures

S. Greiner[1], T. Schleid[1]
[1]Universität Stuttgart, Institut für Anorganische Chemie, Stuttgart, Germany

The strontium rare-earth metal(III) chloride oxoselenates(IV) $Sr_4RECl_3[SeO_3]_4$ with *RE* = Y and Yb are the first representatives for this type of composition. These compounds crystallize in the monoclinic space group *P*2/*c* with the lattice parameters $a = 886.79(5)$ pm, $b = 549.36(3)$ pm, $c = 1715.68(9)$ pm, $\beta = 91.261(3)°$ for *RE* = Y and $a = 887.98(5)$ pm, $b = 548.65(3)$ pm, $c = 1711.46(9)$ pm, $\beta = 91.247(3)°$ for *RE* = Yb and Z = 2. Their crystal structure exhibits one distinct RE^{3+} cation with an eightfold coordination of oxygen atoms in a $[REO_8]^{13-}$ square prism, while two different Sr^{2+}-cation positions occur. $(Sr1)^{2+}$ is surrounded by four oxygen atoms, which belong to four terminal $[SeO_3]^{2-}$ groups, and four Cl^- anions resulting in a $[(Sr1)Cl_4O_4]^{10-}$ square antiprism. In contrast, $(Sr2)^{2+}$ shows a coordination sphere of eight oxygen atoms from both monodentate and bidentate $[SeO_3]^{2-}$ anions in a $[(Sr2)O_8]^{14-}$ square prism. The $[REO_8]^{13-}$ and $[(Sr2)O_8]^{14-}$ polyhedra are connected via common edges to form 2D-$\{[RE(Sr2)O_{12}]\}^{19-}$ layers running parallel to the (100) plane. These layers experience interconnection by the $[(Sr1)Cl_4O_4]^{10-}$ polyhedra via common O···O edges erecting the three-dimensional network of the new $Sr_4RECl_3[SeO_3]_4$ series. Each $[(Sr1)Cl_4O_4]^{10-}$ antiprism connects via common Cl2···Cl2 edges and Cl1 vertices with other $[(Sr1)Cl_4O_4]^{10-}$ units to arrange as corrugated double layers parallel to the 2D-$\{[RE(Sr2)O_{12}]\}^{19-}$ sheets. The Se^{4+} cations are not only responsible for the charge balance, but also bind three oxygen atoms each to form ψ^1-tetrahedral $[SeO_3]^{2-}$ units with stereochemically active lone-pair electrons. This structure description is only possible for $Sr_4YCl_3[SeO_3]_4$ (CSD 432842), due to the same electron density of Y^{3+} and Sr^{2+}. In the case of Yb^{3+}, a mixed occupation of the lanthanoid and both strontium cations was detected for $Sr_4YbCl_3[SeO_3]_4$ (CSD 433799). One position displays an occupation of 60 % Sr^{2+} and 40 % Yb^{3+}, while the second one carries 70 % Sr^{2+} and 30 Yb^{3+}. Just the third position with the mixed chlorine and oxygen coordination sphere exhibits exclusively Sr^{2+} cations, however.

P053

The crystal structure of trisodium hexachloroiridate

M. Etter[1], M. Müller[2], S. Bette[3]
[1]Deutsches Elektronen-Synchrotron DESY, FS-PE, Hamburg, Germany
[2]Universität Duisburg-Essen, Fakultät Physik, Duisburg, Germany
[3]Max-Planck-Institut für Festkörperforschung, Röntgenographie , Stuttgart, Germany

Strongly hygroscopic inorganic compounds exhibit a rich field of unsolved crystal structures as often several hydrated forms exist. However, solving these crystal structures is challenging, since single crystals are in many cases not available and powders usually consist of several hydrated phases at the same temperature and moisture conditions. Such a challenging compound is for instance the highly hygroscopic trisodium hexachloroiridate (Na3IrCl6) which possess multiple hydrated phases and a so far unsolved crystal structure even of the anhydrous phase.

Here, the crystal structure of the anhydrous phase of trisodium hexachloroiridate (Na3IrCl6) at room temperature was solved after a dehydration process using laboratory powder X-ray diffraction. It was found that the crystal structure of Na3IrCl6 crystallizes in space group *P*-31*c* isostructural to the crystal structures of Na3CrCl6, Na3InCl6 and Na3MoCl6 as well as to the recently found crystal structure of trisodium hexachlororhodate (Na3RhCl6) [1] (see figures 1 and 2).

In this presentation structural details about the dehydrated compound will be given as well as an outlook to the variety of hydrated phases.

Fig. 1: Crystal structure of Na3IrCl6 presented along the (110) direction.
Fig. 2: Crystal structure of Na3IrCl6 presented along the *c*-axis.

References

[1] M. Etter, "The crystal structure of trisodium hexachlororhodate (Na3RhCl6)", submitted to Powder Diffraction

Figure 1

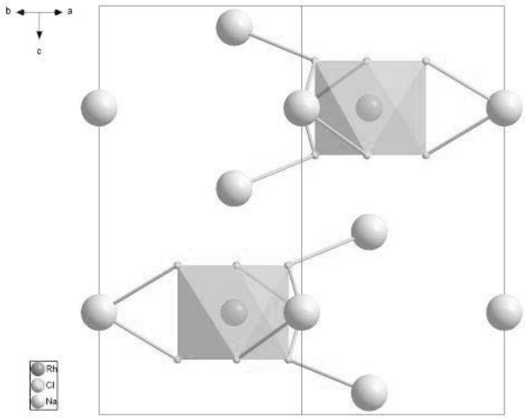

Figure 2

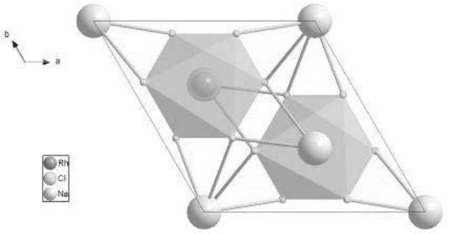

P054

Higher symmetry at lower temperature: reinvestigation of the historic compound caffeinium triiodide monohydrate

G. J. Reiss[1], M. A. Majewski[1], J. Merkelbach[1]
[1]Heinrich-Heine-Universität Düsseldorf, Institut für Anorganische Chemie und Strukturchemie, Düsseldorf, Germany

A report on the first triiodide (strychninium triiodide) dates back to the beginning of the 19th Century [1]. A reinvestigation by combustion analysis in 1865 verified these findings [2]. In the course of this study caffeinium triiodide monohydrate (*caff*$HI_3 \cdot H_2O$) was identified. An earlier attempt to determine the crystal structure of *caff*$HI_3 \cdot H_2O$ at room temperature suggests disorder of the I_3^- anions and an assignment of the space group $P2_1/a$ [3].

As part of a study on polyiodides trapped in hydrogen bonded surroundings [4, 5], we have reinvestigated the system caffeine/HI/H_2O/I_2. In the structure of *caff*$HI_3 \cdot H_2O$ the cations and water molecules are connected by NH···O and OH···O hydrogen bonds. The I_3^- anions are arranged in channels along [100]. At room temperature the structure crystallises in the space group *Pc* (9269 unique reflections, $a = 9.6997(2)$ Å,

$b = 12.2050(2)$ Å, $c = 14.0587(3)$ Å, $\beta = 106.326(2)°$, $R_{gt}(F) = 0.0326$, $wR_{ref}(F^2) = 0.0618$). The organic substructure shows inversion symmetry (black dots in the upper part of the figure). This also holds true for the polyiodide substructure. Both subsystems do not however share their inversion centres, a fact which has been reported for a related structure [4]. Two crystallographically independent I_3^- anions show very loose contacts to neighbouring ones (I···I: 3.834(1) and 3.847(1) Å). On cooling, enthalpic effects in the range of -60 to -80 °C (DSC) are associated with diffuse scattering effects representing reorganisation phenomena. The LT-phase is best described in space group $P2_1/c$ (4482 unique reflections, $a = 9.5860(1)$ Å, $b = 12.0508(1)$ Å, $c = 13.9618(2)$ Å, $\beta = 107.590(1)°$, $R_{gt}(F) = 0.0208$, $wR_{ref}(F^2) = 0.0466$). The dislocation of the subsystems to one another leads to the centrosymmetric LT-phase of *caff*$HI_3 \cdot H_2O$ (lower part of the figure, black dots mark the inversion centres). The asymmetric unit now contains one I_3^- anion, one cation and one water molecule. The phase transition leads to a significant shortening of secondary I···I contact distances within the chains (3.7199(2) Å).

References

[1] P.-J. Pelletier, J. B. Caventou, Ann. Chim. Phys. **10** (1819) 142-177.

[2] W. A. Tilden, J. Chem. Soc. **18** (1865) 99-105.

[3] F. Herbstein, M. Kaftory, M. Kapon, W. Saenger, Z. Kristallogr. **154** (1981) 11-30.

[4] G. J. Reiss, J. S. Engel, CrystEngComm **4** (2002) 155-161.

[5] G. J. Reiss, Z. Kristallogr. CM **232** (2017) 789-795.

Figure 1

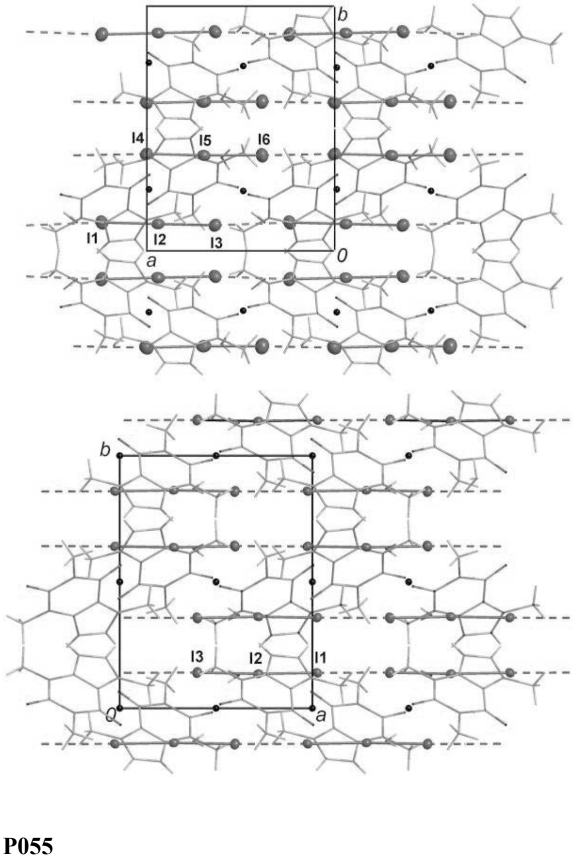

P055

Sr_2*Ln*$Cl_3[SeO_3]_2$ (*Ln* = La – Pr): Strontium Lanthanoid(III) Chloride Oxoselenates(IV) with Mixed Occupation of the Metal Positions

S. Greiner[1], T. Schleid[1]
[1]Universität Stuttgart, Institut für Anorganische Chemie, Stuttgart, Germany

The new strontium lanthanoid chloride oxoselenates(IV) Sr_2*Ln*$Cl_3[SeO_3]_2$ (*Ln* = La – Pr) crystallize in the monoclinic space group $C2/m$ and the lattice parameters $a = 1304.26(5)$ pm, $b = 560.04(3)$ pm, $c = 755.73(5)$ pm, $\beta = 113.672(3)°$ for *Ln* = La (CSD 432843), $a = 1300.74(7)$ pm, $b = 558.65(3)$ pm, $c = 756.29(4)$ pm, $\beta = 113.768(3)°$ for *Ln* = Ce (CSD 432844) and $a = 1297.63(7)$ pm, $b = 557.41(3)$ pm, $c = 757.08(4)$ pm, $\beta = 113.870(3)°$ for *Ln* = Pr (CSD 432845) with Z = 2. One unique Se^{4+} site exists in their crystal structure, but two crystallgraphically different cation positions. Both of them are mixed occupied by Sr^{2+} and Ln^{3+} cations. The *M*1 position is eightfold coordinated by oxygen atoms, which belong to four bidentate $[SeO_3]^{2-}$ units and two Cl^- anions in a $[(M1)O_8Cl_2]$ polyhedron. In contrast the *M*2 position shows a surrounding of five oxygen atoms from monodentate and bidentate $[SeO_3]^{2-}$ units and four Cl^- anions in a $[(M2)O_5Cl_4]$ polyhedron. The $[(M1)O_8Cl_2]$ polyhedra are connected via common O1···O1 edges to one-dimensional chains 1D-$\{[(M1)(O_2)_{4/1}(O1)_{4/2}(Cl_2)_{2/1}]\}$ running parallel to [010]. The $[(M2)O_5Cl_4]$ polyhedra form two-dimensional layers 2D-$\{[(M2)O_{4/2}O_{1/1}(Cl2)_{3/2}(Cl1)_{1/1}]\}$ by sharing Cl2···Cl2 and O···O edges. These layers spread out parallel to (100) and the three-dimensional network of the Sr_2*Ln*$Cl_3[SeO_3]_2$ structure is achieved by interconnecting these layers via common Cl1 vertices. The chains containing the *M*1 cations are arranged in the cavities between the layers and run perpendicular to them. All Se^{4+} cations are coordinated by three oxygen atoms each to form ψ^1-tetrahedral $[SeO_3]^{2-}$ units with a stereochemically active lone pair of electrons at the Se^{4+} centers. Two different coordination spheres of *M* cations are found for the two Cl^- anions, since $(Cl1)^-$ exhibits a linear surrounding, whereas $(Cl2)^-$ is trigonally coordinated in a non-planar fashion.

P056

Cancer treatment by inhibition of nuclear export – crystal structure of a human CRM1-inhibitor complex

A. Shaikhqasem[1], T. Monecke[1], R. Ficner[1]
[1]Georg-August Universität Göttingen, Abteilung für Molekulare Strukturbiologie, Göttingen, Germany

In the last decade, it has been discovered that tumor-growth can be caused or stimulated by a cellular mislocalization of tumor suppressor proteins. CRM1 (chromosome region maintenance 1) is the major export receptor that mediates the transport of a wide range of proteins from the nucleus to the cytoplasm. Interestingly, CRM1 has been identified as nuclear export factor for many tumor suppressor proteins. This renders CRM1 a particularly interesting target for therapeutic intervention in diverse cancer types [1]. Several crystal structures of complexes containing *Saccharomyces cerevisiae* CRM1 bound to different inhibitors have been solved and defined the molecular basis for CRM1-inhibition [2, 3]. Nevertheless, to date there is no structural information available for inhibitors bound to human CRM1 – the real target for cancer treatment. We aim to conceive a crystallization system containing human CRM1 bound to a number of inhibitors. The CRM1 conformation required for the inhibitor binding is stabilized by local and allosteric events including the repositioning of C-terminal helix 21B and the repositioning of the acidic loop of CRM1. To obtain the desired conformation we generated a mutant of CRM1 and co-crystallized it with RanGTP and the inhibitor. Here we present the crystal structure of the well-known nuclear export inhibitor Leptomycin B (LMB) bound to human CRM1 and human RanGTP. Our crystal structure represents a model to explain the mode of action of LMB on human CRM1. The system is also a powerful tool for the characterization and improvement of novel nuclear export inhibiting anti-tumor drugs as it allows rapid screening by crystal soaking.

References

[1] Dickmanns, A., Monecke, T., Ficner, R. Structural basis of targeting the exportin CRM1 in cancer. *Cells* **(2015)** 4: 538-568

[2] Etchin, J., Sun, Q., Kentsis, A., Farmer, A., Zhang, Z.C., Sanda, T., Mansour, M.R., Barcelo, C.,McCauley, D., Kauffman, M.,

Shacham, S., Christie, A.L., Kung, A.L., Rodig, S.J., Chook, Y.M., Look,A.T. Antileukemic activity of nuclear export inhibitors that spare normal hematopoietic cells. *Leukemia*, **2013**, 27:66-74

[3] Sun, Q., Carrasco, Y.P., Hu, Y., Guo, X., Mirzaei, H., Macmillan, J., Chook, Y.M. Nuclear export inhibition through covalent conjugation and hydrolysis of Leptomycin B by CRM1. *Proc. Natl. Acad.Sci. USA*, **2013**, 110(4):1303-1308

P057

Structural aspects of the arene solvation of a ternary halide: Comparison of the crystal structures of [(1,2,4,5-$C_6H_2(CH_3)_4$)Ga][$AlCl_4$] and Ga[$AlCl_4$]

L. Küppers[1], W. Frank[1]
[1]Heinrich-Heine-Universität Düsseldorf, Lehrstuhl für Material und Strukturforschung, Düsseldorf, Germany

In the year 1987 Staffel and Meyer reported the crystal structure of Ga[$AlCl_4$] (**1**) [1,2]. The gallium atom in **1** is surrounded by nine chlorine atoms forming a tri-capped trigonal prism. The Ga-Cl distances range from 3.101 Å to 3.858 Å. The tetrahedral $AlCl_4^-$ unit is slightly distorted, with an average *d*(Al-Cl) = 2.129 Å and Cl-Al-Cl angles ranging from 105.57° to 112.29° [1]. It is interesting to explore the differences of Ga-Cl interactions in the salt **1** and in solvated derivatives like [arene$_n$Ga][$AlCl_4$]. Therefore, by dissolving **1** and durene in chlorobenzene at 80 °C and subsequent crystallization [($C_6H_2(CH_3)_4$)Ga][$AlCl_4$] (**2**) was synthesized. Compound **2** crystallizes in the monoclinic space group *I*2/*m* with $a = 13.3101(6)$ Å, $b = 10.7671(3)$ Å, $c = 21.8878(10)$ Å, $\beta = 93.886(4)°$ and Z = 8 ($R_1 = 0.0345$, $wR_2 = 0.0756$). The [$AlCl_4$]$^-$ tetrahedra in **2** are slightly distorted with *d*(Al-Cl) ranging from 2.1032(14) Å to 2.1382(9) Å and Cl-Al-Cl angles ranging from 105.27(6)° to 111.20(5)°. The Ga1 atom in **2** is surrounded by four [$AlCl_4$]$^-$ units. These [$AlCl_4$]$^-$ tetrahedra are connected to Ga1 by five chlorine atoms forming a pentagonal pyramid. Two chlorine atoms of the [$AlCl_4$]$^-$ tetrahedra form a four membered ring with two [($C_6H_2(CH_3)_4$)Ga]$^+$ units. In total seven chlorine contacts to four [$AlCl_4$]$^-$ tetrahedra are in the environment of Ga2. The Ga-Cl distances range from 3.2362(9) Å to 3.8488(9) Å. Moreover, both Ga1 and Ga2 are coordinated by a durene molecule in a η^6-mode to complete the coordination sphere. In conclusion, the arene complexation in **2** reduces the number of nearest Cl-neighbours for Gallium compared to **1**, by replacing four and two chlorine atoms, respectively, to allow a η^6-coordination to the durene molecule. Consequently, Ga-Cl distances are longer with an average of 3.4738 Å and 3.5849 Å for Ga1 and Ga2 respectively, compared to 3.360 Å in **1** [1].

Figure 1: Coordination of Ga in compound **1** [1].
Figure 2: Coordination of Ga1 and Ga2 in compound **2**.

References

[1] T. Staffel, G. Meyer, *Z. Anorg. Allg. Chem.* **1987**, *552,* 108.

[2] R. K. McMullan, J. D. Corbett, *J. Am. Chem. Soc.* **1958**, *80*, 4761.

Figure 1

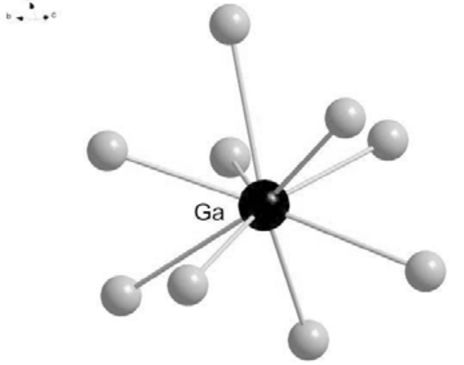

Figure 2

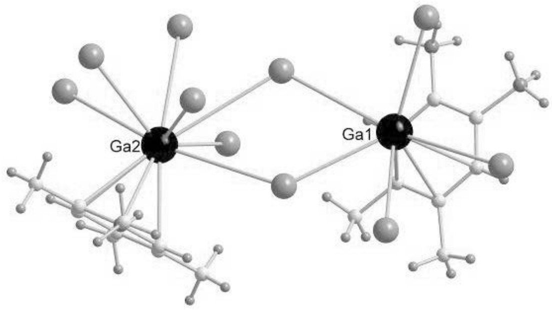

P058

Crystal Structures of Bimetallic Molybdenum and Tungsten Fluoro-Alkoxy Complexes

D. Bockfeld[1], C. Bittner[1], H. Ehrhorn[1], M. Tamm[1]
[1]Technische Universität Braunschweig, Institut für Anorganische und Analytische Chemie, Braunschweig, Germany

During the studies on alkyne metathesis reactions with the molybdenum and tungsten 2,4,6-trimethyl-benzylidyne-fluoro-alkoxy complexes [MesC≡M{OC(CF_3)Me_2}$_3$] (M = Mo, W; Mes = 2,4,6-trimethylphenyl) we observed the formation of Mo_2{OC(CF_3)Me_2}$_6$ [1] and W_2{OC(CF_3)Me_2}$_6$ as a side product formed during the syntheses of the catalysts.

These highly reactive complexes feature severe disorder problems. Beside the individual CF_3-groups, the entire fluoro-*tert*-butoxy groups are prone to disorder. Furthermore, the M≡M-moiety itself exhibits an interesting disorder. The structures are centrosymmetric and feature one half of the molecule in the asymmetric unit. Initial refinements lead to a non-disordered model comprising significant residual electron density in proximity to the metal atoms. Finally, the metal atoms were refined disordered over these positions. The symmetry leads to the generation of eight partly occupied molybdenum positions occupying the edges of an imaginary cuboid (see figure 1). Alternative positions for the ligands could hardly be identified since these can be assumed to be close to their respective averaged positions (see figure 1).

The structures will be discussed in detail and compared to other complexes featuring similar motifs.

References

[1] C. Bittner, H. Ehrhorn, D. Bockfeld, K. Brandhorst, M. Tamm, *Organometallics* **2017**, *36*, 3398–3406.

Figure 1: ORTEP diagram of Mo_2{OC(CF_3)Me_2}$_6$[1] with thermal displacement parameters drawn at 50% probability, hydrogen atoms are omitted for clarity. The fragment containing Mo" was generated via an inversion centre, all four partly occupied Mo positions are shown and connected by dashed lines. The table is showing the distances from the metal positions to the neighboring oxygen atoms.

Figure 1

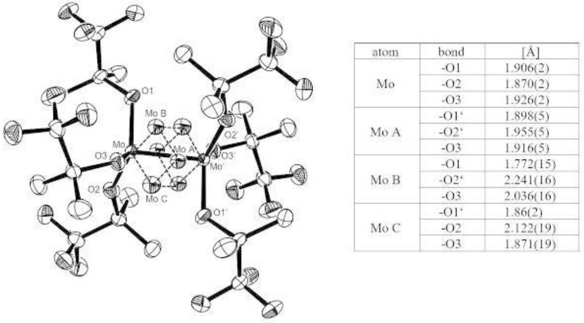

atom	bond	[Å]
Mo	-O1	1.906(2)
	-O2	1.870(2)
	-O3	1.926(2)
Mo A	-O1'	1.898(5)
	-O2'	1.955(5)
	-O3	1.916(5)
Mo B	-O1	1.772(15)
	-O2'	2.241(16)
	-O3	2.036(16)
Mo C	-O1'	1.86(2)
	-O2	2.122(19)
	-O3	1.871(19)

P059

$Dy_3O_2Cl[SeO_3]_2$ and $Er_3O_2Cl[SeO_3]_2$: Two Non-Isotypic Lanthanoid Oxide Chloride Oxoselenates(IV)

S. H. Su[1,2], J. Wontcheu[1], T. Schleid[1,2]
[1]Universität Stuttgart, Institut für Anorganische Chemie , Stuttgart, Germany
[2]International Max Planck Research School for Condensed Matter Science, Stuttgart, Germany

Rare-earth metal(III) oxoselenates(IV) are known as potential host lattices for doping with trivalent lanthanoid cations in luminescent phosphors, which could become an important component in light-emitting diodes. The ψ^1-tetrahedral $[SeO_3]^{2-}$ anions in their crystal structures can provide ligand-to-metal charge transfer and s–p or sp^3–sp^{3*} transition processes at selenium(IV) the non-bonding electron pair. This phenomenon is known as antenna effect, which increases the luminescent efficiency in optoelectronics. Several rare-earth metal(III) oxide chloride oxoselenates(IV) have already shown their ability for luminescent applications, for instance $Y_2O_2Cl[SeO_3]_2$: Eu^{3+} [1]. Some isostructural lanthanoid(III) compounds $Ln_3O_2Cl[SeO_3]_2$ (Ln = Sm, Gd, Tb and Dy) [2, 3] could be successfully synthesized and characterized. They all crystallize in the orthorhombic system with the space group *Pnma* and lattice parameters like a = 533.81(4), b = 1521.03(9), and c = 1076.58(7) pm for $Dy_3O_2Cl[SeO_3]_2$ (CSD-433668), for example. On the other hand, a different crystal structure was detected for $Er_3O_2Cl[SeO_3]_2$ (CSD-433669), which crystallizes in the monoclinic system with the space group *C2/c* and a = 1498.23(9), b = 1102.04(7), c = 547.95(4) pm, β = 105.516(3)° as lattice parameters.

Two crystallographically independent Dy^{3+} cations are found in the structure of $Dy_3O_2Cl[SeO_3]_2$. Eight anions (six O^{2-} and two Cl^-) surround Dy1 building a bicapped trigonal prism, while Dy2 is coordinated by seven O^{2-} and one Cl^- with the shape of a distorted square antiprism. In the polyhedra $[(Dy1)O_6Cl_2]$ and $[(Dy2)O_7Cl]$, there are two and five triangular non-planar $[SeO_3]^{2-}$ groups, respectively, attached via single oxygen atoms (Fig. 1, *top*).

On the other hand, $Er_3O_2Cl[SeO_3]_2$ also has two crystallographically independent Er^{3+} cations in eight- and sevenfold coordination (Fig 1, *bottom*). Whereas the $[(Er1)O_6Cl_2]$ units build up a bicapped trigonal prism again, the $[(Er2)O_6Cl]$ polyhedra lack one $[SeO_3]^{2-}$ ligand in their capped trigonal antiprisms as compared to $Dy_3O_2Cl[SeO_3]_2$.

Both structures contain $[OLn4]^{10+}$ tetrahedra (Ln = Dy and Er), however, which are condensed via common edges to form the double chains $^1_\infty\{[O_2Ln_3\ ]^{5+}\}$ along [100] or [010] (Fig. 2). The structures differ only in the stacking sequence when viewed at the (010) plane.

References
[1] *Z. Kristallogr.* **2011**, 226, 651.
[2] Wontcheu, *Dissertation*, Uni Stuttgart **2004**.
[3] Su, Dissertation, Uni. Stuttgart **2018**.

Figure 1

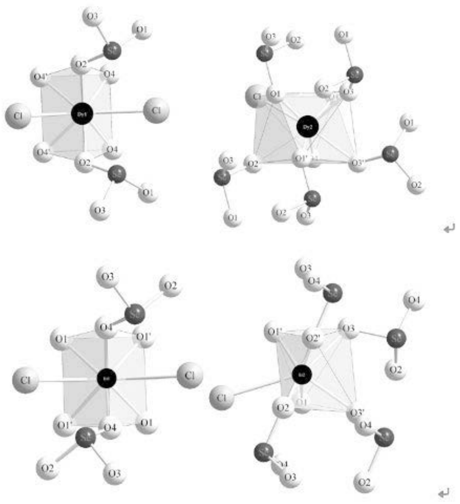

Figure 2

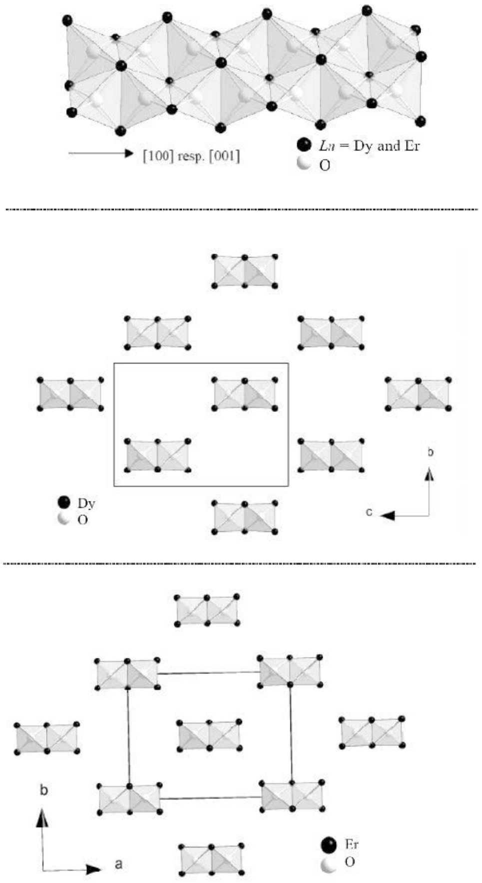

P060

New 2D crystal structures discovered in mixed-valent copper chalcogenide systems

M. I. Sturza[1,2], A. J. E. Rettie[2], D. Bugaris[2], F. Han[2], S. Aswartham[1], D. Y. Chung [2], M. Kanatzidis[2,3], B. Büchner[1]
[1]Leibniz-Institut für Festkörper- und Werkstoffforschung, Institute for Solid State Research , Dresden, Germany
[2]Argonne National Laboratory, Materials Science Division, Argonne, United States
[3]Northwestern University, Department of Chemistry, Evanston, United States

The class of transition-metal chalcogenides that exhibits mixed valency has been of continuing interest for several decades. The emergence of superconductivity with a superconducting transition temperature (Tc∼30 K) in mixed-valence AxFe2−ySe2 (A = K, Rb, Cs, and Tl) phases has further increased interest in the chemistry and physics of complex ternary transition-metal chalcogenides. Copper chalcogenide materials are of considerable scientific interest because of their rich structural and compositional diversity, mixed valency, propensity for phase transitions, charge-density waves, potential for ionic mobility, as well as applications such as high-performance photovoltaic cells.

New results from the chemistry of the A/Cu/Q (A=Na, K, Ba; Q=S, Se) system will be reported. The synthesis, crystal structure, and properties of new layered copper chalcogenide compounds, which are mixed-valent will be presented. Single crystals were grown by the reaction of Cu metal in a molten alkali/ alkaline-earth metal/polysulfide/polyselenide/flux. Single-crystal X-ray diffraction measurements performed on several crystals showed a high quality of the crystals, proven by the good internal consistency of the data collected using the full-sphere mode and an extremely low R factor. Electronic band structure calculations and physical property measurements reveal p-type metallic behavior, with moderately high electrical conductivity and hole carrier mobilities.

P061

Single Crystals of the New Caesium Praseodymium Selenophosphate $Cs_2PrP_2Se_7$

B. Schulz[1], T. Schleid[1]
[1]Universität Stuttgart, Stuttgart, Germany

The caesium praseodymium selenophosphate $Cs_2PrP_2Se_7$ (CSD-433800) crystallizes in the monoclinic space group $P2_1/n$ with the lattice parameters $a = 1021.18(5)$ pm, $b = 724.23(3)$ pm, $c = 2037.41(9)$ pm and $\beta = 98.624(3)°$ for $Z = 4$. Just two other selenophosphate representatives of this formula type were known so far with the lanthanoids cerium and gadolinium and the alkali metals rubidium and caesium [1]. In the crystal structure only unique Pr^{3+} cations exist, coordinated by eight selenium atoms each as bicapped trigonal prismatic $[PrSe_8]$ polyhedra. These are interconnected via common Se3 atoms to one-dimensional1D-$\{PrSe^{t}_{6/1}(Se3)^{v}_{2/2}\}$ chains (t = terminal, v = vertex-sharing) along [010] (Figure 1, *left*). All selenium atoms are part of two different complex selenophosphate anions. There is one tetrahedral $[PSe_4]^{3-}$ unit (Figure 1, *top right*) and one trigonal anti-prism $[P_2Se_6]^{4-}$ (Figure 1, *bottom right*), which exhibits a direct P–P bond. The $[P_2Se_6]^{4-}$ anions connect the one-dimensional 1D-$\{PrSe^{t}_{6/1}(Se3)^{v}_{2/2}\}$ chains via common Se···Se edges to the three-dimensional network of $Cs_2PrP_2Se_7$ (Figure 2). In contrast, the $[PSe_4]^{3-}$ tetrahedra are arranged between the $[PrSe_8]$ polyhedra by sharing Se···Se edges and Se vertices. The resulting hexagonal cavities of the complex anionic units along the [100] direction accommodate the Cs^+ cations, which reside in ten- and elevenfold selenium coordination. They are also generating the charge compensation in $Cs_2PrP_2Se_7$ according to $Cs_4Pr_2[PSe_4]_2[P_2Se_6]$ as mixed selenophosphate(IV) and (V). For its synthesis, praseodymium powder (Pr) was mixed with red phosphorus (P), selenium (Se) and caesium bromide (CsBr) in a molar ratio of 6:6:24:1. The reactants were filled in evacuated glassy silica ampoules and tempered at 950 °C for 4 days. Then the furnace was cooled down to 350 °C within 36 hours, before it was switched off. After washing the raw product with tetrahydrofuran (THF) amber-colored, plate-shaped single crystals of the title compound were obtained and their crystal structure was determined by single-crystal X-ray diffraction at room temperature.

References

[1] K. Chondroudis, M. G. Kanatzidis, *Inorg. Chem.* **1998**, *37*, 3792–3797.

Figure 1

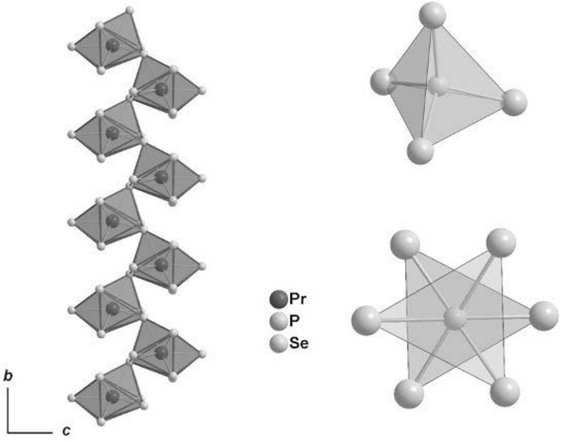

Figure 1 Chain of condensed $[PrSe_8]$ units running along the [010] direction (*left*), $[PSe_4]^{3-}$ tetrahedron (*top right*) and staggered conformation of the trigonal anti-prism $[P_2Se_6]^{4-}$ as Newman projection along the P–P bond (*bottom right*).

Figure 2

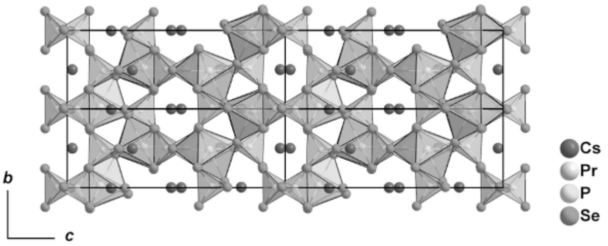

Figure 2 Crystal structure of $Cs_2PrP_2Se_7$ as viewed along [100].

P062

Structure Varieties of Europium(II) Oxoborates: $Eu_2[B_2O_5]$ and EuB_2O_4

C. Funk[1], T. Schleid[1]
[1]Universität Stuttgart, Institut für Anorganische Chemie, Stuttgart, Germany

In nature boron is found in different minerals such as *sassolite* (H_3BO_3) [1] or *berborite* ($Be_2[BO_3](OH)(H_2O)$) [2]. The structure variety of these oxoborates appears quite large. Besides isolated $[BO_3]^{3-}$ triangles like in $Eu_3[BO_3]_2$ [3], there exist vertex-condensed ones like in $[B_2O_5]_{4-}$ entities [4, 5] and infinite chains 1D-$\{[BO^{v}_{2/2}O^{t}_{2/1}]^{-}\}$ [4, 5], layered material like H_3BO_3 [1] as well as 3D-networks of vertex-connected $[BO_4]^{5-}$ tetrahedra, as for example in EuB_4O_7 [5]. Now it was possible to obtain orange-colored needles of $Eu_2[B_2O_5]$ (CSD-433885) and yellow needles of EuB_2O_4 (CSD-433886) as new europium(II) oxoborates.

$Eu_2[B_2O_5]$ (Figure 1, top) crystallizes monoclinically in space group $P2_1/c$ with the lattice constants $a = 778.91(5)$, $b = 534.63(4)$, $c = 1189.02(8)$ pm and $\beta = 92.784(3)°$ for $Z = 4$. The $(Eu1)^{2+}$ cations are surrounded by five $[B_2O_5]^{4-}$ anions via two edges and three vertices. The coordination spheres of the $(Eu2)^{2+}$ cations consist of five $[B_2O_5]^{4-}$ anions, which are coordinating four times with just one and once with two oxygen atoms. The Eu^{2+}–O^{2-} bond lengths range from 243 to 277 pm with a further one at a distance of 303 pm for $(Eu2)^{2+}$, providing a sevenfold oxygen coordination for both Eu^{2+} cations (Figure 1, bottom). The B–O distances of 142 – 144 pm for the terminal and 135 – 136 pm for the bridging ones within the $[B_2O_5]^{4-}$ units, which result from two vertex-connected $[BO_3]^{3-}$ triangles, correspond well with literature data [6].

EuB_2O_4 (Figure 2, left) crystallizes orthorhombically in space group *Pbcn* with a = 1206.91(8), b = 434.32(3) and c = 659.87(5) pm for Z = 4. The crystallographically unique Eu^{2+} cations are coordinated by eight oxygen atoms each (Figure 2, right) stemming from four $1D\text{-}\{[BO^{v}_{2/2}O^{t}_{2/1}]^{-}\}$ chains, generated by vertex-connected $[BO_3]^{3-}$ triangles, which run along the b axis. The Eu–O distances of 253 – 274 pm and the B–O distances of 132 pm for the terminal and 139 – 141 pm for the bridging ones are again in good accordance with literature data [6].

References

[1] M. Schlatti, *Naturwissenschaften* **1967**, *54*, 587–587.
[2] M. Gajhede, S. Larsen, S. Rettrup, *Acta Crystallogr.* **1986**, *B42*, 545–552.
[3] O. Reckeweg, Ch. Funk, F. J. DiSalvo, Th. Schleid, *Z. Anorg. Allg. Chem.* ***2016**, 642*, 1051–1051.
[4] K. -I. Machida, G. -Y. Adachi, J. Shiokawa, *J. Lumin.* **1979**, *21*, 101–110.
[5] K. -I. Machida, G. -Y. Adachi, J. Shiokawa, *Acta Crystallogr.* **1980**, *B36*, 2008–2011.
[6] R. D. Shannon, *Acta Crystallogr.* **1976**, *A32,* 751–767.

Figure 1

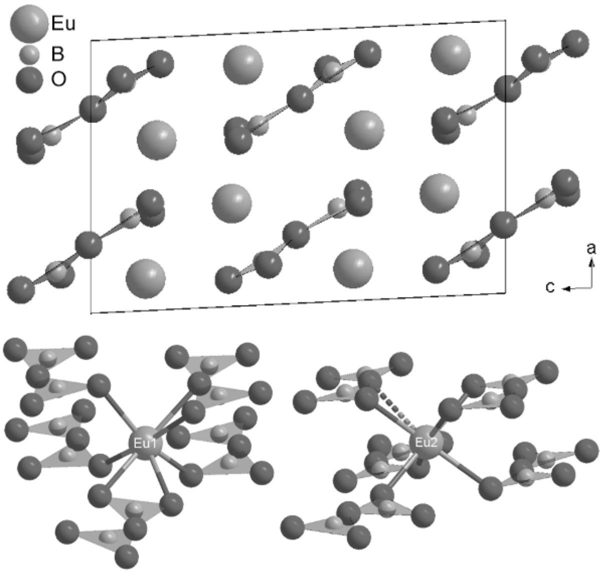

Figure 1. Crystal structure of $Eu[B_2O_5]$ (*top*) and coordination spheres of $(Eu1)^{2+}$ (*bottom left*) and $(Eu2)^{2+}$ (*bottom right*).

Figure 2

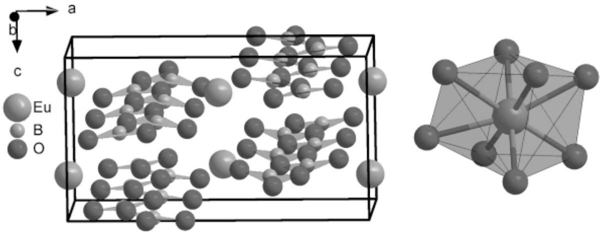

Figure 2. Crystal structure of EuB_2O_4 (*left*) and coordination sphere of Eu^{2+} (*right*).

P063

Crystal Engineering with benzylamines: an inorganic-organic hybrid material containing benzyltrimethylammonium and $[MoOCl_4(H_2O)]^-$ anions.

M. Lichte[1], F. Thoelen[1], W. Frank[1]
[1]Heinrich-Heine-Universität Düsseldorf, Lehrstuhl für Material- und Strukturforschung, Düsseldorf, Germany

In terms of crystal engineering,[1] benzylammonium cations and anionic molybdenum(V) complexes can be adequate compounds for synthesis of inorganic-organic hybrid materials.[2-5]

In this article a new compound is presented containing benzyltrimethylammonium cations and $[MoOCl_4(H_2O)]^-$ anions.

Crystallisation of $[(C_{10}H_{16}N)MoOCl_4(H_2O)] \cdot H_2O$ (**1**) was achieved by cooling of a saturated solution of benzyltrimethylammonium chloride and molybdenum(V) chloride in hydrochloric acid. Platelets of **1** crystallize in the orthorhombic space group *Pbca* (a = 10.726(3) Å, b = 14.2138(3) Å, c = 22.2765(5) Å, Z = 8, 3891 reflections, parameters 191, R_1 = 0.0393, wR_2 = 0.0755). The structure of **1** can be separated into hydrophobic and hydrophilic areas. The hydrophobic regions are formed by the benzyltrimethylammonium cations. The hydrophilic regions contain distorted octahedral $[MoOCl_4(H_2O)]^-$ anions and water. The sixfold coordination of the molybdenum central atom consists of four chlorido ligands (Mo–Cl distances from 2.3645(1) to 2.4032(9) Å), an oxido ligand (Mo=O bond length 1.652(2) Å) and a coordinating water molecule ($Mo–O_{water}$ bond length 2.317(2) Å). Additional water molecules in the hydrophilic layer enable a complex hydrogen bonding network between the complex anions (Fig. 2). Two types of hydrogen bonds can be identified: medium strong hydrogen bonds of the O–H···O type (D–A distance 2.694(4) Å) are present between the coordinating water molecule and water of hydration molecules in the inorganic layer. Weak hydrogen bonds of the O–H···Cl type (D–A distance 3.468(3) Å) are formed between the aforementioned water of hydration and the chlorido ligands of the molybdate anion. Considering graph-set analysis there are two types of ring systems in the hydrogen bond pattern (Fig. 2).[6]

References

[1] G. J. M. Schmidt, *Pure Appl. Chem.* **1971**, *27*, 647.
[2] J. Graf, W. Frank, *Z. Anorg. Allg. Chem.* **2004**, *630*, 1894.
[3] T. Hahn, G. J. Reiß, W. Frank, *Z. Anorg. Allg. Chem.* **2006**, *632*, 2156.
[4] W. Frank, T. Hahn, *Z. Anorg. Allg. Chem.* **2008**, *634*, 2037.
[5] J. van Megen, A. Heymann, W. Frank, *Z. Anorg. Allg. Chem.* **2014**, 2368.
[6] M. C. Etter, J. C. MacDonald, J. Bernstein, *Acta Crystallogr.* **1990**, *B46*, 256–262.

Figure 1: Packing diagram of **1**.
Figure 2: Hydrogen bonds.

Figure 1

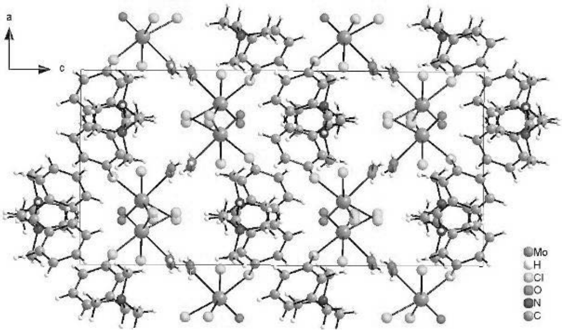

Figure 2

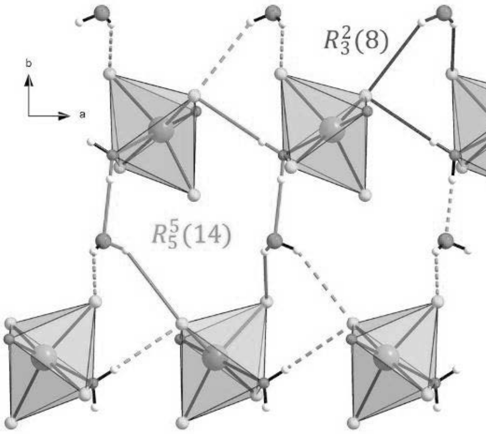

P064

$Cs_3Er_7Se_{12}$ and $Cs_3Tm_7Se_{12}$: Two New Additions at the Far End of the $Cs_3RE_7Se_{12}$ Series

A. H. Geyer[1], A. Elbe[1], T. Schleid[1]
[1]Universität Stuttgart, Institut für Anorganische Chemie, Stuttgart, Germany

Since the late 1990s ternary rare-earth metal chalcogenides with the composition $A_3RE_7Ch_{12}$ (A = K – Cs; RE = Y, Sm, Gd – Er, Yb; Ch = S – Te) [1–7] are known, crystallizing with the $Cs_3Y_7Se_{12}$-type structure [4]. Up to this point, caesium lanthanoid(III) selenides with this formula type were merely known for RE = Y, Sm, and Gd – Ho [4–6]. Due to some unexpected lucky finds, the new compounds $Cs_3Er_7Se_{12}$ and $Cs_3Tm_7Se_{12}$ could be obtained as single-crystalline minority components during the syntheses of Er_2O_2Se and Tm_2O_2Se. The substances crystallize in the orthorhombic space group $Pnnm$ with the lattice parameters of $a = 1276.45(8)$, $b = 2615.71(18)$, $c = 411.06(3)$ pm for $Cs_3Er_7Se_{12}$ (CSD-433902) and $a = 1273.84(8)$, $b = 2610.65(18)$, $c = 408.59(3)$ pm for $Cs_3Tm_7Se_{12}$ (CSD-433903), hosting two formula units per unit cell. The crystal structures display a framework of edge-sharing $[RESe_6]^{9-}$ octahedra (d(Er–Se) = 277 – 297 pm, d(Tm–Se) = 276 – 296 pm), which offers channels along the c axis, where the Cs^+ cations are embedded (d(Cs–Se) = 351 – 391 pm, CN = 6 and 7). Due to electroneutrality and too short $Cs^+\cdots Cs^+$ contacts ($d(Cs\cdots Cs) = 226 – 227$ pm) between the respective Cs^+ cations, the Cs2 position is compelled to be occupied only with half of these, which can be convincingly verified by the structure refinements. This expands the obtainable series of caesium lanthanoid(III) selenides of the formula type $Cs_3RE_7Se_{12}$ by two further representatives since the last addition of the samarium compound in 2012 [5]. Regarding the lattice parameters of $a = 1303.87(9)$, $b = 2667.42(19)$, $c = 423.51(3)$ pm for $Cs_3Sm_7Se_{12}$ [5], the ones in [6] and those shown above, they follow nicely the trend of the lanthanoid contraction.

References

[1] F. Lissner, I. Hartenbach, Th. Schleid: *Z. Anorg. Allg. Chem.* **2002**, *628*, 1552–1555.
[2] M. Folchnandt, Th. Schleid: *Z. Kristallogr. NCS* **2000**, *215*, 9–10.
[3] S.-J. Kim, S.-J. Park, H. Yun, J. Do: *Inorg. Chem.* **1996**, *35*, 5283–5289.
[4] M. Folchnandt, Th. Schleid: *Z. Anorg. Allg. Chem.* **1997**, *623*, 1501–1502.
[5] C. Schneck, A. Elbe, C. M. Schurz, Th. Schleid: *Acta Crystallogr.* **2012**, *E68*, i2–i2.
[6] M. Folchnandt, Th. Schleid: *Z. Anorg. Allg. Chem.* **1998**, *624* 1595–1600.
[7] O. Tougait, H. Noël, J. A. Ibers: *Solid State Sci.* **2001**, *3*, 513–518.

Fig. 1 3D-$\{[RE_7Se_{12}]^{3-}\}$ framework of edge-sharing $[RESe_6]^{9-}$ octahedra in the crystal structure of $Cs_3RE_7Se_{12}$ (RE = Sm, Gd – Tm) forming a tube-like pattern with channels along the c axis, apt to take up the Cs^+ cations.

Figure 1

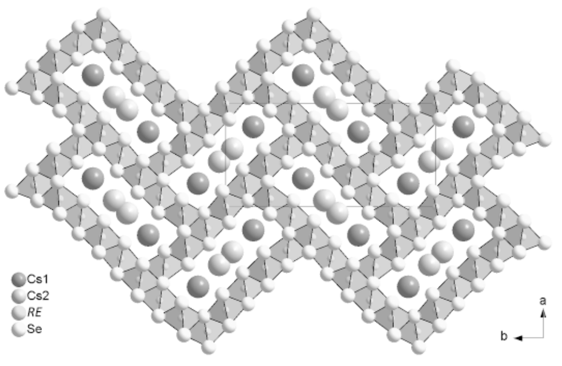

P065

Redetermination of the Crystal Structure of Tetraethylammonium Permanganate at Low Temperatures with Freely Refined Hydrogen Positions

M. Conrad[1], J. Bauchert[1], T. Schleid[1]
[1]Universität Stuttgart, Institut für Anorganische Chemie, Stuttgart, Germany

Abstract

The crystal structure of tetraethylammonium permanganate $[N(C_2H_5)_4][MnO_4]$ was first described in 1991 by *Whang*, *Chung* and *Kim* [1] with $a = 751.2(1)$, $b = 1110.3(1)$, $c = 1476.4(2)$ pm and $\beta = 91.44(1)°$ at room temperature. However, the hydrogen atoms within the structure could not be freely refined in the original data set.

Objectives

Investigations on various alkyl derivatives of ammonium permanganate were conducted as promising precursors for octahedral molecular sieves (OMS) based on porous MnO_2.

Materials and methods

An aqueous solution of barium permanganate $Ba[MnO_4]_2$ was added to an equimolar amount of tetraethylammonium sulfate $[N(C_2H_5)_4]_2[SO_4]$ dissolved in demineralized water. Subsequently, the solution was concentrated and separated from the emerging barium-sulfate precipitate. Drying the purple solution overnight in a desiccator over silica gel lead to the growth of deep purple crystals of tetraethylammonium permanganate $[N(C_2H_5)_4][MnO_4]$.

Results

The crystal structure of tetraethylammonium permanganate was determined at 100 K from single-crystal X-ray diffraction data. $[N(C_2H_5)_4][MnO_4]$ crystallizes in the monoclinic space group $P2_1/c$ (no. 14) with the lattice parameters $a = 745.09(5)$, $b = 1088.56(7)$, $c = 1451.85(9)$ pm and $\beta = 91.324(3)°$ for $Z = 4$. The crystal structure contains a crystallographically unique Mn^{7+} cation surrounded by four crystallographically independent oxygen atoms forming a virtually ideal $[MnO_4]^-$ tetrahedron (d(Mn–O) = 161 pm, $\measuredangle$(O–Mn–O) = 109 – 110°). Furthermore, the structure contains a crystallographically unique nitrogen atom surrounded by four ethyl groups forming a nearly ideal $[N(C_2H_5)_4]^+$ tetrahedron (d(C–N) = 151 – 153 pm, d(C–C) = 150 – 151 pm). It is fixed to the $[MnO_4]^-$ anions via both methylene and methyl protons with remarkably strong hydrogen bonds judged from short O--H distances (d(O--H) = 230 – 253 pm). By reducing both tetrahedral units to their respective centers of gravity, the structure can be described as NaCl-type structure consisting of two commutative partial lattices.

References

[1] D. Whang, S. K. Chung, K. Kim, *Acta Crystallogr*. **1991**, *C47*, 2672–2674.

Figure 1: View at the unit cell of tetraethylammonium permanganate along [100].

Figure 1

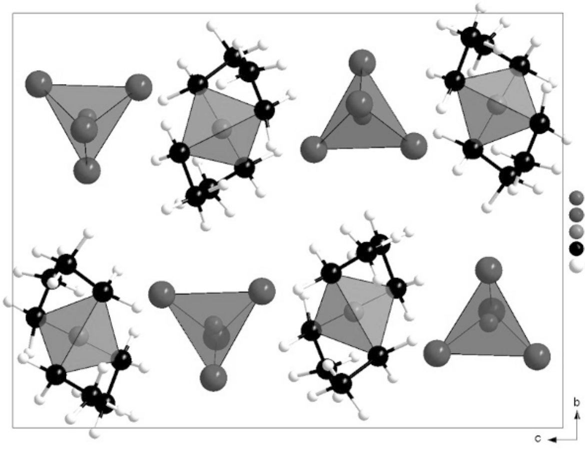

Figure 1: View at the unit cell of tetraethylammonium permanganate along [100].

P066
$CsSc_3S_5$: The First Ternary Sulfide With $CsEr_3Se_5$-Type Structure

C. Buyer[1], D. D. Zimmermann[1], T. Schleid[1]
[1]Universität Stuttgart, Institut für Anorganische Chemie, Stuttgart, Germany

Since the late 1990s ternary rare-earth metal chalcogenides with the compositions ARE_3Ch_5 and $A_3RE_7Ch_{12}$ (A = K – Cs; RE = Y, Sm, Gd – Er, Yb; Ch = S – Te) [1–7] are known, crystallizing with the $CsEr_3Se_5$-type [3] and the $Cs_3Y_7Se_{12}$-type structures [4]. For the first composition, only two representatives have been known so far, namely the archetype itself ($CsEr_3Se_5$ [3]) and $CsHo_3Te_5$ [8]. Due to some unexpected lucky finds, the first ternary sulfide of this structure type $CsSc_3S_5$ could be obtained as single-crystalline minority component during attempts to synthesize ScFS from 1:2:3-mixtures of ScF_3, Sc and S with a surplus of CsF as flux and (unscheduled) reagent. The pale yellow needles crystallize in the orthorhombic space group *Pnma* with the lattice parameters $a = 2036.85(16)$, $b = 374.69(3)$, $c = 1118.92(8)$ pm for $CsSc_3S_5$ (CSD-433904) hosting four formula units per unit cell. The crystal structure displays a framework of edge-sharing $[ScS_6]^{9-}$ octahedra (d(Sc–S) = 252 – 269 pm), which offers channels along the b axis (Figure 1), where the Cs^+ cations are embedded (d(Cs–S) = 346 – 362 pm *plus* 410 pm, CN = 7+1) and coordinated as bicapped trigonal prisms $[CsS_{7+1}]$ (Figure 2). Both the connectivity of and the distances within the $[ScS_6]^{9-}$ octahedra resemble those in the crystal structure of Z-type Sc_2S_3 (257 – 261 pm) [9].

References

[1] F. Lissner, I. Hartenbach, Th. Schleid: *Z. Anorg. Allg. Chem.* **2002**, *628*, 1552–1555.
[2] M. Folchnandt, Th. Schleid: *Z. Kristallogr. NCS* **2000**, *215*, 9–10.
[3] S.-J. Kim, S.-J. Park, H. Yun, J. Do: *Inorg. Chem.* **1996**, *35*, 5283–5289.
[4] M. Folchnandt, Th. Schleid: *Z. Anorg. Allg. Chem.* **1997**, *623*, 1501–1502.
[5] C. Schneck, A. Elbe, C. M. Schurz, Th. Schleid: *Acta Crystallogr.* **2012**, *E68*, i2–i2.
[6] M. Folchnandt, Th. Schleid: *Z. Anorg. Allg. Chem.* **1998**, *624* 1595–1600.
[7] O. Tougait, H. Noël, J. A. Ibers: *Solid State Sci.* **2001**, *3*, 513–518.
[8] J. Yao, B. Deng, D. E. Ellis, J. A. Ibers: *J. Solid State Chem.* **2005**, *178*, 41–46.
[9] J. P. Dismukes, J. G. White: *Inorg. Chem.* **1964**, *3*, 1220–1228.

Figure 1 3D-$\{[Sc_3S_5]^-\}$ framework of edge-sharing $[ScS_6]^{9-}$ octahedra in the crystal structure of $CsSc_3S_5$ forming a tube-like pattern with channels along the b axis, apt to take up the Cs^+ cations.

Figure 2 Coordination polyhedron $[CsS_{7+1}]$ (bicapped trigonal prism) in the crystal structure of $CsSc_3S_5$.

Figure 1

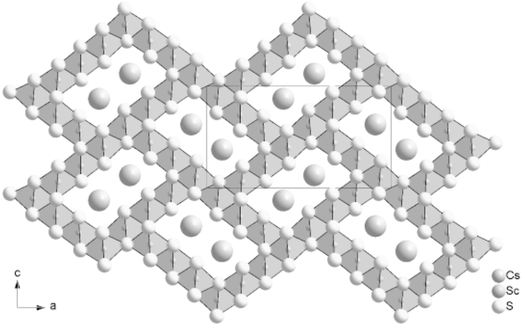

Figure 2

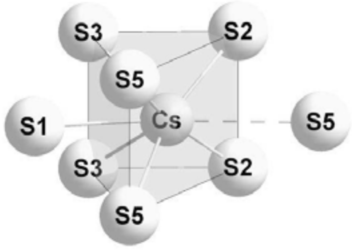

New developments in methods, instrumentation and applications in neutron scattering

P067

FIREPOD – the fine resolution powder diffractometer @ Berlin research reactor BER II

A. Franz[1], A. Hoser[1], S. Schorr[1,2]
[1]Helmholtz-Zentrum Berlin, Structure and Dynamics of Energy Materials, Berlin, Germany
[2]Freie Universität Berlin, Institute of Geological Sciences, Berlin, Germany

The fine-resolution neutron powder diffractometer E9 [1] at the BER II research reactor at the Helmholtz-Zentrum Berlin für Materialien und Energie is dedicated to collect high quality diffractograms suited for crystal structure determinations and Rietveld refinements.

The detector bank consists of eight individual 2D detectors, arranged at an optimized, non-constant distance from the sample, and a radial collimator to reduce background noise. Position-sensitive data integration results in a strongly reduced peak asymmetry.

We provide a large variety of different sample environments, covering temperatures from 1.5 - 2000 K, pressure up to 2.5 kbar, variable magnetic fields (up to 5T) and 10 different gas-adsorption modules (4 K to 1500 K and up to 10000 bar). Possible load gasses include nitrogen, hydrogen, heavy hydrogen, argon and helium. For room temperature measurements we offer a 10-fold automatic sample changer.

References

[1] Helmholtz-Zentrum Berlin für Materialien und Energie. (2017). E9: The Fine Resolution Powder Diffractometer (FIREPOD) at BERII. Journal of large-scale research facilities, 3, A103

Crystallography in nanoscience

P068

Multifunctional nanoparticle superlattices based on engineered protein containers as building blocks

M. Lach[1], M. Künzle[1], T. Beck[1]
[1]RWTH Aachen, Aachen, Germany

We have recently introduced a method for the construction of multifunctional biohybrid material, using protein containers, engineered with opposite surface charge,[1] as atomically precise ligand shells for the assembly of inorganic nanoparticles into highly ordered superlattices.[2] The engineered protein containers form crystalline assemblies, which were characterized with single crystal X-ray crystallography to high resolution. Importantly, using the same building blocks, the composition of the crystals (unitary or binary) and the lattice parameters can be tuned simply by adjusting the crystallization conditions. For example, the coordination number of each protein container in the binary structure can be modified from eight to twelve. The cavity of the protein container can be filled with metal oxide nanoparticles, prior to assembly of the protein containers. The crystallization of oppositely charged protein containers with nanoparticle cargo yields highly ordered nanoparticle superlattices as free-standing crystals, with up to a few hundred micrometers in size. Moreover, the protein matrix can be stabilized by fixation of the crystals with glutaraldehyde without changing the original crystal structure. The application of these biohybrid materials in catalysis was investigated. Cerium oxide nanoparticle superlattices show oxidase-like and peroxidase-like activity, whereas iron oxide nanoparticle superlattices show peroxidase-like activity. In binary nanoparticle superlattices, the combination of two different nanoparticles in the protein scaffold does not influence the activity of the single nanoparticle type.[3] Furthermore, a multifunctional material was constructed with catalytic and magnetic properties.

References

[1] T. Beck, S. Tetter, M. Künzle, D. Hilvert, *Angew. Chemie Int. Ed.* **2015**, *54*, 937–940.
[2] M. Künzle, T. Eckert, T. Beck, *J. Am. Chem. Soc.* **2016**, *138*, 12731–12734.
[3] M. Lach, M. Künzle, T. Beck, *Chem. Eur. J.* **2017**, DOI: 10.1002/chem.201705061.

P069

Synthesis and characterization of rhodium nanoparticles

M. Olejnik[1], M. Epple[1]
[1]Universität Duisburg-Essen, Institut für Anorganische Chemie, Essen, Germany

Introduction

Rhodium nanoparticles (Rh NPs) can be used as catalysts in a large number of reactions, due to their high reactivity and stability in harsh reaction conditions. Essential parameters for the applications of Rh NPs in a heterogeneous and homogeneous catalysis are their size and morphology, which determine the stability, activity and selectivity of NPs.

Objectives

The aim of this work was to synthesize monodisperse Rh NPs with different morphologies (polyhedrons, triangular plates and cubes) and size using the following methods: standard polyol process, polyol process with microwave heating and hydrothermal synthesis.

Materials and Methods

Rh NPs with polyhedron and triangular plate morphologies were synthesized by reduction of rhodium ions ($RhCl_3 \cdot 3\ H_2O$) in various polyol solvents and in the presence of the capping agent polyvinylpyrrolidone (PVP) at different temperatures. Rhodium nanocubes were prepared by two different synthesis methods (polyol process and hydrothermal synthesis) in the presence of potassium bromide (KBr). Afterwards, the nanoparticles were purified by ultracentrifugation, and their size and shape were determined by differential centrifugal sedimentation and transmission electron microscopy.

Results

Rh NPs with different morphologies were successfully synthesized with an average particle diameter between 5 and 15 nm.

Conclusions

The targeted synthesis of Rh NPs with defined shape and size strongly correlates with the reduction potential of the polyol solvents used and the reduction temperature applied. This opens the way for a selective synthesis of such nanoparticles, e.g. in heterogeneous catalysis.

P070

Synthesis of Functionally Polymorphic Pyroxenes

D. Hanaor[1], M. H. Assadi[2], F. Kamutzki[1], A. Mandlule[3], S. Basyar[3]
[1]Technische Universität Berlin, Fachgebiet Keramische Werkstoffe, Berlin, Germany
[2]University of Tsukuba Japan, Tsukuba, Japan
[3]Technische Universität Berlin, Fachgebiet Keramische Werkstoffe, Berlin, Germany

Pyroxene silicate phases constitute a major part of the Earth's crust and have been studied thus far primarily in mineralogical realms. However, accelerated by developments in synthesis and characterisation tools, in recent years pyroxene phases are attracting increasing interest towards applications as functional ceramic systems. Pyroxene compositions are generally of the form $M2M1Si_2O_6$ where M2 and M1 are cations of summed oxidation state +4, and crystallise in both monoclinic and orthorhombic structures, with up to four known polymorphs for certain compositions. These phases are characterised by their assembly of SiO_4 tetrahedra in extended c-axis oriented vertex sharing chains. Often M2 is a larger cation in distorted octahedral coordination while M1 is a smaller octahedra sandwiched between tetrahedral chains.

The versatility of pyroxenes as functional ceramics stems from the diverse range of substitutions that are possible at M1, M2 and tetrahedral sites and the associated ability to tune phase stability and physical properties of these systems. In particular the occurrence of rapid thermomechanically induced displacive phase transformation between pyroxene polymorphs accommodated through kinking and tilting of tetrahedral and octaehedral chains renders these materials of interest towards phase change materials, and in particular transformation toughening ceramics.

In the present work we investigate solution based synthesis methods towards the fabrication of pyroxene phases and in particular examine the role of steric entrapment of cations through chelation polymerisation based methods in crystallisation of nano-structured pyroxenes at low processing temperatures.

The substitution of Zinc at M1 and M2 sites is investigated in the $Ca_yMg_{2-y-x}Zn_xSi_2O_6$ system using precipitation and resin based synthesis methods. This is further supported by computational analysis using DFT simulations, which demonstrate the propensity of Zn to stabilise the Proto-enstatite phase at low Ca contents. Studies demonstrate the role of zinc substitutions in phase stability and further highlight the important role of synthesis tools in achieving non-equilibrium cation distribution and nano-scale crystallites

Figure 1: DFT simulation output for Zn subsitution in enstatite

Figure 2: Morphology of materials fabricated through (a) Precipitation and (b) Pechini resin synthesis

Figure 1

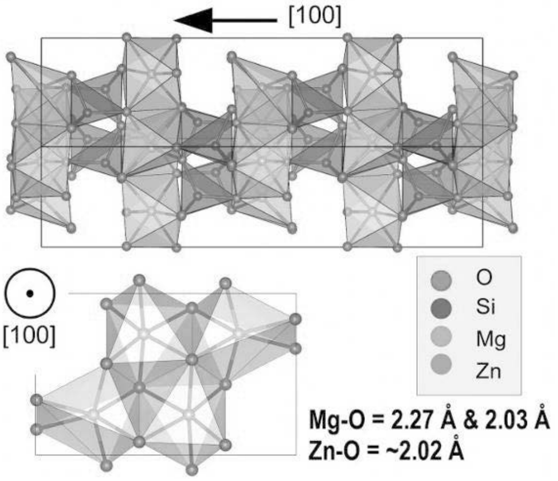

Figure 2

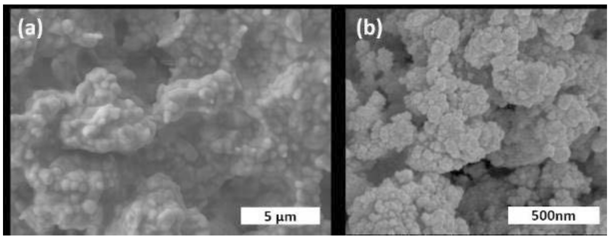

P071

Analysis of Fe stabilized cubic phase Li7La3Zr2O12 solid electrolytes for solid state Li-ion batteries

G. Tian[1], F. Scheiba[1], S. Angelina[1], Z. Zhao[1], A. Fiedler[1], H. Ehrenberg[1]
[1]Karlsruhe Institute of Technology (KIT), Institut für Angewandte Materialien (IAM-ESS), Eggenstein-Leopoldshafen, Germany

Because of doping introduces vacancies into Li sublattice with large entropy and low Gibbs free energy, the cubic phase can be stabilized with high ionic conductivity[2]. The partially suitable supervalent ions replacing Li^+ and Zr^{4+} not only decreases the sintering temperature, resulting in Li^+ loss and energy wastage, but also minimizes the pores or defects, reducing the interface resistance. However, commercial sample contains 8.36% tetragonal phase, so Fe stabilized $Li_{7-3x}Fe_xLa_3Zr_2O_{12}$ (x = 0, 0.12, 0.16, 0.20 and 0.24) garnet solid state electrolyte was prepared via solid-state reaction to obtain the pure cubic phase LLZO garnet.

In Fig. 1, Raman spectra indicate the raw LLZO and the LLZFe0.12 contain a hybrid phase (cubic- and tetragonal phase), whereas the doped LLZFe samples display the cubic phase ($x \geq 0.16$). In Fig. 2, HT-XRD pattern of LLZFe0.16 clearly shows a stable cubic phase up to 900 °C, and the cubic phase does not transform back to the tetragonal phase once the temperature decreases to room temperature. In contrast, an impurity of $La_2Zr_2O_7$ was observed in the raw LLZO above 750 °C. All the diffraction peaks during the stepwise heating process shifts to lower angles, indicating the symmetric cubic structure. Rietveld refinement shows that a lattice parameter of 12.996 Å for raw LLZO. The diffusion of Fe^{3+} ions into the Li+ lattice leads to a decrease in the lattice parameters to around 12.970 Å. It is consistent with the relative ionic radii of Fe^{3+} (60 pm) and Li^+ (76 pm). Fe^{3+} dopant can create enough Li vacancies concentration (0.4~0.5 mol. pfu), which are necessary to stabilize c-LLZO, while excessive Fe^{3+} incorporation levels are also believed to hinder the Li^+ motion in these materials. The experimental results confirm that Fe^{3+} doping can stabilize cubic phase and repress Li loss during the sintering process.

References

[1] H. Buschmann, J. Doïle, S. Berendts, A. Kuhn, P. Bottke, M. Wilkening, et al. Phys. Chem. Chem. Phys. 13 (2011) 19378–19392.
[2] R. Wagner, G.J. Redhammer, D. Rettenwander, G. Tippelt, A. Welzl, S. Taibl, et al. Chemistry of Materials. (2016) acs.chemmater.6b02516.

Figure 1

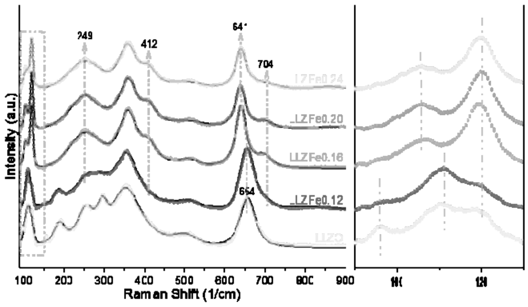

Figure 2

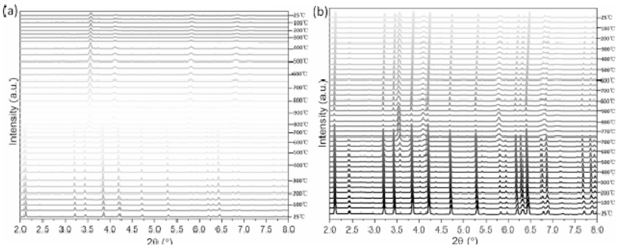

P072

Three dimensional X-ray diffraction imaging of single core-shell-shell nanowires

A. Davtyan[1], V. Favre-Nicolin[2], R. B. Lewis[3], H. Küpers[3], L. Geelhaar[3], D. Kriegner[4], A. Al Hassan[1], U. Pietsch[1]
[1]Universität Siegen, Faculty of Physics, Siegen, Germany
[2]European Synchrotron Radiation Facility (ESRF), Grenoble, France
[3]Paul- Drude-Institute, Berlin, Germany
[4]Charles University Prague, Condensed Matter Physics, Prague, Germany

X-ray diffraction imaging (CXDI) is a powerful tool in structural analysis of single nano objects. In our study we use 3D CXDI to study single core-shell-shell nanowires (NWs) composed by 140nm GaAs core-10nm $In_{0.10}Ga_{0.90}As$ inner shell and 30nm GaAs outer shell grown on (111) silicon substrate. The experiment has been performed at beamline ID01 of the ESRF, Grenoble using coherent x-rays with energy of 9keV and a beam size of 150x200nm² full width at half maximum (FWHM). CXDI in Bragg geometry records the 3D reciprocal space maps around the GaAs (111) from two single NWs at different positions along the growth direction. The first observation shows that the RSMs appear with threefold rotational symmetry. For first NW the orientation of the threefold symmetry preserved along the growth direction. In case of NW2 the orientation of the threefold symmetry is changing along the growth direction which can be explained by the presence of twin domains in the NW. We use ptychography in forward direction to characterize the incoming X-ray wave front and attempt to reconstruct the 3D section of the RSMs taken at different heights on the NWs. We show that the reconstructed phase has also therefore rotational symmetry. Our findings from CXDI measurements are correlated with the 2D ptychography measurements taken at GaAs 111 reflection from the same two NWs.

Structure-property-relationships

P073

$Cu_2ZnSnSe_4$: How far does off-stoichiometry go?

G. Gurieva[1], P. Knoll[2], R. Ferreira[1,3], S. Schorr[1,2]
[1]Helmholz Zentrum Berlin, Berlin, Germany
[2]Freie Universität Berlin, Institute of Geological Sciences, Berlin, Germany
[3]Universidade de Coimbra, Physics Department, Coimbra, Portugal

Quaternary Cu2ZnSnSe4 (CZTSe) is a promising semiconductor material for absorber layer in thin film solar cells due to direct band gap around 1 eV and high absorption coefficient (> 104 cm-1) [1]. Nevertheless, a low open circuit voltage with respect to the band gap is a common phenomenon in CZTSe photovoltaic devices. A plausible reason for this is a reduction in the effective band gap due to inhomogeneities in structure, phase, or composition. The highest conversion efficiency of CZTSe solar cells is above 11%, where the absorber layer of the device exhibits an off-stoichiometric, copper poor zinc rich composition [2]. Stoichiometry deviations lead to formation of intrinsic point defects, which significantly influence the electrical and optical properties of the material [3]. Therefore, a further study of strong deviations from stoichiometry, and the existence region of the kesterite type phase is of great importance for the understanding of device performances.

A comparative study of the phase content of very far off-stoichiometric CZTSe compounds will be presented. The possible limits of the existence region of the kesterite CZTSe will be discussed.Polycrystalline powder samples of eight very far off-stoichiometric CZTSe compounds (off-stoichiometry types A- D) have been grown using the solid state reaction method in evacuated silica tubes. An additional thermal annealing was perfomed, including a very slow cooling, in order to study the influence of annealing on the phase content and stoichiometry of CZTSe phases formed under these conditions. The structural characterization of the synthesized materials before as well as after annealing was carried out by powder X-ray diffraction (PXRD), paying a special attention to the possibility of minimization the content of secondary phases, as well as the changes in the composition of the CZTSe main phase. Wavelength dispersive X-ray spectroscopy (WDX) was used to determine the chemical composition of the obtained phases, paying a special attention to the phase constituents as well as the evolution of the CZTSe phases after the additional annealing.

References

[1] T. Tanaka, et al, J. Phys. Chem. Sol. 66,1978 (2005).
[2] Y.S.Lee, Adv.Energy Mater. 2015, 5, 1401372
[3] S. Chen, et al Adv. Mater. 25,1522-1539 (2013).

P074

The effect of quenching on the spontaneous electric polarization in relaxor ferroelectric Sr0.52Ba0.48Nb2O6 (SBN52) and Ca0.28Ba0.72Nb2O6 (CBN28)

H. A. Graetsch[1]
[1]Ruhr-Universität Bochum, Institut für Geologie, Mineralogie und Geophysik, Bochum, Germany

Quenching SBN crystals from high temperatures is known to cause larger spontaneous electric polarization and higher Curie temperatures [1]. In this contribution, the structural origin of this behaviour is investigated by X-ray single crystal diffraction.

In slowly cooled sbn52 about 10 % of the Me2 sites and almost 30 % of the Me1 sites are vacant [Fig.1). Sr2+ is distributed over both large cation sites whereas Ba2+ is only found on the Me2 site [2]. Quenching causes small changes in the Sr2+ distribution which increase the total occupancy of the Me2 site at the expense of the Me1 site [3]. Changes of occupancy of both Me1 and Me2 sites influences the off-centre shifts of the Nb atoms (Fig.2). Cooperative off-centre shifts of Nb in adjacent octahedra are the main cause of spontaneous electric polarization. Increase of the cation population on Me2 reduces the average displacement of Nb1 through enhanced cation-cation repulsion while the corresponding decrease of the Sr2+ concentration on Me1 let the average shift of Nb2 increase. The multiplicity of Nb2 is four times higher than the multiplicity of Nb1 so that a larger overall polarization results.

The two dimensional incommensurate displacive modulations of the oxygen atoms [4] also seem to be coupled to the cation distribution so that quenching slightly increases the modulation amplitudes. Reheating and subsequent slow cooling removes the structural changes.

CBN crystals show a different response to quenching. No changes of cation distribution or modulation amplitudes were found. The tetragonal symmetry, however, is broken as one of the two dimensions of the modulations is lost. Diffuse intensity replaces the corresponding satellite reflections.

The different behaviour of SBN52 and CBN28 on quenching may be ascribed to the different sizes of Ca2+and Sr2+ resulting in a more ordered cation distribution for CBN28 as no or only very few Ca2+ are built-in on the Me2 site. The disorder of the modulation waves can be due to medium range effects such as changes of the ferroelectric domain size or shape on quenching

References

[1] Guo RT et al. (1989) *Ferroelectrics,* 93, 397
[2] Jamieson PB et al. (1968) *J. Chem. Phys.* 48, 5048
[3] Graetsch HA (2017) *Acta Cryst.* B73, 820
[4] Woike T et al. (2003) *Acta Cryst.* B59, 28

Figure 1

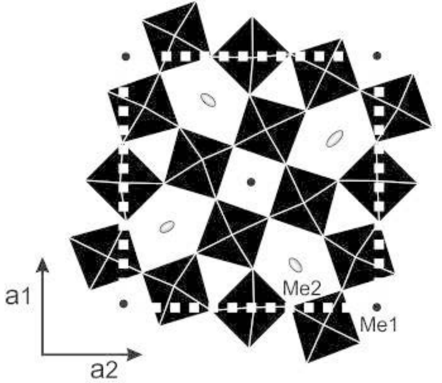

Fig. 1

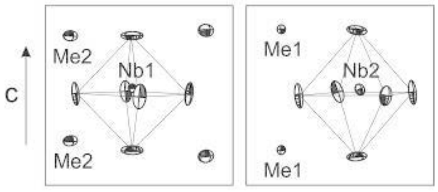

Fig. 2

P075

Influence of mixed crystal formation on the magnetic properties of thiocyanate coordination Polymers

C. Wellm[1,2], M. Rams[2], T. Neumann[1], C. Näther[1]
[1]Christian-Albrechts Universität zu Kiel, Institut für Anorganische Chemie, Kiel, Germany
[2]University of Krakow, Institute of Physics, Krakow, Poland

In the last years were are working on the synthesis and the magnetic properties of coordination polymers based on thiocyanate or selenocyanate of transition metal cations and organic N-donor ligands. In this context, compounds with the general composition $[\mathrm{M(NCS)_2(L)_2}]_n$ (M = Mn Fe, Co, Ni), in which the metal cations are mostly bridged by pairs of anionic ligands, are of most importance. In a few cases networks are observed, in which the cations are connected by both, pairs and single anionic ligands. This is the case, e.g., for the compounds $[\mathrm{M(NCS)_2(4\text{-}acetylpyridine)_2}]_n$ (M = Co, Ni). [1,2]

Both of them show ferromagnetic ordering where the critical temperature of the nickel compound (T_c = 8.6 K) is roughly 7.3 K higher than the ordering temperature of the cobalt compound (T_c = 1.3 K). [2,3] Based on this results the questions arose whether mixed crystals of these compounds could be prepared, if they are homogenous and to which extend the magnetic properties are influenced by mixed crystal formation.

Mixed crystals of these compounds can be obtained by reaction in solution, although the content of nickel in the mixed crystals is higher than that used in synthesis.

Magnetic measurements show that the mixed crystals also show ferromagnetic behavior, while the critical temperature T_c decreases with increasing cobalt content. Also there is evidence that no homogeneous samples were obtained if the synthesis is performed at room temperature. Therefore the synthesis was optimized to obtain compounds for which the magnetic measurements prove, that a higher level of homogeneity was accomplished. The dependence of T_c as function of the actual Ni:Co ratio was also confirmed by heat-capacity measurements.

References

[1] J. Werner, M. Rams, Z. Tomkowicz, T. Runčevski, R. Dinnebier, S. Suckert, C. Näther, *Inorg. Chem.* **2015**, *54*, 2893.
[2] J. Werner, T. Runčevski, R. Dinnebier, S.G. Ebbinghaus, S. Suckert, C. Näther, *Eur. J. Inorg. Chem.* **2015**, *20*, 3236.
[3] S. Suckert, M. Rams, M. Böhme, L. Germann, R.E. Dinnebier, W. Plass, J. Werner, C. Näther, *Dalton Trans.* **2016**, *45*, 18190.

P077

Structure Property Relationships in Magnetic 1D and 2D $\mathrm{Ni(NCS)_2}$ Coordination Polymers

A. Jochim[1], T. Neumann[1], C. Wellm[1], M. Rams[2], I. Jeß[1], C. Näther[1]
[1]Christian-Albrechts Universität zu Kiel, Institut für Anorganische Chemie, Kiel, Germany
[2]University of Krakow, Krakow, Poland

The rational access to compounds with distinct magnetic properties is an important step for the development of new materials. In this regard coordination compounds might be of interest, in which paramagnetic centers are connected *via* ligands that can mediate magnetic exchange. In such compounds the strength of this interaction and the overall magnetic behavior depends strongly on a number of parameters and therefore, systematic investigations on the influence of a chemical and a structural modification on their magnetic properties is crucial for an optimization of such compounds.

In this context we have reported on coordination polymers with the general composition $[\mathrm{M(NCS)_2(L)_2}]_n$ (M = Mn, Fe, Co, Ni; L = N-donor co-ligand), in which the metal cations are octahedrally coordinated and linked into chains by pairs of anionic ligands.[1,2] Depending on the metal cation and the organic co-ligand different magnetic properties are observed, which predominantly depend on the strength of the magnetic exchange along the chains. In most cases the N, respectively S atoms of the anionic ligands as well as the N atoms of the co-ligand are in *trans*-arrangement leading to linear chains, but in the course of our project we obtained a number of new $\mathrm{Ni(NCS)_2}$ compounds with pyridine derivatives substituted in 4-position, that show a different metal coordination. This includes a linear chain with *cis*-coordinating N, respectively S atoms of the anionic ligands as well as a number of zig-zag-like chains in which the metal cations shows either an alternating or an exclusively *cis-cis-trans*-coordination.[3] With other substituents in 4-position also 2D networks are observed, in which the metal cations are linked by single and double thiocyanate anions into layers.[4] For all 1D compounds the magnetic exchange constant was determined from the susceptibility curve and from heat-capacity measurements, which showed a strong dependence of J on the actual metal coordination and the geometry of the chain.

References

[1] J. Werner, T. Runčevski, R. Dinnebier, S. G. Ebbinghaus, S. Suckert, C. Näther, *Eur. J. Inorg. Chem.*, **2015**, *2015*, 3236.
[2] S. Wöhlert, T. Runčevski, R. Dinnebier, S. G. Ebbinghaus, C. Näther, *Cryst. Growth. Des.* **2014**, *14*, 1902.
[3] S. Suckert, M. Rams, M. M. Rams, C. Näther, *Inorg. Chem.* **2017**, *56*, 8007.
[4] S. Suckert, M. Rams, M. Böhme, L. Germann, R. Dinnebier, W. Plass, J. Werner, C. Näther, *Dalton Trans.*, **2016**, *45*, 18190.

P079

Structures, thermodynamic relations and magnetism of novel stable and metastable $\mathrm{Ni(NCS)_2}$ coordination polymers

T. Neumann[1], I. Jess[1], M. Rams[2], L. S. Germann[3], R. E. Dinnebier[3], C. Näther[1]
[1]Christian-Albrechts-Universität zu Kiel, Institut für Anorganische Chemie, Kiel, Germany
[2]University of Krakow, Krakow, Poland
[3]Max-Planck-Institut für Festkörperforschung, Stuttgart, Germany

Recently, we have reported on a number of compounds in which 3d metal cations are octahedral coordinated by thio- or selenocyanate anions and different N-donor co-ligands and are linked by pairs of anionic ligands into chains.[1] Dependent on the nature of the metal cation, the anionic and the neutral ligand, different magnetic properties are observed.[2,3] Based on these results we started a project in which the influence of a chemical and a structural modification on the magnetic properties of such compounds should be investigated in detail. In this context, compounds with same composition but different structures are of special importance, because their physical properties directly depend on the structural changes.

In the course of this project we prepared new $\mathrm{Ni(NCS)_2}$ compounds with 4-aminopyridine. From solution a 2D compound was obtained, in which the metal cations are connected by single thiocyanate bridges into linear chains, which are additionally linked by the co-ligands into layers. On thermal annealing of a 4-aminopyridine-rich precursor a different isomer was obtained, in which the cations shows a *cis-cis-trans*-coordination of the anionic ligands, which leads to the formation of zig-zag-like chains. On further heating this compound loses half of the 4-aminopyridine ligand and transforms quantitatively into a new more condensed network, in which thiocyanate chains are linked by $\mathrm{NiS_2Ni}$ bridges into double chains. Further investigations reveal that the 2D isomer is thermodynamically stable at room-temperature but becomes metastable at higher temperature. This transformation can also be observed in the solid state using DSC measurements, where an endothermic signal is observed, indicating that both forms are related by enantiotropism. The magnetic properties of all compounds were investigated by a combination of dc and ac susceptibility measurements and heat-capacity measurements, which show significant differences in the magnetic exchange constant J in dependence of the topology of the coordination network.

References

[1] J. Werner, M. Rams, Z. Tomkowicz, T. Runčevski, R. Dinnebier, S. Suckert, C. Näther, *Inorg. Chem.*, **2015**, *54*, 2893.
[2] S. Suckert, M. Rams, L. Germann, R. Dinnebier, C. Näther, *Cryst.Growth.Des.* **2017**, *17*, 3997.
[3] S. Suckert, M. Rams, M. Böhme, L. Germann, R. Dinnebier, W. Plass, J. Werner, C. Näther, *Dalton Trans.*, **2016**, *45*, 18190.

P080

Tuning of the intrachain interactions by mixed crystal formation of the anionic ligands in magnetic 1D coordination polymers

I. Jess[1], T. Neumann[1], Z. Tomkowicz[2], M. Rams[1,2], C. Näther[1]
[1]Christian-Albrechts Universität zu Kiel, Institut für Anorganische Chemie, Kiel, Germany
[2]University of Krakow, Institut of physics, Krakow, Germany

In recent years, the synthesis of new coordination polymers has been the subject of extensive investigations with the goal to design new materials exhibiting definite magnetic properties. Independent of the nature of the compounds, one key-parameter is represented by the strength of the exchange constant, which depends to a large extend on the ligand that mediates the magnetic exchange. Therefore, replacement of one ligand by a different one without changing the overall topology of the coordination network is one step to control the strength of the exchange and thus, the magnetic properties in more detail. However, in this case only discrete steps in the exchange constants are expected and therefore, the idea arose whether this can be controlled more precisely by the preparation of mixed crystals of ligands that mediate magnetic exchange differently. For a prove of principle we selected the isotypic quasi-1D ferromagnets $[Co(NCS)_2(pyridine)_2]_n$ and $[Co(NCSe)_2(pyridine)_2]_n$.

Synthetic investigations have shown, that compounds with the composition $[Co(NCS)_x(NCSe)_{2-x}(pyridine)_2]_n$ can be directly obtained from solution, but are also available by thermal decomposition of mixed crystals of a precursor complex with the composition $Co(NCS)_x(NCSe)_{2-x}(pyridine)_4$. The formation of mixed crystals is indicated by comparison of the XRPD pattern of the mixed crystals with that of physical mixtures with the same ratio between the anionic ligands. EDX investigations on several batches also indicate that homogenous samples were obtained.

For all samples dc magnetic measurements at low fields were performed and the exchange constant J was determined by fitting of the cT vs. T curve, whereas the critical temperature Tc was obtained from the derivative of the χ vs. T curve. Both parameters were additionally determined from heat capacity measurements. These investigations reveal that with increasing selenocyanate content J and Tc increase continuously and that within the experimental error no significant differences between the mixed crystals prepared from solution and by thermal decomposition is observed.

References

[1] J. Boeckmann, C. Näther, Dalton Trans.,**2010**, 39, 1019.
[2] J. Boeckmann. C. Näther,Chem. Commun., **2011**, 47, 7104.
[3] M. Rams, M. Böhme, V. Kataev,Y. Krupskaya, B. Büchner, W. Plass, T. Neumann, Z. Tomkowicz, C. Näther, Phys. Chem. Chem. Phys., **2017**, 19, 24534.

P081

Structural consequences of synthesis parameters in the semiconductor $ZnGeN_2$

A. Glibo[1,2], J. Breternitz[1], S. Schorr[1,2]
[1]Helmholtz-Zentrum Berlin, Structure and dynamics of energy materials, Berlin, Germany
[2]Freie Universität Berlin, Berlin, Germany

Zinc-group IV-nitride ($Zn(Si, Ge, Sn)N_2$) materials have a great potential as absorber material in solar cells, since the bandgap of these materials can be tuned in a wide range which spans the visible part of the electromagnetic spectrum. Furthermore, the lattice parameters for $ZnGeN_2$ and $ZnSnN_2$ [1] have a smaller mismatch than the lattice parameters of GaN and InN. [2] With these properties, those materials promise great potential as earth-abundant solar materials that potentially circumvent issues like structural instability and limited miscibility.

The crystal structure of $ZnGeN_2$ thought as a hettotype of wutzite-type GaN, where Ga is replaced alternatingly with Zn and Ge atoms. By arranging the cations in a way that each anion is surrounded by two Zn and two Ge ions, the local valence requirements are fully met. This type of substitution allows the formation of two types of structures that obey the octet rule: an orthorhombic structure in space group $Pna2_1$ and with sixteen atoms per unit cell and a second orthorhombic structure in space group $Pmc2_1$ and with eight atoms per unit cell. [3] We will describe the difference of the structural models and their occurrence in materials prepared under different conditions of a given protocol.

Polycrystalline $ZnGeN_2$ is prepared in a two-step process with the first step being the synthesis of a precursor material, Zn_2GeO_4, *via* a citrate route method. [4] Zn_2GeO_4 then undergoes a reaction with ammonia at high temperatures to form $ZnGeN_2$. [5] Particularly the reaction conditions of this second step greatly influence the physical and structural features of the produced material and we will focus on these relationships in the presentation to allow the targeted preparation of the $ZnGeN_2$ with optimal properties.

References

[1] A. Punya, T. R. Paudel, W. R. L. Lambrecht, **Phys. Status Solidi C**, 2011, **8**, 2492.
[2] H. Morkoç, Handbook of nitride semiconductors and devices, **WILEY-VCH**, 2008, **1**.
[3] E. W. Blaton, K. He, J. Shan, K. Kash; **J. Cryst. Growth**, 2017, **461**, 38.
[4] G. Taglieri, M. Tersigni,P. L. Villa, C. Mondelli; **Int. J. Inorg. Mater.**, 1999, **1**, 103.
[5] R.Viennois, T. Taliercio, V. Potin, A. Errebbahi, B. Gil, S. Charar, A. Haidoux, J.-C. Tédenac; **Mater. Sci. Eng. B**, 2001, **82**, 45

P082

Crystal growth, crystal structures, vibrational spectroscopy and optical properties of antimony tartrates of monovalent cations

L. Bohatý[1], P. Becker[1], P. Held[1], I. Matulková[2], I. Cisarova[2], I. Nemec[2]
[1]Universität zu Köln, Institut für Geologie und Mineralogie, Köln, Germany
[2]Charles University Prague, Department of Inorganic Chemistry, Faculty of Science, Prague, Czech Republic

A stimulated Raman scattering (SRS) study in crystals of the tetragonal $Ba[Sb_2((+)C_4H_2O_6)_2]\cdot 3H_2O$ [1] as well as the determination of the SHG-tensor [d_{ijk}] (SHG = second harmonic generation) of the hexagonal $Sr[Sb_2((+)C_4H_2O_6)_2]\cdot 2H_2O$] [2] reveal remarkable nonlinear optical properties of these antimony tartrates of divalent metals. In addition, attractive linear optical properties were found, which allow the realization of phase matching conditions for different nonlinear optical processes [2,3]. In the present work we focus our attention to antimony tartrates of monovalent cations $M^I_2[Sb_2((+)C_4H_2O_6)_2]\cdot xH_2O$ (M^I = alkali metal) and present the synthesis and crystal structures of:

$Li_2[Sb_2((+)C_4H_2O_6)_2]\cdot 6H_2O$ (space group $C2$)

$Na_2[Sb_2((+)C_4H_2O_6)_2]\cdot 4.5H_2O$ (space group $C2$)

$KLi[Sb_2((+)C_4H_2O_6)_2]\cdot 4H_2O$ (space group $C2$)

$Cs_2[Sb_2((+)C_4H_2O_6)_2]\cdot 3.5H_2O$ (space group $P1$)

$Cs_2[Sb_2((+)C_4H_2O_6)_2]\cdot 2H_2O$ (space group $P2_12_12_1$)

$K_2Na[Sb_2((+)C_4H_2O_6)_2]NO_3\cdot 3H_2O$ (space group $P2_12_12_1$)

Using a standard technique of controlled evaporation of the solvent at constant temperature (in our experiments 38°C) we have been growing large single crystals (volume of several cm^3) of optical quality of $Li_2[Sb_2((+)C_4H_2O_6)_2]\cdot 6H_2O$ and $KLi[Sb_2((+)C_4H_2O_6)_2]\cdot 4H_2O$ from aqueous solutions. A typical growth period amounts 12 to 14 weeks, examples of grown crystals are shown in the figures below.

Crystals of $Li_2[Sb_2((+)C_4H_2O_6)_2]\cdot 6H_2O$ were studied by IR and Raman spectroscopy. Further, refractive indices and their dispersion of these crystals were measured in the wavelength range from 400 to 1080 nm. Based on Sellmeier fits of the refractive index data phase matching (PM) conditions for collinear SHG were evaluated for fundamental laser wavelengths from 1100 nm to 550 nm. Both, type I PM and type II PM, including non-critical PM, can be realized in crystals of $Li_2[Sb_2((+)C_4H_2O_6)_2]\cdot 6H_2O$. This promising result motivates, as a next step, a determination of the coefficients of the SHG tensor of this monoclinic antimony tartrate.

References

[1] A.A.Kaminskii et al., Ann. Phys. **529** (2017)1600295
[2] L. Bayarjargal et al., Cryst. Res. Technol. **43** (2008) 508.
[3] L. Bohatý et al., Cryst. Res. Technol. **34** (1999) 533.

Figure 1

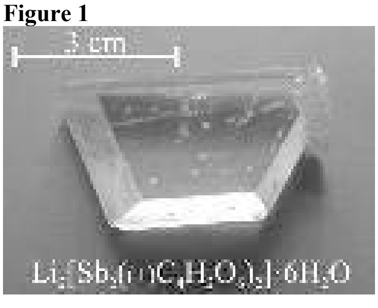

Figure 2

P083

In plane and asymmetric XRD investigation of magnetic thin films

Z. Balogh-Michels[1], A. Neels[1], O. ztürk[2,3], B. Sakar[2,3], A. Ahsen[2,3]
[1]Empa, Swiss Federal Laboratories for Materials Science and Technology, Center for X-ray Analytics, Dübendorf, Switzerland
[2]Gebze Technical University, Physics Dept, Kocaeli, Turkey
[3]Gebze Technical University, Nanotechnology Institutes, Kocaeli, Turkey

Introduction

For magnetic materials the orientation of the grains is highly important as the easy axis of magnetization determines their magnetic properties. This is especially true for the hexagonal cobalt. The typical symmetric scans are not suitable to study very thin films (<10 nm) since the signal to background ratio is low. Moreover such scans cannot differentiate between textured and epitaxial films as only the dominant out of plane peak will be revealed.

Objectives

In this work we applied two techniques to reveal the structural properties of two specimens with Pt/Co/Pt (pcp) and Ti/Pt/Co/Pt (tpcp) stacking order using a Bruker D8 Discovery DaVinci diffractometer. Detector scans with grazing incidence (i.e. asymmetric scans) and in-plane reciprocal space maps. The two films have shown different magnetization characteristics. Both samples were grown on Naturally Oxide Si(111) surface by using Magnetron Sputtering in UHV conditions. Magnetic measurements for the easy magnetization axis of the samples are investigated by using *surface sensitive magneto-optical Kerr effect method (SmartMOKE Magnetometry system-Nanosan Instruments). Hysteresis loops of* tpcp shows perpendicular (or out of plane) magnetization and PCP shows in-plane magnetization.

Results

Clear structural differences between the two specimens are shown in the asymmetric scans. The tpcp film, the one with out-of-plane magnetization has shown a strong preferred orientation for the Pt, while the pcp films is random oriented. That is why pcp does not have perpendicular magnetic anisotropy but show in-plane magnetization (Fig 1). Multiple Co reflections are also visible for the pcp film (Fig. 2 left). The in plane reciprocal space map also revealed the presence of all main Pt reflections (111, 200, 220, 311) as broad, continuous rings (Fig. 2 right).

Conclusion

Asymmetric scans and in plane investigations reveal useful information on the texture of the thin films. In this case, the out-of-plane magnetization properties can be correlated with the presence of preferred orientation for the Ti/Pt/Co/Pt films since the existence of Ti Buffer layer promotes this orientation.

Fig. 1: M-H Measurement of the Sample tpcp by P_Moke. (left) M-H Measurement of the Sample_pcp by P_Moke and L_Moke (right)

Fig. 2: GI asymmetric scan of both specimens (left) in plane reciprocal space map of the pcp specimen (right)

Figure 1

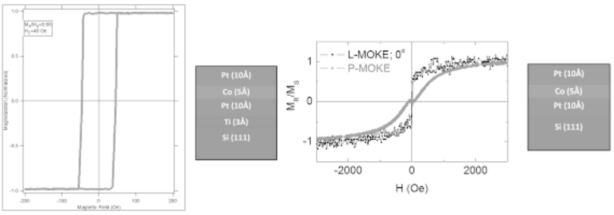

Figure 2

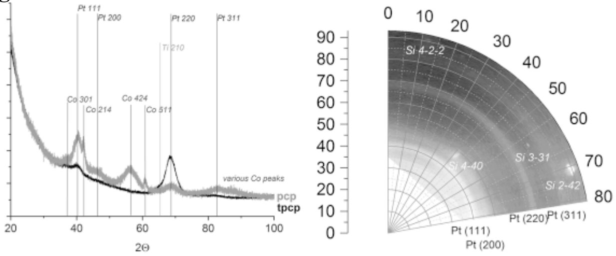

P084
The Nature of Symmetric and Asymmetric Liquid Crystals based on Hydrogen-bonded Assemblies

M. Pfletscher[1], S. Hölscher[1], C. Wölper[2], M. Mezger[3,4], M. Giese[1], M. Pfletscher[1]
[1]Universität Duisburg-Essen, Institut für Anorganische Chemie, Essen, Germany
[2]Universität Duisburg-Essen, Institut für Anorganische Chemie, Essen, Germany
[3]Johannes Gutenberg-Universität Mainz, Physik, Mainz, Germany
[4]Max Planck Institut, Polymer Chemistry, Mainz, Germany

In recent years, Supramolecular Chemistry has become a powerful tool to create smart materials. Since the macroscopic properties of such materials are closely related to their supramolecular architecture, a comprehensive understanding of these non-covalent interactions is necessary to design and synthesize novel functional materials in a rational manner.[1]

Supramolecular liquid crystals (SmLCs) are functional assemblies showing molecular order as well as structural complexity,[2] and so far, just few examples are known who employ hydrogen bonds to create mesogenic assemblies.[3] Therefore, we apply this principle as a modular concept (Lego brick principle), which allows to specifically investigate changes in the self-organization processes of hydrogen-bonded aggregates (Figure 1, red and blue moieties).

A variety of phenol-based SmLCs has been prepared in order to investigate their structural characteristics (morphology) relating to their liquid crystalline behaviour. This series, where the SmLCs consist functional photo-switchable groups (blue moiety), were studied in their nature of the solid structure. The results indicate that the total number and the relative position of the hydroxyl groups determined the mesoscopic geometry (linear, *V*- *vs. U*-shaped structures).[4] Furthermore, a correlation of the crystalline structure with their macroscopic property gives a deep insight into the structure-property relationships (*SPR*s) of SmLCs, providing a fundamental explanation of liquid crystallinity.[5]

References

[1] T. Kato, N. Mizoshita, K. Kishimoto, *Angew. Chem. Int. Ed.* **2006**, *45*, 38-68;
[2] X. Yan, F. Wang, B. Zheng, F. Huang, *Chem. Soc. Rev.* **2012**, *41*, 6042-6065;
[3] T. Wöhrle, I. Wurzbach, J. Kirres, A. Kostidou, N. Kapernaum, J. Litterscheidt, J. C. Haenle, P. Staffeld, A. Baro, F. Giesselmann, S. Laschat, *Chem. Rev.* **2016**, *116*, 1139-1241;
[4] M. Pfletscher, C. Wölper, J. S. Gutmann, M. Mezger, M. Giese, *Chem. Commun.* **2016**, *52*, 8549-8552.
[5] M. Pfletscher, S. Hölscher, C. Wölper, M. Mezger, M. Giese, *Chem. Mater.* **2017**, *29 (19)*, 8462-8471.

Figure. The design of novel materials can be easily achieved by using the modular concept based on non-covalent interactions (Lego brick principle). The application of such a concept simplifies the synthetic complexity and offers a facile recover of the subunits.

Figure 1

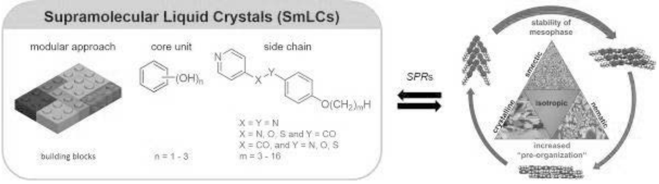

P085
Advantages of chalcogenide bonded metals as basis for potential Al-ion conducting materials

F. Meutzner[1,2], M. Zschornak[1], T. Nestler[1], A. A. Kabanov[2], T. Leisegang[1,2], V. A. Blatov[2], D. C. Meyer[1]
[1]Technische Universität Bergakademie Freiberg, Institut für Experimentelle Physik, Freiberg, Germany
[2]Samara National Research University, Samara, Russian Federation

Due to its high abundance and triple charge, Al is highly interesting for future electrochemical energy storage solutions. Especially for stationary applications, to balance the demand and offer of the energy grid, large quantities of active mass are necessary. Currently, Li and Pb dominate the battery market, but especially Li may show substantial supply challenges in the future. Therefore, the search for new chemistries and technologies for a diversification of applications will become increasingly important.
Within the crystalline structure of potential Al-ion conductors, the high charge of the trivalent Al ion poses the challenge of high attraction towards anions and high repulsion from cations. In this context, an optimised crystal structure is of paramount importance. By analysing the necessities for good ionic transport and applying this knowledge to large crystallographic databases by means of high-throughput crystal-chemical analyses, we address the identification of promising materials for a future Al-ion battery technology.

We opened up the chemical composition space of potential Al-ion conductor materials by first analysing bonding differences in Al and O, S, or Se-containing materials. Due to the decreasing electronegativity and increasing size, we found an increasing polarisation of the chalcogenides and a better shielding of charge from the Al-ions. We have studied varying ternary spinel-like structures by means of DFT calculations to quantitatively evaluate the chemical bonding in Al-chalcogenides.

Eventually, this knowledge was applied to the ICSD to filter out interesting O-, S-, and Se-containing materials for the conduction of Al-ions. We applied Voronoi-Dirichlet partitioning to first geometrically filter for materials with interconnected interstitial voids that are large enough to host Al-ions. Secondly, bond-valence site-energies were calculated to estimate respective activation energies for the percolation of Al-ion conduction paths. As a last step, DFT will be used to simulate a full, dynamic diffusion process for the most interesting candidates ab initio.

We will present our findings for the differences of bonding in different chalcogenides based on Bader-partitioning and demonstrate the results of our crystal-chemical screening algorithm.

This work is funded by the German BMBF (R2RBattery: 03SF0542A), the Russian Megagrant (14.B25.31.0005), and the RSF (16-13-10158).

P086

TomG performs O-methylation in Tomaymycin Biosynthesis via an on-line Tailoring Reaction on the NRPS TomA

J. Pippel[1], A. von Tesmar[2,3], M. Hoffmann[2,3], A. Abou Fayad[2,3], S. Dausend-Werner[2], A. Bauer[4], W. Blankenfeldt[1,5], R. Müller[2,3]
[1]Helmholtz Centre for Infection Research, Structure and Function of Proteins, Braunschweig, Germany
[2]Helmholtz Institute for Pharmaceutical Research Saarland, Department of Microbial Natural Products (MINS), Saarbrücken, Germany
[3]German Center for Infection Research (DZIF), Braunschweig, Germany
[4]Sanofi-Aventis Deutschland GmbH, R&D Therapeutic Area Infectious Diseases, Frankfurt am Main, Germany
[5]Technische Universität Braunschweig, Institute for Biochemistry, Biotechnology and Bioinformatics, Braunschweig, Germany

Introduction

The pyrrolo[4,2]benzodiazepine (PBD) tomaymycin is produced by *Streptomyces achromogenes* and exhibits antibiotic and anticancer potential. Biosynthesis of the tomaymycin core structure is facilitated by the two NRPS TomA and TomB which catalyze the condensation of anthranilic acid and proline derivatives (Li *et al.*, 2009; von Tesmar *et al.*, 2017). NRPSs are modularly organized proteins that generate various natural product and diversity of these products is achieved since most NRPS accept a wide range of unusually modified building blocks. In tomaymycin biosynthesis, modification of 5-hydroxy anthranilic acid is performed by TomE/F as well as TomG which catalyze 4-hydroxylation and O-methylation, respectively. However, timing of these tailoring reactions remained unknown.

Objectives

By combining X-ray crystallography with mass spectrometry (MS) and *in-silico* experiments, we aimed at deciphering the timing of the tailoring reactions to gain information in tomaymycin biosynthesis.

Results

Structural analysis revealed that TomG requires two adjacent hydroxyl groups for methylation of the anthranilic acid moiety leaving us to conclude that TomE/F-mediated 4-hydroxylation takes place prior to O-methylation. MS-based experiments furthermore demonstrated that 5-hydroxy anthranilic acid is the preferred substrate of TomA, whereas 4,5-dihydroxy anthranilic acid is not accepted by TomA. Additionally, a post-NRPS methylation was ruled out leaving us to conceive an most likely on-line scenario for 4-hydroxylation and subsequent O-methylation while the substrate is loaded to TomA. This was in good agreement with our structural and *in-silico* analysis revealing a spacious and solvent-exposed substrate-binding pocket for TomG.

Conclusion

The combination of MS-based experiments and structural analysis gave valuable insights into the substrate specificity and timing of the NRPS-mediated tomaymycin biosynthesis. Thus, this approach was proven appropriable to decipher NRP biosynthesis and might further pave the way for industrial applications.

Li, W. *et al.* (2009). Cloning and characterization of the biosynthetic gene cluster for tomaymycin, an SJG-136 monomeric analog. *Appl Environ Microbiol.* 75(9)*:*2958-2963.

Von Tesmar A *et al.* (2017). Total Biosynthesis of the Pyrrolo[4,2]benzodiazepine Scaffold Tomaymycin on an In Vitro Reconstituted NRPS System. *Cell Chem Biol.* Oct 19;24(10):1216-1227.

Figure 1

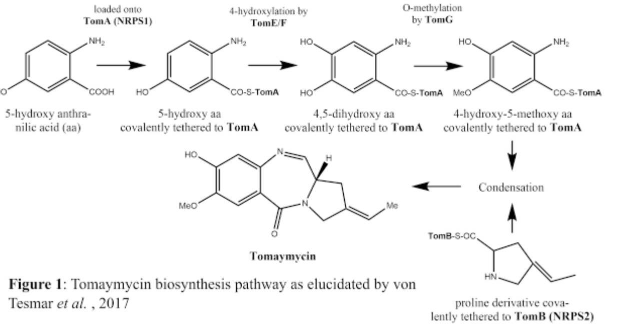

Figure 1: Tomaymycin biosynthesis pathway as elucidated by von Tesmar *et al.* , 2017

P087

Determination of structure-property-relations from single crystal X-ray diffraction data

T. Weigel[1], M. Zschornak[1], T. Behm[1], C. Funke[1], S. Jachalke[1], H. Stöcker[1], T. Leisegang[1,2], D. C. Meyer[1]
[1]Technische Universität Bergakademie Freiberg, Insitut für Experimentelle Physik, Freiberg, Germany
[2]Samara National Research University, Samara, Russian Federation

The increase in energy efficiency is an ubiquitous issue becoming particularly important for future economic dynamics in terms of innovative materials, corresponding devices and decreasing production costs. The latter offers a high potential, especially given the fact that today, according to estimates more than 72 % of the converted energy worldwide gets lost in the form of waste heat. A large amount thereof, 63 % is low-temperature waste heat for which new highly efficient materials are needed for conversion into, e. g., versatile electric energy. To make this waste heat usable, materials exhibiting the pyroelectric effect can be utilized. For the estimation of such materials and crystals properties, beside a structural characterization, additional measurements of the physical properties are necessary. A direct evaluation of structure-property-relations from structural data is usually difficult. However, a multitude of material *property* variations is caused by the changes in their specific structure, which are measurable values. For example, the pyroelectric effect has its origin in temperature dependent changes of the spontaneous polarization based on atomic displacements.

This work shows an approach, how these measurable structural changes can be used for the determination of pyroelectric and thermal expansion behaviors of the material, without any further measurements. Deviations of the crystal structure have been investigated with single crystal X-ray diffraction in a temperature range from 80 K to 400 K. The pyroelectric standard and well-known material system lithium niobate (LiNbO3) was used as sample. As a result, spontaneous polarization, pyroelectric coefficient as well as thermal expansion coefficients have been calculated and show a high comparability with theoretical and experimental data. Therefore, this work may be of wide interest for the pyroelectric community.

This work was financially supported by the German BMBF (CryPhysConcept: 03EK3029A) and DFG (DFG ME 1433/15-1).

P088

Perovskites as potential electrocatalysts for electrochemical oxygen evolution reaction

S. Ortatatli[1], X. Deng[1], M. Haiduk[2], H. Tüysüz[1], C. Weidenthaler[1]
[1]Max-Planck-Institut für Kohlenforschung, Heterogeneous Catalysis, Mülheim an der Ruhr, Germany
[2]Ruhr-Universität Bochum, Institut für Geologie, Mineralogie und Geophysik, Bochum, Germany

Perovskites are an interesting class of materials as their crystal structures can tolerate non-stoichiometry, cationic substitutions as well as structural disorder [1]. Therefore, perovskites have diverse applications as cathode catalysts employed in solid oxide fuel cells (SOFCs) [2], catalytic CO and CH_4 oxidation [3], as well as oxygen evolution reaction (OER) [4], etc. In general, solid-state reaction is used to synthesise perovskites which causes sintering of particles at elevated temperatures giving rise to particle sizes on micrometer scale. The goals of this study were to synthesise perovskites from simple to substituted compositions using a more practical method and investigating the influence of compositional changes on the electrocatalytic activity for OER. In our study perovskites with various chemical compositions were synthesised using a hard-templating method starting from metal nitrate precursors. In order to investigate the influence of reaction temperature on the structure, some samples were calcined at 450, 550 and 700 °C. For revealing the average bulk structures of the samples X-ray powder diffraction (XRPD) was used. XRPD data showed that not only simple but also substituted perovskites could be synthesised at 550 °C and 700 °C with domain sizes on nanoscale. For example, $LaCoO_3$ and $La_{0.8}Ca_{0.2}Ni_{0.5}Co_{0.5}O_{3-\delta}$ could be synthesized already at 550 °C (Fig. 1).

Figure 1: XRPD data of the samples synthesised at 550 and 700 °C: (a) $LaCoO_3$, (b) $La_{0.8}Ca_{0.2}Ni_{0.5}Co_{0.5}O_{3-\delta}$. Tick marks indicate the reference reflection positions.

On the other hand, XRPD data of the samples calcined at 450 °C could not provide beneficial information about the crystal structures due to reflection broadening. Elucidation of the local structures of the amorphous samples calcined at 450 °C was performed by pair distribution function (PDF) analysis. Influence of chemical composition on the OER activity was evaluated by comparing the activities of as-synthesised pure and substituted perovskites. OER measurements show that among the simple perovskites, $LaCoO_3$ outperformed $LaNiO_3$ and $LaFeO_3$. For systematic substitution of A- and B-cationic sites it was found that Co substitution enhances the OER activity of $LaNiO_3$. (Manuscript was submitted).

References

[1] C. Artini, *J. Eur. Ceram. Soc.*, **2017**, 37, 427-440,
[2] J. Kim et al., *ChemSusChem.*, **2014**, 7, 1669-1675,
[3] S. Royer et al., *Appl. Catal. A*, **2005**, 282, 273-284,
[4] J. Suntivich et al., Science, **2011**, 334, 1383-1385.

Figure 1

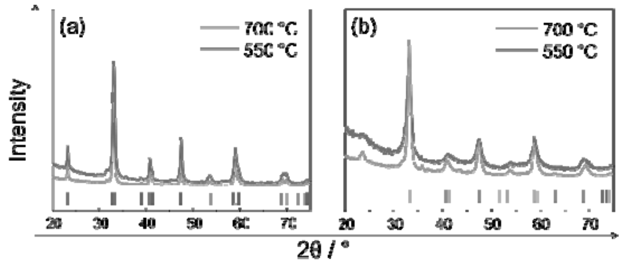

P089

Triclinic pedial sarcosinium hydrogen L-tartrate: Crystal growth, pyroelectric and linear optical properties

L. Bohatý[1], L. Bayarjargal[2], L. Andersen[3], P. Becker[1]
[1]Universität zu Köln, Institut für Geologie und Mineralogie, Köln, Germany
[2]Goethe-Universität Frankfurt am Main, Institut für Geowissenschaften, Frankfurt am Main, Germany
[3]Universität zu Köln, II. Physikalisches Institut, Köln, Germany

Crystals that belong to the triclinic pedial space group *P*1 possess - with the exception of translation -no further symmetry elements, in particular, neither symmetry elements of rotation nor rotoinversion. According to Neumann´s Principle [1] in such crystals no symmetry restriction exists for the anisotropy of macroscopic crystal properties. In this general case the anisotropy possesses the maximum degree of freedom. To our best knowledge, reliable detailed crystal physical investigation of tensor properties of a crystal with point group symmetry 1 was published in [2] only. In [2], in particular, the piezoelectric and elastic properties of lithium oxalate $LiHC_2O_4 \cdot H_2O$ were reported, including the determination of all components of the relevant tensors. Twinning of left- and right-handed individuals made the study of $LiHC_2O_4 \cdot H_2O$ more difficult.

In the present work we report on triclinic pedial (*P*1) sarcosinium hydrogen L-tartrate ($C_3H_8NO_2$-L-$C_4H_5O_6$; Sar^+-L-$tartrate^-$) [3, 4] which can easily be obtained in large crystals. The handedness of the L-tartrate structural units fixes the handedness of the crystals. Therefore, twinning combining left- and right-handed crystals cannot occur.

Single crystals of sarcosinium hydrogen L-tartrate (Sar^+-L-$tartrate^-$) were grown from aqueous solution containing sarcosine and L(+)-tartaric acid in stoichiometric ratio 1 : 1 of the constituents using the controlled evaporation method of the solvent at 38.5°C. Crystals of optical quality and dimensions up to 25x25x40 mm^3 have been grown during periods of 10 to 14 weeks. Refractive indices and their dispersion in a wavelength range from 365 to 1083 nm were determined. Based on this linear optical data, phase matching conditions for collinear second harmonic generation (SHG) were analyzed and discussed.

In addition, the length and the orientation of the pyroelectric vector ***p*** and its temperature dependence between 100 K and 310 K were determined. In this temperature range the value of ***p*** increases nearly linearly from 19 to 24 $\mu CK^{-1}m^{-2}$ and the orientation of ***p*** changes only very slightly keeping its direction approximately perpendicular to the alternate sarcosinium and hydrogen tartrate layers.

References

[1] J. F. Nye, *Physical Properties of Crystals*, Oxford, 1957.
[2] S. Haussühl, Z. Kristallogr. **194 (**1991) 57.
[3] R. V. Krishnakumar et al., Acta Crystallogr. C **57** (2001) 165.
[4] M. Fleck et al., J. Mol. Struct. **1045** (2013) 95.

Figure 1

P090

Structure transformation and magnetic properties of iron oxides and hydroxides

N. Dudchenko[1], A. Brik[1], V. Ponomar[1]
[1]M.P. Semenenko Institute of Geochemistry, Mineralogy and Ore Formation, Physics of mineral structure and biomineralogy, Kyiv, Ukraine

Question

Ukraine has significant resources of weathered iron ores and iron-containing waste (e.g. tailings). Both consist of iron oxides and hydroxides (hematite, goethite) of various particle sizes. Occupying a large area and polluting the environment of mining regions, such wastes should be processed. One of the possibilities of their processing is the transformation of weakly magnetic iron oxides and hydroxides (hematite, goethite, etc.) into a strongly magnetic magnetite. Newly formed magnetite can be easily extracted from the raw materials by the magnetic separation.

Methods

Phase transformation of the structure of synthetic (nanoscale) and natural hematite and goethite under reducing conditions (temperature – 600 °C, atmosphere – carbon monoxide).

Results

Phase transformations were performed using a custom-built facility that enables to generate carbon monoxide. Reduction of hematite and goethite with carbon monoxide was performed under heating to 600 °C. Mineral composition of the source and the resulting samples was investigated using XRD. The source synthetic samples consist of pure hematite and of pure goethite, while natural samples are represented by quartz/hematite ore and by quartz/goethite/hematite ore. The resulting samples are characterized by the formation of a new strong magnetic mineral attributed to magnetite. It has been shown that the reduction of synthetic hematite starts at 340 °C, while the starting temperature of goethite reduction is 260 °C. The reduction of natural minerals occurs at higher temperatures. Saturation magnetization of all samples obtained after reduction increases significantly. The subsequent magnetic separation of the reduced natural samples leads to the extraction of magnetite from the ores. The resulting magnetite concentrate has the iron content of 69.5 wt. %. The saturation magnetization of the magnetite concentrate is about 90 Am2/kg.

Conclusions

The reduction of hematite into magnetite occurs at temperatures higher than 340 °C. Goethite reduces to magnetite at 260 °C and more. The transformation performed for natural ores allows the extraction of iron in the form of magnetite by magnetic separation.

This work was supported by Science and Technology Center in Ukraine within Project 6176.

P091

Growth, Structure, and Properties of La2*BB*"O6 (B = Co, Ni, Mg, and Zn; B" = Ru, Ir) Double Perovskite Single Crystals

R. Morrow[1], M. I. Sturza[1], L. T. Corredor[2], A. Wolter-Giraud[1], S. Wurmehl[1,3], B. Büchner[1,3]
[1]IFW Dresden, Dresden, Germany
[2]Universidade Federal do Rio Grande do Norte, Natal, Brazil
[3]Technische Universität Dresden, Dresden, Germany

Double perovskites have received a great deal of attention in recent times due to their magnetic properties. However, the vast majority of experimental data thus far in this field has been generated with powder samples resulting in numerous open questions concerning the underlying principles governing the magnetic properties of these complex oxides. Here it is shown that, using a flux method, double perovskite iridate single crystals as large as 3 mm with formula La2*BB*"O6 (*B* = Co, Ni, Mg, and Zn; *B*" = Ru, Ir) have been grown. The structure and properties of the crystals are characterized and are in agreement with previous powder data. Therefore, future more detailed experiments will be possible on a variety of double perovskite single crystals with numerous electronic configurations.

P092

The thermal expansion behaviour of Mn, Fe, Co and Ni olivines

P. Schmid-Beurmann[1], H. Kroll[1], A. Sell[1], J. Büscher[1], R. Dohr[1], A. Kirfel[2]
[1]Universität Münster, Institut für Mineralogie, Münster, Germany
[2]University of Bonn, Steinmann Institut, Bonn, Germany

In order to complete the data set for comparing the thermal behaviour of end-member olivines containing cations of the transition element series Mn ($3d^5$), Fe ($3d^6$), Co (3d7), Ni (3d8 subshell) the thermal expansivity of Co and Ni olivine has been studied by powder diffraction at ambient pressure and temperatures between 25°C and 1000°C. The anisotropy of the thermal expansion was analyzed using the Kumar equation-of-state (EoS) coupled with the thermal Mie-Grüneisen EoS.

Axial expansivities αi are controlled by compressibilities $\beta T,i$ and thermal pressures $(\partial P/\partial T)V,i$ according to $\alpha i = \beta T,i\ (\partial P/\partial T)V,i$. For olivines, the isothermal compressibilities can be related to structural properties and suggest a sequence of compressibilities with $\beta T,b > \beta T,c > \beta T,a$ (SG Pbnm). Compression along *a* involves compression of Si tetrahedra which are rigid. M2 octahedral layers, which are free of Si sites and thus more easily to compress, extend normal to *b*. The M2 octahedra share O-O edges with Si tetrahedra being parallel *c*. According to White et al. (1985) the "thermal expansion is a response to thermal pressure $(\delta P/\delta T)V$ and is the greater the more compressible the material or direction". Thus, axial expansivities αi and compressibilities $\beta T,i$ are expected to follow the same ranking, i.e. $ab > ac > aa$. The expectation is fulfilled for Mg and Mn olivines but not for Fe, Co and Ni olivines. In Fe olivine, although $\beta T,b$ is largest *ab* is smallest while in Ni and Co olivine *ab* plots in between *aa* and *ac*. This unusual behaviour can be related to the anisotropic behaviour of the axial thermal pressure $(\partial P/\partial T)V,i$ as this quantity is part of the thermodynamic identity $\alpha i = \beta T,i\ (\partial P/\partial T)V,i$. In the case of Mg and Mn olivine, $(\partial P/\partial T)V,i$ values are similar whereas for Fe olivine the anisotropy is pronounced reducing towards Co and Ni olivine. It is instructive to discuss the thermal expansion behaviour of Co and Ni olivine as a part of the transition element series. While Mn olivine with its isometrical (3d5) electron configuration exhibits only little anisotropy, this is much larger in Fe (3d6) olivine showing decreasing tendency towards Co (3d7) and Ni (3d8) olivine.

White GK, Roberts RB, Collins JG (1985) High Temp - High Press 17: 61-65

In-situ methods

P094

In situ synchrotron pair distribution function analysis of amorphous photocatalysts for hydrogen generation

E. Onur Sahin[1], G. H. Moon[1], H. Tüysüz[1], C. K. Chan[2], W. Schmidt[1], C. Weidenthaler[1]
[1]Max-Planck-Institut für Kohlenforschung, Heterogeneous Catalysis, Mülheim an der Ruhr, Germany
[2]Arizona State University, Materials Science & Engineering, Tempe, United States

The photocatalytic production of H_2 from water has been considered as a big challenge since the solar energy conversion efficiency is quite low for its practical applications. Among different photocatalysts, TiO_2 is an interesting candidate because the energy levels of the conduction band (CB) and valence band (VB) potential are suitable for overall water-splitting. In addition, low material costs, high durability, and the environmentally benign nature of the material make TiO_2 an attractive compound for photocatalysis. Very recently, we reported that amorphous TiO_2, prepared by the direct injection of Ti precursors into an aqueous solution containing 10 vol.% methanol and further irradiation with UV light, resulted in a high photocatalytic activity for H_2 production even higher than that of a commercial TiO_2 (P25).[1,2] Because the local structures of amorphous compounds are not accessible by conventional X-ray diffraction methods, local probes such as Pair Distribution Function analysis (PDF) are required.[3] In the present study we monitor the formation of TiO_2 and Ta_2O_5 based solid-state photocatalysts, their structures and the dependence of the degree of crystallization from the synthesis parameters by means of *in situ* XRD/PDF studies. Total scattering data were collected *in situ* using a photocatalytic setup installed on ID11 beamline at ESRF. Firstly, metal alkoxide precursors were added to a solution of methanol and water. After this the solution was pumped continuously from the reaction vessel through a flow cell and scattering data were collected. Turning on a UV light source realizes working conditions of catalysts in photocatalytic reactions. Changes of the color of the Ti catalysts from white to black are an indication for changes in the oxidation state which may also change the local structure.[1] Potential changes of the catalysts structures during UV irradiation were recorded with time. Application of additional characterization techniques including Raman spectroscopy, X-ray photoelectron spectroscopy, and electron microscopy are required to complete the picture of the state of the different photocatalysts.

P095

In situ cryocrystallisation of chiral liquids

N. Nöthling[1], R. Goddard[1], C. W. Lehmann[1], R. W. Seidel[2]
[1]Max-Planck-Institut für Kohlenforschung, Chemical Crystallography and Electron Microscopy, Mülheim an der Ruhr, Germany
[2]Martin-Luther-Universität Halle-Wittenberg, Institut für Pharmazie, Halle (Saale), Germany

The efficiency of asymmetric synthesis using chiral catalysts is conveniently determined by HPLC on chiral columns. This technique provides information about the relative concentrations of the enantiomers, but not their absolute configuration. The absolute configuration of chiral compounds is currently established using optical rotatory dispersion, vibrational circular dichroism, the use of chiral shift reagents in proton NMR and Coulomb explosion imaging [1]. Recently, we have had success in crystallising the industrially important feedstocks, anisole (*T*m = -37 °C) [2], acetic anhydride (*T*m = -73.1 °C) [3] and adiponitrile (*T*m = +1.9 °C) [4] by *in situ* crystallisation [5] in an open glass capillary using the technique of zone melting in a cold N2 gas stream. The crystal structure determinations yield important information about the intermolecular interactions that the molecules undergo. In extension of this work, we have crystallised small amounts (*ca.* 2 μl ≈ 2 mg) of the chiral liquids (*S*)-2-chloropropionic (*T*m = -3.1 °C) and (*S*)-2-methylbutyric (*T*m = -70 °C) acids by *in situ* cryocrystallography and confirmed their absolute configurations by determining the absolute structures of their crystals. We compare these crystal structures with those of (*R*) and (*rac*)-2-bromo-3-methylbutyric acids. In favourable cases, *in situ* cryocrystallography provides a rapid and non-invasive method of determining the absolute configuration of chiral liquids.

References

[1] P. Herwig *et al.*, *Phys. Rev.* **2014**, A90, 052503.
[2] R. W. Seidel, R. Goddard, *Acta Cryst.* **2015**, C71, 664-666.
[3] R. W. Seidel, R. Goddard, N. Nöthling, C. W. Lehmann, *Acta Cryst.* **2016**, C72, 753-757.
[4] R. W. Seidel, R. Goddard, N. Nöthling, C. W. Lehmann, *Acta Cryst.* **2017**, C73, 937-940.
[5] H. S. Kaufman, I. Fankuchen, *Rev. Sci. Inst.* **1949**, 20, 733-734; R. Boese, *Z. Kristallogr.* **2014**, 229, 595-601.

P096

In-situ analysis of ZnMn2O4 as High Performance Anode for Lithium-Ion Batteries

Z. Zhao[1], Q. Fu[1], A. Sarapulova[1], H. Ehrenberg[1], S. Dsoke[1]
[1]Karlsruhe Institute of Technology (KIT), Institute for Applied Materials-Energy Storage Systems, Eggenstein-Leopoldshafen, Germany

Spinel ternary transition metal oxides have received intensive attention as conversion electrode materials for electrochemical energy storage due to their high gravimetric/volumetric capacity. The tetragonal spinel ZnMn2O4 is included in this group of materials. As Zn can alloy with Li, ZnMn2O4 can deliver the high capacity of 1008 mAh g-1 in the first lithiation, and 784 mAh g-1 in the subsequent cycles. Considering also its safety and low cost, ZnMn2O4 became a promising anode material for Li ion batteries.

The electrochemical energy storage mechanism of this material is reported in literature. During the first lithiation, the spinel oxides are reduced to metallic nanoparticles embedded in an amorphous Li2O matrix. Then the metallic Zn reacts with Li to form the ZnLi alloy. During the following delithiation, firstly, ZnLi de-alloys and then the metallic Zn and Mn are oxidized to MnO and ZnO. The spinel ZnMn2O4 will not recover its initial status. However, the underlying reaction and phase transitions upon the initial lithiation has not been deeply investigated. In the present work, in situ XRD analysis has been applied to elucidate the process of the multi-steps lithium insertion.

According to the potential profile, three sections can be distinguished: (a) section I: uptake of the first 2 Li per formula unit, (b) section II: uptake of >2 Li until 11 Li per formula unit, (c) section III: uptake of >11 Li per formula until the end of lithiation. In section I, the beginning of Li uptake, a slight shift of the reflections occurred due to an expansion of the *a* axis and the shrinkage of the *c* axis. The intensity of the reflections exhibits no change indicating that the crystalline material is not converted into a new product at this stage. In section II, 9 Li per formula unit are inserted. Theoretically, 6 Li per formula unit should be inserted, so the extra 3 Li per formula unit are consumed to form SEI. The intensities of the patterns collected in this section decrease indicating the transformation of the crystal structure to amorphous phase. Some new weak peaks appear at the plateau of 0.5 V vs. Li/Li+, evidencing the formation of an interphase during the transformation. In section III, no reflection peaks are observed in the pattern, implying the amorphous structure of the Li2O and metallic Zn and Mn. At potential below 0.2 V vs. Li/Li+ one Li per formula unit is inserted indicating the formation of Li-Zn alloy.

Figure 1

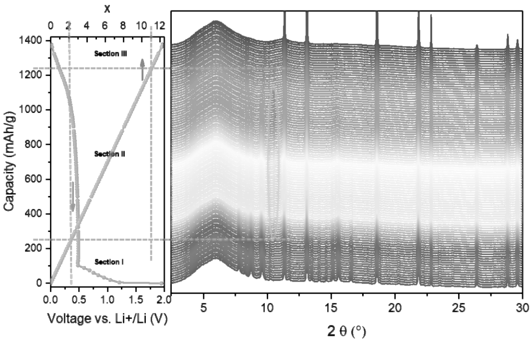

P097

Detecting the structural change and density anomaly in liquid iodides by in-situ synchrotron x-ray diffraction and absorption measurements under high pressures

K. Fuchizaki[1,2], N. Hamaya[3]
[1]Ehime University, Physics, Matsuyama, Japan
[2]The University of Tokyo, The Institute for Solid State Physic, Kashiwa, Japan
[3]Ochanomizu University, Graduate School of Humanities and Sciences, Tokyo, Japan

Recently, we have succeeded in detecting a density anomaly in liquid tin tetraiodide by in-situ synchrotron x-ray absorption measurements under high pressures [1]. The same technique allowed us to show firmly the existence of the liquid-liquid critical point in tin tetraiodide [2]. The technique has been developed through our synchrotron x-ray diffraction study for measuring in situ the pressure-induced liquid-liquid transition (LLT) in tin tetraiodide [3] and germanium tetraiodide [4]. Although the method was primarily developed for observing liquids, we believe that it is useful for solids as well.

The key ingredient for the method is a sample container, for which the following conditions must be required: i) It must have a strength for withstanding a high pressure applied. ii) It must be transparent to x rays. iii) It should not react with a sample. For density measurements, iv) it must be processed with high precision to determine the distance of a path along which x rays travel, whereas, for diffraction measurements, the Bragg peaks from the container should not "interfere" with the halo from the liquid. We have finally arrived at to find diamond that satisfies all the conditions listed above.

Because diamond is not deformed, a part that can transmit pressure is a cover, for which we employed pyrolytic BN (PBN), a substance with the following quite interesting feature; although PBN is hard at room temperature, it becomes flexible when the temperature exceeds about 500 K. It is then possible to increase pressure not by loading but by increasing temperature (see Fig. 4 of [5]). It thus permits us to control subtly pressure with relative ease. A way of estimating pressure inside the container was described in [5].
The method introduced here must be useful for measuring in situ a chemically active sample at a high temperature when subtle control of pressure is required.

References

[1] K. Fuchizaki *et al.*, Talk presented at StatPhys26, July 18-22, 2016, Lyon, France; in preparation.
[2] K. Fuchizaki *et al.*, Talk presented at 54th EHPRG, September 4-9, 2016, Bayreuth, Germany; in preparation.
[3] K. Fuchizaki *et al.*, J. Chem. Phys. **135**, 091101 (2011).
[4] K. Fuchizaki *et al.*, J. Phys.: Condens. Matter, in press.
[5] K. Fuchizaki and N. Hamaya, Phys. Rev. B **84**, 144105 (2011).

P098

Following the effects of micelle expanders on SBA-15 synthesis with *in-situ* SAXS

H. Rasmussen[1], F. Mariano-Neto[2,3], M. C. d. A. Fantini[4], C. L. Oliveira[3]
[1]University of Aarhus, Department of Chemistry and iNANO Interdisciplinary Nanoscience Center, Aarhus, Denmark
[2]Universität Duisburg-Essen, Institut für Anorganische Chemie, Essen, Germany
[3]University of São Paulo, Institute of Physics - Department of Experimental Physics, São Paulo, Brazil
[4]University of São Paulo, Institute of Physics - Department of Applied Physics, São Paulo, Brazil

Introduction

The synthesis of ordered mesoporous silica SBA-15 has been studied ever since it was first discovered in 1998. The large pores present in this material make it possible for its application in several areas, such as biotechnology and electronics. The addition of micelle expanders might present an alternative way to larger pores, but at the same time the narrow pore size distribution and the ordering of the pores that SBA-15 is well known for are lost.

Objectives

The objective of this work is to follow the synthesis process of the SBA-15 silica using Small Angle X-ray Scattering, and determining the experimental parameters of the material as it is being formed. That is made possible by a theoretical model that takes into account both the spatial ordering and the morphology of the cylindrical micellar structures formed by the Pluronic P123 polymer during the process2,3. We also investigate the behavior of these structures when micelle expanding substances are added, notably TMB (trimethylbenzene) and TIPB (triisopropylbenzene).

Results

The theoretical model was fitted with a least-squares procedure. The evolution of the curves indicates clearly when the transition occurs from separate structures into a more ordered, hexagonal phase. From the time when it occurs, this process seems to be triggered by the addition of the silica source (TEOS). The same effect is observed in the samples with micelle expanders.

Conclusion

From the evolution of the fit parameters during the synthesis time, it is possible to characterize the behavior of the system when different proportions of micelle expanders are used. In this way, one can tune the pore sizes according to the desired application.

References

[1] Zhao, D. et al. Triblock copolymer syntheses of mesoporous silica with periodic 50 to 300 angstrom pores. Science (80-.). 279, 548–52 (1998).
[2] Sundblom, A., Oliveira, C. L. P., Palmqvist, A. E. C. & Pedersen, J. S. Modeling in situ small-angle X-ray scattering measurements following the formation of mesostructured silica. Phys. Chem. C 113, 7706–7713 (2009).
[3] Sundblom, A., Oliveira, C. L. P., Pedersen, J. S. & Palmqvist, A. E. C. Decoupling particle formation from intraparticle ordering in mesostructured silica colloids. Microporous Mesoporous Mater. 145, 59–64 (2011).

Fig.1: SAXS curves obtained for the *insitu* study of SBA-15 synthesis.

Figure 1

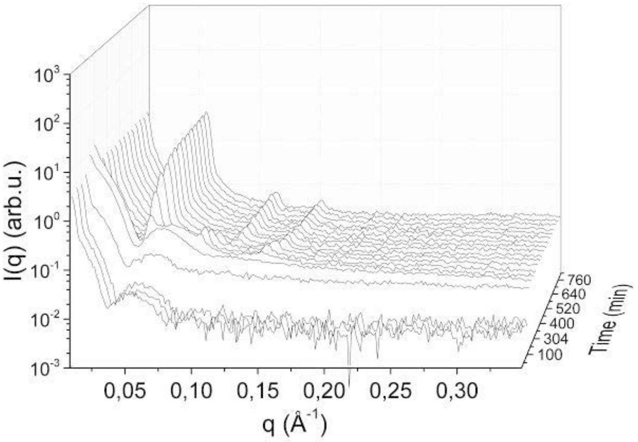

P099

Low temperature X-ray investigations on silver-based Kesterites

M. Tovar[1], G. Gurieva[1], S. Schorr[1,2]
[1]Helmholtz-Zentrum Berlin, Berlin, Germany
[2]Freie Universität Berlin, Berlin, Germany

Using a Guinier diffractometer for low temperature X-ray powder diffraction allows most accurate investigations of lattice parameters at non-ambient conditions. Therefore, we are able to trace subtle changes in cell metrics such as cell parameter deviations or symmetry breaking. In this contribution, we will apply this technique to kesterite-type solar absorber materials, especially silver-based. For Kesterite-type materials unusual thermal behaviour like negative thermal expansion is reported (1). Outcome of low temperature X-ray investigations of $(Ag,Cu)_2ZnSnSe_4$ will be presented and compared to formerly results.

References

[1] Schorr, S., Sheptyakov, D., J. Phys.: Condens. Matter 20 (2008), 104245

Figure 1

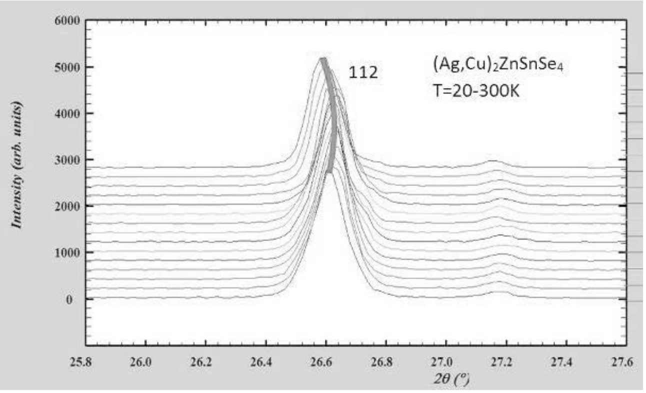

Electron microscopy

P100

Ab-initio Calculations of electronic structure of TlInS2

N. Ismayilova[1]
[1]Azerbaijan National Academy of Sciences, Institute of Physics, Baku, Azerbaijan

Abstract

The electronic structure was calculated for TlInS2 from first principle. In the literature there are some experimental data about electronic spectrum of the crystal TlInS2. In Ref. [1, 2, 3] authors have obtained the optical indirect gap of Egi =2.27 eV and the direct gap of Egd =2.47 eV. In contradiction with these works, experimental works [4, 5] reveals that it is direct gap semiconductor with energy gap Eg =2.25 eV. But in the literature there are no theoretical data on the electronic structure of the crystal. Taking this into account in this paper presented theoretically investigations of electronic structure of crystal.

Method and result

Calculation carrid out by implementing the Density Functional Theory (DFT) [6] method within the Local Density Approximation (LDA) [7] and using the Atomistix Tool Kit program software (ATK, http://quantumwise.com/). The electron-ion interactions were taken into account through pseudopotentials Hartwigsen–Goedecker– Hutter (HGH). The wave function was expanded taking into account plane waves with energies up to 150 Ry, which provided a good convergence of the total energy. The primitive cell of TlInSe2 was optimized with force and stress tolerances of 0.0001 eV/Å and 0.0001 eV/Å3 respectively.

Fig.1 Calculated electronic structure of compound TlInS2

Calculation of the electronic structure with LDA reveals that TlInS2 is a direct gap semiconductor with a direct energy gap. Such that the VBM and CBM are located at the Γ-point of the BZ. Calculated electronoc structure (Figure 1) has been shown that band gap of compound is Eg=1.43 eV.

References

[1] Hanias M.P., Anagnostopoulos A.N., Kambas K., Spyridelis J. Physica *B*, 1989, v. 160, p.154-160
[2] El-Nahass M.M., Sallam M.M. Egypt. J. Solids, 2008, v.31, No.1, p.31-44
[3] El-Nahass M.M., Sallam M.M., Abd Al-Wahab A.H.S. Current Applied Physics 2009, v.9, p.311–316
[4] Kalomiros J.A., Anagnostopoulos A.N. Phys. Rev. B, 1994, v.50, No.11, p.7488-7494
[5] Allakhverdiev K.R., Mammadov T.G., Suleymanov R.A., Gasanov N.Z. J. Phys., Condens. Matter, 2003, v.15, No.8, p.1291-1298
[6] P. Hohenberg, W. Khon. Phys. Rev. B 136, 864 –871. (1964)
[7] W.Kohn, L.Sham. *Phys.*Rev., 140 (1965) A1133–A1138.

Figure 1

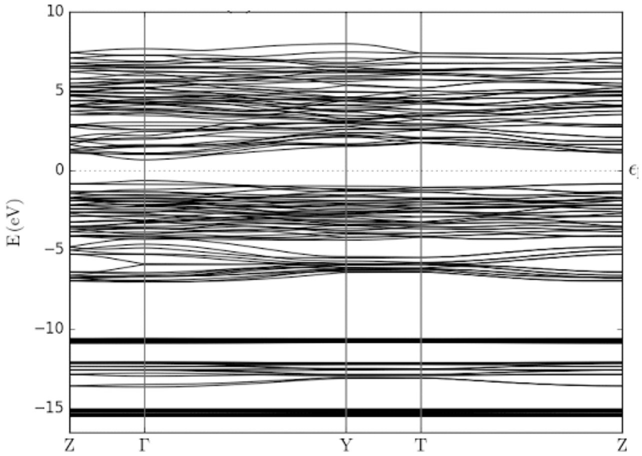

P101

Transrotational structure with complicated lattice misorientations revealed by TEM for 2 kinds of spherulites growing in amorphous films

V. Kolosov[1]
[1]Ural Federal University, Institute of Natural Sciences & Mathematics, Ekaterinburg, Russian Federation

Last 30 years the growing interest for synthesis and studies of objects, structures with unusual for condensed matter atom packing is observed starting from the findings of quasicrystals, fullerenes and nanotubes.

This paper presents some experimental results for the formation and microstructure on the nano-, meso-, and microscale of the other less-known "**transrotational**" microcrystals discovered for diverse films of semiconductors, oxides and metals produced by different methods. We focus on the complicated crystallographic orientations for 2 type of spherulites observed. The main data is obtained by diffraction transmission electron microscopy (TEM), primarily bend-contour method.

It was shown earlier [1] that the growth of crystals in nanothin amorphous films (below 100 nm) is often accompanied by strong (up to 100 degrees per 1 μm) internal "crystal lattice bending" of non-dislocational nature. Up to now the phenomenon has been revealed for many substances and materials of different chemical bonding and various preparation conditions (Se-C, Se-Te, Sb, Sb2Se3, Sb2S3, Ge-Sb_2Se_3, Ge-Te, Tl-Se, Cu-Te, α-Fe_2O_3, Cr_2O_3, Co-Pd, Re, W, amorphous metals, ferroelectrics, phase change materials and some other. For such extraordinary microcrystals the new term "**transrotational**" crystals was introduced [2] since the **trans**lation of the crystal unit cell is accompanied by slight permanent **rotation** (up to ~ 0,1 degrees per unit cell) around the axis lying in the film plane. In the rather usual case of spherulites growing in thin films the azimuthal misorientations are thus complicated by such "transrotation" and very complex textured crystalline aggregates are formed in result. Main features of crystallographic orientations are shown below, Figs.1-2 (better seen in colors). For the last case skyrmion- like order for [001] can be stated.

References

[1] Bolotov I.E., Kolosov V.Y., Kozhyn A.V.*Phys. Stat. Sol.*1982, 72a, 645.
[2] Kolosov V.Yu., Tholen A.R. Acta Mater. 2000,48, 1829.

Fig. 1. Spherulite (hexagonal Se) with regular perturbation around 2 poles where [001] is normal to the film plane. At the nucleation center in between poles [001] is parallel to the film plane as it is

also everywhere at the periphery of the growing crystal (around the central area including the poles).

Fig.2. Spherulite (α-Fe_2O_3) with alternating circular single-crystalline ([001] tends to be normal to the film) odd zones and fine-grained ([001] is close to the film) even zones.

Figure 1

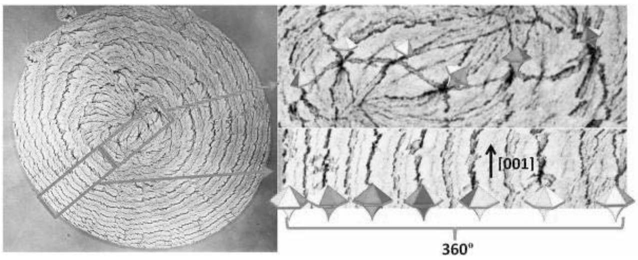

Figure 2

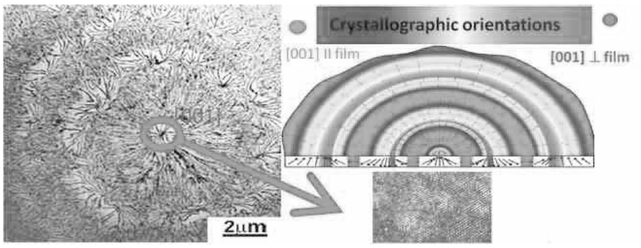

Experimental electron density

P102

Topological Analysis of two [2]Catenanes based on Electron Densities from Invariom Refinements

P. Luger[1], B. Dittrich[1]
[1]Freie Universität Berlin, Institut für Chemie, Berlin, Germany

The catenanes are currently of increasing interest as potential building blocks of molecular machines. In their smallest forms as [2]catenanes they consist of two macrocycles which are mechanically interlocked. This unusual structural architecture cannot be opened without breaking at least one covalent bond. This "non-covalent" interaction allows a high mutual mobility of the contributing molecules, which can be exploited in the design of larger mobile systems.

As far as we know an electron density (ED) study in this class of compounds has not been reported, although based on the unique structural characteristics unusual topological properties and Hirshfeld or electrostatic potential (ESP) surfaces would make such study interesting. We carried out invariom based ED studies [1] on the data sets of the [2] catenane coded H22 in ref. [2], and the [2]catenane coded H4L7 in ref. [3]

The intra and intermolecular interactions are characterized not only by classical N-H···N and C-H···O hydrogen bonds, but also by C-H···π and π ·· π interactions, most of them are verified by local electron density concentrations visible on the corresponding Hirshfeld surfaces. Inspection of the ESP"s on iso-electron density surfaces is in progress.

References

[1] B. Dittrich et al., *Acta Crystallogr.*, **2013**, B69, 91 – 104.
[2] D. A. Leigh, P. J. Lusby, A. M. Z. Slawin, D. B. Walker, *Angew. Chem. Int. Ed.*, **2005**, *44*, 4557 - 4564.
[3] D. A. Leigh et al., *J. Am. Chem. Soc.*, **2009**, *131*, 3762 - 3771.
[4] C. B. Hübschle, P. Luger, *J. Appl. Crystallogr.*, **2006**, *39*, 901-904.

Fig. 1.Left: Hirshfeld surface of molecule 2 of H4L7, molecule 1 is shown in ball and stick form, right: ESP surface of mol. 2 of H22, MOLISO representations [4]

Acknowledgement: We thank Prof. A. Slawin, Univ. of St. Andrews, and Prof. D. Leigh, Univ. of Manchester, for the X-ray data of H22 and H4L7.

Figure 1

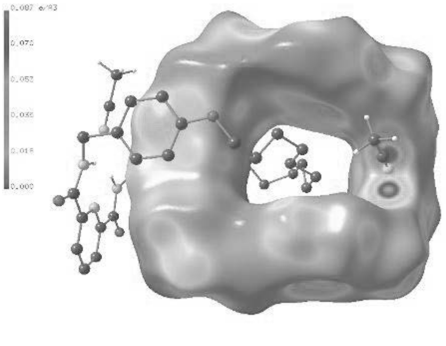

Moliso (c) 2007 Christian B. Hübschle

Figure 2

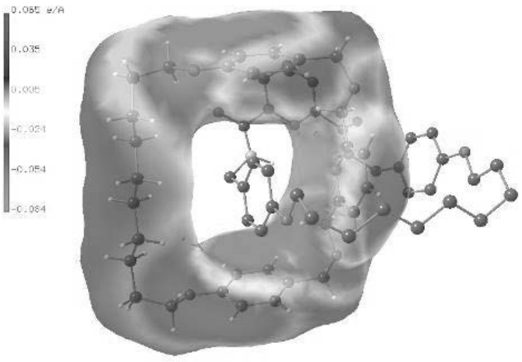

Moliso (c) 2007 Christian B. Hübschle

P103

Charge Density Analysis of Cobalt(II) phosphate

H. Keil[1], D. Stalke[1], R. Herbst-Irmer[1]
[1]Georg-August Universität Göttingen, Institut für Anorganische Chemie, Göttingen, Germany

Cobalt phosphate can be applied as a catalyst in the oxidative dehydrogenation of ethane and propane [1] as well as in the oxidation of water in the presence of solar light [2] – to name just a few examples. In order to learn more about the properties of cobalt phosphate and to make an attempt to understand its catalytic effect, we embarked on an experimental charge density analysis. Suitable crystals were obtained from the melt and high resolution X-ray diffraction data up to 0.3 Å were collected on our home Ag microfocus source. After structure refinement based on the Hansen-Coppens multipole model [3] the charge density distribution was analysed according to Bader´s Quantum Theory of Atoms in Molecules (QTAIM) [4]. The different coordination geometries and electron density distributions of the two cobalt atoms in the asymmetric unit hint at various catalytical activities. VSCCs (valence shell charge concentrations) around the cobalt atoms are shown in Figure 1. They correspond to the maxima of the electron density concentration around the metal. Due to the high resolution, it was also possible to analyse the d-orbital population of the cobalt atoms.

References

[1] Aaddane, M. Kacimi, M. Ziyad, *Cat. Let.,* 2001, 73, 47–53.
[2] W. Kanan, J. Yano, Y. Surendranath, M. Dinca, V. K. Yachandra, D. G. Nocera, *J. Am. Chem. Soc,* 2010, 132, 13692–13701.
[3] K. Hansen, P. Coppens, Acta Crystallogr. 1978, A34, 909-921.
[4] F. W. Bader, Atoms in Molecules: A Quantum Theory. 1990, Oxford.

Figure 1

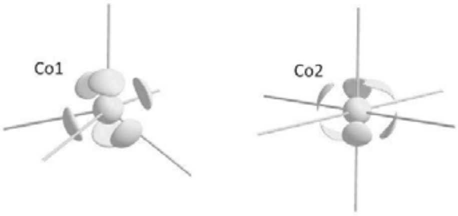

P104

Experimental Charge Density Study of Alkyllithium Compounds

A. Münch[1], D. Stalke[1], R. Herbst-Irmer[1], L. Knauer[2], C. Strohmann[2], H. Ott[3]
[1]Georg-August Universität Göttingen, Institut für Anorganische Chemie, Göttingen, Germany
[2]Technische Universität Dortmund, Institut für Anorganische Chemie, Dortmund, Germany
[3]Bruker AXS GmbH, Chemical Crystallography, Karlsruhe, Germany

Organolithium compounds are used widely in organic as well as inorganic syntheses. Their ambiguous character underlines this importance as they might be employed as strong bases or as nucleophiles. Due to their strongly polarized carbon lithium bond, organolithium compounds tend to form aggregates which tempers their reactivity.[1] Over the past years, this structure/reactivity relationship was in the center of interest.[2] For understanding their reactivity, the investigation of the molecular and electronic structure of reactive species is of great importance. Herein, we present the first experimental charge density analysis of aggregates of tert-butyllithium and iso-propyllithium with the rigid monodentate donor ligand quinuclidine. High-resolution single crystal X-ray data were used for a multipole refinement according to the Hansen & Coppens method.[3] The topological analysis based on QTAIM by Bader gives insight to the bonding situation of the carbon lithium contact.[4]

References

[1] T. Stey, D. Stalke, *The chemistry of organolithium compounds* **2004**.
[2] a) H. Ott, C. Däschlein, D. Leusser, D. Schildbach, T. Seibel, D. Stalke, C. Strohmann, *J. Am. Chem. Soc.* **2008**, *130*, 11901 - 11911; b) V. H. Gessner, C. Däschlein, C. Strohmann, *Chem. Eur. J.* **2009**, *15*, 3320; c) C. Strohmann, V. H. Gessner, *Angew. Cje,. Int. Ed* **2007**, *46*, 8281.
[3] N. K. Hansen, P. Coppens, *Acta Crystallogr. A, Foundations of crystallography* **1978**, *34*, 909.
[4] a) R. F. W. Bader, *Chem. Rev.* **1991**, *91*, 893; b) R. F. W. Bader, *Atoms in Molecules. A Quantum Theory*, Clarendon Press, Oxford, New York, **1990**.

Figure 1

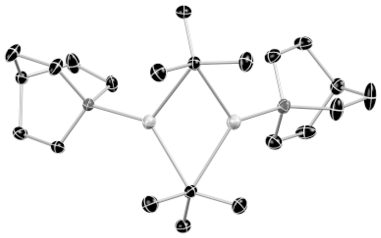

Figure 2

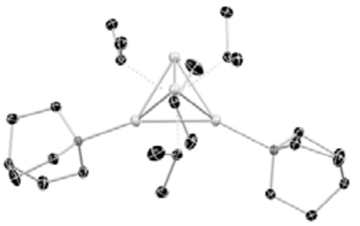

P105

Comparison of Different Strategies for Modelling Hydrogen Atoms in Charge-Density Analysis

C. Köhler[1], D. Stalke[1], J. Lübben[1], L. Krause[2], R. Herbst-Irmer[1]
[1]Georg-August Universität Göttingen, Institut für Anorganische Chemie, Göttingen, Germany
[2]Aarhus University, Department of Chemistry, Aarhus, Denmark

This work compares the quality of various approximation methods for modelling anisotropic displacement parameters (ADPs) and C-H bonding distances of hydrogen atoms in charge-density investigations with results derived from neutron data. While hydrogen atom parameters based on neutron diffraction experiments are commonly regarded as "gold standard", these experiments can only be conducted at a small number of highly specialized institutions in the world.

Figure 1: Structures of used model compounds.

A multipole refinement[1] was performed against high-resolution X-ray data of 9-diphenylethiophosphanyleanthracene (**1**) and 9,10-bis-diphenylethiophosphanyleanthracene (**2**). Hydrogen atom parameters derived from our collected neutron data sets were compared with those obtained from the SHADE-server[2], the software APD-Toolkit[3] based on the INVARIOM[4] database and the results of anisotropic hydrogen refinement. Surprisingly, the hydrogen ADPs obtained from refinement against X-ray data turned out to yield the smallest deviations from neutron data. However, the refinement of bond directed quadrupole parameters turned out to be critical for the quality of the resulting ADPs. In both model structures, SHADE and to a lesser extent APD-Toolkit showed problems in dealing with hydrogen atoms bonded to carbon atoms with refined Gram-Charlier parameters[5].

The unconstrained refinement of hydrogen atom positions against X-ray data with ADPs derived from all used approximation methods showed that even with well approximated hydrogen ADPs the resulting C-H bonding distances were still significantly underestimated.

References

[1] N. K. Hansen, P. Coppens, *Acta crystallographica. Section A, Foundations of crystallography* **1978**, *34*, 909.
[2] A. O. Madsen, A. A. Hoser, *J Appl Crystallogr* **2014**, *47*, 2100.
[3] J. Lübben, L. J. Bourhis, B. Dittrich, *J Appl Crystallogr*, **2015**, *48*,1785.
[4] B. Dittrich, C. B. Hübschle, K. Pröpper, F. Dietrich, T. Stolper, J. J. Holstein, *Acta Crystallographica Section B-Structural Science* **2013**, *69*, 91.
[5] C.K. Johnson, H. A. Levy in *International Tables for X-ray Crystallography*, Kynoch Press, Birmingham, **1974**, pp. 311-336.

Figure 1

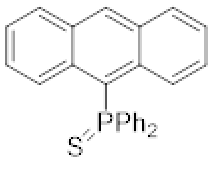

1

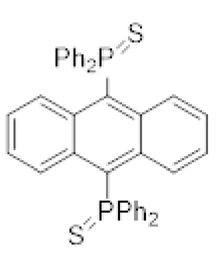

2

P106

Halogen bonds involving TFDIB: Answers from experimental electron density

R. Wang[1], D. Hartnick[1], M. Kremer[1], I. Karl[1], U. Englert[1]
[1]RWTH Aachen, Institute of Inorganic Chemistry, Aachen, Germany

A "halogen bond" denotes a short contact between an electron donor D and a halogen atom X as the electrophile [1]. The electrophile is usually approached by the donor in a region of depleted electron density opposite to its s bond, the so-called "s hole". Tetrafluorodiiodobenzene (TFDIB, Scheme below) and DMAPY and DABCO represent particularly well-suited partners for halogen bonds (N…I-C in almost linear geometry).

To understand the halogen bonds involving TFDIB [2,3], intensity data are accurately measured at low temperature (100K) and up to high resolution. Multipole refinement [4,5] and interpretation of the experimental electron density have been done according to Bader's *AIM* theory [6].

Acknowledgement: We gratefully acknowledge financial support by DFG (project EN309/10-1: Experimental electron density of halogen bonds and interhalogen contacts).

References

[1] P. Metrangolo, G. Resnati, *Chem. Eur. J.* **2001**, 7, 2511.
[2] M. Bolte, *CSD Communication (Private Communication),* **2004**.
[3] L. C. Roper, C. Prasang, V. N. Kozhevnikov, A. C. Whitwood, P. B. Karadakov, D. W. Bruce, *Cryst. Growth Des.* (**2010**) 10, 3710
[4] N. K. Hansen, P. Coppens, *Acta Crystallogr. Sect. A* **1978**, 34, 909.
[5] A. Volkov; P. Macchi; L. J. Farrugia; C. Gatti; P. Mallinson; T. Richter; T. Koritsanszky, *XD2016*, **2016**.
[6] R. F. W. Bader, *'Atoms in Molecules - a Quantum Theory'*, Clarendon Press, **1990**.

Figure 1

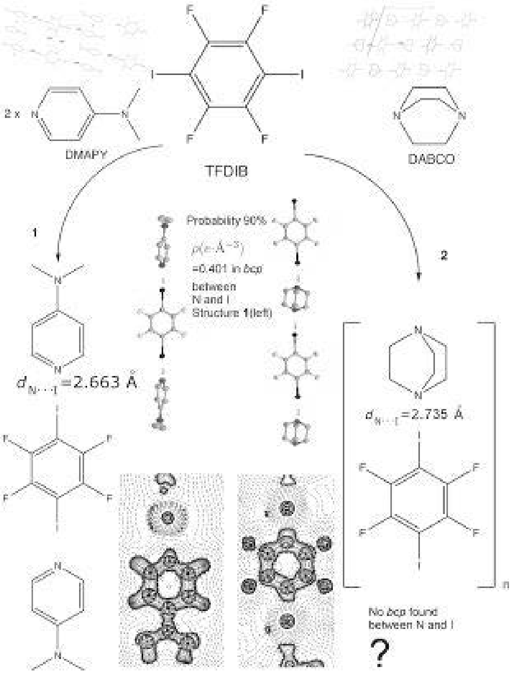

Spectroscopic methods in crystallography

P107

Substitution and doping in iron pnictides

M. Merz[1], P. Nagel[1], M. J. Huang[1], R. Eder[1], T. Wolf[1], S. Schuppler[1]
[1]Karlsruhe Institute of Technology (KIT), Institut für Festkörperphysik, Eggenstein-Leopoldshafen, Germany

For insight into the composition-dependent electronic structure of iron pnictides, we performed a systematic study of spatial structure and electronic states by x-ray diffraction and x-ray absorption. A large number of compositions in the $(Ba,Sr,AM)(Fe,TM)_2(As,P)_2$ family of compounds was investigated, covering the substitution of Ba by Sr or alkali metals (AM); of Fe by transition metals (TM); and of As by P. Our observations on doping effects upon such substitutions include "reluctant" doping (charge carriers are only partially transferred away from the substituent) or "site-decoupled" doping (transferred charge carriers affect either Fe sites or As sites but not both). Here, we focus on isovalent substitutions and on substitutions with high Ni content. The energy-level schemes derived from electronic and spatial structure differ from the "standard" ones in ways that may help explain the systematics in these substitution systems. Indirect, structural effects of substitution appear to be more important for magnetism and superconductivity in iron pnictides than the direct, charge-carrier doping effects.

P108

Application of Raman spectroscopy for identification of anhydrous $CaCl_2$, $KCaCl_3$ and $K_3NaFeCl_6$ in natural inclusions

S. Grishina[1], P. Kodera[2], L. Uriarte[3], A. Oreshonkov[4], Y. Maximovich [1], E. Roginskii[5], F. Imko[6]
[1]Sobolev Institute of Geology and Mineralogy Siberian Branch of the Russian Academy of Sciences, Mineralogy, Novosibirsk, Russian Federation
[2]Comenius University, Economic Geology, Bratislava, Slovakia
[3]Université de Lorraine, GeoRessources laboratory, Vandoeuvre-lès-Nancy, France
[4]Kirensky Institute, Krasnoyarsk, Russian Federation
[5]St.Petersburg State University, Ioffe Institute, St. Petersburg, Russian Federation
[6]Slovak Academy of Sciences, Institute of Inorganic Chemistry, Bratislava, Slovakia

Anhydrous chlorides - $CaCl_2$, $KCaCl_3$ (chlorocalcite) and $K_3NaFeCl_6$ (rinneite) were identified as mineral inclusions in halite from the Siberian Large Igneous Province at the contact of magmatic intrusions and evaporates. Chlorocalcite was also found as daughter mineral in polyphase hypersaline inclusions. While Raman spectra of $KCaCl_3$ (chlorocalcite) in natural inclusions are similar to spectra of synthetic analogue, the Raman spectra of natural $CaCl_2$ do not correspond to the published Raman spectra of synthetic $CaCl_2$. Simulations of Raman spectra using *ab initio* density-functional theory (DFT) allowed us to calculate the spectra of individual polymorphs of $CaCl_2$ and to discriminate anhydrous $CaCl_2$ phases in natural inclusions and synthetic $CaCl_2$. In the spectrum of the Pbcn polymorph of $CaCl_2$ twelve different peaks could be identified at 74, 95, 99, 107, 124, 158, 164, 179, 212, 236, 244, 256 cm-1 in contrast to five peaks in the spectrum of the Pnnm polymorph of $CaCl_2$ at 115, 157, 160, 211 and 252 cm-1. Naturally occurring $CaCl_2$ in inclusions in halite consist of Pbcn polymorph only, which probably results from a mechanical stress on cooling from magmatic to ambient temperatures. However, the Raman spectra of the synthetic $CaCl_2$ corresponds to the Pnnm phase with small contributions of the Pbcn phase.

Raman spectra of the synthetic $KCaCl_3$ with main peaks at 58, 67, 90, 97, 133, 139, 147, 193 cm-1 agrees well with the spectra of chlorocalcite in the natural inclusions. Positions of each atom in the $KCaCl_3$ structure were refined using the density-functional theory. There are no imaginary phonon modes for the optimized structure, indicating that the structure of $KCaCl_3$ is stable. Calculated Raman spectrum is in a good agreement with the Raman spectrum of synthetic $KCaCl_3$.

In this study we show different Raman spectra of $CaCl_2$ polymorphs and very similar spectra of isostructural rinneite ($K_3NaFe^{2+}Cl_6$) and saltonseaite ($K_3NaMn^{2+}Cl_6$).

This work is financialy supported by the Russian Foundation for Basic Research (grant no. 15-05-09345, 18-05-00682) and VEGA grant 1/0560/15.

Structurally complex materials

P109

Magnons in the multiferroic phase of cupric oxide

F. Ziegler[1], S. Schwesig[1], O. Sobolev[1], A. Maity[1], G. Eckold[1]
[1]Georg-August Universität Göttingen, Institute of Physical Chemistry, Göttingen, Germany

Introduction

Cupric oxide (Cu(II)O) has attracted renewed interest over the last years after the existence of a high-temperature multiferroic phase was discovered. Unlike other multiferroics with phase transition temperatures well below 50 K, CuO shows multiferroic behaviour in the incommensurate antiferromagnetic phase already in the temperature regime between 230 and 213 K.

Objective

The magnetic structure of the multiferroic phase is characterised by a cycloidal spin arrangement in contrast to the collinear antiferromagnetic low-temperature phase. However, not much is known about the magnetic dynamics of the incommensurate phase, since only magnons at temperatures below 213 K were studied so far. We therefore performed an inelastic neutron scattering study in the multiferroic phase as well as in the low-temperature phase for comparison. For all investigations, we used the new neutron polarisation analysis of PUMA@FRMII [1]. With this setup, it is possible to detect both spin states of the neutron beam simultaneously. Measurements in different Brillouin-zones allow us to distinguish magnons with different polarisation which helps for a better understanding of the individual excitations.

Results

As an example, Fig.1 shows the results of a constant-Q-scan up to 15 meV at the position of the magnetic satellites within the (002)-Brillouin zone in the multiferroic phase. The red circles (spin flipped neutrons) correspond to a magnon polarised perpendicular to the cycloidal plane with a pronounced spin band gap of about 4 meV. Non-spinflip scattering (black squares) shows a different behaviour without any sign of a spin gap. This magnon can be attributed to a phason mode of the spin cycloid. It is equivalent to the magnon spectra observed in the Brillouin zone (-202) depicted in Fig.2 where the intensity in both channels, spin flip as well as non-spin flip, corresponds to the same excitation polarised within the cycloidal plane.

Conclusion

In conclusion, we are able to present the first spectra of magnons in the multiferroic phase of cupric oxide ever observed. Furthermore, the polarisation analysis allows us to assign all magnons observed in different Brillouin-zones and both antiferromagnetic phases.

References

[1] Schwesig S., Maity A., Sobolev O., Ziegler F. and Eckold G. 2018 *Nuclear Instruments and Methods in Physics Research Section A* **877** 124.

Figure 1

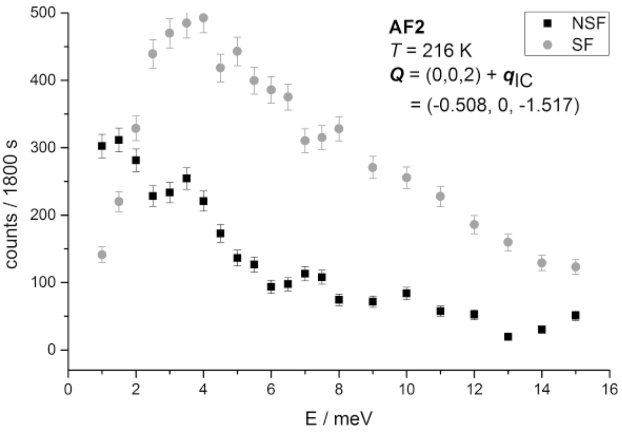

Figure 2

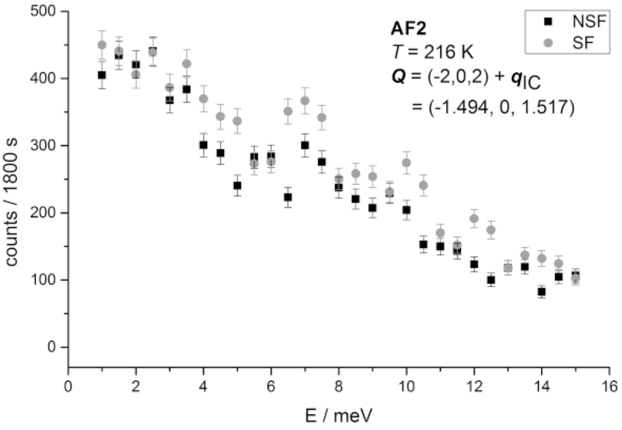

P111

The phonon density of states (PDOS) and the crystal growth of deuterated bis-2-phenylethylamine-$CuCl_4$, -$MnCl_4$ ($(PEA)_2CuCl_4$, $(PEA)_2MnCl_4$) and their mixed crystals

M. Schomber[1], H. Gibhardt[1], J. Park[2], I. H. Oh[3], W. Lohstroh[2], G. Eckold[1]
[1]Georg-August Universität Göttingen, Institute of Physical Chemistry, Göttingen, Germany
[2]Heinz Maier-Leibnitz Zentrum, München, Germany
[3]Korea Atomic Energy Research Institute, Daejeon, South Korea

Introduction

$(PEA)_2CuCl_4$ and $(PEA)_2MnCl_4$ and their mixed crystals provide interesting systems for thermoelectric applications. This is due to its layered crystal structure provided by MCl_6 corner-sharing octahedra (with M = Cu, Mn) separated by large organic spacer molecules as shown in Fig. 1[1]. The space group of both compounds is Pbca at ambient conditions. The dynamical properties of this complex system have been studied using inelastic neutron as well as optical Raman scattering.

Objectives

The thermoelectric figure of merit is essentially determined by the competing effects of the electric and thermal conductivities. While the former is almost confined to the electronic properties of the inorganic layers, the latter is determined by the propagation of phonons. The large organic spacer molecules are supposed to act as efficient damping elements that reduce the thermal conductivity. Moreover, it is expected that the thermoelectric performance can be improved by the substitution of the transition metals.

Results

First Raman-results obtained from large single crystals are presented which provide information of low lying Gamma-point optical modes. Moreover, the PDOS is obtained by incoherent neutron scattering from hydrogen atoms of the organic spacer molecules using the Time-of-Flight spectrometer (TOFTOF) at the FRM2 in Garching/Munich. The TOFTOF data show a strong temperature dependence of the inelastic neutron scattering (INS) which indicates a strong anharmonicity and therefore an efficient damping of phonons which are responsible for the thermal conductivity. More detailed information about the low-frequency dynamics can be expected from coherent scattering experiments from deuterated single crystals. We have obtained a deuteration grade of more than 90%, as confirmed by ^{1}H-NMR spectroscopy, using the deuteration reaction of PEA with the mixed Pd/C-Pt/C catalyzers. Platelet single crystals with dimensions of a few mm edge lengths and up to 1mm thickness were obtained from aqueous solution.

Conclusion

We report on phonon investigations of PEA-$CuCl_4$ and PEA-$MnCl_4$ using INS and light scattering which help to understand the basic mechanisms of the thermal conductivity. Furthermore an efficient route for the deuteration of PEA and the crystal growth of deuterated PEA-$CuCl_4$ for further investigation with coherent neutron scattering is shown.

Fig. 1: $(PEA)_2MCl_4$, M = Cu, Mn

References

[1] A. Polyakov, A. Arkenbout, Chem. Mater., **24**, 133 (2012)

Figure 1

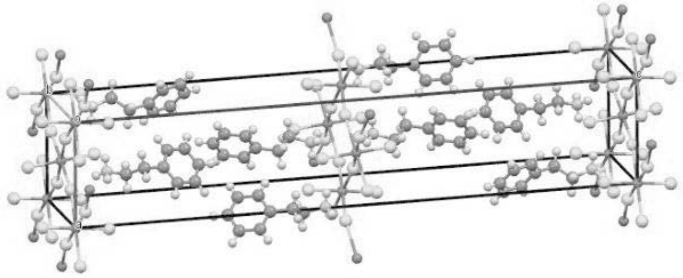

P112
Jump Rate and Jump Length in a Triple Well Potential

M. Ouahmane[1], L. Arfa[1], L. Elarroum[1]
[1]Ben M'sik University Hassan II Casablanca, Faculty of Science, Casablanca, Morocco

The diffusion mechanism of Brownian particles non interaction in a triple-well potential is studied using the Fokker-Planck equation (FPE). The FPE is solved numerically by the matrix continued fraction method (MCFM). The main objective of this work is to study the effect of the structure of the potential on the diffusion by calculating the jump rate and the probability distribution of the jump lengths as function of friction for different values of ration of the barrier height of the potential are presented.

P113
Cyclic Coordination Compounds "Donuts" and their Host-Guest-Complexes with Fullerenes

C. Göb[1], L. Sturm[1], T. Sato[1], I. Oppel[1]
[1]RWTH Aachen, Institute of Inorganic Chemistry, Aachen, Germany

C_3-symmetric triaminoguanidinium based ligands are able to coordinate soft metal ions like Pd(II), Cd(II) or Eu(III) as well as hard metal ions like Ti(IV) or Zr(IV) in their trisdentate chelating [NNO] binding pockets.[1] As the combination of ligands and metal ions provides flexible coordination environments, a variety of different discrete supramolecular coordination cages, such as tetrahedra, octahedra and trigonal bipyramids, are accessible. Some of these compounds showed activity in ring opening polymerization of lactide. Several cyclic coordination compounds using Zn(II) ions were synthesized in a self-assembly process in the presence of (pseudo-)halides and a base. The resulting products exhibit large cavities which can incorporate guest molecules like fullerene C_{60} and C_{70}.[2]

References

[1] C. Von Eßen, C. R. Göb, I. M. Oppel, *Top. Heterocycl. Chem.* **2015**.
[2] C. R. Göb, L. Sturm, T, Sato, Y. Tobe, I. M. Oppel, *manuscript in preparation.*

Figure 1

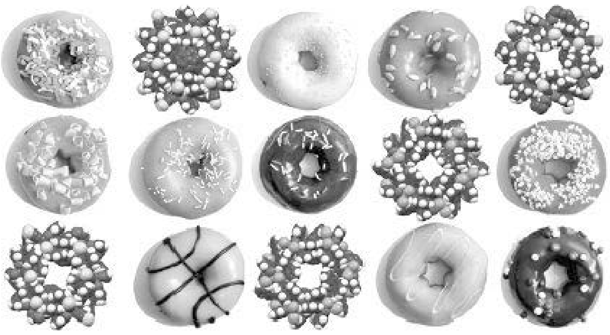

P114
Comparisons of the microstructure from two bivalve shells: *Pinctada martensii* and *Anodonta cynea*

J. He[1], E. Griesshaber[2], W. W. Schmahl[2], U. Bismayer[1]
[1]Universität Hamburg, Mineralogisch-Petrographisches Institut, Hamburg, Germany
[2]Ludwig-Maximilians-Universität München, Department of Earth and Environmental Sciences and GeoBioCenter, München, Germany

Biominerals, such as mollusc shells, often present a highly ordered organic-inorganic hierarchical structure, which has been the main interest of study in biomineralization. In this work, the shells of two bivalve species from different living habitats have been studied with SEM, microprobe and advanced EBSD measurements. Electron backscatter diffraction (EBSD) has been widely acknowledged as an effective and accurate method to resolve the texture of biominerals. Detailed analyses showed that the two shells have a similar mesoscopic structure, which are consisted of three layers: periostracum layer, prismatic layer and nacreous layer. The prismatic layers of *Pinctada martensii* and *Anodonta cynea* shells are composed by calcite and aragonite crystallites respectively. In the former one, each prism has a "single-crystalline" outlook; the c-axis of crystallites within one prism are arranged almost in one direction: either parallel or perpendicular to the surface of the shell. In the later one, each prism is polycrystalline and full of mesoscale twinning. The nacreous layers of *Pinctada martensii* and *Anodonta cynea* shells are both composed by aragonite crystallites. The differences of crystallite grain size and mesoscale twining structure of nacreous layers have also been investigated and discussed.

P115

Diaquabis(1,10-phenanthroline)zinc(II) dinitrate, a modulated structure

A. Schönleber[1], S. W. Ng[2]
[1]University of Bayreuth, Laboratory of Crystallography, Bayreuth, Germany
[2]The University of Nottingham Malaysia Campus, Semenyih, Malaysia

The crystal structure of diaquabis(1,10-phenanthroline)zinc(II) dinitrate, $[Zn(H_2O)_2(C_{12}H_8N_2)_2](NO_3)_2$, exhibits strong satellite reflections up to 6th order in its diffraction pattern. The peaks can be uniquely indexed by a monoclinic (**b**-unique) lattice with parameters a = 9.5949(7) Å, b = 15.9348(15) Å, c = 15.8943(15) Å, β = 96.145(7) and a modulation wave vector **q** = 0.2957(2) **a*** - 0.2171(2) **c***.

Crystals were synthesized by evaporation of a stoichiometric mixture of zinc nitrate hexahydrate and 1,10-phenanthroline monohydrate in ethanol.

The coordination geometry of the zinc ion is described as distorted octahedral, comprising two O atoms from two coordinated water molecules and four N atoms from two 1,10-phenatroline molecules. The stability of the structure is enhanced by extensive O–H···O hydrogen-bonding interactions, linking the nitrate anions to the water molecules of the metal complex.

In our contribution we will propose a structural model for the modulated structure applying superspace group symmetry $P2_1/n(\alpha 0 \gamma)0s$ within the higher-dimensional superspace approach.

Developments in molecular crystallography

P116

Pressure effect on the arene-perfluoroarene interaction

A. Friedrich[1], K. Radacki[1], J. Ruiz-Fuertes[2,3], I. E. Collings[4], D. Sieh[1], M. B. Todd[1]
[1]Julius-Maximilians-Universität Würzburg, Institut für Anorganische Chemie, Würzburg, Germany
[2]Universitat de Valencia, Departament de Física Aplicada, Valencia, Spain
[3]Universidad de Cantabria, Santander, Spain
[4]European Synchrotron Radiation Facility (ESRF), Grenoble, France

The arene-perfluoroarene interaction is a robust supramolecular synthon, which is used for the development of highly oriented, stacked π-systems [1,2]. It describes the attractive interaction between fluorinated and non-fluorinated aromatic molecules, which have opposite charge distribution, resulting in a face-to-face association in contrast to the edge-to-face stacking (herringbone-type) of pure aromatic molecules [3]. While the arene-perfluoroarene interaction has been extensively applied in crystal engineering, only few high-pressure studies have been reported [4,5]. The aim of our study was the structural investigation of arene-perfluoroarene co-crystals at high pressure in order to obtain insight into the pressure evolution, stability, and strength of the arene-perfluoroarene interaction.

High-pressure single-crystal synchrotron X-ray diffraction data were collected on the 1:1 co-crystals of octafluoronaphthalene with naphthalene (NOFN) and anthracene (AOFN) up to 20 and 30 GPa, respectively, at beamline ID15B at the ESRF.

While NOFN maintains its structure and crystallinity up to 19 GPa, AOFN shows a pressure-induced phase transition at about 25 GPa. At this pressure the intermolecular distances approach 2.6 Å, a critical distance previously proposed for inducing intermolecular addition reactions, which may lead to polymeric products [3,6]. We have shown that in AOFN the stacking direction (*a* axis) is strongly compressed at the phase transition indicating the breakdown of the π-π stacking interaction. In summary, the parallel π-stacking arrangement induced by the arene-perfluoroarene interaction is more stable towards pressure than the herringbone-type packing, in which the molecules first tend to rearrange in a parallel way on pressure application [3]. The breakdown pressure, however, is similar to that reported for another co-crystal and polycyclic aromatic hydrocarbons (20-25 GPa) [3,5,6].

The authors thank the ESRF for synchrotron beamtime. Financial support from ESRF and University of Würzburg is greatly appreciated. J.R.-F. thanks the Spanish MINECO for the Juan de la Cierva Program (IJCI-2014-20513).

References

[1] T. Dahl. *Acta Chem. Scand. A* 1988, **42**, 1
[2] J.C. Collings et al. *New J. Chem.* 2001, **25**, 1410
[3] F. Capitani et al. *J. Phys. Chem. C* 2016, **120**, 14310
[4] S. Desgreniers et al. *J. Chem. Phys*. 1985, **83**, 480
[5] Y. Wang et al. *J. Phys. Chem. C* 2016, **120**, 29510
[6] L. Ciabini et al. *Nat. Mater.* 2007, **6**, 39

P117

The new Chemical Crystallography Beamline P24 at Petra III (PEX-E), Desy

C. Paulmann[1], M. Tolkiehn[2], U. Bismayer[1], H. Schulz-Ritter[2], A. Berghäuser[3]
[1]Mineralogisch-Petrographisches Institut, Universität Hamburg, Hamburg, Germany
[2]DESY Photon Science, Hamburg, Germany
[3]European XFEL, Hamburg, Germany

The shutdown of DORIS III discontinued some successful beamlines which served as main stations for a wide field of crystallographic applications ranging from diffuse scattering studies, charge density analysis, phase transitions, disordered and modulated structures all at ambient and non-ambient conditions.

A collaboration of a joint research BMBF project and Desy build up a new beamline at Petra III dedicated to all fields of crystallographic research. The beamline will start full user operation in spring 2018 and consists of two experimental hutches housing a refurbished Eulerian diffractometer (EH2) and a new heavy-load Kappa-diffractometer (EH2). Both instruments offer a compatible range of detectors (eg. Pilatus 1M CdTe, MarCCD, Ketek drift detector) and sample environments (10K-1300K, electrical fields, DACs).

The diffractometers are installed at a standard PETRA III undulator (2m, U29) using a CEMO-type water-cooled DCM (Si111/Si311) with preceding water-cooled mirrors for higher harmonic rejection (Rh/Pt-coated, 1.5 – 3.0 mrad). Due to heat-load restrictions of the CEMO-DCM, additional Cu-coated diamond windows will reduce the low-energy range providing an optimised continous range between 15keV – 44keV and a smaller range around 8keV. The calculated horizontal and vertical beam profiles at 80m source distance and 17.7keV are 1.5 x 0.7 mm^2 and 0.6 x 0.3 mm^2 FWHM and FW90%M, respectively. Additional Be-CRLs are foreseen for further beam-focusing down to 6 µm.

The Kappa-diffractometer (ca. 3.5 tons) offers two independent detector circles able to take loads of 30 kg each equipped with motorized counter-weights to balance a detector travel of 500 mm. The sphere of confusion (SOC) of the main circles (incl. Omega) for multi axis movements is below 10 µm and repeatability below 2x10^{-4} degrees. The inner circles (Kappa, Phi) provide a SOC below 25 µm for loads up to 5 kg with a maximum load of 10 kg. The Phi circle includes a motorized xyz-stage offering an accuracy in the micrometer range. The available space for sample environments is 190 mm, extendable to 250 mm by removing the stage. In combination with a modular mounting system, an easy exchange of different detectors or sample environments is possible.

Characterization of defects in crystalline materials

P118

Radiation-damaged pyrochlore

U. Bismayer[1], P. Zietlow[1], T. Beirau[2], J. Schlüter[1], C. Paulmann[1], L. A. Groat[3]
[1]Universität Hamburg, Geowissenschaften, Hamburg, Germany
[2]Martin-Luther-Universität Halle Wittenberg, Institut für Geowissenschaften, Halle (Saale), Germany
[3]University of British Columbia, Department of Earth and Ocean Sciences, Vancouver, Canada

Metamict pyrochlores are radiation-damaged and locally disordered because of intrinsic decay of uranium and thorium nuclei. Resulting structural damages are metastable and determine the macroscopic properties. Thermal annealing re-establishes the long-range structural order to a certain extent. Such healing phenomena are of interest for material sciences and in general for a better understanding of embedding materials for actinides in radioactive waste.

The analysis of pyrochlores exposed to different radiation doses on annealing using X-ray diffraction, Raman and IR spectroscopy respectively, gives insight into the structural damage and the recrystallization behaviour on different length scales [1].

References

[1] Zietlow, P., T. Beirau, B. Mihailova, L.A. Groat, T. Chudy, A. Shelyug, A. Navrotski, R.C. Ewing, J. Schlüter, R. Škoda, Radek and U. Bismayer (2017): Thermal annealing of natural, radiation-damaged pyrochlore. Z. Kristallogr. **232**. 25-38.

P119

CuGaS2:Mn chalcopyrite as intermediate band absorber material

J. Marquardt[1,2], S. Levcenco[1], A. Franz[1], C. Stephan-Scherb[3,2], S. Schorr[1,2]
[1]Helmholtz-Zentrum Berlin, Berlin, Germany
[2]Freie Universität Berlin, Institut für Geologische Wissenschaften, Berlin, Germany
[3]Bundesanstalt für Materialforschung und -prüfung (BAM), Berlin, Germany

By now, the progress in manufacturing Cu(Ga,In)(S,Se)2 absorbers used for thin film solar cells led to conversion efficiencies of 22.6% [1]. The Shockley-Queisser limit for chalcopyrite type semiconductors is at 32% [2]. Applying absorber materials with an intermediate band (IB) energy level in between the valence and conduction bands it is proposed that the efficiency can be raised up to 63.3% in ideal conditions [3]. Martí et al. [4] suggested different transition elements which may cause an intermediate band within the energy band gap of chalcopyrite type CuGaS2.

Part of this study aims for establishing the solubility limits of manganese in CuGaS2. The initial composition of the studied solid solutions follows the pseudo-binary section of CuGaS2 and MnS as well as CuGaS2 and CuMnS2. Thus different series of powder samples were synthesized by solid state reaction of pure elements in evacuated silica tubes. Before an additional annealing the samples were ground and pressed to pellets.

The chemical composition and phase content of the synthesized material were determined by wavelength dispersive spectroscopy (WDX) analysis using an electron microprobe. The structural properties of the obtained compounds were analyzed by X-ray and neutron powder diffraction (HZB, BER II, E9). In addition we have performed photoluminescence measurements to determine the optoelectronic properties.

The presentation will summarize structural trends of lattice parameters, tetragonal distortion and tetragonal deformation in dependence on the Mn content in CuGaS2 as well as off-stoichiometry. Moreover the observed photoluminescence spectra will be interpreted with calculations of the band diagram from Zhao et al. [5] and correlated with the cation distribution obtained from average neutron scattering length method.

References

[1] Jackson *et al*., Phys. Status Solidi RRL, 10 (2016)
[2] R. Scheer, H. W. Schock, Chalcogenide photovoltaics: physics, technologies, and thin film devices (Wiley-VCH, 2011)
[3] A. Luque *et al*., Physica B, 382 (2006)
[4] A. Martí *et al*., J. Appl. Phys., 103 (2008)
[5] Y.-J. Zhao *et al*., Phys. Rev. B, 69 (2004)

P120

Extension of X-Ray Diffraction Laminography: A 4D Imaging Method for the Investigation of Defect Dynamics in Crystalline Materials

S. Bode[1], D. Hänschke[2], E. Hamann[2], M. P. Kabukcuoglu[2,3], S. Haaga[2,3], L. Helfen[2,4], A. N. Danilewsky[3], T. Baumbach[1,2]
[1]Karlsruhe Institute of Technology (KIT), Laboratory for Applications of Synchrotron Radiation (LAS), Eggenstein-Leopoldshafen, Germany
[2]Karlsruhe Institute of Technology (KIT), Institute for Photon Science and Synchrotron Radiation (IPS), Eggenstein-Leopoldshafen, Germany
[3]Albert-Ludwigs-Universität Freiburg, Kristallographie, Freiburg i. Br., Germany
[4]European Synchrotron Research Facility (ESRF), Grenoble, France

Introduction

The defect-free growth of crystalline materials still remains a challenge. Even in previously dislocation-free materials microscopic flaws may trigger defect generation and formation of slip-bands during processing [1]. Imaging techniques are an essential tool to gain insight into these complex processes.

Objectives

In the last years, X-Ray diffraction laminography (XDL) has been developed to investigate the 3D structure of defects in crystalline materials and applied to static problems. The method is compatible with large and laterally extended samples, i.e. wafers [2]. Topographic images are acquired from different angles by rotating the crystal about a reciprocal lattice vector. Using these 2D projections a 3D image of the selected volume can be reconstructed. For the imaging of dislocations in silicon (Si) a spatial resolution of 2-5 µm was achieved while capturing a volume of a few mm3. The combination with other methods like X-ray white beam topography even allowed a full determination of the Burgers vector distribution within dislocation structures [3]. Meanwhile, XDL has also been applied to stronger absorbing materials like gallium arsenide. However, due to the time-consuming measurement procedure a speed-up is required to investigate dynamical processes.

Results

Recently, the XDL approach was extended regarding instrumentation and techniques to evaluate acquired data. Compiling a dedicated sample-manipulator (compare Fig. 1) ensured a highly precise and stable motion of the sample, allowing the automatization of several measurement steps. Furthermore, the set-up enables combination of XDL with methods like rocking curve imaging to link the defect structure to residual strain. Employing well suited reconstruction algorithms led to a reduction of the required number of projections, speeding up the method even more and enabling the observation of dislocation dynamics emerging from Franck-Read sources in Si during a gradual annealing (see Fig. 2).

Conclusion

Concluding, we will present the basic concept of XDL and the recent development entailing the extended capabilities, focusing on the progress in instrumentation and algebraic techniques for the 3D reconstructions.

References
[1] A. N. Danilewsky et al. (2011), J. Cryst. Growth, *318, 1157-1163*
[2] D. Hänschke et al. (2012), Appl. Phys. Lett., *101*, *244103*
[3] D. Hänschke et al (2017), PRL, in print

Fig. 1: Scheme of XDL-setup
Fig. 2: Projections of evolving dislocation structure

Figure 1

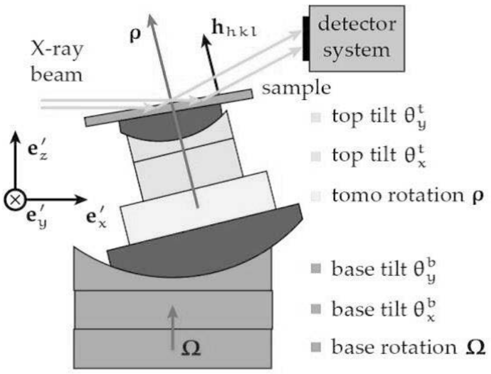

Figure 2

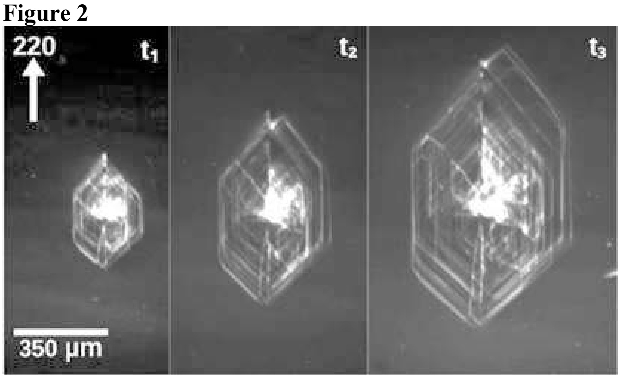

P121
Defect and Strain Characterization of 4H-SiC

M. Roder[1], P. Wellmann[2], A. N. Danilewsky[1]
[1]Albert-Ludwigs-Universität Freiburg, Kristallographie, Freiburg i. Br., Germany
[2]Friedrich-Alexander-Universität Erlangen-Nürnberg, Grystal Growth Lab, Erlangen, Germany

According to the physical and chemical properties of SiC its importance for high temperature and high power devices becomes apparent. Although the applications variety is high, the quality of the grown crystal is rather low, leading to an influence on the device performance [1]. In this work two SiC wafers, grown by Physical Vapor Transport (PVT) were characterized. Synchrotron white beam X-ray topography (SWBXT) performed in the TopoTomo Beamline at IPS was used in back-reflection geometry, which is the most suitable technique for the imaging of defects [2]. As can be seen in figure 1 the observed defects include closed-core and hollow-core screw dislocations (SDs), but reveal also features which does not fit in the description of screw dislocations, having shapeless structures and relative large diameters. In addition small angle grain boundaries are located between the SDs. The same areas on the wafer were then measured in transmission geometry. The resulting features were compared to those of the back-reflection images and identified as dislocations, having the shape of two straight, parallel lines with a strong contrast. For the strain investigation, polarization microscopy was used. While hollow-core dislocations are identified by large ,interference halos, the shapeless structures have a relatively small interference halo and can be identified as voids which are usually considered to be in a relaxed state [3]. For the real structure analysis high resolution X-ray diffractometry (HRXRD) measurements were performed at the two areas, where the topograps are shown in fig.1. The two rocking curves (RCs) differ in their curve shape and full-width at half maximum (FWHM), suggesting a difference in their crystal quality in terms of defects and mosaicity. Depending on the dominant defect type in the measured area, also the relation of strain and tilt in the RSMs changes. While the RSM of the first position (fig. 1a) indicates more crystal lattice tilt initiated by small angle grain boundaries, the RSM of the second position (fig. 1b) indicates less lattice tilt but the same amount of lattice strain as for position a, mainly initiated by voids.

References
[1] Ph G Neudeck, W Huang, and M Dudley, Solid State Electron, 42(12):2157–2164,1998.
[2] F Dudley, W Huang, S Wang, JA Powell, P Neudeck, and C Fazi.,J. Appl. Phys. D: A. Phys.,
28(4A):A56, 1995.
[3] V Presser, A Loges, and KG Nickel., Philos. Mag., 88(11):1639–1657, 2008.

Fig1 SWBXT 0004 reflections used for HRXRD

Figure 1

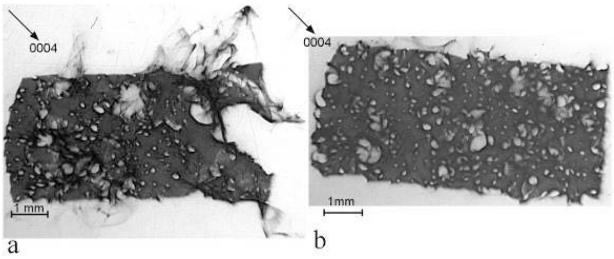

P122
3D Imaging of Crystalline Defects in Highly Absorbing Semiconductor Materials with X-Ray Diffraction Laminography (XDL) on the Example of GaAs Wafers

S. Haaga[1,2], D. Hänschke[2], E. Hamann[2], M. P. Kabukcuoglu[1,2], S. Bode[3], L. Helfen[2,4], T. Baumbach[2,3], A. N. Danilewsky[1]
[1]Albert-Ludwigs-Universität Freiburg, Kristallographie, Freiburg i. Br., Germany
[2]Karlsruhe Institute of Technology (KIT), Institute for Photon Science, Karlsruhe, Germany
[3]Karlsruhe Institute of Technology (KIT), Laboratory for Application of Synchrotron Radiation (LAS), Karlsruhe, Germany
[4]European Synchrotron Radiation Facility (ESRF), Grenoble, France

Introduction

To reduce defects in semiconductor crystals the availability of proper imaging methods is of major importance. Gallium arsenide (GaAs) for example is an important material for the fabrication of micro-electronic devices and is not available defect free. Recently, X-ray diffraction Laminography (XDL) has been developed for the non-destructive 3D imaging of crystalline defects within the bulk of crystals. It has been successfully applied to image dislocation patterns in almost perfect silicon. However, the applicability of XDL is not only limited on weakly absorbing materials with nonzero growth related dislocation densities. Therefore, we will present the first measurements on GaAs wafers by XDL to show its potential in the field of stronger absorbing materials.

Objectives

The basic principle of XDL is similar to well-known tomographic X-ray methods like Computed Tomography. By rotating a crystalline sample around a selected reciprocal lattice vector and recording a sufficient number of topographic projections the defect structure in the crystal bulk can be reconstructed. For weakly absorbing material like silicon XDL achieves a few µm spatial resolution inside large sample volumes (i.e. complete wafer thickness and several mm^2 field of view) . In Comparison with other non-destructive volume methods like X-ray Section Topography (XST) [1], a more than one order of magnitude higher spatial resolution can be achieved. Since XDL is a very general method it can be adapted to stronger absorbing materials like GaAs, nevertheless the results and resolutions will change due to a significantly higher absorption coefficient and a difference in the defect structures.

Results
We will present our results of the first XDL measurements on Liquid Encapsulated Czochralski grown GaAs (Fig. 1), focusing on the methodological challenges entailed by the properties of high-Z materials as well as on the achievable spatial resolutions. Furthermore, we will compare XDL reconstructions with corresponding XST scans.

Conclusion
XDL, a non-destructive 3D X-ray imaging method to reveal the defect structure in monocrystalline materials has been applied on GaAs for the very first time. We will present the results of these measurements as an example of XDL in the field of higher absorbing materials.

[1] D. Allen et al., **J. Appl. Crystallogr**., 44(3), 2011
Fig. 1: X-ray White Beam topograph of a GaAs wafer (left). Rendered XDL reconstruction of the marked area (right).

Figure 1

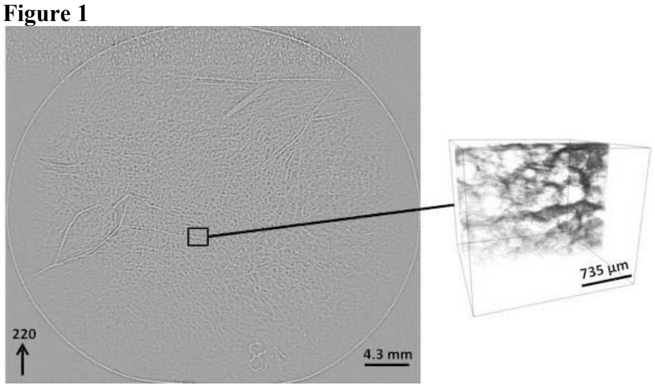

P123

4D Investigation of the Dislocation Propagation and their Interaction Depending on Thermal Stress by Means of X-ray Diffraction Laminography

M. P. Kabukcuoglu[1,2], D. Hänschke[2], E. Hamann[2], S. Bode[3], S. Haaga[1,2], L. Helfen[2,4], T. Baumbach[2,3], A. N. Danilewsky[1]
[1]Albert-Ludwigs-Universität Freiburg, Kristallographie, Freiburg i. Br., Germany
[2]Karlsruhe Institute of Technology (KIT), Institute for Photon Science and Synchrotron Radiation (IPS), Eggenstein-Leopoldshafen, Germany
[3]Karlsruhe Institute of Technology (KIT), Laboratory for Applications of Synchrotron Radiation (LAS), Eggenstein-Leopoldshafen, Germany
[4]European Synchrotron Radiation Facility (ESRF), Grenoble, France

Introduction
Silicon (Si) is the main material for many applications like microelectronic devices. In semiconductor industry, wafer processing and handling can cause damage to Si wafers which during thermal treatment acts as trigger for dislocation nucleation and propagation into dislocation free areas before [1]. A deeper understanding of the temporal evolution of dislocations depending on thermal strain is crucial for the avoidance of slip band formation.

Objective
Recently, X-ray diffraction laminography (XDL) has been developed to investigate the three-dimensional (3D) defect structures in laterally extended crystalline samples non-destructively. The method is capable of imaging complex dislocation patterns with a few µm spatial resolution in several mm3 volumes. By combining XDL with other complementary methods, like X-ray white beam topography, mesoscopic (on the micrometer scale: the 3D arrangement of dislocations within the emerging slip bands), and microscopic/atomistic (Burgers vectors) aspects can be linked enabling a comprehensive characterization of static dislocation structures [2]. Now, we want to capture the emergence and propagation of dislocations in 3D as a function of time.

Results
Si wafers were nano-indented creating initial damage sights to serve as Frank-Read sources. A double ellipsoidal mirror oven was calibrated to perform rapid thermal annealing (RTA) and thereby heat the wafers above the brittle-to-ductile transition temperature to create the thermal driven forces necessary for the generation and propagation of dislocations (Fig.1). Then, XDL scans were performed to follow the temporal evolution of dislocations after each RTA step (Fig. 2). Our measurements enable the imaging of the early formation of slip bands in 3D where dislocations propagate on {111} planes. It is now possible to measure propagation distances even of single dislocations and relate these to the duration and maximum temperature of the respective RTA step. Furthermore, the interactions of dislocations emerging from different Frank-Read sources were captured.

Conclusion
Concluding, we will present results from the first quasi 4D XDL measurement on dislocation dynamics and their interaction with other dislocations within complex arrangements in Si wafers.

References
[1] A. Danilewsky et al., J. Cryst. Growth, 318, 2011
[2] D. Hänschke et al., PRL, accepted

Fig.1: Tempereature profile of RTA
Fig.2: Topographic projection of the evolution of dislocations

Figure 1

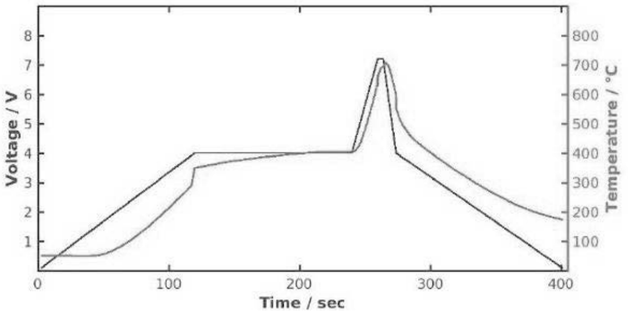

Figure 2

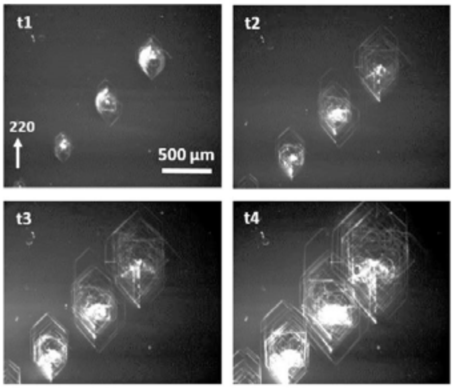

Powder diffraction / PDF

P124

Structural effects of Ni-incorporation into malachite

J. Heese[1], A. Hüttner[1], M. Behrens[1]
[1]Universität Duisburg-Essen, Essen, Germany

Nickel substituted malachite phases with varying Cu:Ni ratio between 100:0 and 90:10 were synthesized by constant-pH coprecipitation in an automated laboratory reactor system. Powder XRD patterns indicate the formation of single-phase materials which exhibit a characteristic shift of the (201-) and (211-) reflections towards higher angles with increasing Ni content. (Figure 1) This is related to the gradual decrease of the Jahn-Teller distortion in the malachite structure. The Jahn-Teller elongated axes are oriented nearly perpendicular to the (201-) and (211-) planes, so that an average contraction of the elongated axes leads to a decreasing spacing between the mentioned lattice planes and accordingly to a peak shift to higher angles in the XRD patterns. To quantify the structural changes caused by the Cu/Ni substitution a whole-pattern refinement was performed by using the Pawley method. The structural analysis showed an anisotropic contraction of the unit cell and Vegard-type linear trends for all lattice parameters. It becomes evident that the monoclinic angle β, a-, and c-axes decrease, while the b-axis slightly increases as a function of the nickel addition.

Figure 1

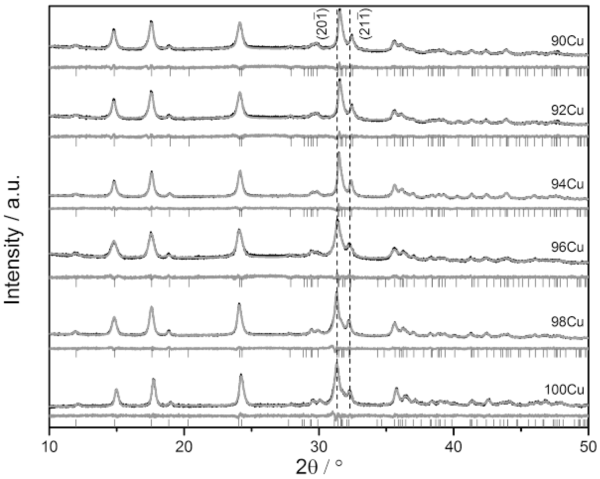

P125

Crystal structure of $La_{0.7}Ca_{0.3}Mn_{0.5}Fe_{0.5}O_3$

S. Jabarov[1,2]
[1]Joint Institute for Nuclear Research, Dubna, Russian Federation
[2]Azerbaijan National Academy of Sciences, Institute of Physics, Baku, Azerbaijan

The structural, magnetic and electron transport properties of mixed-valence manganites of the $R_{1-x}A_xMnO_3$ type (where R is a rare-earth element, A is a divalent alkaline-earth element) attract much interest of scientific community due to the colossal magnetoresistance effect. The unique properties of mixed-valence manganites are reflected in the rich magnetic phase diagram and are determined in particular by complex spin, charge and orbital ordered phases. Magnetic phase diagram includes high-paramagnetic, ferromagnetic, and antiferromagnetic phases, noncollinear spin ordering phase, and the spin-glass phase. In our work, we report experimental results of the neutron powder diffraction investigated at temperatures between 10 and 350 K in $La_{0.7}Ca_{0.3}Mn_{0.5}Fe_{0.5}O_3$ manganite perovskite samples.

$La_{0.7}Ca_{0.3}Mn_{0.5}Fe_{0.5}O_3$ samples were synthesized using standard ceramic procedures by heating stoichiometric mixtures of La_2O_3, $CaCO_3$, Mn_2O_3 and Fe_2O_3 in air at 1320 C, consistently for 15 h and then for 5 and 15 h and finally at 1375 C for 22 h, with intermittent grindings. According to x-ray diffraction data, samples have orthorhombic space group Pnma (a = 5.447(2) Å, b = 7.709(3) Å, c = 5.467(3) Å). The same structure orthorhombic space group Pnma was found in $La_{0.7}Ca_{0.3}Mn_{1-y}Fe_yO_3$ with $x = 0.3$ and $y = 0.0$, 0.03, 0.07 and 0.09. Neutron diffraction measurements of the $La_{0.7}Ca_{0.3}Mn_{0.5}Fe_{0.5}O_3$ samples were performed with DN-12 spectrometer at IBR-2 high-flux pulsed reactor (Frank Laboratory of Neutron Physics, Dubna, Russia). In the temperature range of neutron diffraction measurements from 10 to 300 K the $La_{0.7}Ca_{0.3}Mn_{0.5}Fe_{0.5}O_3$ samples correspond to the orthorhombic space group Pnma with disordering of Mn and Fe. The intensities of the diffraction patterns peaks at interplanar spacing d = 4.45 Å are increased with decreasing temperature.

Our neutron diffraction measurements indicate the formation of antiferromagnetic long-range ordering of G-type throughout the studied temperature range. According to the literature, the $La_{0.7}Ca_{0.3}MnO_3$ doping with iron ions leads to the substitution of Mn^{+3} by the Fe^{+3} and, as a result, to the double exchange mechanism disturbance and to suppression of the ferromagnetism associated with double exchange such a way, the 50% substitution of Mn/Fe leads to a complete suppression of the ferromagnetism in $La_{0.7}Ca_{0.3}Mn_{0.5}Fe_{0.5}O_3$, and the results obtained in our studies confirmed these facts.

P126

In situ X-Ray Diffraction During the Crystallization of Sulfidic Solid Electrolytes

H. Stöffler[1], M. Yavuz[1], S. Indris[1], H. Ehrenberg[1]
[1]Karlsruhe Institute of Technology (KIT), Eggenstein-Leopoldshafen, Germany

All-solid-state batteries (ASSB) using inorganic solid electrolytes instead of flammable organic liquid electrolytes are highly desired for improving the safety of lithium-ion batteries. Sulfide solid electrolytes enable the fabrication of bulk-type ASSBs because of their high ionic conductivity at room temperature and high ductility which enables good contact to the cathode by simply cold-pressing.

Here, we investigated sulfidic solid electrolytes based on Li_2S-P_2S_5. The materials were prepared by ball milling Li_2S and P_2S_5 (3:1) until glass formation was completed and no Bragg reflections were observable by X-ray powder diffraction (XRD). The glass formation process was observed by XRD after different ball milling times. *In situ* high temperature X-Ray diffraction (HT-XRD) was used to observe the crystallization and phase evolution in the temperature range of 25 °C – 700 °C. Thermogravimetric analysis was performed and compared with the HT-XRD experiment.

P128

Structure determination of cesium heteropolyacids with Keggin anions: Cs2.3H0.7[PMo12O40]

K. Hofmann[1], J. Steffan[1], N. Dürr[1], K. Kantchev[1], H. Vogel[1], B. Albert[1]
[1]Technische Universität Darmstadt, Fachbereich Chemie, Darmstadt, Germany

Heteropolyacids with Keggin anions are used in heterogeneous catalysis to partially oxidize methacrolein to methacrylic acid. While there are crystal structures of several representatives in the literature (e.g. K^+, NH_4^+[1]), no detailed structural information based on diffraction data seems to be available for the important cesium series of salts with the [PMo12O40]$^{3-}$ anion. We synthesized crystalline powders of the title compound and determined its crystal structure using highly resolved powder data.

$Cs_{2.3}H_{0.7}[PMo_{12}O_{40}]$ crystallizes isostructural to $(NH_4)_{2.4}H_{0.6}[PMo_{12}O_{40}]$ in the cubic crystal system, space group *Pn*-3*m* (No. 224, *a* = 1177.99(1) pm). The unit cell and the structure of the anion are shown in Fig. 1. The positions of molybdenum (24*k*), phosphorous (2*a*) and oxygen (3x 24*k*, 8e) atoms are fully occupied. The cation site (6*d*) is shared by cesium and hydrogen atoms with a refined ratio of 0.755(2) to 0.245(2). All isotropic displacement parameters except those of the hydrogen atoms were refined freely to give reasonable values. Bond lengths and angles are comparable to those of the potassium analogue described in literature.

Figure 1

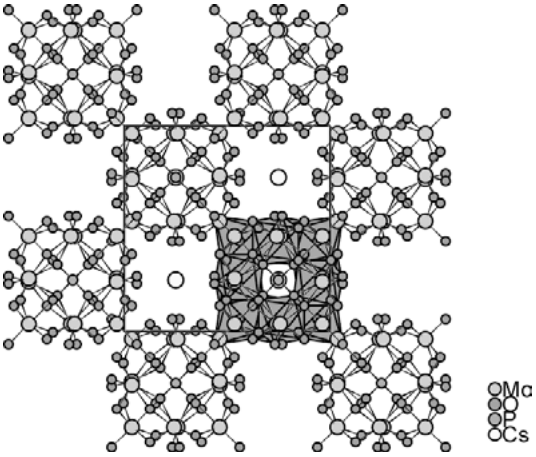

Figure 2

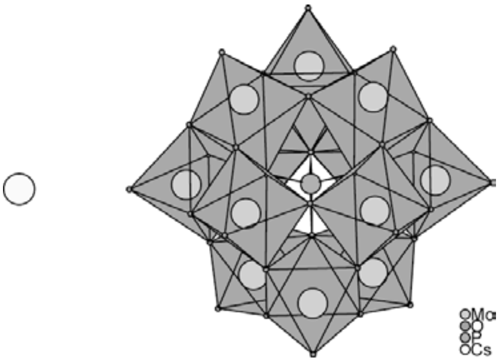

P129

High temperature XRD and PDF studies of Li-argyrodite Li6PS5Cl

R. Giesecke[1,2], M. Yavuz[2], S. Indris[2], T. Hupfer[1], H. Ehrenberg[2]
[1]Robert Bosch GmbH, Renningen, Germany
[2]Karlsruhe Institute of Technology (KIT), Karlsruhe, Germany

All solid state batteries have been attracting much attention over the last couple of years. In comparison to liquid-based batteries, they are expected to be safer and to have better thermal stability, higher ionic conductivity over broader temperature range and longer cycle life. Many solid state electrolytes have now reached the conductivity of liquid electrolytes and some solid state electrolytes even outperform them. One example for such a solid state electrolyte is the Li+ argyrodite (Li6PS5Cl), providing exeptional high Li-ion conductivity (in the range of 10-2 to 10-3 S cm-1 at RT).

In this work, we present a high temperature XRD study of Li6PS5Cl. Changes of structure with temperature are monitored to understand the correlation between structure and conductivity of this system. In addition, synchrotron pair distribution function analysis (PDF) was used to obtain more information about the evolution of the short-range order of this material during heat treatment. A fair amount of disagreement between the observed and calculated PDF in the range below 5 Å is observed. This could be either the evolution of the intra-tetrahedral P-S and S-S distances during crystallization or the coexistence of the glass-ceramics [1]. These structural changes have an impact on the ionic conductivity of the Li6PS5Cl, which makes it important for the further investigations with respect to the application of all-solid-state batteries.

Figure 1

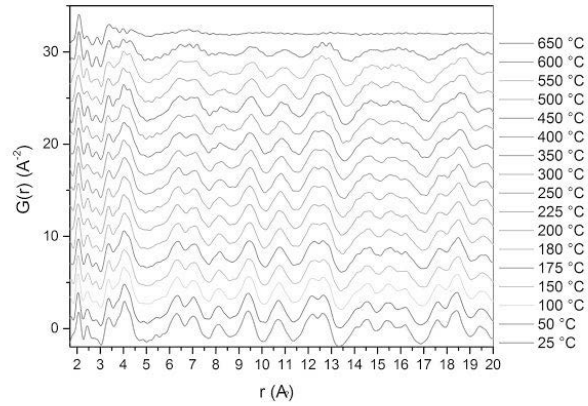

Other Topics

P130

Comparison of structures applying the tools available in the Bilbao Crystallographic Server

G. de la Flor [1,2], D. Orobengoa[1], E. Tasci[3], J. M. Perez-Mato[1], M. I. Aroyo[1]
[1]University of the Basque Country UPV/EHU, Física de la Materia Condensada, Leioa, Spain
[2]Universität Hamburg, Geowissenschaften, Hamburg, Germany
[3]Hacettepe University, Physics Engineering, Ankara, Turkey

Introduction

A quantitative comparison of similar crystal structures is often convenient to cross-check different experimental and/or theoretical structural models of the same phase coming from different sources. It is also important for the identification of different phases with the same symmetry, and it is fundamental for the still open problem of the classification of structures into structure types. In most cases, even if the setting of its space group is fixed, there is more than one equivalent description for a given structure. The existence of various equivalent structure descriptions makes the comparison of different structural models a non-trivial task in general.

Objectives

The aim of this contribution is to present the inew version of the program COMPSTRU [1] available on the *Bilbao Crystallographic Server* (http:// www.cryst.ehu.es) [2-3] for the comparison of structures with the same and different competition.

Results

The program COMPSTRU measures the similarity between two structures having the same space-group symmetry (or space groups that form an enantiomorphic pair) with the same or different compositions, and under the condition that the sequence of the occupied Wyckoff positions is the same in both structures (isopointal structures). Among other applications, this program can be used as a complementary tool for the classification of isopointal structures into isoconfigurational structure types. The efficiency and utility of the program are demonstrated by a number of illustrative examples.

Conclusion

The *Bilbao Crystallographic Server* is in constant improvement and development, offering free of charge tools to study an increasingly number of crystallographic problems which includes the comparison and classification of structures into structure types.

References

[1] G. de la Flor et al. (2016) *J. Appl. Cryst.*, **16,** 1-12
[2] M. I. Aroyo et al. (2006) *Z. Kristallog.*, **221**, 15-27
[3] M. I. Aroyo et al. (2011) Bulgarian Chemical Communications, 43(2), 183-197

P132

Elaboration and electrical properties of metal phosphate glasses

F. E. Dardar[1], M. Gross[2], S. Krimi[3], M. Couzi[4], A. Lachgar[2], A. El Jazouli[1]
[1]Ben M'sik University Hassan II Casablanca, Faculty of Science, Casablanca, Morocco
[2]Wake Forest University, Department of Chemistry, Winston Salem, NC, United States
[3]Ben M'sik University Hassan II Casablanca, Faculty of Science, Casablanca, Morocco
[4]Université de Bordeaux, Bordeaux, France

Abstract

Metal phosphates in both crystalline and vitreous forms are extensively studied for their potential application in heterogeneous catalysis [1], renewable energy [2], biomedical engineering [3], and environmental remediation [4]. Among these phosphates, those belonging to Nasicon family have attracted much attention due to their diverse properties [5]. Many compounds of Nasicon family can be prepared also in the glassy form, they are called Nasiglasses (Na super ionic glass) [6].

Nasiglasses belonging to systems [Na2O - Li2O - CaO - TiO2 - P2O5] and [Na2O - CaO - TiO2 – GeO2- P2O5] were synthesized and characterized by DSC, DTA, PXRD, Raman, density and ionic conductivity measurements. When Na+ is gradually replaced by Li+ in phosphates NaxLiyCazTit(PO4)3 some physical properties (density, molar volume, glass transition temperature, and ionic conductivity) vary in a non-linear manner, as a result of the mixed ions effect. Raman spectroscopy study shows that the glasses contain short -Ti-O-Ti-O-Ti- chains, and P2O7 (Q1) and PO4 (Q0) groups. The presence of -Ti-O-Ti-O-Ti- chains indicates that the TiO6 octahedra are linked to each other through corners.

Key word: Metal phosphates; Glass; PXRD; DTA; DSC; Raman; Ionic conductivity.

Reference

[1] S. Sebti, M. Zahouily, H. B. Lazrek, J. A. Mayoral and D. J. Macquarrie, "Phosphates: New Generation of Liquid-Phase Heterogeneous Catalysts in Organic Chemistry", Current Organic Chemistry, (2008), 12, 203-232
[2] M. Minakshi, D. Mitchell, R. Jones and F. Alenazey, "Synthesis, structural and electrochemical properties of sodium nickel phosphate for energy storage devices", Nanoscale. (2016); 8(21):11291-305.
[3] P. N. Kumta, C. Sfeir, D-H Lee, D. Olton, D. Choi, "Nanostructured calcium phosphates for biomedical applications: novel synthesis and characterization", Acta Biomaterialia 1 (2005) 65–83
[4] N. Lyczko, A. Nzihou and P. Sharrok, "Calcium phosphate sorbent for environmental application", Procedia Engineering 83 (2014) 423–431.
[5] N. Anantharamulu, K. Koteswara Rao, G. Rambabu, B. Vijaya Kumar, Velchuri Radha, M. Vithal, "A wide-ranging review on Nasicon type materials", J Mater Sci (2011) 46:2821–2837
[6] S. Susman, C.J. Delbecq, J.A. McMillan, M.F. Roche, "NASIGLAS: A new vitreous electrolyte", Solid State Ionics (1983) Vol. 9–10, Part 1, pp. 667-673.

P133

Directional solidification and characterization of Fe – 4.25%C eutectic alloy

M. Trepczynska-Lent[1]
[1]UTP University of Science and Technology, Faculty of Mechanical Engineering, Bydgoszcz, Poland

Using a vacuum Bridgman-type device with liquid metal cooling, Fe – 4.25% C alloy was directionally solidified with growth rate of 300 mm/h (83.3 μm/s). The microstructure of the rod sample was studied on the longitudinal and cross-section. Eutectic phase have been observed using optical microscopy and scanning electron microscopy. Measurements were made using the XRD and EBSD technique. The grain boundary shape and morphology details were described. The morphology and microtexture of the eutectic cementite were determined.

P134

The discovery of a molecule-like (without nucleus) structure of atoms

G. Shpenkov[1]
[1]Independent researcher, Bielsko-Biala, Poland

Considering atoms as wave formations, we found that they have a quasi-spherical shell-nodal (molecule-like, without nucleus) structure coincident with the nodal structure of standing waves in a three-dimensional wave space-field. Each atom with Z ≥ 2 represents a specific elementary molecule of the hydrogen atoms, to which we refer *proton*, *neutron* and *protium* (1H1). Reality of the found structure was verified by different ways. The direct confirmation was made on graphene. According to the modern data, a two-dimensional hexagonal lattice of graphene has six-fold rotation symmetry in a plane perpendicular to the axis of rotation. On the contrary, according to the shell-nodal structure of carbon atoms, graphene is anisotropic and has two-fold rotation symmetry. Laboratory tests completely confirmed this prediction, which is a natural consequence of the shell-nodal structure of the atoms. Namely, the polar diagrams of conductivity measured on one-atom thick graphene layers in all directions (from 0 to 360 degrees) along a plane have demonstrated the characteristic elliptical form inherent in anisotropic materials. Thus, we have all rights to state about a key discovery in physics approaching as closer to cognition of the true structure of the atoms. In this connection, it is inevitably should be undertaken efforts to revise some theoretical concepts of crystallography.

P135

X-Ray Optics for Optimized Performance between 10 eV and 40 keV

P. U. Pennartz[1]
[1]Rigaku Innovative Technologies Inc., Eschweiler, Germany

Over recent years, multilayer optics (ML) have found their application in WDXRF and e-beam applications. In our days, one can say there is no WDXRF system sold without several multilayer structures included. We will give a short overview on materials used and applications in this field of instrumentation, which can be found either close to the process control or even within the process flow as an inline metrology tool.

Picture 1 (left) shows the reflectivity curve for several ML structures and the XRF relevant absorption edges for some interesting light elements. The graph shows how to select the best materials to optimize the performance for the different elements to be detected. The detection of light elements are especially of high interest.

Besides the application of ML optics discussed above, there is another wide field of application in the EUV lithography industries. EUV Optics ranging from small monochromators to large condensers for application in EUV lithography machines include some of the big optic tools we are able to produce. Some of these optics are literally big, being 75 cm and more in diameter.

But besides that, metrology machines using the 13.5 nm wavelength are also needed. For such machines, so called replicated optics are a good choice for an optimized optical path. We will show results obtained with these replicated optics. These principles are also finding application in outer space optics such as Walther Objectives. Picture 2 below shows the shape of typical replicated optics.

The geometrical parameters of the shape can be adapted to the needs of the optical specifications and design. The idea of such optics is to produce a mandrel of high precision, which is then used as the core and all "outer" layers are put on top of this core. At the end the core is extracted and the hollow pipe-like structure shown is used.

Picture 3 (left) shows different structures of these replicated optics which can be used from hard x-rays (8 keV leftmost in the picture) to 100 eV (rightmost in the picture).

In the presentation we will show the most recent results obtained with this technology.

Figure 1

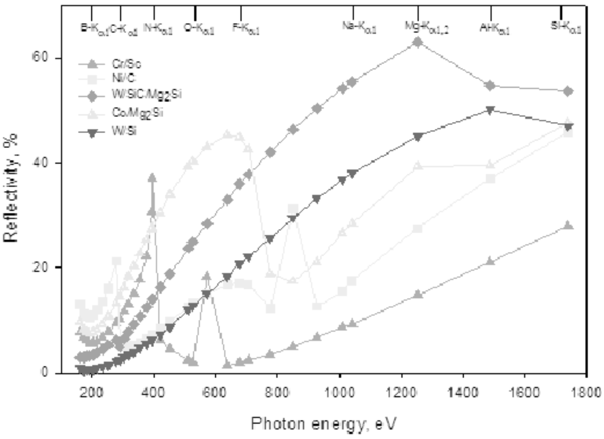

Figure 2

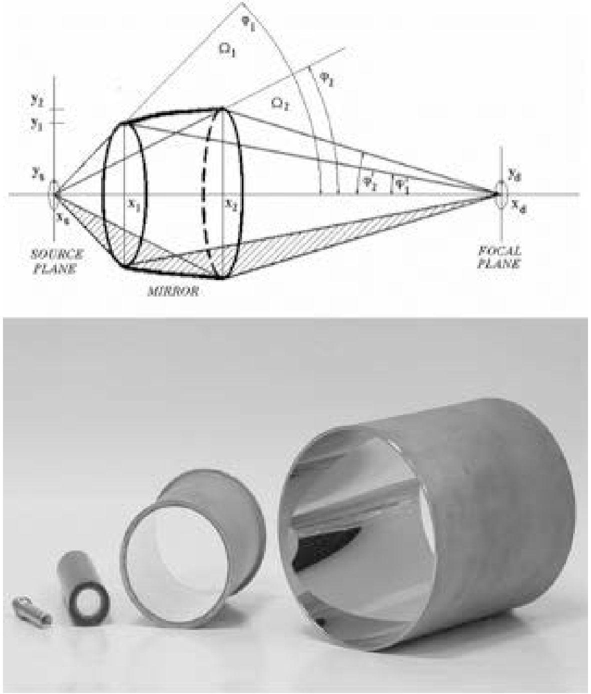

P136

Pump-probe setups for the ultrafast measurements of optical properties in ZnSe

J. Davaasambuu[1], T. Baatarchuluun[1], P. Munkhbaatar[1], T. Khos-Ochir[1], N. Tuvjargal[1], G. Munkhbayar[1], O. Tegus[2]
[1]National University of Mongolia, Department of Physics, Ulaanbaatar, Mongolia
[2]Inner Mongolia Normal University, Key Laboratory for Physics and Chemistry of Functional Materials, Hohhot, China

Optical pump-probe experiments are a powerful tool to study the ultrafast optical response of effects in condensed matters. In pump-probe spectroscopy, the system is excited with a pump pulse and the absorption and/or reflection (response) of a probe pulse is measured as a function of the delay time and the pump and probe frequences [1-2].

We present the main and unique features of the ultrafast pump-probe setup, which is mainly based on a femtosecond laser that emits approximately 6 fs optical pulses at the central wavelength of 800nm with a pulse energy of 4 nJ at a repetition rate of 75 MHz and a regenerative amplifier system that generates high energy (1,5mJ) optical pulses with temporal length of 35 fs at a repetition rate of 5 kHz. The setup can be efficiently utilized for various femtosecond time-resolved optical spectroscopic studies.

This work was supported by the Asian Research Center Project (Grant No. P2017-1303), National University of Mongolia (Grant No. P2017-2407) and Mongolian Foundation for Science and Technology.

References

[1] J. Michael Holles, Modern spectroscopy, Wiley, 2004
[2] R. Paschotta, Encyclopedia of Laser Physics and Technology, Springer, 2005

P137

The Crystal Structure of β-Boron

C. Eisele[1], S. Mondal[2], S. Dey[1], I. Chuvashova[3], C. Paulmann[4], S. van Smaalen[1]
[1]University of Bayreuth, Laboratory of Crystallography, Bayreuth, Germany
[2]CSIR-Central Glass & Ceramic Research Institute, Sensor and Actuator Division, Kolkata, India
[3]University Paris 13, Institut Galilée, Villetaneuse, France
[4]University of Hamburg, Geowissenschaften, Hamburg, Germany

The crystal structure of β-boron and its chemical bonding are still under debate [1]. The most widely accepted structure model of β-rhombohedral boron is the one published by Slack *et al.* in 1988 [2].
According to Slack's model β-boron crystallizes in space group *R-3m* and comprises 320.6 atoms per hexagonal unit cell.
Building blocks of B_{12} icosahedra and triply-fused icosahedra (B_{28} units) make up a complex three-dimensional framework including 15 crystallographically independent boron atoms.
Additional interstitial sites, which are only partially occupied (abbreviated POS), and vacancies in the framework cause distortions from the ideal icosahedral geometry [2].
The concept of these interstitial POS, where single boron atoms act as "dopants", gives rise to the striking thermodynamic stability of β-boron at ambient pressure in all temperatures areas below the melting [1]. We have reinvestigated the crystal structure of β-boron with reduced symmetry based on high-resolution X-Ray data at 100 K. The aim is to get a more detailed structure model of β-boron along with a topological analysis of its chemical bonds as a key for a deeper understanding of its peculiar physicochemical properties.

References

[1] T. Ogitsu, E. Schwegler, and G. Galli, *Chem. Rev.* **113**, 3425 (2013).
[2] G.A. Slack, C.I. Hejna, M.F. Garbauskas, and J.S. Kasper, *J. Solid State Chem.* **76**, 52 (1988).

P138

Systematic errors in least-squares refinements against diffraction data

J. Henn[1]
[1]University of Bayreuth, Bayreuth, Germany

Some important and popular systematic errors are discussed.

P139

Valorization of waste from the wood industry (sawdust) and their use as adsorbent material: physicochemical characterization, modeling and optimization adsorption using Response Surface Methodology (RSM)

S. Asmaa[1]
[1]Ben M'sik University Hassan II Casablanca, Faculty of Science, Settat, Morocco

Abstract

The present work reports on simple and effective ecofriendly approach for the valorization of sawdust (waste from the wood industry) in the environmental application as adsorbent biomaterials. After determination the physicochemical properties of the tested sawdust: pH, conductivity, the biomaterial was characterized using various instrumental techniques including scanning electron microscope (SEM), energy dispersive spectroscopy (EDS) and Fourier transformed infrared spectroscopy (FTIR).

Keywords: waste, wood industry, sawdust, physicochemical characterization, modeling, optimization, RSM.

P140

The Crystal Structure Transformation In $La_{0.8}K_{0.6}Ca_{1.6}Mn_2O_7$ Double Layered Perovskite Manganite

C. G. Nlü[1], A. Tekgül [2], M. Acet[3], M. Farle[3]
[1]Pamukkale University, Department of Biomedical Engineering, Denizli, Turkey
[2]Uludag University, Department of Physics, Bursa, Turkey
[3]Universität Duisburg-Essen, Faculty of Physics, Duisburg, Germany

Perovskite-type manganite oxides have attracted much attention due their unusual electrical and magnetic properties. Recently, apart from the ABO_3 type perovskite manganites, the layered perovskite manganite Ruddlesden-Popper phases attracted considerable attention due to their novel physical properties. In some of the Ruddlesden-Popper perovskites, the porosities in their structures have been observed which directly affect to physical properties of the material.

In this study, we have added K in place of La in $La_{1.4}Ca_{1.6}Mn_2O_7$ to obtain $La_{0.8}K_{0.6}Ca_{1.6}Mn_2O_7$ by sol-gel process. The doped K is removed from the crystal structure of materials by heat-treatment procedure. Therefore, we obtained the space for the changing of the crystal structure. As seen the figure 1, the crystal structure were transformed from orthorhombic to tetragonal and then from tetragonal to rhombohedral by temperature. These crystallographic informations are compatible with the magnetostructural transition temperature in the magnetic measurement.

Figure 1. The peaks at around 49◦ are determined by fit-function to indicate the characteristic peaks of O-T-R phases. Black line is shown the original data and red, blue and purple lines indicate the O-T-R phases, respectively. The sum of fitted curves in a figure creates the original data. (a) 112 K, (b) 120 K, (c) 180 K, (d) 200 K, (e) 222 K, (f) 295 K.

Figure 1

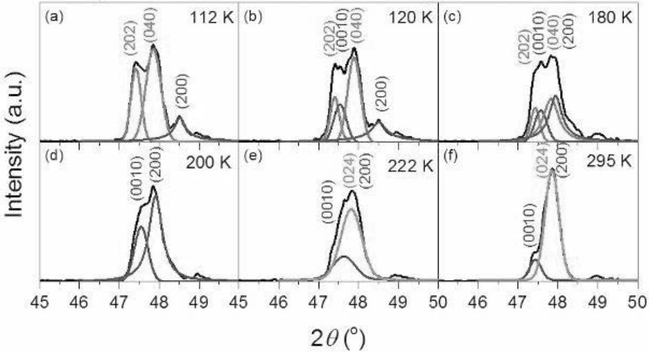

P141

Crystallography in the context of the energy transition: The battery of tomorrow.

T. Leisegang[1,2], F. Meutzner[1,2], T. Nestler[1], M. Zschornak[3], R. Schmid[1], A. A. Kabanov[2], R. A. Eremin[2], V. A. Blatov[2], D. C. Meyer[1]
[1]Technische Universität Bergakademie Freiberg, Institut für Experimentelle Physik, Freiberg, Germany
[2]Samara National Research University, Samara Center for Theoretical Materials Science, Samara, Russian Federation
[3]Helmholtz-Zentrum Dresden Rossendorf, Institute of Ion Beam Physics & Materials Research, Dresden, Germany

Climate change, dwindling resources, and population growth demand for novel efficient ways of energy transition, distribution, and storage. This is a major issue of the German *Energiewende*. Among, the storage of a surplus of electric energy is of high relevance. In recent years several storage test facilities on base of the Li-ion technology have been installed and used for the regulation of supply and demand of electric energy. However, energy density and thus price of such systems are still not sufficient for large-scale distribution. Therefore currently other ways of regulations are discussed for times when the demand of electric energy is low or photovoltaic and wind farms offer high capacities. Those can be the installation of large immersion heater facilities to convert already produced electric energy back to thermal energy in order to exterminate surpluses of electric energy in the Megawatt range, then without meaningful use. Hence, novel high energy density and low-cost electrochemical storage is of particular importance for the efficient storage of electric energy from renewable energies. Beside such stationary systems the electromobility is another driving force for the development of these so-called post-Li batteries.

This is where crystallography can contribute to the *Energiewende*. In order to increase energy density of batteries novel materials, such as solid electrolytes or intercalation cathodes for high-valent elements, need to be identified and prepared. Especially Al as pure anode material appears a promising starting point, since it is the most abundant metal in the earth"s crust and possesses four times the volumetric capacity of Li. For this purpose, we established a combined approach of different theoretical methods to scan for Al containing materials: Voronoi-Dirichlet partitioning (VDP), bond-valence site-energies (BVSE) and density functional theory (DFT) calculations employing the nudged elastic band method. This strategy was able to suggest Al-ion conducting materials.

The presentation gives an overview of new developments in post-Li battery materials, introduces crystallography-based strategies for identifying novel solid-electrolyte and intercalation cathode materials, specifies promising structural motifs for fast Al-ion diffusion, and eventually provides the current state of the Al-ion battery.

This work is funded by the BMBF (R2RBattery: 03SF0542A), Russian Megagrant (14.B25.31.0005), and RSF (16-13-10158).

Figure 1

Author index

Weitere empfehlenswerte Titel


MULTI-COMPONENT CRYSTALS

Multi-Component Crystals
Synthesis, Concepts, Function
Edward Tiekink, Julio Zukerman-Schpector (Eds), 2017
ISBN 978-3-11-046365-1, e-ISBN 978-3-11-046495-5

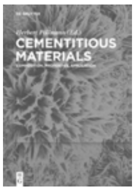
CEMENTITIOUS MATERIALS

Cementitious Materials
Composition, Properties, Application
Herbert Pöllmann (Ed.), 2017
ISBN 978-3-11-047373-5, e-ISBN: 978-3-11-047372-8

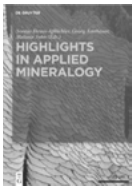
HIGHLIGHTS IN APPLIED MINERALOGY

Highlights in Applied Mineralogy
Soraya Heuss-Aßbichler, Georg Amthauer, Melanie John (Eds.), 2017
ISBN 978-3-11-049122-7, e-ISBN 978-3-11-049734-2


ZEITSCHRIFT FÜR KRISTALLOGRAPHIE SUPPLEMENT

Series: Zeitschrift für Kristallographie Supplement

Published titles in this series:

Vol. 37: 25th Annual Conference of the German Crystallographic Society, March 27-30, 2017, Karlsruhe, Germany (2017)

Vol. 36: 24th Annual Conference of the German Crystallographic Society, March 14–17, 2016, Stuttgart, Germany (2016)

Vol. 35: 23rd Annual Conference of the German Crystallographic Society, March 16–19, 2015, Göttingen, Germany (2015)